Lehrstuhl für Elektrische Antriebssysteme und Leistungselektronik

Prof. Dr.-Ing. Ralph Kennel

Design of a modern aircraft's electrical network system with focus on power quality and network stability via multi-level modeling

Martin Raphael Kuhn

Vollständiger Abdruck der von der Fakultät für Elektrotechnik und Informationstechnik der Technischen Universität München zur Erlangung des akademischen Grades eines

Doktor-Ingenieurs (Dr.-Ing.)

genehmigten Dissertation.

Vorsitzender: Prof. Dr.-Ing. Alexander W. Koch
Prüfer der Dissertation:
1. Hon.-Prof. Dr.-Ing. Martin Otter
2. Prof. Dr.-Ing. Ulrich Wagner

Die Dissertation wurde am 25.09.2017 bei der Technischen Universität München eingereicht und durch die Fakultät für Elektrotechnik und Informationstechnik am 21.12.2017 angenommen.

Abstract

Aiming at global energy optimization of aircraft, the concept "More Electric Aircraft" (MEA) and "All Electric Aircraft" (AEA) becomes more interesting for the aeronautical industry. Electric equipment is replacing hydraulic, pneumatic and mechanical equipment in the domains of propulsion, control and auxiliary systems. This architecture provides much room for optimization but interactions of components have to be analyzed on a bigger scale. This thesis contributes to the design and analysis of the electrical network system by model-based methods which are suitable for modern large aircraft systems.

The thesis starts with a proposal to improve the pre-design of aircraft generators by using multi-objective optimization over design rules taking nonlinear loads and power quality of the network into account. In this phase very simplified, static models are utilized. The power quality is assessed in a new, approximate way using negative sequence inductances. The goal is to show trade-offs between generator weight and power quality.

Afterwards, new methods are introduced which enable the analysis of electrical network systems with regards to power quality and network stability based on models of the electrical equipment. The modeling includes detailed behavioral models, abstracted functional models and time-invariant harmonic models.

- Power quality analysis is performed in periodic steady-state of the overall system, for example by calculation of Total Harmonic Distortion. Traditional simulation methods need long ramp-up phases to reach this state. In the thesis a new method is proposed to directly initialize electrical networks with rectifiers in near periodic steady-state by a suitable combination of harmonic and behavioral component models. This solution includes a new way to model rectifiers. Furthermore, a novel method is proposed to automatically detect when periodic steady-state is reached.
- The network stability is analyzed with several approaches, namely impedance-based methods, Modal Analysis, structured singular value μ analysis and anti-optimization. The advantages and disadvantages of the various methods are analyzed, discussed and exemplified at hand of an aircraft electrical network system.

The last section is devoted to the analysis of network interactions, using detailed large-scale electrical network simulation to perform virtual testing of the electric power network of MEAs. All modeling is based on the object-oriented modeling language Modelica.

Kurzzusammenfassung

Mit dem Ziel der globalen Energieoptimierung von Flugzeugen wird das Konzept "More Electric Aircraft" (MEA) und "All Electric Aircraft" (AEA) für die Luftfahrtindustrie immer interessanter. Hydraulische, pneumatische und mechanische Systeme sollen in den Bereichen Antrieb, Steuerung und Hilfssysteme durch elektrische Systeme ersetzt werden. Diese Architekturen bieten großes Optimierungspotenzial, wobei die Wechselwirkungen von Komponenten großflächig analysiert werden müssen. Diese Arbeit trägt zur Konzeption und Analyse des elektrischen Energienetzes für moderne Großraumflugzeuge durch modellbasierte Methoden bei.

Die Arbeit beginnt mit einem Vorschlag zur Verbesserung des Vorentwurfs von Flugzeuggeneratoren durch die Verwendung von mehrzielieger Optimierung und Entwurfsregeln unter Berücksichtigung nichtlinearer Lasten und der Spannungsqualität des Energienetzes. In dieser Phase werden sehr vereinfachte, statische Modelle verwendet. Die Spannungsqualität wird auf neue, approximative Weise mit Hilfe von Gegeninduktivitäten bewertet. Ziel ist es, Zielkonflikte zwischen Generatorgewicht und Spannungsqualität aufzuzeigen.

Anschließend werden neue Methoden vorgestellt, die es ermöglichen, elektrische Energienetze auf Basis von Modellen des elektrischen Systems hinsichtlich Spannungsqualität und Netzwerkstabilität zu analysieren. Die Modellierung umfasst detaillierte "behavioral models", abstrahierte "functional models" und zeitinvariante harmonische Modelle.

- Die Analyse der Spannungsqualität erfolgt im periodisch stationären Zustand des Gesamtsystems, z.B. durch Berechnung der Gesamtharmonischen Verzerrung (THD). Herkömmliche Simulationsmethoden benötigen lange Anlaufphasen, um diesen Zustand zu erreichen. In der Arbeit wird eine neue Methode vorgeschlagen, um elektrische Netze mit Gleichrichtern in einem nahezu periodisch stationären Zustand direkt zu initialisieren, indem eine geeignete Kombination von harmonischen und detaillierten Komponentenmodellen verwendet wird. Diese Lösung beinhaltet eine neue Möglichkeit, Gleichrichter zu modellieren. Darüber hinaus wird eine neuartige Methode vorgeschlagen, um automatisch zu erkennen, wann der periodisch stationäre Zustand erreicht wird.
- Die Netzwerkstabilität wird mit mehreren Verfahren analysiert, nämlich impedanzbasierten Methoden, Modalanalyse, μ-Analyse und Anti-Optimierung. Die Vor- und Nachteile der verschiedenen Verfahren werden analysiert, diskutiert und exemplarisch an einem elektrischen Energiesystem eines Flugzeugs demonstriert.

Der letzte Abschnitt widmet sich der Analyse von Netzwechselwirkungen. Dazu werden detaillierte und umfangreiche Simulationen des elektrischen Netzes benutzt, um das elektrische Energienetz von MEAs virtuell zu testen. Die gesamte Modellierung basiert auf der objektorientierten Modellierungssprache Modelica.

To my family

Acknowledgments

Contents

1 Introduction

In a conventional aircraft system architecture, fuel is converted into power by the engines. Most of this power is used for the propulsion of the aircraft. The power of the aircraft systems is transmitted via, and converted into, four main types of non-propulsive power. This is pneumatic, mechanical, hydraulic and electrical power:

- Pneumatic power is generated by the compressor stages to power the Environmental Control System (ECS) and supply hot air for the Wing Ice Protection System (WIPS).
- Mechanical power from the engines shafts drive the central hydraulic pumps and other mechanically driven subsystems, and the main electrical generator.
- Hydraulic power by the hydraulic pumps feeds the actuation systems for flight control, landing gear and numerous ancillary systems.
- Electrical power by the generator supplies electric energy to the avionics, to cabin and aircraft lighting, to the galleys, and to other commercial loads.
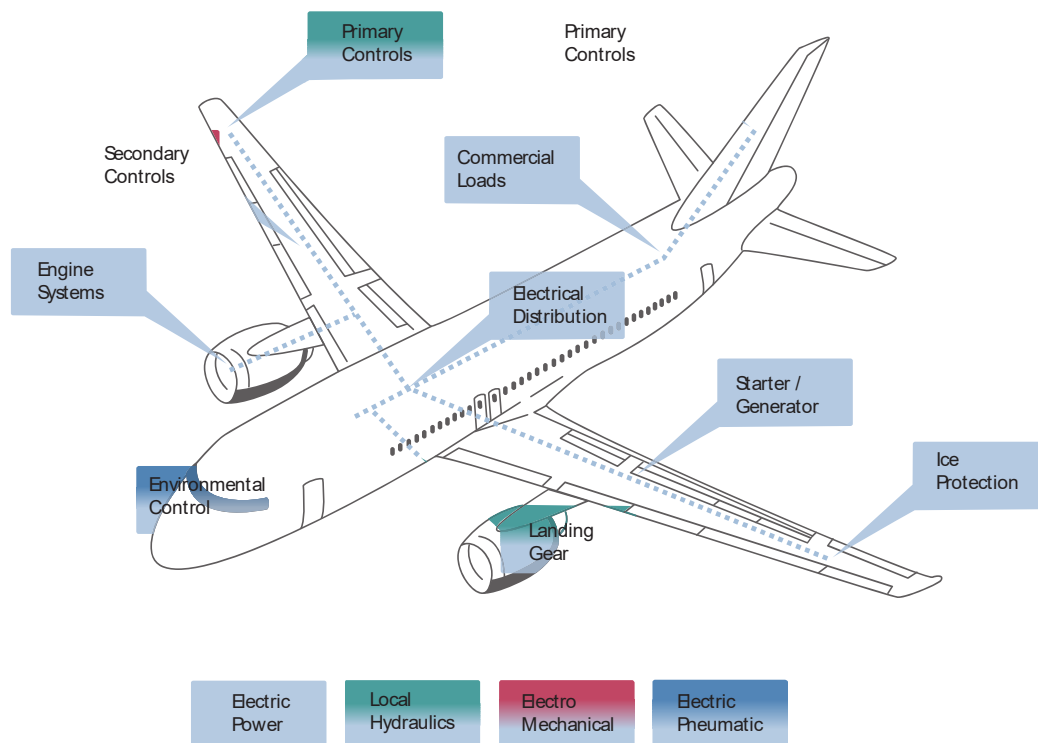
Figure 1.1: Concept of "More Electric Aircraft"

Currently, each aircraft system has become more and more complex over decades of developments. The resulting architecture provides much room for optimization. Aiming at global energy optimization of aircraft, the concept "More Electric Aircraft" (MEA) and "All Electric Aircraft" (AEA) becomes more interesting for the aeronautical industry. Electric equipment is replacing hydraulic, pneumatic and mechanical equipment in the domains of propulsion, control and auxiliary systems. Therefore, a power optimized aircraft architecture depicted in Figure 1.1 has been proposed (Schallert et al., 2006). Using more electric energy could substantially reduce the consumption of non-propulsive power. Possible approaches here include variable frequency networks without gearbox, bleedless engines with an electric Environmental Control Systems (ECS) and electrothermal wing ice protection, local electro-hydraulic and electro-hydrostatic actuators, and more
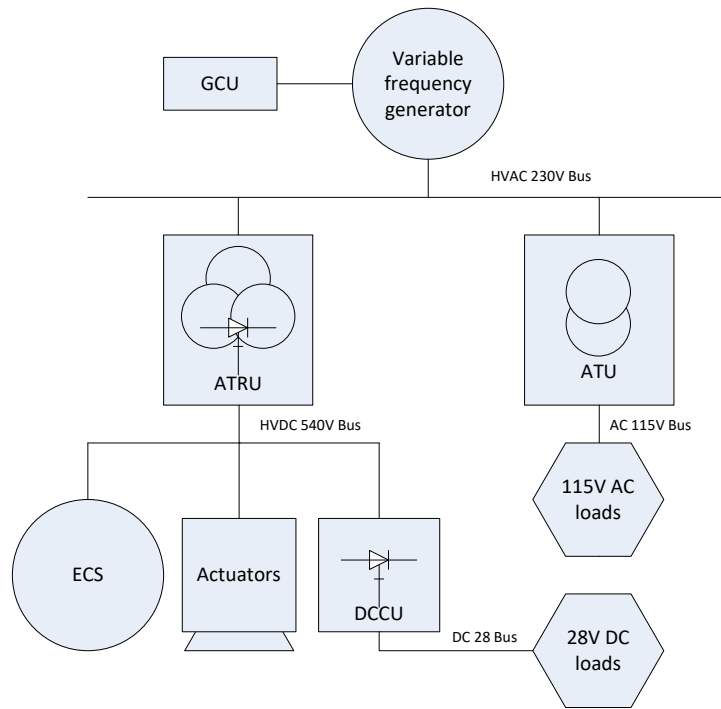
Figure 1.2: Possible architecture for a More Electric Aircraft with local HVDC network

electromechanical actuators. Compared with the conventional power distribution network, the More Electric Aircraft Architecture demonstrated weight gains, reduced maintenance requirements and increased reliability and also increased passenger comfort.

Although the aircraft industry clearly tends to design future aircraft with more electric power, the discussions about the optimal power distribution network is still ongoing. The high voltage DC power distribution system (HVDC) is gaining more attention (Roboam, 2011). Compared to the AC power distribution system it shows benefits like mass/volume saving in the feeders and possible use of regenerated energy from electric actuators. Alternatively, new aircraft concepts based on a classical architecture with AC power distribution tend to distribute more power to non-linear and switching loads which are connected via local HVDC networks, like in Figure 1.2.

This architecture contains an 18-pulse Auto-Transformer Rectifier Unit (ATRU) which transfers 230V AC voltage to 540V DC voltage. The local DC network supplies DC loads such as electric environmental system and electric actuators. The term "High voltage DC" is used to differentiate it from the DC 28 Volts low voltage network rather than to denote a power grid in the order of hundreds of kilovolts.

1.1 State of the art in generator design

Starter generators are significant contributions to the concept of More Electric Aircraft. The replacement of conventional hydraulic, pneumatic and mechanical loads by electric systems and drives increases the on-board electrical load significantly. Classic airplane generators in the range of 100kVA are replaced by generators in the range of 150 to 250 kVA for the Boeing 787 "dreamliner" (Sinnett, 2007). The most commonly used type of machine to generate the electrical power is the externally excited synchronous machine with interior rotor (Sinnett, 2007). For this machine high efficiency can be combined with high reliability via a minimum of electronics, which is essential for aerospace industry. External excitation enables controlled output voltage at the variable shaft speed. It was introduced in newer aircraft such as A380 or B787. With the ongoing modification of existing aircraft
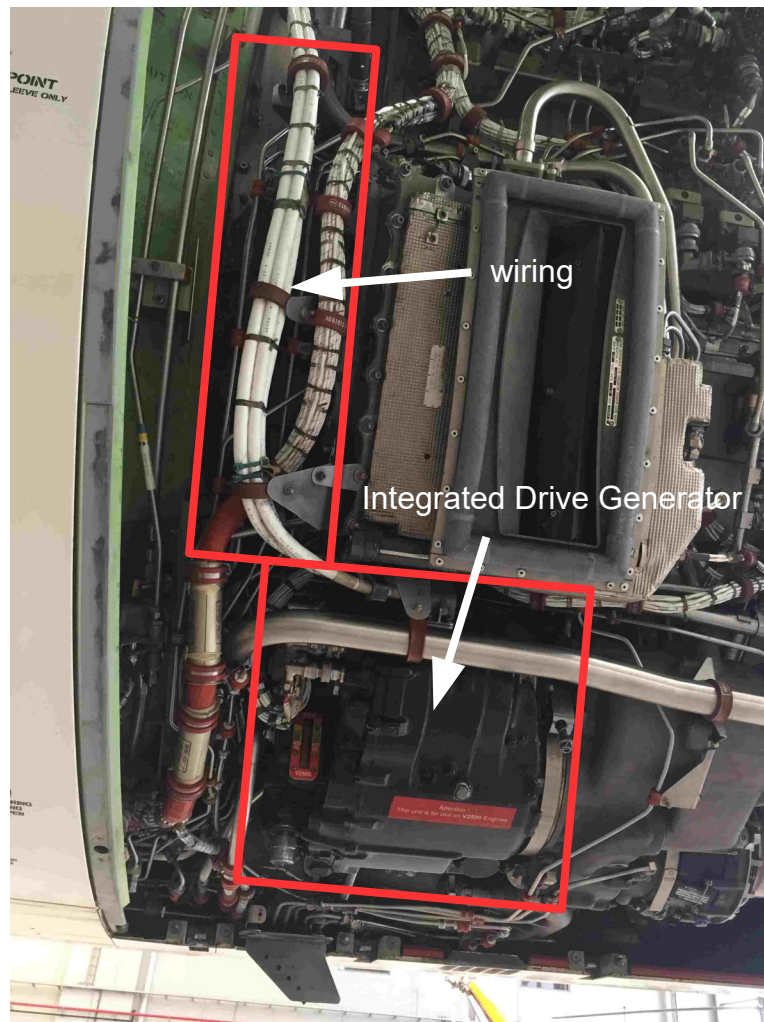
Figure 1.3: Generator in IAE V2500 turbine; DLR A320 research airplane "ATTRA"; source: J. Hammer, DLR

like A320NEO or semi-new aircraft like A350 the existing generator concepts have to be sized for higher power. Simultaneously, they have to face new demands from the growing portion of rectified load: While the power distribution network becomes more extensive for future airplanes, at the same time the type of loads changes from mainly AC resistive loads to more non-linear and switching loads and large high-voltage DC networks. In most modern electrical power transmission networks for vehicles or power grids, this conversion of AC to DC voltage is performed by transistor-based actively-switching circuits, at higher frequencies. For aircraft, DC rectification based on passive switching is still under consideration due to its significant better reliability; its power quality is critical due to slow switching and propagation of harmonics into the network that does affect the source and leads to the necessity of filters. At the same time, the regulated loads in the DC network can be unstable in combination with the input filter and source impedance due to their negative resistance at low frequencies. Therefore, it is necessary to investigate the stability of the whole electric network both at small signal level for steady state conditions and large signal level for transients, impacts and network reconfiguration.

In the last years a lot of research was spent on analyzing and designing power quality and network stability of the MEA electrical power distribution system (Sun et al., 2008) (Areerak et al., 2008) or subsystems (Chandrasekaran et al., 2002). Techniques to design the network structure, the

filters and control schemes were developed in detail. Also new types of generators like the switched reluctance generator were subject of attention in research of MEA (Lafoz et al., 2016). The impact of growing portions of local HVDC load to the externally fed synchronous generators attained little attention, also almost all new commercial airplanes rely on them.

To get an impression of the setup and environment of an electrical generator of an aircraft, Figure 1.3 shows the generator of an Airbus A320. It is a traditional design with a constant-speed drive for fixed AC frequency.

1.1.1 Aircraft design process for suppliers

The design process of the aircraft electrical power system can be divided into four major phases: concept phase, system specification phase, system development&validation phase and system verification phase. Major stakeholders in the aircraft systems design process are the aircraft manufacturer, the system supplier and the equipment suppliers. The role of the system suppliers is gaining more weight with a transition from a purchaser-supplier relationship to the collaboration as risk-sharing partners. The development process of systems is like this: (based on (Moir and Seabridge, 2008), (Kuhn et al., 2015), (Giese et al., 2010), (Becker and Giese, 2011), (Ji, 2016))

- Concept phase: During concept phase an aircraft concept is selected which fits to the strategic needs and available technology. The global energy system architecture is fixed in the end of the phase. The manufacturer defines high-level functional requirements which are translated into a concept of a power-optimized system architecture by the system supplier. The equipment suppliers actively participate in the systems definition. They transfer the needs of the architecture into needs of their component and vice versa. They give a bid for the component including the offered key-features.
- System specification phase: In this phase, a frozen energy system concept is provided by the aircraft manufacturer. Additionally, more detailed aircraft data about power consumers, engine and electrical power generation are available. The selected system suppliers conduct full concept definition where all the requirements and risks are understood. The aircraft manufacturer's requirements is transformed to the level of equipment suppliers by the system suppliers. Basic stability studies and failure analysis of aircraft electrical network are typical activities during the system specification phase. The component suppliers participate with consolidated and complete definitions of the requirements.
- System development and validation phase: In this phase preliminary and detailed design of equipment takes place. Verification plans on system level and validation plans on equipment level are generated. Components are produced and dynamic interactions of the systems are assessed. All equipment is described by preliminary functional and behavioral models to allow first network stability tests.
- System verification phase: in this phase the system integration into the physical and functional aircraft takes place. The objective in the system verification phase is to demonstrate the maturity of the systems in a realistic environment. Models are extended to be representative for the real equipment. The virtual integration platform for energy systems allows addressing integration issues prior to their physical integration on the test rigs and also extend test coverage. Power quality investigation of the integrated network will be of the interest in this phase. All equipment is tested in-house at the supplier and on integration test-rigs at the aircraft manufacturer.

Whilst the product cycles of an aircraft type can be thirty years and longer, the pre-studies of the development process start much earlier in research programs. As soon as a real aircraft program is started, the suppliers get information on the component requirements and some information on the

concepts. Based upon this information they can show concept alternatives and refine the require-ments and submit a bid of the components. Major assessment criteria are cost of equipment and fea-tures of equipment. Here and always later on in the design process, a key-factor for the success of the development of the more electric aircraft in general and the suppliers in particular is the early assessment of requirements and network interactions in the design process. It helps the equipment designers to optimize the design, find contradictory requirements, prevent re-designs and reject uni-lateral burdens from integration issues.

1.1.2 Procedures for power quality, network stability and integration

The performance of the electrical network is investigated and optimized from the very beginning of the design process. In later design phases, the design has to be verified in terms of power quality and network stability. Power quality is related to the harmonic contents which are generated by switching power electronic devices. The harmonics can have a significant influence on power distri-bution and communication lines (Arrillaga and Watson, 2003):

1) transformers are subject to additional losses and have to face the additional thermal load in the iron core; 2) all systems are being impacted by additional wear; 3) the power factor of the en-ergy system is decreased; 4) measurements suffer from additional noise; 5) relays and over-voltage detectors could be malfunction; 6) the radiated interference can distort the nearby data and commu-nication buses, including (flight) control.

While power quality is improved by filters, the electric network is susceptible to instability by interaction of the loads with an ill-conditioned impedance of input filter and power source. Con-trolled loads can change the power demand swiftly and draw even more current at voltage drops to keep the power constant. Stability issues are tightly linked with detailed filter design and might be found late in the aircraft development process. Standard tests on mathematical stability of the elec-trical network include impedance-based methods like Middlebrook criterion (Middlebrook, 1976), Modal analysis for eigenvalue-based stability (Barruel et al., 2005) (Han et al., 2008) or more ab-stract methods like passivity (Brayton and Moser, 1965) (Blankenstein, 2005) (Jeltsema et al., 2005).

In industrial processes the system is usually not observed for internal stability but the behavior of the output signals are tested for conformance with the industrial requirements. The studies on power quality, network stability, and transient and spectral performance are performed by simula-tion and hardware based tests in specific test conditions. General demands which are applicable to several (sub-)systems are generalized in industrial standards, for example MIL-STD-704F (STD-704F, 2004) or airframer specific standards, for example the AirBus Directives (ABD). For the large-scale integration tests, the simulation of the virtual integration platform is a very challenging task: A higher amount of more complex systems can possibly suffer from more integrated networks with less energy buffers. This increases the complexity of the simulations and the necessary scale of testing.

Anyhow, the current design process of the aircraft systems is still a document-based develop-ment (Becker and Giese, 2011). The behavior of the system is defined by textual requirements, pseudo code, tables, block diagrams, logic diagrams and mathematical expressions. Currently, test beds are stated textually by the airframer and often are used only in the systems verification phase to integrate the network rather than be used for matched design in the system design phase. No de-tailed network description is known to the component suppliers which could support better knowl-edge of the system interactions and thus more robust and lighter components. Voltage control and network stability is checked and adapted mainly after the design phase. For the model-based test on

standards conformance, each component supplier has to re-implement in-simulation and post-processing property observers of the requirements.

There are three lessons to learn:

In later design phases detailed models are required. But a model based concept is applicable for every design phase in the aircraft development process. Some of the requirements are known from prior aircraft programs and may be included in the design phase already. A key factor for model-based studies are re-usability of models and generic libraries of the equipment, networks and standardized test cases with requirement monitors.

Second, issues on power quality, network stability and on transient performance are addressed late in the design process. System suppliers have to perform additional extended studies on quality and stability while equipment suppliers should do. The system development and the supplier can benefit from extended knowledge in earlier design phases and may partially use the knowledge to influence the requirements. The industrially defined stability may not be sufficient. But for industrial applicability the methods should be model-based.

Third, cooperation in a model-based process partially takes place. More integrated studies could help to find integration issues earlier in the design process. A key factor of applying a model based design approach is dedicated modeling and simulation techniques.

Among various available modeling languages and tools in this regard, Modelica is gaining more attention and acceptance in the aircraft society thanks to its strong capability to conveniently model complex physical systems containing, e.g., mechanical, electrical, hydraulic, thermal, control, electric power or process-oriented sub components. In combination with the powerful commercial simulation environment Dymola (Dassault Systèmes, 2017), a convenient platform is provided to accomplish multidisciplinary system simulation and integration of complete electric networks including all sub-systems.

The technology readiness level of Modelica as simulation tool of future aircraft electrical systems has been improved and demonstrated step by step; e.g. in the European Commission funded projects VIVACE[1] and MOET[2] in cooperation with aircraft industry.

1.2 Challenges and thesis overview

This thesis contributes to the field of model-based methods for design and analysis of the electrical network systems of a modern aircraft, with focus on the generators manufacturer perspective. This work was motivated by two main drivers: The need of the generator manufacturer Thales to include advanced measures of the network interactions in the system design phase; and the need of Airbus France to demonstrate the feasibility of a Modelica based development process, with focus on the large-scale integration tests in the validation&verification phase. Both studies are tightly linked, since the generator model and hardware test data are essential brick-stones of the V&V studies. The design and analysis studies of the electrical network rely on models with different levels of abstraction. The work proposes models and infrastructures of the industrially standardized levels, and applies an additional layer with harmonic models. The model-based approach and the use of simulation and other analysis tools are applicable for the system development phase and the systems validation phase of the aircraft development process.

The thesis addresses four major issues. The first one is specific to the generator design, while the last three ones are of general interest:

[1]VIVACE (Value Improvement Through A Virtual Aeronautical Collaborative Enterprise); www.vivaceproject.com
[2]MOET (More Open Electrical Technologies); www.eurtd.com/moet/

The first issue is about the design of the Thales "MEGEVE" generator. The design function is based on analytical functions, taking into account electrical, mechanical, thermal constraints and constraints on the dimensions. The design was originally hand-tuned. The challenge was to develop an appropriate framework for the efficient multi-objective optimization of the generator, taking into account the various constraints. The second objective is about power quality. For future aircraft, the installed electrical power tends to grow. At the same time, a trend towards a larger share of AC rectified load can be observed, to feed brush-less DC drives and converters. This may have an impact on existing and future generators. The issue was to include measures for power quality in the generator design. The third issue treats the network stability and possibly define design margins. The electric network tends to instability if the controlled loads interact with an ill-conditioned source impedance of input filter and power source. Model-based methods shall be found which can evaluate the stability behavior. In this context stability can be defined by the mathematical definition with internal stability or the industry defined stability criteria on output stability. The last topic is about the implementation of model based system level studies and detailed simulation. The increased complexity of the aircraft power network demands sophisticated models and test-beds for simulation based studies. There was a need to improve the technology readiness level of the Modelica based models and Dymola based simulations to enable the studies. The four main challenges contribute to the assessment of a component in an electrical network. Figure 1.4 shows the research fields and individual contributions of this thesis.

The topics are closely related, since they contribute to the assessment of components and systems. The research field is highly fragmented into specialized disciplines. Therefore, this thesis presents the state of the art and challenges chapter wise. The individual contributions are stated at the end of each chapter.

This thesis is structured as follows:

At the beginning of the thesis, in **chapter 2** the multi-level modeling concept of the aircraft electrical network is discussed. The representation of the models in a rotor-fixed reference frame, and by base-band representations is illustrated. The first one has benefits for the analysis of the low-frequency behavior of an AC network, while the second one is representative for the harmonic content in periodic steady state. Throughout this thesis the methods are tested and demonstrated by a small electrical network model. The most important components, generator and passive 6-pulse rectifier, are discussed and implementation issues are addressed. The correctness of the generator model is verified by coherency checks of model and hardware measurements.

Chapter 3 deals with improvement of the generator design. The basic steps of machine design are briefly reviewed to understand the implementation and results of the multi-objective optimization of the machine. The design function itself was given by Thales. In a next step, the design is extended by measures for power quality. A two-stage setup, with optimization for Pareto-optimal solutions and simulation-based measures is shown.

The computation time of the simulation model for power quality stays a critical issue and is addressed in **chapter 4**. The model can be simplified by replacing the controller by a constant value. It is proven that this simplification has no impact on the accuracy of the steady-state result of the simulation. This modification improves the simulation speed at the expense of a longer ramp-up phase. Anyhow, an essential part of the simulation time results from the initially needed ramp-up phase to periodic steady-state. A method using combined modeling in the frequency domain and the time domain can reduce the ramp-up time drastically. The method is discussed theoretically and an infrastructure with models is shown.

The presence of a periodic steady state condition has to be tested by appropriate detectors. **Chapter 5** compares two methods from literature with two new, FFT based ones. The implementation, including windowing and sampling, is discussed in detail.

Chapter 6 deals with the stability issue of the electric network. The applicability of Impedance-based methods, Modal Analysis, µ-Analysis and Anti-optimization is investigated. Implementation issues for automatic evaluation in a model-based design process are discussed.

Chapter 7 deals with the framework for detailed large-scale system studies with unitary testing of equipment and network integration tests. The necessary models, tools and scripts of a model-based virtual testing process are discussed.

Chapter 8 summarizes the thesis, highlights the contributions and

Chapter 9 gives an outlook on potential future research activities.

The **Appendix** shows additional material and information:

- An introduction to simulation with Modelica/Dymola and the optimizer MOPS.
- The Modelica-based aircraft library for virtual testing.
- Property monitors for transient and spectral properties.
- Filter weight determination for integrated studies of system weight, network stability and power quality.
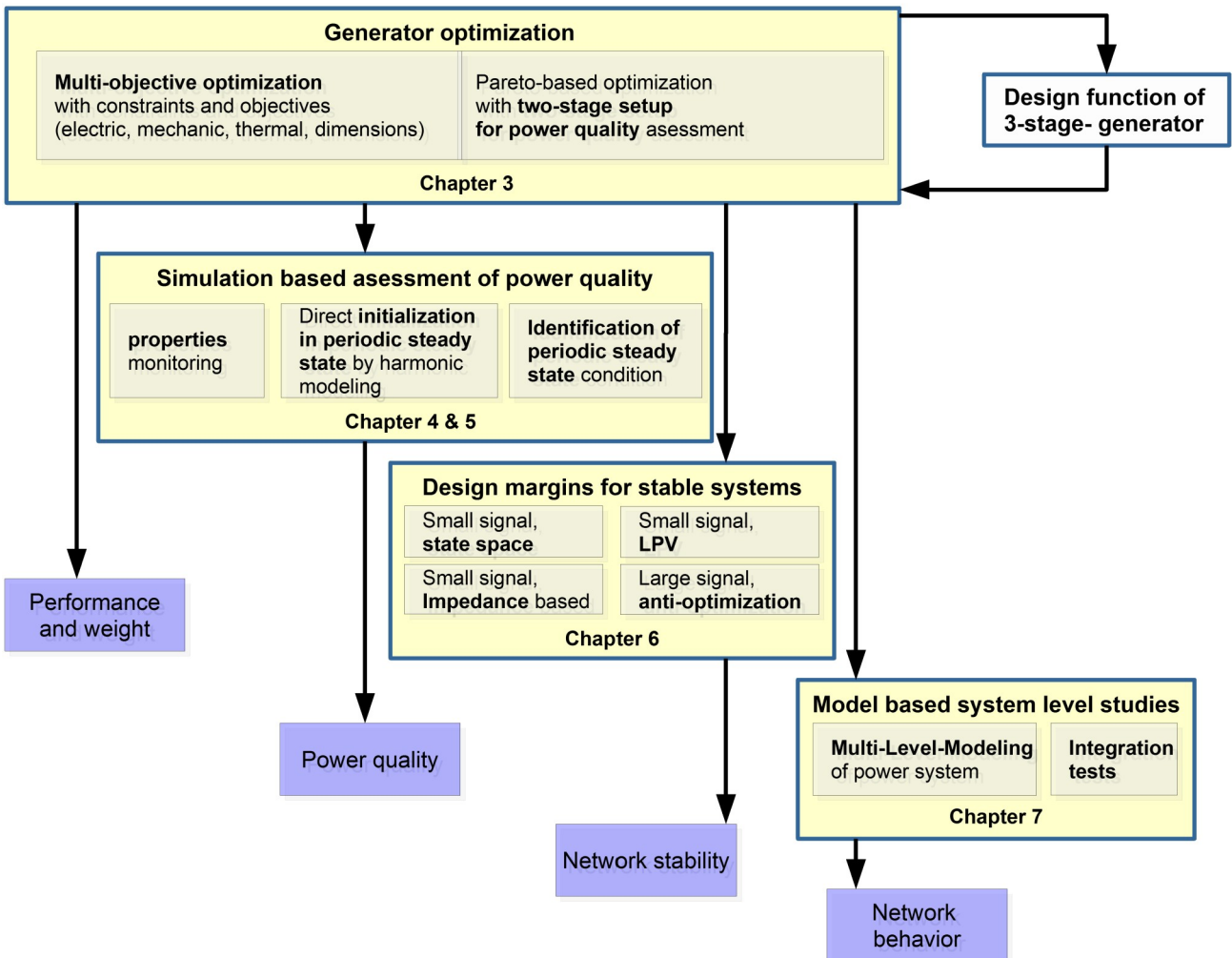
Figure 1.4: Overview of topics and challenges; yellow: main fields of challenge; grayish: contributions; white: pre-existing know-how

2 Modeling of the components of the aircraft electrical network

This thesis proposes several model based design extensions for the design of the aircraft electrical network system. The level of detail of the model has to match the requirements of the design method in terms of complexity and abstractness. The same component model may be needed for different types of studies; or the same study may rely on different abstraction levels of the same component.

This chapter is structured as follows: First, appropriate levels of abstraction are defined. The next sub-chapter derives models of electrical components in different levels of abstraction, which are relevant and used by the design methods. The generator model is of special interest due to the focus of this thesis to the perspective of the generator supplier. The validity of the model is shown by coherency tests between the models in different levels, and of the models to hardware measurements. An outlook is given on design considerations of an efficient multi-level infrastructure which could be used for integration of several abstraction levels.

2.1 Levels of abstraction and mathematical methods

For the industrial design, evaluation and certification process of the energy distribution networks, often several models exist which represent different modeling accuracies of the same system. It is not always useful to take the most detailed one, as it may not improve the overall accuracy but will slow down the simulation drastically. Electrical power system simulation includes studies from quasi stationary power flow till high frequent electromagnetic compatibility studies. Depending on the desired evaluation of an electrical network (power consumption, network stability, power quality), system simulations with models of different levels of accuracy are much better suited. The simulation time of the simplest, architectural level of a model is usually in the order of seconds while power electronic events demand resolutions in the nanosecond to microsecond level. Thus, this behavioral level of the model is 2 to 3 orders of magnitude slower. Conversely, the architectural models are applied for the simulation of flight cycles while the behavioral models are used for simulation of time-limited steady-state conditions and at critical transient conditions.

In the following the different levels are defined. They rely on the nomenclature of Airbus for the purpose of aircraft electrical system design and validation. This was presented in (Kuhn et al., 2008). This nomenclature may be used differently in the American literature but will be standardized by (AE-7M, 2016). At supplier level these levels may not necessarily fit the needs. But in many cases the supplier's component is virtually tested in-house, with models for the same purpose as in integration testing at the airfamer.

The concept of multi-level modeling and the benefits of functional modeling in the qd0 system was discussed in (Kuhn et al., 2008). It was an input to the work of the SAE AE-7M standardization committee "Aircraft Electrical power systems. Modelling and simulation. Definitions" (AE-7M, 2016) of Bozhko, Kuhn and others in SAE AE-7M standardization committee.

In an aircraft design process the following levels apply:

2.1.1.a Level 1: Architectural level

The top architectural level aims on steady-state power consumption. Usually, modeling involves algebraic equations describing the energy balance between ports and considers the global system to be in steady state. No dynamic response is covered. AC waveforms are not applicable but the power consumption shall be representative for the real system. Architectural models are typically used for

power budget calculations in the aircraft pre-design phase or systems specification phase or for management of energy and network reconfiguration. For example in (Schallert, 2010), an aircraft power distribution network is investigated with respect to reliability and components' power demand, based on architectural models.

2.1.1.b Level 2: Functional level

The functional layer extends the range to the low-frequent transient behavior but without covering the high-frequent switching effects. For AC networks the maximum of the dynamics is clearly delimited from the base grid frequency. Waveforms between the real system and functional models should only deviate by the high frequency content but not in base amplitude or phase. For example for a 360-800 Hz aircraft variable frequency network, the maximum may be set roughly to one third which is 100 to 150 Hz. The purpose of functional models includes control theoretical and simulation-based stability studies of the electrical power system, studies of transient behavior at switching or change of loads and studies of power quality of low frequent conducted emission. For example, inrush currents of transformers can be studied at this level (Ji and Kuhn, 2013).

2.1.1.c Level 3: Behavioral level

The behavioral (or behavioural[3]) layer is representative for actual wave forms including switching and HF injection behavior for studies on conducted EMC. Modeling typically is based on lumped parameter subsystem models with high fidelity up to 100 kHz. Models are abstracted from physical implementation as they do not cover all parasitic effects or do not use the most detailed methods as finite element modeling. The modeling detail is driven from the need to handle the complexity of the simulation of the total system and subsystem, within appropriate time.

The purpose is detailed validation of the hardware, network power quality studies including filter design and EMC issues.

(AE-7M, 2016) defines four abstraction layers. Some of them may be divided into sub-levels. Since this work will make use of it, a further intermediate level is introduced:

2.1.1.d Harmonic Layer or harmonic functional level

The harmonic layer is a special type of functional layer. It is representative of the DC value and amplitude and phase of the AC base frequency and in addition it also includes harmonic frequencies. Mathematically, it is based on multiple frequency selection through base-band transformation modeling techniques. This means the system is modeled in the frequency domain by amplitudes and phases of a selection of harmonics. Amplitudes may be constant or slowly varying. The purpose is basic investigation of power quality and unbalanced load and extended network stability including filter design.

2.1.1.e Level 4: Component or device physical level

The component layer is representative for models exceeding the demands of the behavioral layer. This includes the most detailed physical effects and effects only visible in the interior of the component which can be abstracted at the ports. This level may be needed as part of the components' detailed design process.

---

[3]Throughout this thesis American English is used; in European aircraft projects all terms are labeled in British English. Therefore both way of writings of "behavioural" or "behavioral" will appear.

Name of level	Purpose of simulation	Abstractness and level of modeling complexity	Complexity of simulation
Architectural	Predesign phase electric power system (EPS) sizing for weight and cost; power management, reconfiguration	Power balances without dynamics, idealized control loops.	Very simple, allows simulation of missions at aircraft level.
Functional	Fine EPS sizing and check for network stability and low-frequency power quality; includes check of energy management, fault propagation and clearance.	Dynamic state average models at steady-state, trajectories represent the moving averages; representative of stability properties; open loop models representative for closed loop design; modeling is elaborated.	Medium complexity; allows simulation of systems at mission level.
Functional (harmonic)	Special investigations: Studies on non-balanced AC, power quality.	Very abstract modeling by advanced base-band transformation, requires complex methods for modeling and model interfaces.	Medium complexity; allows simulation of systems for medium periods of time.
Behavioural	Verification of models against hardware or abstract levels; in-depth analysis; studies and design for power quality.	Models close to physical behavior with idealized switches, abstraction only where no effect on the network.	Very complex to initialize and run at component and much more on network level; very slow, only short periods.
Component	Simulation and design at supplier level, verification of lower abstraction layers.	Models close to physical behavior with arbitrary level of detail.	Simulation of local network, only short periods.

Table 1: Overview of modeling levels

In Figure 2.1 the multi-level modeling concept is visualized. Lower levels exhibit increased level of detail at the cost of higher complexity. The level concept is summarized in Table Table 1.

An illustration of the tree-level concept by means of simulation results is given in Figure 2.2. It shows simulations of a DC/DC buck converter. The architectural layer input current shows large simulation steps neglecting the detailed effects which can be seen at the behavioral layer model simulation. The functional layer model covers the waveform of the detailed model without switching effects.
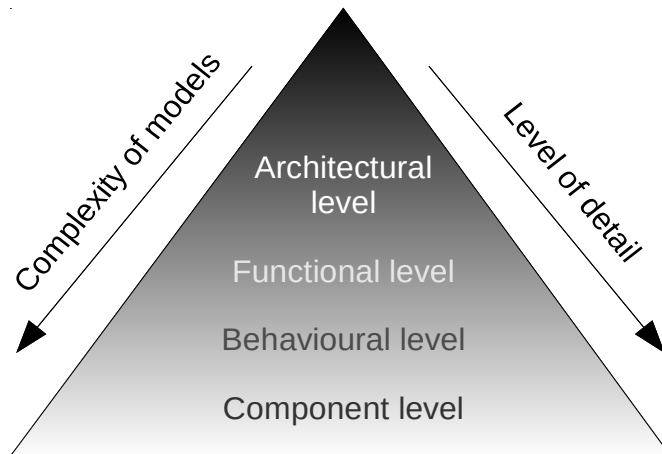
Figure 2.1: Modeling by multi level models

The original level description by Airbus focuses on the purpose of the airframer's analysis study. For the standard (AE-7M, 2016), not all levels are specified in detail. Especially for the functional level, alternative modeling paradigma may be applied.

For the purpose of the electric network design with focus on the generation channel in this thesis, no need of architectural level models was identified. On the detailed level with behavioural models, no general modeling paradigma have to be discussed since they are close to the hardware level with moderate abstraction. In contrast to this, the implementation of functional models shall be defined more clearly since they are both relevant and complex in implementation.
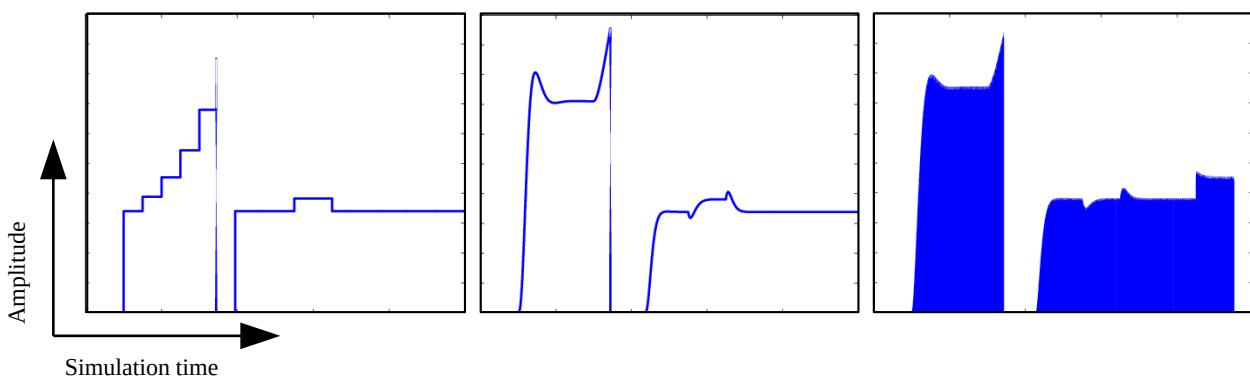
Figure 2.2: Illustration of the 3 layer concept by means of simulations of a DC/DC buck converter: architectural level | functional level | behavioural level

Functional models are of major importance for fast simulation at medium detail and analysis. Since the implementation of the functional levels is both not standardized and may use complex

mathematical modeling, implementations for functional and harmonic functional modeling are proposed in the following, highlighting their advantageous for specific studies.

2.1.2 Functional modeling by use of qd0 or "Park" transformation

While the architectural layer is defined to contain only static energy balance equations and the behavioral models to contain all effects which are relevant in the network, the definition of the functional models is not as straight forward. Functional models have to be applicable for linearization, for stability investigations with methods of control theory for linear time-invariant systems. For DC systems, those have to be deduced from the complex models by averaging the switching models on a time interval and order reduction techniques. For AC systems, the time-variant characteristics of the sinusoidal alternating currents prevents a time invariant steady state condition and hence linearization and therefore must be treated specially:

For electrical power systems, fast dynamics occur due to inductive and capacitive couplings of magnetic and electric fields. These are the electromagnetic transients. For all classical power networks with power conversion of mechanical power into electrical power by generators, there appear slower dynamics due to the interaction between mechanical energy and electric energy. These Electromagnetic transients are tight to the dynamics of the mechanical system which exhibits essentially larger time constants. Therefore, for an alternating frequency power transmission network, the spectrum of the phase variables shows a bandpass restricted signal which is centered at the network frequency.

For studies on the power transmission behavior, this inherent physical property of the electrical system gives motivation to use a reference frame linked to the slow varying system. This acts like a shift of the spectral content from the network frequency to the center of the spectral axis. The Park, dq or qd transformation is such a kind of transformation.

Starting from the 1920s, R.H Park (Park, 1929) and others developed an approach for mathematical modeling of electrical machines. By use of a general transformation, all time-varying inductances, stator and rotor variables are mapped to variables associated with fictitious windings. The transformation contains two steps: First a mapping to a reference frame with perpendicular axis is performed. This is also called "Clarke transformation". Then, the system is rotated by an angle θ. The angle may be time varying with a rotational speed of ω. In this reference system the perpendicular axes are the direct axis (d) and the quadratic axis (q). Offsets which are are common to all phase variables are mapped to the zero axis (0).

The general three-phase AC system instantaneous values χ_a, χ_b and χ_c can be written as

$$
\begin{aligned}
\chi_a &= \sqrt{2}\,\chi_{as}\cos\left(\theta_a\right) \\
\chi_b &= \sqrt{2}\,\chi_{bs}\cos\left(\theta_b\right) \\
\chi_c &= \sqrt{2}\,\chi_{cs}\cos\left(\theta_c\right)
\end{aligned}
\tag{1}
$$

Where $\chi_{\_s}$ may be time variant. In case the alternation of the sinusoidal phases is coupled, they are equally displaced in phase (120° for three phase system) and the mean parts are of equal length ($\chi_{as}=\chi_{bs}=\chi_{cs}=\chi_s$), the variables are called a balanced set (Krause et al., 2002):

$$\begin{aligned}
\chi_a &= \sqrt{2}\,\chi_s \cos(\theta_e) + \chi_o \\
\chi_b &= \sqrt{2}\,\chi_s \cos\left(\theta_e - \frac{2\pi}{3}\right) + \chi_o \\
\chi_c &= \sqrt{2}\,\chi_s \cos\left(\theta_e + \frac{2\pi}{3}\right) + \chi_o
\end{aligned} \tag{2}$$

θ_e may be linearly dependent on time with a constant or quasi constant angular velocity ω_e.

$$\omega_e = \frac{d\theta_e}{dt} \tag{3}$$

χ_s may be a slowly time varying at change rates well below net frequency. χ_0 may be an offset common to all phases. All electric variables of a system are balanced in case all sources are balanced and all loads are linear and balanced. For example an ideal three phase generator connected with three linear phases to ground impedances of equal size only exhibits symmetric phase currents.

The transfer into the qd0 system is performed by matrix multiplication of the phase variables χ_a, χ_b, χ_c by the transformation matrix:

$$\begin{bmatrix} \chi_q \\ \chi_d \\ \chi_0 \end{bmatrix} = T \cdot \begin{bmatrix} \chi_a \\ \chi_b \\ \chi_c \end{bmatrix},$$
$$T = \frac{2}{3} \begin{bmatrix} \cos(\theta_e) & \cos(\theta_e - 2\pi/3) & \cos(\theta_e + 2\pi/3) \\ \sin(\theta_e) & \sin(\theta_e - 2\pi/3) & \sin(\theta_e + 2\pi/3) \\ 1/2 & 1/2 & 1/2 \end{bmatrix} \tag{4}$$

where χ are the voltages v or the currents i. The transformation is generally valid, for example for flux linkage or electric charge. The length of the variables in the qd system is given by trigonometric identities:

$$\chi_q^2 + \chi_d^2 = \chi_s^2 \tag{5}$$

The relation of χ_q and χ_d keeps the information on the phase of the sinusoidal phase quantities. Sometimes the variables are sorted in the order dq0 and called dq transformation. Mathematics is the same but just the rows are permuted.

The inverse transformation back into phase variables can be performed with the following matrix multiplication:

$$\begin{bmatrix} \chi_a \\ \chi_b \\ \chi_c \end{bmatrix} = T^{-1} \begin{bmatrix} \chi_q \\ \chi_d \\ \chi_0 \end{bmatrix},$$
$$T^{-1} = \begin{bmatrix} \cos(\theta_e) & \sin(\theta_e) & 1 \\ \cos(\theta_e - 2\pi/3) & \sin(\theta_e - 2\pi/3) & 1 \\ \cos(\theta_e + 2\pi/3) & \sin(\theta_e + 2\pi/3) & 1 \end{bmatrix} \tag{6}$$

Unfortunately, two types of dq transformations are commonly used: the value invariant transformation and the power invariant transformation. They differ in a pre-factor of $\sqrt{3/2}$ in the matrices in Equations (4) and (6). In this thesis, value invariant transformation is used exclusively.

Details on the transformation and use in other reference frames, the history and mathematical properties can be found for example in (Krause et al., 2002).

The transformation equations are of full rank and invertible. They are applicable regardless of the input waveform. Nevertheless, the transformation is most useful in case the input values form a balanced 3-phase set with equal-amplitude sinusoidal quantities displaced by $2\pi/3$.

In case the rotation speed of the transformation matrix matches the rotation speed of the phase variables with a reference frame phase displacement of θ_0, the transformed values in qd system reflect the base band signal χ_s, where:

$$
\begin{aligned}
\chi_q &= \sqrt{2} \cdot \chi_s \cdot \cos\left(\theta_{ef} - \theta_0\right) \\
\chi_d &= -\sqrt{2} \cdot \chi_s \cdot \sin\left(\theta_{ef} - \theta_0\right) \\
\chi_0 &= \chi_o
\end{aligned}
\tag{7}
$$

and:

$$
\sqrt{v_q^2 + v_d^2} = \hat{v}_{a/b/c} = \sqrt{2} \cdot v_{RMS\,a/b/c}
\tag{8}
$$

The total instantaneous power can be calculated as

$$
pow_{qd0} = pow_{abc} = \frac{3}{2}\left(v_q\,i_q + v_d\,i_d + 2\,v_0\,i_0\right)
\tag{9}
$$

For synchronous machines, the rotor time-varying inductances are eliminated in case the transformed variables are referred to the synchronously rotating reference frame by setting the reference frame angle θ_e to the rotor angle θ_r. In this case the transformed system and all variables of three-phase symmetric linear circuits powered by the synchronous generator exhibit steady-state time invariant equations in case of constant operation. Also, in case the AC load is symmetric and no common voltage is injected into the star point of the generator for other reasons, voltages and currents of the zero system remain at zero.

Example: for a symmetrical 3-phase inductive circuit with no mutual line to line inductance, the equation system is

$$
\boldsymbol{v}_{abc} = \boldsymbol{L} \cdot p \cdot \boldsymbol{i}_{abc}
\tag{10}
$$

with the differentiation operator p, three-phase voltages $\boldsymbol{v}_{abc}$ and currents $\boldsymbol{i}_{abc}$ and the inductance matrix $\boldsymbol{L} = diag\left(L_s\right)$. Application of the transformation results in

$$
\boldsymbol{T} \cdot \boldsymbol{v}_{abc} = \boldsymbol{v}_{qd0} = \boldsymbol{T} \cdot \boldsymbol{L} \cdot p \cdot \boldsymbol{i}_{abc} = \boldsymbol{T} \cdot \boldsymbol{L} \cdot p \cdot \boldsymbol{T}^{-1} \cdot \boldsymbol{i}_{qd0}
\tag{11}
$$

And after some symbolic manipulation:

$$
\begin{aligned}
v_q &= \omega \cdot L_s \cdot i_d + p \cdot L_s \cdot i_q \\
v_d &= -\omega \cdot L_s \cdot i_q + p \cdot L_s \cdot i_d \\
v_0 &= p \cdot L_s \cdot i_0
\end{aligned}
\tag{12}
$$

The zero system of the Park transformed system is skipped in the thesis if not indicated otherwise. For aircraft electrical systems in normal operation there is no substantial common current. While the generator's star point is grounded in today's aircraft electrical networks, the system fed by the power supply is designed to have little line to ground coupling via resistive, capacitive or inductive impedances. Sources of coupling could be capacitive coupling of the star point of a motor or

phase to ground filter capacitances. Relevant common currents can only occur when powering the system on, due to loading of the line to ground capacitances. In contrast to this, heavy common phase currents occur in abnormal operation in case of line to ground short circuits. This allows the short circuit identification by current sensing in the generator's star point connection. But in nominal operation and simulation of the nominal system, the zero system has no influence. In case of asymmetric loading the variables in qd system show a high frequency content at double system frequency.

Due to the benefits of steady-state equations in a rotation fixed reference, Park transformation is the standard way of modeling generators and motors insofar no emphasis is placed on asymmetry in the machine. Also it is used for the control of motors where the transformation is evaluated numerically using a rotational position sensor or the estimated position.

For functional models which must be non-switching and linearizable, limitations for time triggered switching and level-triggered switching devices can be circumvented by using averaged models. Especially for self commutating rectifiers there is a need for calculating the mean output voltage/current, averaged on a commutation interval. Therefore, for functional models of AC components, representation in Park transformation is used in this thesis. The equations for the most important components are given in the modeling chapter. Theory on other electric components, the transformation and averaged models can be found for instance in (Krause et al., 2002).

In simulation of AC electrical power transmission systems, the transformation to a net-frequency fixed system exhibits substantial benefits of simulation speed. The dynamics of the system can be separated into a net-frequency related part and the deviation from it. For example, for the current: "$i(t)=i(\omega_{net})+\Delta i(t)$". In simulation, the model uses $\Delta i(t)$ as state rather than $i(t)$. In stationary operation with constant load and no dynamic variation of the speed, $\Delta i(t)=0$ and $i(t)=i(\omega)$. This time invariant system also results in much faster simulation. The Nyquist criterion limits the maximum permissible step size for an integration algorithm in relation to the maximum occurring frequency. In case $\Delta i(t)$ changes slower than the original $i(t)$, simulation speed may be improved.

When recalling the definition of the functional modeling, this would allow for a more simple type of modeling. In qd0 transformation, the balanced set of AC quantities is represented by variables in direct or quadratic axis plus zero axis in case of a common share. This allows the reconstruction of the amplitude and the phase in relation to the base rotation angle. In the method of **equivalent DC voltages**, only the amplitude χ_s of a balanced set of AC variables are considered. This means the functional model of the AC system is represented by an equivalent one phase DC electrical circuit. The phase information is not preserved by this method where phase displacement comes from inductors and capacitors. The reactive losses can only be represented by inserting equivalent resistors under assumption of a given net frequency. This does not allow exact but only approximate treatment of the losses. The dynamics from the interaction of the phases is neglected. For example, for the inductor in Equation (12), assuming excitation only in q axis, the cross coupling from the $\omega L_s i_q$ term induces a voltage in d axis which could be compensated by capacitive elements or could drive reactive losses in the transmission lines.

The method of equivalent DC voltages is popular in industry due to its simplicity. But as it lacks the important information on phase displacement it may not be sufficient for investigations on network stability phenomena and also phase information can not be gained for direct comparison with behavioural models. Therefore this approach was only pursued for functional modeling in the industrial large-scale V&V study in chapter 7.1.

2.1.3 Harmonic functional modeling

Park transformation is an exact transformation independent of the waveform, which has benefits for balanced sets at quasi constant net frequency and low frequency perturbations of the signals. This is the case for the synchronous generator fed network, where the AC system is driven by the mechanical rotation frequency of the generator, where an ideal designed generator induces only balanced voltages.

In case of asymmetries, the Park transformation does not result in steady-state conditions but an alternative implementation including harmonics may suit better. The alternative representation includes harmonics but no switching. Therefore the level is called harmonic functional level:

In case a load, which is connected to a balanced voltage source, exhibits a non balanced impedance

$$Z_{abc} = \begin{bmatrix} Z_a \\ Z_b \\ Z_c \end{bmatrix} \tag{13}$$

with $Z_a \neq Z_b \neq Z_c$, the currents may be not balanced. They form an unbalanced set which may be expressed as

$$\chi_{abc}(t) = \begin{bmatrix} X_a \cos(\omega t + \theta_a) \\ X_b \cos(\omega t - \dfrac{2\pi}{3} + \theta_b) \\ X_c \cos(\omega t + \dfrac{2\pi}{3} + \theta_c) \end{bmatrix} \tag{14}$$

χ_x may be currents but the theory holds for all types including varying impedances. Non balanced means the amplitudes X_x are not identical but time invariant and the phases of the m variables are not displaced equally by $360°/m$.

By the method of symmetrical components (e.g. (Kundur, 1994)) this unsymmetrical three-phase system can be expressed by three balanced systems:

$$\chi_{abc}(t) = \chi_{abc,p}(t) + \chi_{abc,n}(t) + \chi_{abc,z}(t) \tag{15}$$

Where the first one is the positive sequence component

$$\chi_{abc,p}(t) = X_p \begin{bmatrix} \cos(\omega t + \theta_p) \\ \cos(\omega t - \dfrac{2\pi}{3} + \theta_p) \\ \cos(\omega t + \dfrac{2\pi}{3} + \theta_p) \end{bmatrix} \tag{16}$$

and the second is called negative-sequence component

$$\chi_{abc,n}(t) = X_n \begin{bmatrix} \cos(\omega t + \theta_n) \\ \cos(\omega t + \dfrac{2\pi}{3} + \theta_n) \\ \cos(\omega t - \dfrac{2\pi}{3} + \theta_n) \end{bmatrix} \tag{17}$$

The phase offset of the negative sequence components b and c are exchanged when compared to the positive sequence components.

Last, the zero sequence component can be written as:

$$\chi_{abc,z}(t) = X_z \begin{bmatrix} \cos(\omega t + \theta_z) \\ \cos(\omega t + \theta_z) \\ \cos(\omega t + \theta_z) \end{bmatrix} \tag{18}$$

Note, the definition of a "zero sequence system" differs from the zero sequence system in Park transformation. In French literature, the transformation into symmetrical components is generally referred to as Fortescue's transformation (Fortescue, 1918).

The combination with qd0 transformation gives some very valuable information about non-balanced systems. Writing the unbalanced set (15) in qd0 coordinates (4) gives

$$\chi_{qd0}(t) = \chi_{qd0,p}(t) + \chi_{qd0,n}(t) + \chi_{qd0,z}(t) \tag{19}$$

with a positive sequence system

$$\chi_{qd0,p}(t) = X_p \begin{bmatrix} \sin(\theta_p) \\ \cos(\theta_p) \\ 0 \end{bmatrix} \tag{20}$$

which is the only content in case of balanced currents. The negative-sequence component is given as

$$\chi_{qd0,n}(t) = X_n \begin{bmatrix} -\sin(2\omega t + \theta_n) \\ \cos(2\omega t + \theta_n) \\ 0 \end{bmatrix} \tag{21}$$

at double system frequency.

The zero sequence is

$$\chi_{qd0,z}(t) = X_z \begin{bmatrix} 0 \\ 0 \\ \cos(\omega t + \theta_z) \end{bmatrix} \tag{22}$$

The currents are induced by unbalanced voltages or unbalanced loads. The transformation of balanced loads, e.g. three equal sized resistors, with qd0 transformation matrix $T(t)$ (4) results in time invariant loads in qd0 system Z_{qd0}. For non equal loads, the transform $Z \cdot T(t)$ leads to time variant loads $Z_{qd0}(t)$.

One can see from (19) to (22), for a qd0 system synchronized with net frequency, an unbalanced set induces content with double system frequency in the negative sequence. Therefore unbalanced loads exhibit a spectrum in qd0 system consisting of time invariant content (positive sequence), double system frequency (negative sequence) and system frequency (zero system).

Other higher harmonics at k multiples of the net frequency may appear through non-linearities in the system. For example passively switching diode rectifiers also act as unbalanced loads but around switching frequency at six times ω_e.

Alternatively, in the following a formulation based on dynamic complex phasor transform analogue to (Chen et al., 1999) is deduced to express the harmonic quantities. Very close relations to the Park transformation will be apparent. Nevertheless this type of representation will be shown to exhibit certain benefits.

Any periodic signal can be expanded into a Fourier series of the form

$$\chi(\tau) = \sum_{\omega=-\infty}^{\infty} \mathbf{X}(j\omega) \cdot e^{j\omega\tau}, \ \tau \in [0..T] \tag{23}$$

with $\chi(\tau)$ being periodic in the time interval τ from zero to period length T. X are called the (complex) phasors. In case the spectrum consists of band restricted portions that are centred at the harmonics $k\omega_e$ and are restricted to a spectral width of ω_e, which means they do not overlap, the spectrum can be written as the sum of adjacent spectral packages:

$$\mathbf{X}(j\omega) = \sum_{k=-\infty}^{\infty} \mathbf{X}_k \cdot e^{jk\omega_e\tau} \tag{24}$$

ω_e is the base angular velocity while k times ω_e are harmonics of ω_e.

A typical spectrum with a baseband signal around ω_e and harmonic contents around multiples of ω_e can be seen in Figure 2.3
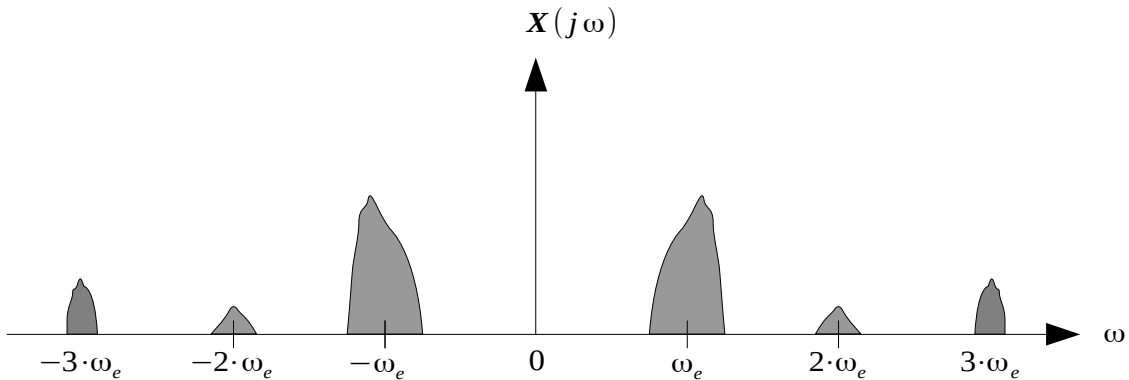
Figure 2.3: Spectrum with higher harmonics

While the Fourier transform of periodic only signals clearly differs from the matrix style transformation rule to qd0 system, the phasors in Equation (24) can be used similarly as the variables in qd0 system to represent signals in a periodic steady-state by static variables. For linear electrical circuits, modeling in Fourier domain is a standard method (Chua et al., 1987).

The theory can be extended to allow time variant phasors, in case the variation rate stays well below the fundamental frequency. The slowly time varying complex variables $X_k(t)$ are called dynamic phasors. The mathematics can be found for example in (Demiray, 2008).

With a choice of K dynamic phasors, Equations (23) and (24) can be generalized for non-strictly periodic signals to

$$\chi(\tau) \approx \sum_{k \in K} X_k(\tau) \cdot e^{j k \omega_e \tau} \tag{25}$$

where τ denotes the nearly cyclic time dependency within $\tau \in [t-T, t]$. The coefficients are determined by

$$X_k(t) = \frac{1}{T} \int_{t-T}^{t} x(\zeta) e^{-j k \omega_e \zeta} \, d\zeta \tag{26}$$

This equation can also be used for transformation of the input signals to the system, for example by direct use of Fourier series.

In case all $X_k(t)$ do not show time variation at some time instant and there exists at least one $X_k(t) \neq 0$ at one $k > 0$, the system is said to be in a periodic steady-state condition.

Equation (26) can be expressed alternatively by the inner product

$$X_k(t) = \langle x(t), e^{j k \omega_e t} \rangle = \langle x(t) \rangle_k \tag{27}$$

$\langle x(t) \rangle_k$ highlights the source of the phasor in time domain.

The differentiation of the signal in time domain corresponds to a superposition of the derivatives of the signals of the basebands, with a part for the strictly periodic content and a part for the deviation from it:

$$\left\langle \frac{d x(t)}{d t} \right\rangle_k = j k \omega_e X_k(t) + \frac{d X_k(t)}{d t} \tag{28}$$

The product of time domain signals equals to convolution in frequency domain. In analogy to this, the dynamical phasors combine convolutions and products:

$$\langle x(t) y(t) \rangle_k = \sum_{l=-\infty}^{\infty} \left(X_{k-l}(t) Y_k(t) \right) \tag{29}$$

For real valued signals, there is the identity

$$X_{-k}(t) = X_k(t)^* \tag{30}$$

with the complex conjugate.

Modeling by phasors and Park transformation can be combined. The qd0 transformation, which was introduced in Equation (4), transforms the time varying phase quantities χ_{abc} into a reference system χ_{qd0} which rotates synchronously with the generator's rotor.

$$\begin{bmatrix} \chi_q(t) \\ \chi_d(t) \\ \chi_0(t) \end{bmatrix} = \boldsymbol{T} \cdot \begin{bmatrix} \chi_a(t) \\ \chi_b(t) \\ \chi_c(t) \end{bmatrix} \tag{31}$$

As noted earlier, this reference frame is most natural for modeling of the synchronous machine equations and exhibits benefits in case of balanced condition since the variation of the qd0 transformed signals vary much slower than the instantaneous values of the values in abc system. The qd0

transformation itself is an analytic approach. In order to come to a steady-state condition, even for higher harmonic contents, the variables in qd0 system can be expanded further by approximation of the qd0 signals by a Fourier series:

$$\chi_{qd\,0}(\tau) = \sum_{h=-\infty}^{\infty} X_{qd0\,(h)}(t) \cdot e^{jh\omega_{base}t} \tag{32}$$

Since all harmonics of the passively commutated rectifier are induced by the base angular velocity, ω_{base} is taken for ω. Only a choice of n harmonics may be used to approximate the signal. For example, for unbalanced loads, there is essential harmonic content at double system frequency at a counter-rotating frequency and with system frequency in zero system. For diode based six pulse rectifiers, apart from the base content, harmonics at fifth and seventh and higher harmonics occur.
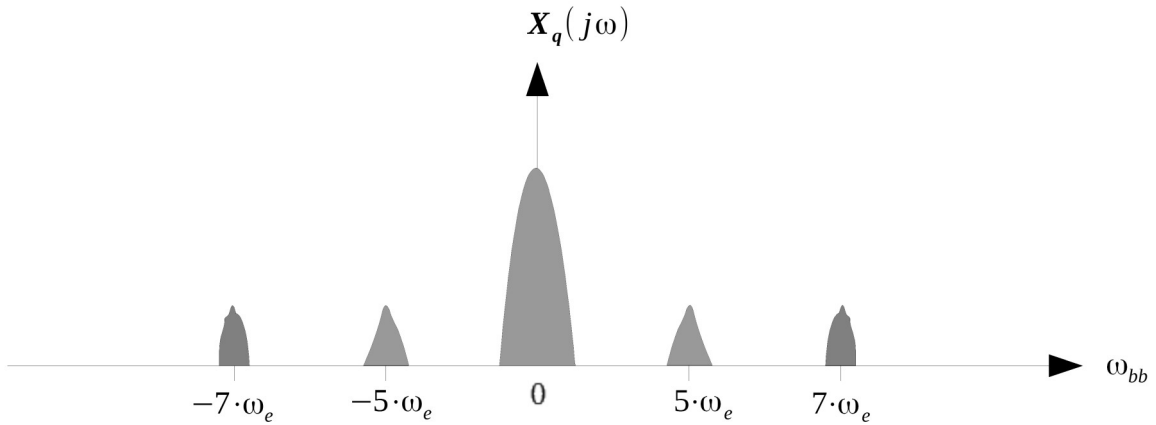
Figure 2.4: Spectrum in base band representation

With the dynamic phasor representation in qd0 system, Equation (32) becomes

$$\chi_{qd\,0}(\tau) = \sum_{h \in H} X_{qd0\,(h)}(t) \cdot e^{jh\omega_{base}t} \tag{33}$$

The spectrum of such a base-band representation is depicted in Figure 2.4.

Going one step further, the negative harmonics can be neglected by using the right half side of the Fourier spectrum since $x_{qd\,0}(t)$ represents real variables:

$$x_{qd\,0}(t) = \left(\sum_{h=0}^{\infty} X_{qd\,0(h)} \cdot e^{jh\omega_{base}t} \right) + \left(\sum_{h=1}^{\infty} X_{qd\,0(h)}^{*} \cdot e^{-jh\omega_{base}t} \right) \tag{34}$$

The *abc* to *qd 0* transformation **T** can be brought to the complex domain by Euler's identities.

$$\cos\theta = \frac{e^{j\theta} + e^{-j\theta}}{2}, \sin\theta = \frac{-j \cdot e^{j\theta} + j \cdot e^{-j\theta}}{2}. \tag{35}$$

Substitution of (35) in (4) and $\theta = \theta_0 + j \cdot \omega \cdot t$ gives the complex transformation **P**

$$P = P_1 \cdot e^{j\omega t} + P_2 \cdot e^{-j\omega t} + P_0 \tag{36}$$

where

31

$$P_1 = \frac{1}{3} \cdot e^{j\theta_0} \cdot \begin{bmatrix} 1 & e^{j4\pi/3} & e^{j2\pi/3} \\ -j & -j \cdot e^{j4\pi/3} & -j \cdot e^{j2\pi/3} \\ 0 & 0 & 0 \end{bmatrix}$$

$$P_2 = \frac{1}{3} \cdot e^{-j\theta_0} \cdot \begin{bmatrix} 1 & e^{j2\pi/3} & e^{j4\pi/3} \\ j & j \cdot e^{j2\pi/3} & j \cdot e^{j4\pi/3} \\ 0 & 0 & 0 \end{bmatrix} \tag{37}$$

$$P_0 = \frac{1}{3} \begin{bmatrix} 0 & 0 & 0 \\ 0 & 0 & 0 \\ 1 & 1 & 1 \end{bmatrix}$$

Similar to Equation (34), the *abc* variables can be decomposed into a Fourier series (which may be half sided):

$$\chi_{abc}(t) = \sum_{h=-\infty}^{\infty} X_{abc(h)}(t) \cdot e^{jh\omega t} \tag{38}$$

Combining equations (4),(36), and (38) results in

$$\chi_{qd0}(\tau) = T \cdot \chi_{abc}(\tau) = \sum_{h \in H} X_{qd0(h)}(t) \cdot e^{jh\omega_{base}t},$$
$$where \, X_{qd0}(t) = P * X_{abc} \tag{39}$$

For a signal with balanced and unbalanced variables with oscillation at $m \cdot \omega_{base}$, the phase rotation of the ABC spectrum in Equation (39) is positive for angular velocities $(m+1) \cdot \omega_{base}$ and counter-rotating for $(m-1) \cdot \omega_{base}$. With (34) and assuming only half-sided spectrum and a choice of harmonics $m \in \{0 .. m_{max}\}$ gives:

$$X_{qd0(m)} = P_1 \cdot X_{abc(m-1)} + P_2 \cdot X_{abc(m+1)} + P_0 \cdot X_{abc(m)} \tag{40}$$

The evaluation of Equation (40) may be restricted to frequencies with harmonic content. For an unbalanced three-phase load this would be m=0 with content in $-\omega_{base}$ and ω_{base}; for a rectifier with harmonics in 5th and 7th harmonic it would be m=6.

The inverse Park transformation in complex variables PT is given by

$$PT = PT_1 \cdot e^{j\omega t} + PT_2 \cdot e^{-j\omega t} + PT_0 \tag{41}$$

With

$$PT_1 = \frac{1}{2} \cdot e^{j\theta_0} \cdot \begin{bmatrix} 1 & -j & 0 \\ e^{-j2\pi/3} & -j \cdot e^{-j2\pi/3} & 0 \\ e^{j2\pi/3} & -j \cdot e^{j2\pi/3} & 0 \end{bmatrix}$$

$$PT_2 = \frac{1}{2} \cdot e^{-j\theta_0} \cdot \begin{bmatrix} 1 & j & 0 \\ e^{j2\pi/3} & j \cdot e^{j2\pi/3} & 0 \\ e^{-j2\pi/3} & -j \cdot e^{-j2\pi/3} & 0 \end{bmatrix} \tag{42}$$

$$PT_0 = \begin{bmatrix} 0 & 0 & 1 \\ 0 & 0 & 1 \\ 0 & 0 & 1 \end{bmatrix}$$

The transformation to phase variables

$$X_{abc(m)} = PT_1 \cdot X_{qd0(m-1)} + PT_2 \cdot X_{qd0(m+1)} + PT_0 \cdot X_{qd0(m)} \tag{43}$$

In this thesis, models of the different layers will be demonstrated and used: The behavioral models are used in studies of power quality, analysis of network stability and integrated network simulation and analysis. The functional models are used for calculation of steady-state values and for analysis of network stability. More simple functional models are taken for the simulation of the integrated network. The harmonic functional models are used for automated initialization of behavioral models for power quality checks. For the initialization, the harmonic functional models are used only with constant (=non time variant) coefficients.

2.2 Implementation of simulation infrastructure by Modelica/Dymola

Modeling and simulation of electrical, mechanical, electro-mechanical and other physical systems is usually performed by mathematical representation of the system by Differential Algebraic Equation systems (DAE):

$$0 = f_{implicit}(x, \dot{x}, y, u, t) \tag{44}$$

$$0 = g(x, y, u, t) \tag{45}$$

Their time domain solution defines the trajectories of the state-space variables x as a function of the recent state of the system, at time t, with the algebraic variables y and input variables u. Instantaneous memory-less relations of algebraic variables in relation to x are implicitly defined by Equation (45). Algebraic relations often result from interconnection of the modeled subsystems.

Differential Algebraic Equation systems may be transformed into ordinary differential equations (ODE)

$$\dot{x} = f(x, t, h(x, y, u, t), u) \tag{46}$$

in case the algebraic equations in (45) can be explicitly solved for $y = h(x, y, u, t)$.

The time-domain trajectories can be calculated numerically by integration algorithms in combination with algorithms for solving algebraic equations. There exist integration algorithms like Dassl (Breman et al., 1989) which can calculate the trajectories from the differential-algebraic equation system directly. In any case, the integration algorithms are known to allow more efficient and reliable computation in case the equation system is brought to explicit state space description first.

For numerical integration, the initial boundary value problem has to be solved first. By assumptions, constraints and additional equations, some initial equation system has to be built and solved for initial values x_0 and u_0 at $t = t_0$.

$$d\,x_0/dt = f\left(x_{0,}\,y_{0,}\,u_0\right)$$
$$\mathbf{0} = g\left(x_{0,}\,y_0\right) \tag{47}$$

In case these initial values represent a steady-state equilibrium condition of the system, then equation (46) can be linearized to get the linear state-space descriptions. This is the base for small signal stability analysis:

$$\Delta\,\dot{x} = A \cdot \Delta\,x + B \cdot u \tag{48}$$

Matrices A and B can be obtained via the Jacobians

$$A = \frac{\partial\,f}{\partial\,x}\bigg|_{x_0,\,u_0,\,t_0}\,, B = \frac{\partial\,f}{\partial\,u}\bigg|_{x_0,\,u_0,\,t_0} \tag{49}$$

Solution of (45) for y and calculation of steady-state conditions require algebraic manipulations. An analytic solution is often possible for simple systems. In case the algebraic equations can not be solved symbolically, algebraic loops may appear which require iterative numerical calculations which usually slows down the computation drastically.

The demands on efficient modelling of the components of the electrical network were seen as best met by the object-oriented modelling language Modelica (ModelicaAssociation, 2017) with the Modelica based simulation environment Dymola (Dassault Systèmes, 2017). Several strategies for initialization of (47) can be applied. Additional equations may be defined, which are processed symbolically into the equation system of the initial values. Also guess values for the state variables may be set. The remaining initial conditions are set automatically by default values using zero for the states or state derivatives. Modelica/Dymola is used throughout the thesis for physical modelling of the electrical networks. The "Modelica/Dymola" section in the appendix gives an example of Modelica code and the graphical layout.

2.3 Components of small onboard electrical network model

For an airplane multi-phase power transmission system, the following components are of primary importance:

- Power source: The generators supply sinusoidal voltage at net frequency. Calculation of voltage and current is usually performed in a rotor-fixed system (synchronous machine).
- Symmetrical loads: for symmetrical resistive, inductive and capacitive loads, as well as synchronous motors, the current/voltage relations are fixed to net frequency.
- Other loads: Switches, diodes, unsymmetrical loads and time variant loads do not have simple steady-state dependencies upon net frequency.

In chapter 2.1 the levels of abstraction were defined. The following paragraph gives the equations of the most relevant models for the investigations of this thesis, which are generator and rectifier. The harmonic functional models and the advanced rectifier model are treated in chapter 4.3.1. An overview of the models of a large aircraft-network, which was developed in a research activity on simulation based validation and verification of the electrical network, can be found in the chapters 7.1 and A2.

2.3.1 Modeling of generator

2.3.1.a Behavioural model

The equations of the synchronous machine can be found in literature like (Krause et al., 2002). The following chapter will rely on the specific adaptions of saturation and harmonics in (Kutt, 2012) for the Thales generator.

The generator treated in this thesis is a y-connected 3-phase synchronous machine, which is modeled in *qd 0* reference-frame. The stator windings are identical sinusoidal distributed with a two-layer arrangement. The machine is excited by the field windings only in d-axis. One damper circuit for each q and d axis is foreseen. The model can include saturation effects and a triple space harmonic, which is parameterized from the no-load back-emf waveform. For all tests the shaft was driven in constant speed operation. Therefore, no equations for inertia or friction are taken into consideration. The machine's behavior can be represented by the following set of equations in *qd 0* system:

The fundamental angular velocity of the electrical network is coupled to the mechanical angular velocity via the number of pole pairs p

$$\omega_e = p \cdot \omega_{mec} \tag{50}$$

The magnetic fluxes ϕ in the machine are

$$\begin{bmatrix} \phi_{qs} \\ \phi_{ds} \\ \phi_{0s} \\ \phi_{kq} \\ \phi_{kd} \\ \phi_{fd} \\ \phi_{rem} \end{bmatrix} = \boldsymbol{L} \cdot \begin{bmatrix} i_{qs} \\ i_{ds} \\ i_{0s} \\ i_{kq} \\ i_{kd} \\ i_{fd} \\ i_{fd\,rem} \end{bmatrix} \tag{51}$$

With the matrix L:

$$\boldsymbol{L} =$$

$$\begin{bmatrix} -L_{ls}-k_{sat}L_{mq} & 0 & 0 & k_{sat}L_{mq} & 0 & 0 & 0 \\ 0 & -L_{ls}-k_{sat}L_{md} & 0 & 0 & k_{sat}L_{md} & k_{sat}L_{md} & L_{md} \\ 0 & 0 & -L_{ls} & k_{sat}\dfrac{L_{0s1}}{2} & k_{sat}\dfrac{L_{0s2}}{2} & k_{sat}\dfrac{L_{0s2}}{2} & \dfrac{L_{0s2}}{2} \\ -k_{sat}L_{mq} & 0 & -k_{sat}L_{0s1} & k_{sat}L_{mq}+L_{lkq} & 0 & 0 & 0 \\ 0 & -k_{sat}L_{md} & -k_{sat}L_{0s2} & 0 & k_{sat}L_{md} & L_{lkd}+k_{sat}L_{md} & L_{md} \\ 0 & -k_{sat}L_{md} & -k_{sat}L_{0s2} & 0 & L_{lfd}+k_{sat}L_{md} & k_{sat}L_{md} & L_{md} \\ 0 & 0 & 0 & 0 & 0 & 0 & L_{md} \end{bmatrix} \tag{52}$$

The subscripts *qs* and *ds* denote q axis respectively d axis quantities in the stator. $0s$ stands for zero axis and *fd* field winding in d axis. *kq* and *kd* are related to the damper windings. $L_{m\_}$ denotes magnetizing inductances while $L_{l\_}$ denotes leakage inductances. The static remanence units are written with the subscripts "*rem*".

35

The third harmonic is a result of the hardware-implementation of the machine. It is modeled by a phase dependent linkage with amplitude k_{3h} and phase displacement ϕ_{3h}. Amplitudes and phases can be calculated from hardware measurements.

$$L_{0s1} = 2 L_{mq} k_{3h} \cos\left(3 \omega_e t + \varphi_{3h}\right)$$
$$L_{0s2} = 2 L_{md} k_{3h} \sin\left(3 \omega_e t + \varphi_{3h}\right)$$

(53)

The ferromagnetic rotor core can show a remanence effect. This is equivalent to an offset in the current of the field winding. This effect accounts for minor excitation currents of the controller than anticipated without the effect. It can be calculated from hardware measurements. At no load and no excitation at angular velocity ω_{etest}, the voltage at the output terminals is the remanence voltage v_{rem} which can be related to the remanence current:

$$i_{fd\,rem} = \sqrt{2} \, v_{rem} / \left(\omega_{e\,sat} L_{md}\right)$$

(54)

For optimal exploitation of the machine, the core is driven into saturation of the ferromagnetic material. The saturation is modeled by a saturation coefficient k_{sat} of the magnetizing inductances L_m in dependency of all flux-generating magnetizing currents i_{md} and i_{mq}:

$$i_{md} = \frac{\left(-i_{ds} + i_{fd} + i_{kd}\right)}{k_{fd}}$$
$$i_{mq} = \frac{\left(-i_{qs} + i_{kq}\right)}{k_{fd}}$$
$$i_m = \sqrt{i_{md}^2 + i_{mq}^2}$$

$$k_{sat} = \frac{\sqrt{2}\left(v_{sat} - v_{rem}\right)}{i_m \omega_{e\,test} L_{m0}}$$

(55)

with the measured non-saturated magnetizing inductance L_{m0}

$$L_{m0} = \frac{\sqrt{2}\left(v_{nom} - v_{rem}\right)}{\omega_{e\,test}}$$

(56)

the measured saturation function

$$v_{sat} = f\left(i_m\right)$$

(57)

and the field winding to stator ratio k_{fd}, with the number of field windings *nfd* and number of stator windings *ns*:

$$k_{fd} = 2/3 \; Nfd/ns$$

(58)

The electrical torque is

$$
\begin{aligned}
T_e = \quad & \frac{3}{2}\, p\, k_{sat}\big(\big(-i_{ds}+i_{fd}+i_{kd}\big)i_{qs}L_{md}+i_{ds}\big(-i_{kq}+i_{qs}\big)L_{mq} \\
& +6\, i_{0s}\big(i_{fd}+i_{kd}\big)k_{3h}L_{md}\cos\big(3\,\omega_e+\varphi_{3h}\big) \\
& + L_{md}\big(i_{qs}+6\, i_{0s}k_{3h}\cos\big(3\,\omega_e+\varphi_{3h}\big)\big)\big(i_{fd\,rem}\big) \\
& -6\, i_{0s}i_{kq}k_{3h}L_{mq}\sin\big(3\,\omega_e+\varphi_{3h}\big)\big)
\end{aligned}
\tag{59}
$$

The voltage in the machine's terminals are induced by

$$
\begin{aligned}
v_{qs} &= -R_s i_{qs}+\omega_e\phi_{ds}+\dot\phi_{qs} \\
v_{ds} &= -R_s i_{ds}-\omega_e\phi_{qs}+\dot\phi_{ds} \\
v_{fd} &= \ R_{fd}i_{fd}+\dot\phi_{fd}
\end{aligned}
\tag{60}
$$

The dampers in q and d axes represent short-circuit coils with:

$$
\begin{aligned}
0 &= R_{kq}i_{kq}+\dot\phi_{kq} \\
0 &= R_{kd}i_{kd}+\dot\phi_{kd}
\end{aligned}
\tag{61}
$$

Later on in this thesis, the model is parameterized directly from machine design data. For sake of completeness all relations are quoted here. The model parameters can be related to the output parameters, where:

The stator magnetizing inductances $L_{m\_}$ are the difference of synchronous inductances $L_{\_}$ and stator winding leakage inductance L_{ls}

$$
\begin{aligned}
L_{md} &= L_d-L_{ls} \\
L_{mq} &= L_q-L_{ls}
\end{aligned}
\tag{62}
$$

The field winding leakage inductance L_{lfd} is calculated from the subtransient inductance in d-axis L_d', where all rotor quantities are seen from stator side

$$
L_{lfd}=L_{md}\frac{L_d'-L_{ls}}{L_{md}+L_{ls}-L_d'}
\tag{63}
$$

The damper (leakage) inductances are calculated with the sub-transient inductances $L_{\_}''$

$$
\begin{aligned}
L_{lkd} &= \big(L_d'-L_{ls}\big)\frac{L_d''-L_{ls}}{L_d'-L_d''} \\
L_{lkq} &= L_{mq}\frac{L_q''-L_{ls}}{L_{mq}+L_{ls}-L_q''}
\end{aligned}
\tag{64}
$$

Also the rotor resistance has to be mapped to

$$
r_{fd}=\frac{2}{3}\frac{r_r}{k_{fd}k_{fd}}
\tag{65}
$$

The saturation effect can be switched off by setting $k_{sat}=1$. The 3rd harmonic is deactivated by setting the variables L_{0s2}, L_{0s1} and k_{3h} to zero.

The implementation of the simulation model by Equations (50)-(65) is straightforward. Just for the saturation function (57), the direct implementation of $v_{sat} = f(i_m)$ results in a set of differential algebraic equations with an algebraic loop, where the magnetizing current has to be calculated from a function by itself and other variables $vars_1$ by
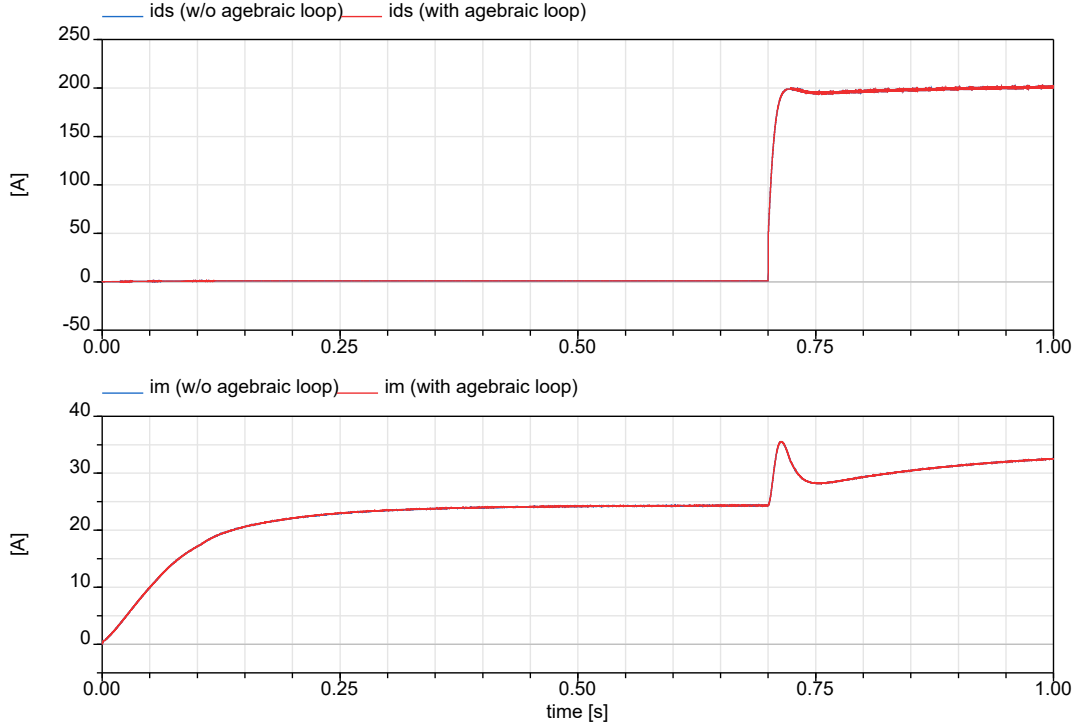
Figure 2.5: Check of influence of smoothing of magnetizing inductance by first order filter

$$i = f(i, vars_1) \tag{66}$$

This results in larger equation systems with nonlinear loops and was responsible for critical numerical performance and bad finding of initial conditions. The calculation of the saturation factor in Equation (55) can be smoothed by a first order filter to reduce numerical issues:

$$\dot{k}_{sat} = \left(k_{sat} - f(i_m, vars_2)\right) \cdot 1/T_1 \tag{67}$$

with a time constant T_1 well below the subsynchronous time constant and some constants "vars". This will cut the algebraic loop and restrict the variability of the saturation. It will be found later that this change is essential for improved initialization. The validity of the implementation with Equation (67) was checked experimentally. Figure 2.5 shows the results of a simulation with a load step from 2kW to 50kW at 0.7 seconds. The results do coincide at a time constant T_1 of 1e-6 seconds. For a time constant of 1e-4 seconds, they would not.

The generator model is shown in Figure 2.6 (machine_beh). In the AC connectors (blue circles) the interface variables $\{i_a, i_b, i_c, v_a, v_b, v_c\}$ are exchanged.

2.3.1.b Functional model
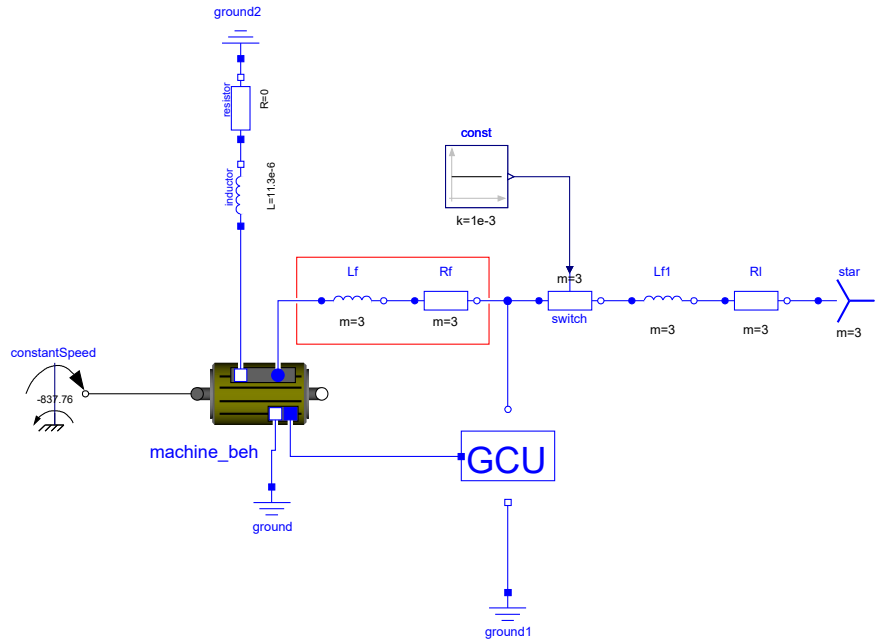
Figure 2.6: Test model with generator (machine_beh), behavioral level
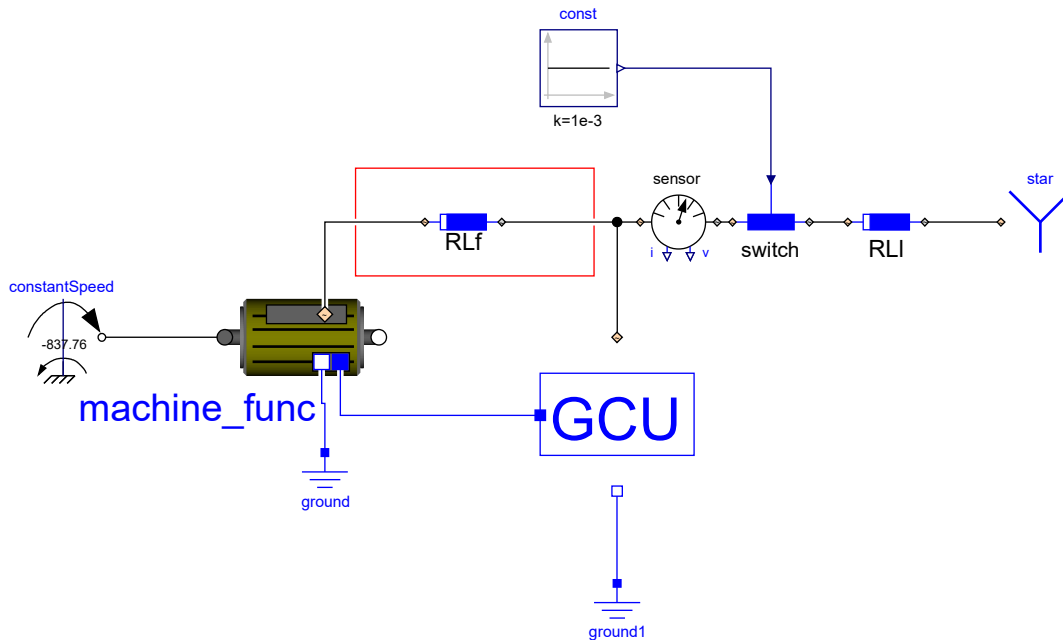
Figure 2.7: Test model with generator (machine_func), functional level

The functional model of the generator in $qd0$ system is basically the same as the behavioral model without the tripple harmonic. The model is shown in Figure 2.7 (machine_func). In the AC connectors (diamonds) the interface variables $\{i_q, i_d, i_0, v_q, v_d, v_{0,}\theta_e\}$ are exchanged with the machine's electrical phase angle θ_e.

In the test model, the 3-phase resistive/inductive impedances "Rlf" and "RLI", with symmetric values, were modeled in qd0 system by

$$\boldsymbol{L}_{qdo} \cdot \dot{i}_{qd0} + \omega_e \cdot \boldsymbol{yL}_{qdo} \cdot i_{dq0} + \boldsymbol{R}_{qdo} \cdot i_{qd0} = v_{qd0} \tag{68}$$

With $d\theta_e/dt = \omega_e$,

$$\boldsymbol{R}_{qd0} = \begin{bmatrix} R & 0 & 0 \\ 0 & R & 0 \\ 0 & 0 & R \end{bmatrix}, \boldsymbol{L}_{qd0} = \begin{bmatrix} L+3/2\cdot M & 0 & 0 \\ 0 & L+3/2\cdot M & 0 \\ 0 & 0 & L \end{bmatrix} \tag{69}$$

with self inductance L and line to line mutual inductance M. Furthermore $\boldsymbol{yL}_{qdo} = \boldsymbol{y}\cdot\boldsymbol{L}_{qdo}$, where

$$\boldsymbol{y} = \begin{bmatrix} 0 & 1 & 0 \\ -1 & 0 & 0 \\ 0 & 0 & 0 \end{bmatrix} \tag{70}$$

The model "switch" is a resistive element with low conductance in "open", and low resistance in "open" state.

2.3.2 Modeling of diode rectifier

2.3.2.a Behavioural model

$$i = i_{ds}\left(e^{v/vt} - 1\right)$$
$$\left(vt = \frac{kTn}{q}\right)$$

$$v = V_{knee} + s\cdot\begin{cases} 1 & \forall\, c_jf \\ R_{on} & \forall\, else \end{cases}$$

$$i = Gc_jf\cdot V_{knee} + s\cdot\begin{cases} G_{c_jf} & \forall\, c_jf \\ 1 & \forall\, else \end{cases}$$

$$c_jf = s<0$$
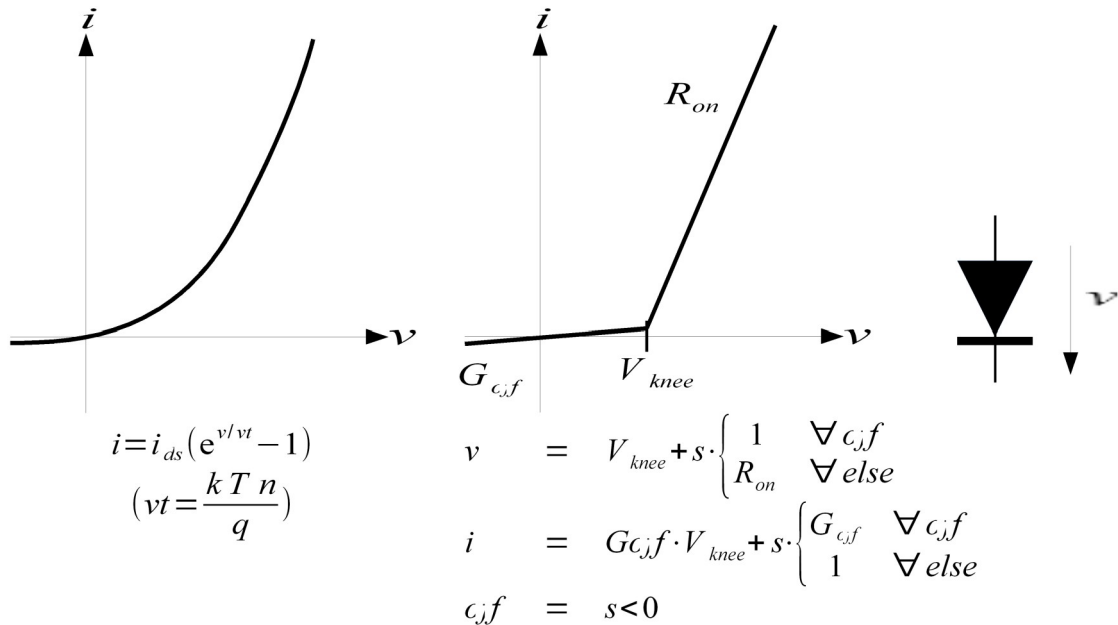
Figure 2.8: Diode models, used by rectifier (s: parameter of s- parametrization)

The auto-commutated full bridge or 6-pulse rectifier is the least-complex type of an AC/DC converter. It injects considerable harmonic currents and voltages into AC and DC side. The different modes of operation, which will be discussed further on in this chapter, make it highly unpredictable. Nevertheless, for aircraft applications the simple structure with six equally sized diodes has big advantageous in terms of reliability, compared to actively switching converters. For larger loads the number of switching circles can be increased by autotransformer-rectifier-units. Rectifiers are also used in testing as a parallel source of distortion to the tested equipment.

The diodes can be described by the equations in Figure 2.8. The user may choose between the continuous, but exponential, Shockley diode equation (left) and section wise defined linear equations (right). Both are models of the Modelica standard library.

2.3.2.b Functional model
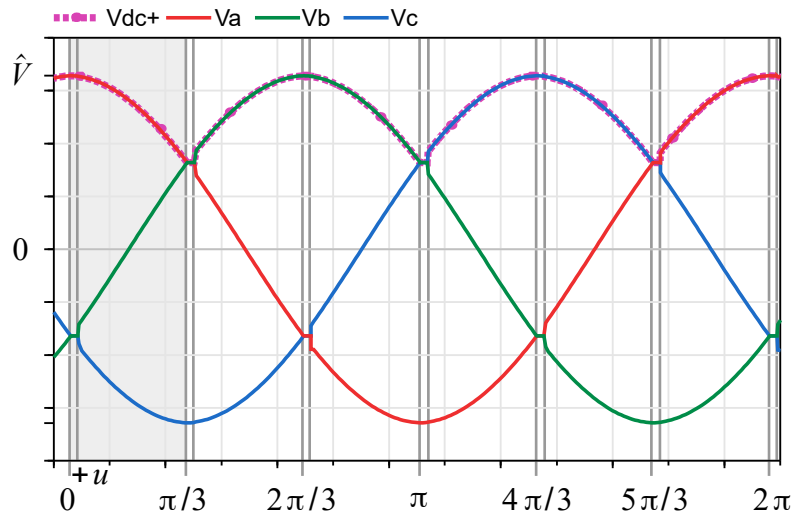
Figure 2.9: Switching intervals of 6-pulse rectifier; voltage [V] vs. phase angle [rad]

The 6-pulse rectifier is a highly-nonlinear element due to its phase-dependent switching. For network stability studies it is not necessary to consider time scales above net frequency. The trajectories just have to be representative for the moving averages along the trajectories of the original system. The stability properties of the original and approximate systems have to be identical. The func-
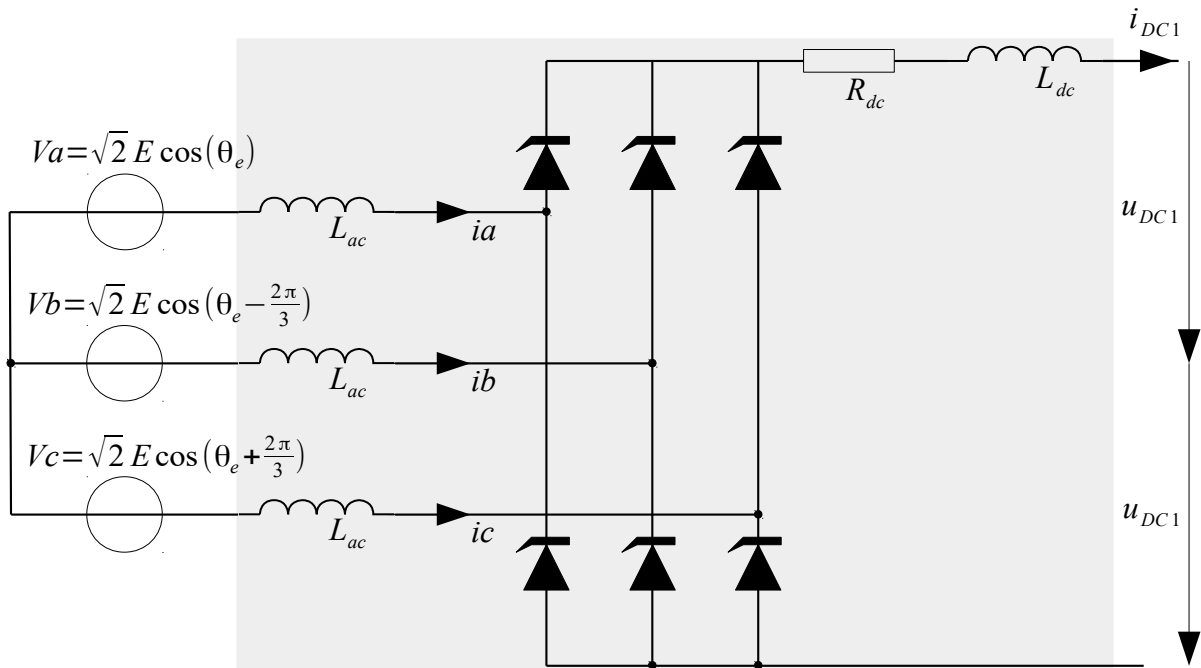
Figure 2.10: 3-phase full converter circuit; circuit approximated by the functional model is high-lighted in grey

tional model can be identified by state space averaging technique.

Figure 2.9 shows the different switching intervals of a rectifier with continuous DC current. The circuit which is approximated can be seen in Figure 2.10. The impedances are embedded as part of the functional model.

41

In the "conduction interval" from phase u to $\pi/3$, the voltage of the positive pin of the DC output $Vdc+$ equals the envelope of the AC voltage Va. If the source shows inductive behavior, then the conduction interval is followed by the "commutation" interval from $\pi/3$ to $\pi/3+u$, where both Va and Vb equal to $Vdc+$. Va is kept to $Vdc+$ by the inductance. If the DC voltage is stabilized by a capacitor, then instead of a commutation interval the conduction interval may end earlier with an interval where $Vdc+$ stays above the source voltages. All considerations apply accordingly to the following switching intervals and the negative side.

The functional equations of the 6-pulse rectifier can be taken from (Krause et al., 2002). It derives the model by integration and time-averaging of the currents and voltages in the switching intervals. Limitations are

- The RMS amplitude of the AC source may not change swiftly.
- The change of DC load current needs to stay constant within one interval.
- One commutation takes place at a time.

All AC quantities are treated in the transformed Park system. The terminal quantities have to be rotated into a local system with d-axis voltage $vdg=0$ by the angle $thetaX$, with the new variables $\{vqg, vdg, iqg, idg\}$.

$$thetaX = atan2(vq, vd)$$
$$\begin{bmatrix} vqg \\ vdg \end{bmatrix} = \begin{bmatrix} \cos(thetaX) & -\sin(thetaX) \\ \sin(thetaX) & \cos(thetaX) \end{bmatrix} \cdot \begin{bmatrix} vq \\ vd \end{bmatrix}$$
$$\begin{bmatrix} iq \\ id \end{bmatrix} = \begin{bmatrix} \cos(thetaX) & \sin(thetaX) \\ -\sin(thetaX) & \cos(thetaX) \end{bmatrix} \cdot \begin{bmatrix} -iqg \\ -idg \end{bmatrix}$$
$$(71)$$

The currents are the sum of the averaged currents in commutation and conduction phase:

$$i_{qg} = i_{qg\,com} + i_{qg\,cond}$$
$$i_{dg} = i_{dg\,com} + i_{dg\,cond}$$
$$(72)$$

where

$$i_{dg\,com} =$$
$$\left(\begin{array}{l} -6E\left(\sin(u)(\cos(u)-1)\cos(\alpha)^2 + \cos(u)\sin(\alpha)(\cos(u)-1)\cos(\alpha) - \frac{(\sin(u)\cos(u))}{2} + \frac{u}{2}\right)\sqrt{2} \\ +6L_s i_{DC1}\left(\left(\frac{-\cos(\alpha)\sin(u)}{3} - \frac{\sin(\alpha)(\cos(u)-1)}{3}\right)\sqrt{3} + \cos(\alpha)(\cos(u)-1) - \sin(\alpha)\sin(u)\right)\omega_e \end{array} \right)$$
$$\Big/ 2L_s \omega_e \pi$$
$$(73)$$

$$i_{qg\,com} =$$
$$\left(\begin{array}{l} -(6(\cos(u)\cos(\alpha)^2 - \sin(u)\sin(\alpha)\cos(\alpha) - (1/2)\cos(u) - 1/2))E(\cos(u)-1)\sqrt{2} \\ -2L_s((\cos(\alpha)(\cos(u)-1) - \sin(\alpha)\sin(u))\sqrt{3} + 3\cos(\alpha)\sin(u) + 3\sin(\alpha)(\cos(u)-1))i_{DC1}\omega_e \end{array} \right)$$
$$\Big/ 2L_s \omega_e \pi$$
$$(74)$$

$$i_{qg\,cond} = \big(-(((\cos(u)+1)\cos(\alpha)-\sin(\alpha)\sin(u))\sqrt{3}-3\cos(\alpha)\sin(u)-3\sin(\alpha)(\cos(u)-1))i_{DC1} \big) \Big/ \pi \tag{75}$$

$$i_{dg\,cond} = \big(-i_{DC1}((\cos(\alpha)\sin(u)+\sin(\alpha)(\cos(u)+1))\sqrt{3}+(3\cos(u)-3)\cos(\alpha)-3\sin(\alpha)\sin(u)) \big) \Big/ \pi \tag{76}$$

with the RMS value E of the AC voltage vqg. In case the diodes are replaced by thyristors, the DC voltage can be controlled by the initial "firing angle" α. Otherwise α equals zero.

The equations for the commutation angle u and the derivative of the DC current i_{DC1} are adapted from (Krause et al., 2002). The commutation angle u may not exceed theoretic values and $\dot{i}_{DC1}$ is limited in case the output voltage exceeds the theoretic DC voltage because of a DC capacitor:

$$u = -\alpha + acos\left(\left\{ -1 < \cos(\alpha) - \frac{L_s \omega_e i_{DC1}\sqrt{2/3}}{E} < 1 \right\} \right) \tag{77}$$

$$\dot{i}_{DC1} = \frac{\left\{ max\left(u_{DC1}, \dfrac{3\sqrt{6}\,E\cos(\alpha)}{\pi} \right) \right\} \pi + (-i_{DC1}R_{dc} - u_{DC1})\pi - 3\,i_{DC1}L_s\omega_e}{(L_{dc} + 2\,L_s)\pi} \tag{78}$$
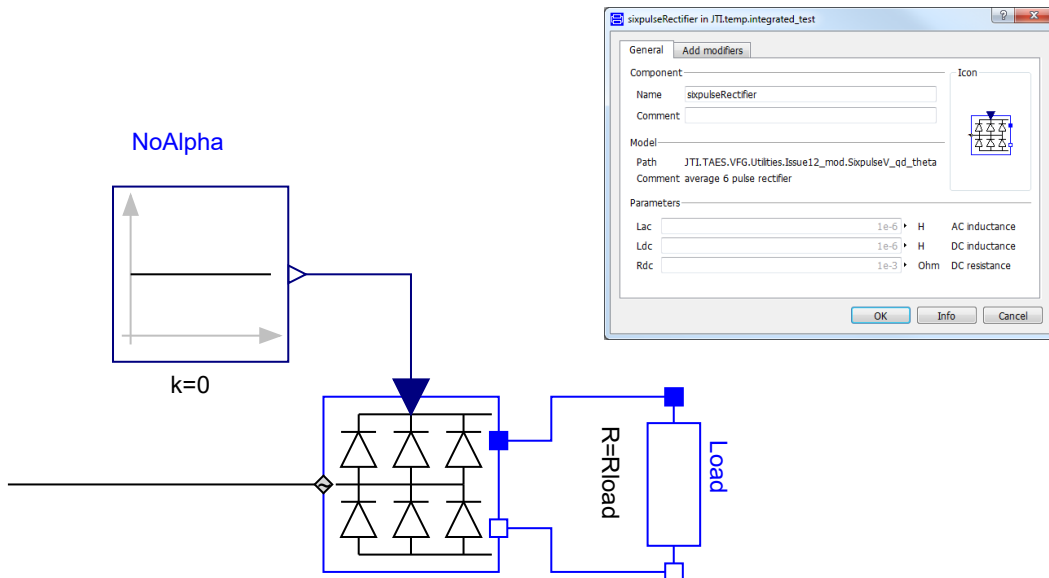
Figure 2.11: Functional model of 6-pulse rectifier in Modelica, with parameter interface

The implementation of the model in Modelica can be seen in Figure 2.11. The AC interface was explained in the generator section.

The validity of the model is demonstrated in Figure 2.12. Both, behavioral and functional rectifier, are powered by a voltage ramp and loaded by a resistive load: The DC voltage is basically the same, with additional noise at the behavioral model.
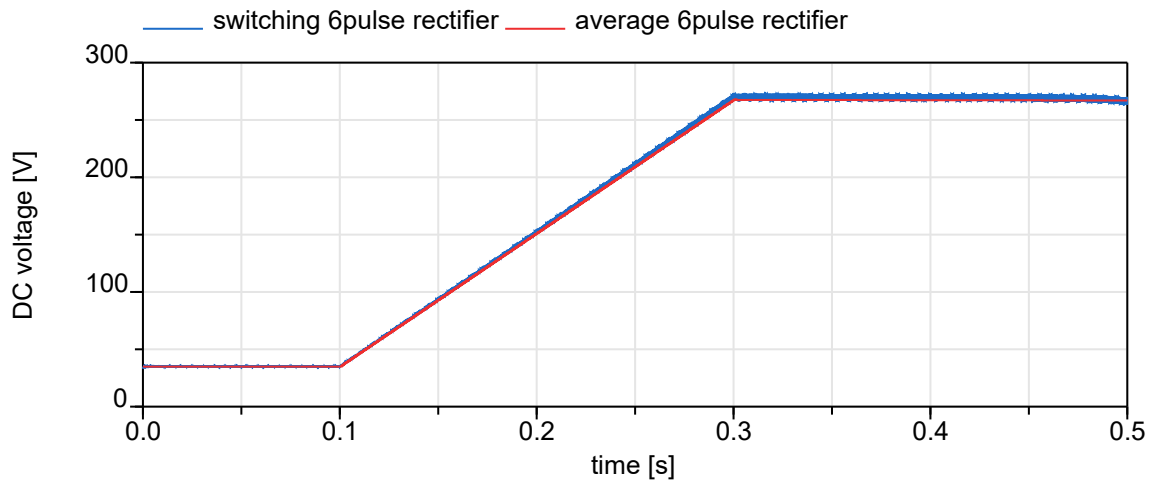
Figure 2.12: Comparison of behavioral and functional models of 6-pulse rectifier; ramp 15...155V AC

Further details on an infrastructure for multi-level modeling can be found in (Kuhn et al., 2008) and (Kuhn et al., 2009). The papers describe a unified framework for both detailed behavioral models and functional averaged models. They highlight the benefits of describing a complex system with Modelica in terms of modelling simplicity and capability of automatically performing procedures such as initialization and linearization. The papers demonstrate the modelling approach and its potential for stability analysis of complex vehicular power systems.

2.3.3 Validation of generator model against hardware

The design of the Thales "MEGEVE" generator matured within several research programs. Details on the hardware development in the European Community funded 5th research framework program are published in (Delhasse and Biais, 2006). Later research improved the machine and added more detailed design and modeling (Kutt, 2012). The machine was validated as part of the "COPPER Bird®"[4] ground electrical test rig. The work on the test bench was started in 2002 to test innovative more electrical aircraft architectures in the context of the POA (Power Optimised Aircraft) European project. The test bench is used by all follow-up programs.

For network integration and verification studies, the validity of all equipment models must be checked by coherency tests. Coherency tests are quality checks which ensure the validity of models versus hardware tests and validity among the models with different levels of abstraction. Conversely, for simulation assisted design studies it is essential that the simulation model is representative for the real properties. In the following the correctness of the generator model is demonstrated by means of a coherency test between test rig data and simulation data. The testing was part of the V&V studies in CleanSky SGO project which are addressed in chapter 7.1. All data and plots were pre-published in (Ji, 2016).

---

[4]Safran "COPPER Bird", https://www.safran-electrical-power.com/media/20150504_copper-birdr-lps-benefits-unique-test-rig-use-research-more-electric-aircraft
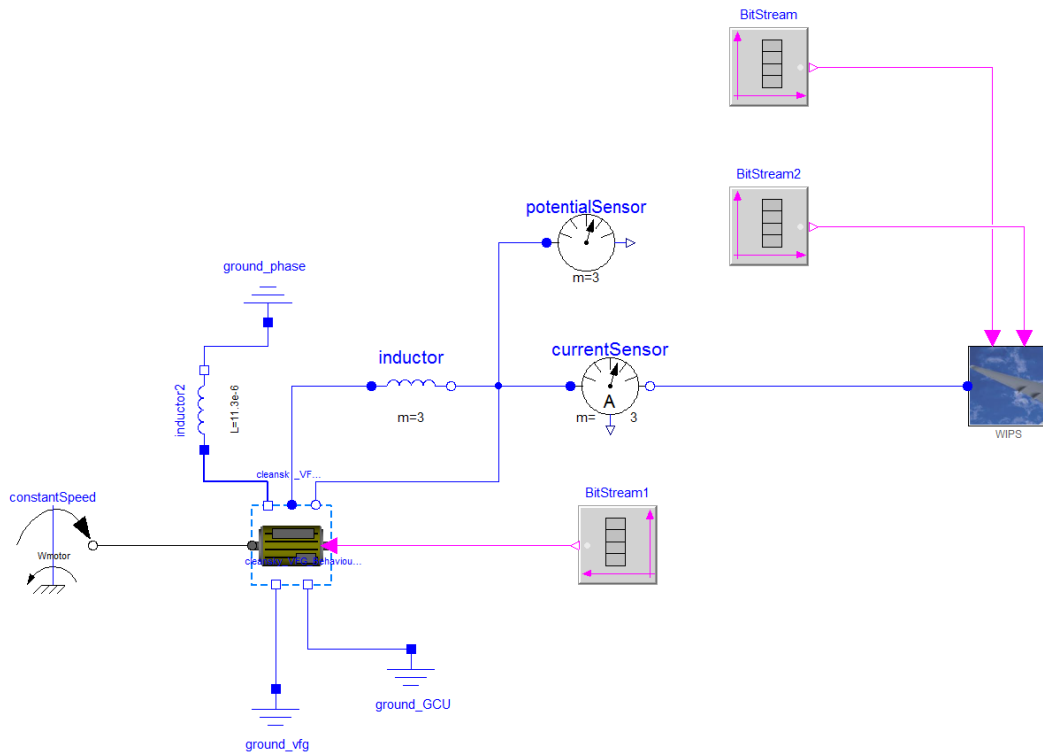
Figure 2.13: Coherency test of variable frequency generator between measurement data and be-havioral model

The simulation result is said to be coherent with the hardware measurement if the criterion $C_{err}(t)$ stays below a threshold value c_{thresh} at all times of evaluation:

$$C_{err} = \frac{1}{T_c} \int_t^{t+T_c} \frac{|X_{meas}(u) - X_{simulation}(u)|}{|X_{meas}(u)| + 0.01\, X_n}\, d\,u \leq c_{thresh}\ \forall\, t \tag{79}$$

where $X_{meas}(t)$ are the reference data and $X_{simulation}(t)$ are the simulation data. The period T_c is an averaging interval which filters high frequent oscillations and X_n is a nominal value which suppresses errors at small amplitudes. The criterion shall be lower than 5% at any time for a period T_c of 5 µs.

Exemplary for all coherency tests, Figure 2.13 shows a test bench of the variable frequency generator at 400Hz which is loaded by the Wing Ice Protection System (WIPS). WIPS is a resistive load. Figure 2.14 shows the phase A currents and voltages at disconnection of the load.

The result in Figure 2.15 prove the coherency of the models and hardware test.

2.3.4 Contributions

This chapter gives the equations of the two most relevant components of this thesis, the generator and the rectifier. Minor contributions include
- *the validated implementation of the generator models in Modelica*
- *the numerical efficient re-formulation of the generator*
- *the first implementation of a state-space averaged functional model of the rectifier in Mod-elica*
- *the implementation of the interface-infrastructure in Modelica for functional modeling in Park system*

Relevant publications:
"A Multi Level Approach for Aircraft Electrical Systems Design" (Kuhn et al., 2008)
  • *contribution of the author: implementation of the infrastructure*
"A components library for simulation and analysis of aircraft electrical power systems using Mod-
elica" (Kuhn et al., 2009)
  • *contribution of the author: implementation of the infrastructure, basic models and source*
    impedance identification of generators and rectifiers
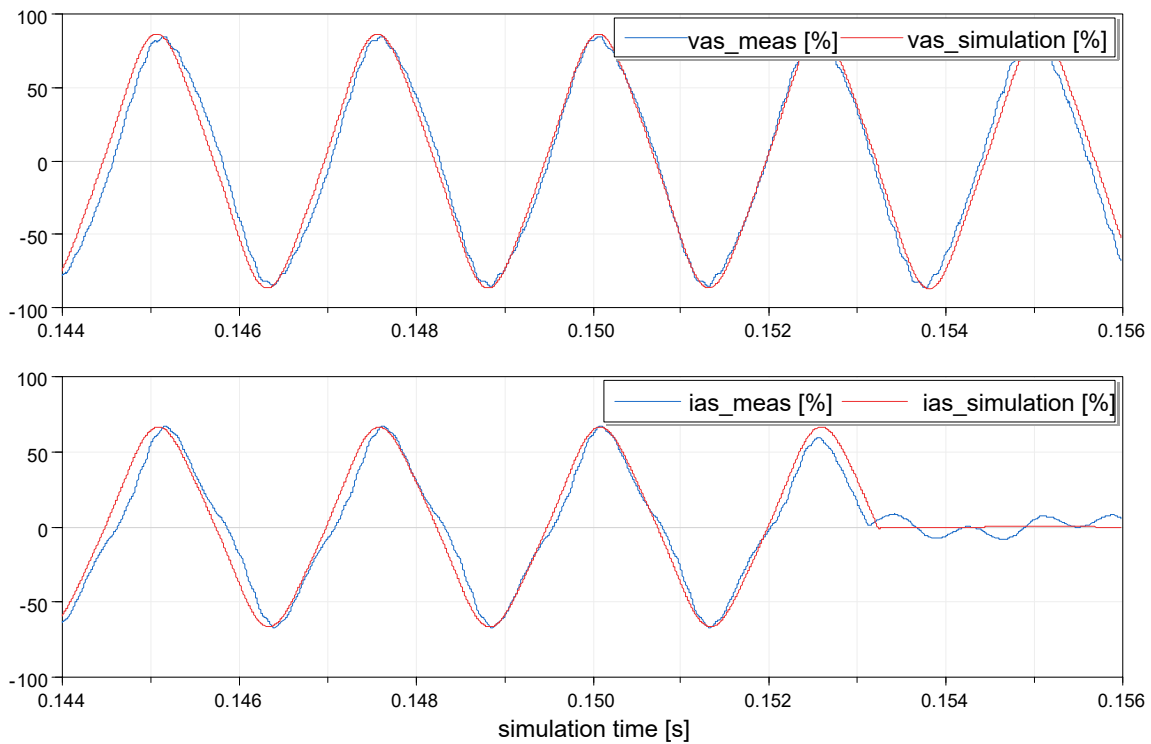
Figure 2.14:Quantities of phase A of the coherency test between measurement data and simula-
         tion; unit quantities referring to base current i-base and v_base
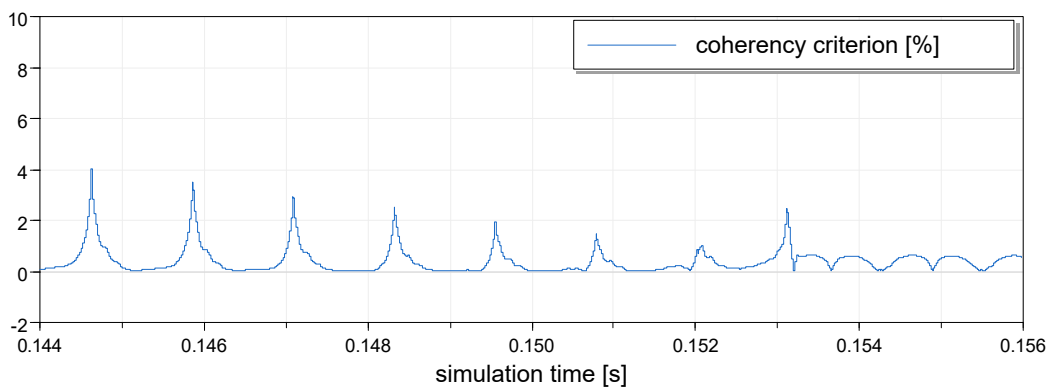
Figure 2.15:Coherency test criterion for phase A voltage

3 Improved generator design

In upcoming and future more-electric airplanes, more of the electrical loads connected to the power distribution network will behave non-linearly and will be switching. This will induce advanced demands on the network to keep the power quality. Trade-offs between performance, weight, and power quality, have to be made and design choices have to be supported by qualitative and quantitative measures.

This chapter aims on the improvement of the generator design and investigates the impact of the new demands on the generator. The supplier Thales developed advanced calculation routines for the "MEGEVE" generator and validated the results by hardware tests (Delhasse and Biais, 2006). Trade-offs in the design parameters are known to the experienced engineers. No further numerical optimization was used before this study. Furthermore, no relations of the generator design to the ratio of non-linear loads were known with respect to power quality.

The objective of this work was to

- develop an appropriate framework for the efficient multi-objective optimization of the generator,
- perform the optimization of the aircraft generator design and analyze the result,
- develop a methodology to analyze the impact of higher ratios of rectified load and implement the criteria into the optimization framework, and
- analyze the design trade-offs using suitable methods.

This chapter will first show the state of the art in electrical power generation of aircraft. Then, a brief background of electrical machine design is given. It is followed by the implementation of the multi-objective optimization and results are discussed. In a second step, the generator is investigated for use with a higher ratio of non-linear rectified loads. This work proposes simulation based methodology for analysis and optimization. In the last sub-chapter the results and trad-offs are discussed.

3.1 Aircraft starter generators

The aircraft electrical network in commercial airplanes is powered by up to four generators, which are driven by the shafts of the aircraft's turbines. The generators are not connected to each other, but feed different loads to prevent failure propagation. The variation of the turbine speed can be compensated for (variable speed, constant frequency), for example, using hydraulic gears with constant output speed to the generators (e.g. A340) or by intermediate DC stages and electronic inversion (e.g. B777). In newer aircraft, such as the A380 or B787, no compensation of speed is done. The generators are driven by variable shaft speed directly (Moir and Seabridge, 2008) but only stabilize the AC voltage amplitude (fixed voltage/variable frequency). This allows simpler designs for the mechanical and generator part, but loads must be capable to handle variable frequency AC voltage. For variable frequency, output voltage must be controlled via variable excitation of the rotor's field windings.

The aircraft's gas turbines were traditionally started using pneumatic pressure. For newer designs, the generator can act as an electro-mechanical starter. For this concept, the power is supplied via an inverter, which is disconnected after the starting of the engines. For this reason, the machine is called a starter-generator. The motor operation is usually done at lower power ratings than the generator operation. Design considerations for the motor operation of the machine are not part of this thesis.

Type of machine
3-phase synchronous machine (SM) star point wye-connected stator windings are identical sinusoidal with distributed windings rotor of SM equipped with field winding and damper windings in q and d axis.

Rated parameters	
Total three-phase apparent power (max)	S_n= 209kVA
RMS phase voltage	U_{as}= 230V
Variable electrical frequencies	f_e=360-800Hz
Power factor	$\cos \varphi_n$=0.75..1
Number of pole pairs	3

Table 2:Ratings of nominal starter-generator

For this thesis, a three-phase starter generator was considered with a variable shaft speed and controlled output voltage of 230 volts RMS. The machine was originally designed for a traditional aircraft network, with mainly symmetric resistive loads according to standard (ABD100.1.8, 2002). For an externally excited synchronous machine, the current of the rotor field is controlled. The power has to be supplied to the rotor, for example, from the stationary environment to the shaft by slip-rings. For an airplane generator, high demands apply on a reliable and wear-free design; therefore, it is implemented using a brushless design. For this, the starter generator actually comprises of three synchronous machines: In a first machine, the permanent-magnet rotor generates three-phase AC voltage in the stator, which is rectified to DC and powers the stationary Generator Control Unit (GCU). The controller excites the one-phase stator of the second machine. The voltage of its three-phase rotor is rectified and feeds the field windings of the main machine. The three-phase stator output is the generator's output. The structure of the machine is depicted in Figure 3.1. Table 2 lists the basic parameters of the generator. In this thesis, the first two machine stages are not taken into further consideration: The power stage is considered to supply the power to the control unit without interaction. The second machine stage is considered to have fast and well-damped dynamics, compared to the dynamics of the field windings of the main machine. Therefore, it can be represented as a GCU-controlled, variable-voltage source to the field windings.

In recent research projects, alternative generation concepts are being investigated. The permanent-magnet excited synchronous generator is a particularly promising approach. The output voltage can not be adapted at this machine, but it is proportional to the mechanical rotation speed. Therefore, all loads have to be designed for variable frequency and variable voltage. This drawback is compensated by a much simpler generator structure, consisting of only one machine and without stages for voltage control. On the other hand, this machine was found to be critical in the case of faults. Since the output voltage can not be controlled, in the case of an emergency, the generator has to be decoupled from the network at nominal voltage conditions. The switches must be capable of
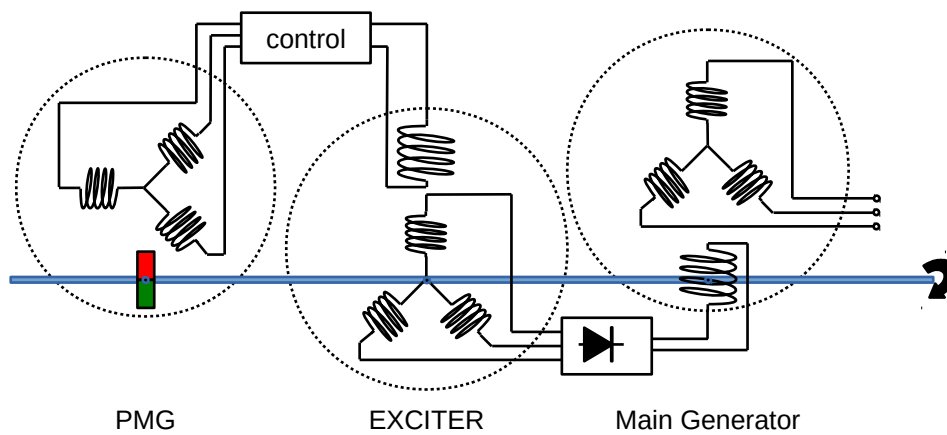
Figure 3.1: Three-stage machine structure

reliably interrupting the lines at maximum power flow. By contrast, the externally excited machine may turn the machine voltage off before disconnection. Due to this weakness, the classic three-stage machine is still a good solution.

3.2 Basics of machine design

The basic steps of designing a synchronous machine are well known from literature, but constraints and details of the design are very specific to the application. Starting with the design as proposed in (Müller et al., 2008), the most crucial part in machine design is to fix the basic design choices. First, the type of machine is chosen e. g. synchronous or interior rotor. Then, with the help of design rules, a preliminary, main geometric layout and the magnetic circuit is designed. Afterwards, dependent geometric properties and electrical characteristics can be calculated. In the next step, the final machine is found from numerical parameter optimization. Thus, machine design is always an iterative process, to find the parameters that satisfy the specification. Often, verification by numeric magnetic field computation concludes the design. In addition to the basic electro-mechanical layout, thermal, liquid-cooling, pressure and mechanical constraints of the generator have to be taken into account.

In the following, a rough overview of the design of the synchronous machine by design rules is given, with some references on the design choices of the generator. It is assumed that the reader already understands the operation principle and mechanical composition of synchronous machines. Information can be taken from the references. Only three-phase machines are investigated. The information on machine design is taken and quoted from (Müller et al., 2008) and (Soong, 2008). Practical applications on optimization can be found in (Besnerais et al., 2008) or for the industrial design, (Delhasse and Biais, 2006).

The equations used for the design of the electromagnetic components of the machine, are constrained by maximum air gap induction and specific electric loading of the field windings. However, the real challenges are related to the thermal aspects. The electromagnetic active components and insulation can only withstand limited temperatures. Therefore, efficient design limits both the losses, especially in critical components, and considers heat dissipation through sufficient cooling, to limit maximum temperatures. Apart from the basic equations, there are many design choices. Constraints include geometric dimensions, choice of cooling and economic aspects, such as the best utilisation of material and production costs.

The "inner apparent power" P_{si} is an important basic characteristic in the design of the machine. It is calculated by the equation

$$P_{si} = C_S D^2 l_i n_0 \tag{80}$$

with the main dimensions diameter D, length l_i, and nominal speed n_0. The utilization factor of apparent power C_S is calculated by a function which depends on the machine's layout. The equation of the inner apparent power visualizes the basic relations for the main geometries: It can be seen that the machine's power is dependent upon the volume via diameter and length, can be increased by higher speeds, while the torque $\tau = P_{si}/n_0$ can not, and by the utilization factor. Therefore, for low volume and thus, low weight machines, this utilization factor needs to be optimized by a good design.

Other publications, such as (Soong, 2008) do not use the term utilization factor C_S but deduce the equations with the more physically influenced parameter shear (normal) stress σ:

$$P_{si} = 2 \cdot V_r \cdot \sigma \cdot n_0 \tag{81}$$

Where V_r is the rotor's volume. σ is the stress acting on the current-carrying conductors on stator side. It is calculated as the electromagnetic force in the machine's airgap, normalized by the area of the conductors:

$$\sigma = \frac{F}{Area} \tag{82}$$

The electromagnetic force is calculated by

$$F = B \cdot I \cdot l \tag{83}$$

with an uniform magnetic field B and windings of length l. While the term "utilization factor" points out the need for a high exploitation, the term "shear stress" reminds us that the design is stressed mechanically. Both utilization factor and shear stress are parameters characteristic of a machine type. Once this factor is known from detailed calculations or prior designs, new designs can be extrapolated from it easily.

In the preliminary design phase, typical process input parameters include rated power, electrical and mechanical frequency, voltage, power factor and number of phases. Additional constraints may include output voltage quality, reactances and time constants. For the generator design, the inner apparent power is the dimensioning element, since both real power and reactive power are associated with power lost through heat. For the generator, the rotor flux is excited by an external current (in contrast to permanent magnetic poles). Therefore, coils for both stator and rotor must be designed. Apart from the parameters, the basic design considerations are identical for both (for permanent excited machines, usually the stator is designed first; and afterwards the rotor is designed as part of the magnetic circuit).

The first step in machine design is to find starting values for the geometric dimensions D and l by help of Equation (80) (the basic parameters are visualized in Figure 3.2). Amongst others, they are functions of torque, poles and utilization factor. Their ratio can be found later in the design process, as a trade-off between good cooling in short machines with higher diameter and better winding length, and moment-of-inertia for long machines with lower diameter. For the aircraft generator design, the electrical speed range is fixed. It is defined by the industrial standards to be between 360 to 800 Hz. The ratio of electrical to mechanical speed can be varied by the pole pair number (and further to the engine by gear stages). The maximum mechanical speed is limited by mechanical stress.

The number of strand windings, also known as number of turns in series per phase, is dimensioned for the demanded voltage induction by the fundamental flux wave, at no-load-condition at maximum speed. As some of the most important parameters, start values for the amount, width and length of the notches are specfied. Also, the maximum iron magnetic field intensity is given. With this data, the winding number can be calculated. The span of a coil across several notches calculates from the number of notches per pole and phase. The windings are distributed geometrically, which may lead to a sub-optimal degree of utilization of the flux generation. It is taken into account by the winding factor, which varies slightly from one machine to another. This non-perfect coupling may have disadvantages in terms of utilization, but also some interesting benefits; the effect can be used for smoother sinusoidal voltage and torque waveforms (see winding scheme, next).

On the rotor side, the ratio of the impedances in the q and d axis can be adapted. The difference in any type of axis specific impedance $L_d^x - L_q^x$ is called "saliency" and can be varied by the layout of the iron core. High saliency rotors support high reluctance torque, but can cause mechanical asymmetries and bad voltage quality in the case of rectified loads (Bonfert, 1962). Design for low saliency will always have some degree of non-symmetry, in case the field winding is not symmetrical but is aligned only in the d axis. Symmetric excitation can be found in double-fed induction machines, but is not standard for synchronous machines. The machine treated in this thesis has excitation in the d axis only, but is designed for low saliency. Machines with a high number of pole pairs tend to have negligible saliency.
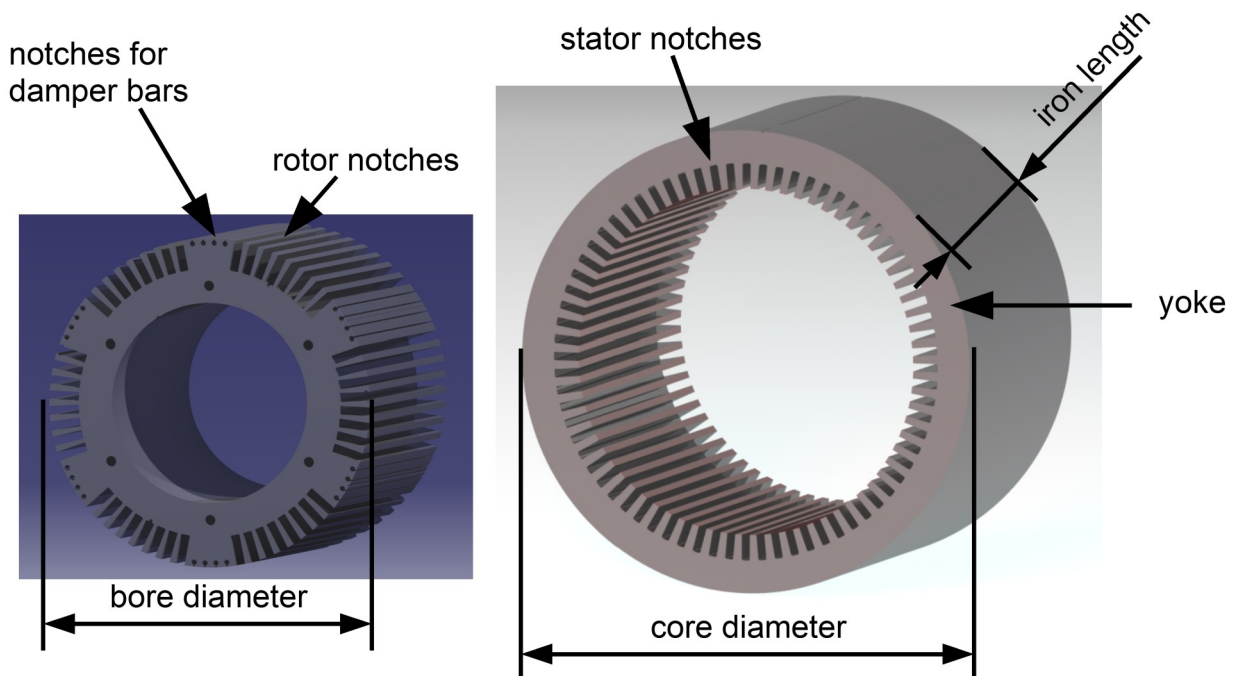
Figure 3.2: Generator's iron core of rotor and stator, with nomenclature; CATIA model

For illustration of the design of the active part of the generator, the iron core of a generator layout is visualized in Figure 3.2 (CATIA model, with data from design routine). Both the inner rotor and the outer stator contain slots to embed the copper windings. The rotor contains notches to embed the damper windings.

The winding scheme is of central importance for the production effort and also on the voltage harmonics. It arranges the conductors to coils with a certain geometrical alignment. A design choice of the conductor shape has to be made, which can vary from round wire to solid bars. Coils can be wound regularly with an integral number of slots per pole, which is called integral slot winding. Al-

ternatively, a scheme can be applied to spread the number of slots per pole, where the mean number is a fraction. Therefore, it is called a fractional slot winding. This method is used for smoother flux waveforms, but also might be used to prevent linkage of any harmonics between the armature and the field winding. If there are several symmetric winding packages per phase, they can be connected in series or in parallel. Packages can also be ordered in multiple layers, with coils sitting on top of each other. Depending on the winding scheme, the output's voltage harmonics can be influenced, where the shape can vary between an ideal sinusoidal voltage to a square wave voltage. Square waves are beneficial for low harmonic content on the DC side, while the sinusoidal waves exhibit lower harmonic content on the AC side. For the objective of this thesis, the output voltage has to meet strict industrial standards for power quality, with minimal harmonics being allowed.

With the turn number known and the wire diameter determined from the maximum current density, the coils that fill the notches can be calculated. Based on the space needed for the wires, the notch width and height can be calculated. Constraints have to be checked for the heat dissipation, the flux linkage with limitation of leakage and the maximum induction in a tooth. Skin effect could limit the effective conductor cross section. Therefore, it should be addressed if precautions need to be taken. In the case of asynchronous loading, negative sequence fields would induce large currents in the stator. Furthermore, load steps could result in swinging of the system. In non-salient pole rotors, currents induced in the iron counteract against this effect. To reduce it further, short circuit windings in the rotor notches, called 'dampers', are used for additional damping; for example in Figure 3.2 on the left, short circuit windings are foreseen to the four open holes in the six wide teeth of the rotor.

After the electro-mechanical parts have been considered, the magnetic circuit has to be designed. The field winding is dimensioned for the induced voltage at the nominal speed. With an estimate on the field strengths of the active parts, the missing geometries for the magnetic circuit are designed with the help of some design rules. These rules include the thickness of the pole cores, the yoke and the airgap. The yoke has the purpose of closing the magnetic circuit, but it also has to be designed to withstand the strong mechanical forces. Estimates on the leakage of the magnetic fields are needed, for sufficient dimensioning of the effective flux path and mechanical stress. The width of the air-gap is limited by efficiency on the upper side and by mechanical robustness and electrical stability on the lower side.

3.3 Numerical optimization of the design

After the design phase, the machine can be further analyzed and adapted in the "calculation phase". Supplementary performance measures can be introduced, which were not considered during the analytic layout phase. The most important difference compared to the prior design phase, is that more design variables are taken as parameters. The values which were found by the analytic design rules are taken as starting values. The designs are validated and constrained by additional functions for the electrical, magnetic, mechanical and thermal domain. In the following, the set of all sub-functions which are used to calculate the design properties is called the "design function".

For the Thales generator, this company developed an advanced design function over the years. The output of the design function was validated by hardware tests. An early result was proposed in (Delhasse and Biais, 2006). The original parametrization of the Thales generator was tuned manually at the manufacturer. The following chapter proposes the implementation, and the results of a multi-objective optimization of the Thales generator. The Thales design function is implemented as MATLAB m-file.

3.3.1 Implementation of multi-objective optimization

Name	*Type*	*Name*	*Type*	*Name*	*Type*
Pole pair number	d	Iron length	c	Yoke stator height	c
Notch width	c	Notch height	c	Number of statoric turns in series/phase	d
Bore diameter	c	Yoke rotor height	c	Number of rotor notches	d
Rotor notch width	c	Rotor notch height	c	Number of excitation turns/pole	d
Airgap	c	Number of damper bars /pole	d	Diameter of damper bar	c

Table 3: List of tuners (c: continuous, d: discrete)

In the Thales design function, the winding scheme and turn numbers are used as inputs again. The iron geometry, including the number of notches and dimensions, are also immediate input parameters. Table 3 gives an overview of the input parameters. Calculation steps include the computation of the magnetic circuit and electrical characteristics, including voltage harmonics of the open-circuit voltage. The currents and the losses are of primary interest, as they give information on the dissipated heat and also on the degree of efficiency. The wire dimensions are set where the diameter has a strong impact on the dissipated heat, called copper losses. Thus, the maximum operating temperatures do constrain the wires. Characteristics for the mechanical stress can be extracted for the normal operation, but also with special focus on the worst-case conditions, as asymmetrical load. The term stress and shear stress was introduced as design characteristic in Equation (82). High stress values are desired for compact designs but result in structure-borne noise and may end up in material fatigue of the core material. Therefore, for this design optimization the stress is constraint by a maximum value.

From the Thales design routine, the motor impedances and time constants can be extracted. The resistances and reactances are necessary inputs to the subsequent design phase, which is the check of the machines behavior at different operating conditions through simulation. Again, electrical stability has to be considered. Last and most important, as soon as all parameters are fixed, information on material cost and weight can be supplied.

In the following, a procedure for the optimization of the generator using the generator design function is given. At this stage, the single objective function is the weight of the generator active part.

The generator optimization task can be formulated as a constraint optimization problem

$$\begin{cases} \min_{X} \boldsymbol{crit}\left(\boldsymbol{X}\right) \\ subject\,to\,\boldsymbol{constr}\left(\boldsymbol{X}\right) \leq \boldsymbol{0} \end{cases} \qquad (84)$$

where

- **X** is the vector of the tuner values from Table 3. The "type" field indicates continuous variability or variability in discrete only increments.
- **crit** is the criteria vector to be minimized, which is the weight of the generator.
- **constr** is the inequality constraint vector of criteria, which may not exceed the limitations. The vector of constraints is of length 31, with constraints in Figure 3.3:
  - Vector of thermal constraints (max temperatures),
  - distance to critical speed, that excites the natural frequency of the mechanics,
  - mechanical stresses on rotor teeth and yoke,
  - maximum excitation current which can be delivered by the recent control,
  - other constraints on geometrical dimensions and windings alignment.

For a good convergence of the optimization, the following considerations had to be taken into account:

1) The mechanical synchronous speed n_s of the driving shaft, is linked to the electrical frequency f by

$$n_s = \frac{60\,f}{p} \qquad (85)$$

where the AC network's variable frequency is constrained between 360 and 800Hz. Since the ratio of turbine speed and shaft speed n_s can be adapted by a mechanical gear ratio, the pole-pair number p does not need to be constrained. The ratio may vary between 1,2,3 or 4. The selection of p has a substantial influence on most generator-sizing equations. Equation (80) shows the dominant influence of the mechanical speed on the apparent power. Lower p's with higher n_s are beneficial for power density, but the diameter is constrained by the mechanical forces. Therefore, the steep transition of criteria values between adjacent p's, prevent an optimization in one step; independent optimizations were run instead, for each number of pole-pairs.

2) Input variables to the analytic generator layout function need to be broken down into their atomic elements. For example, the number of notches *nes* is a multiple *k* of the pole pair number *p*:

$$nes = k \cdot p \qquad (86)$$

Thus, *nes* can be varied by the independent tuners *k* and *p*.

3) Optimization algorithms do have difficulties with complex constraints on tuners. It should be considered to have unconstrained, continuous variables and adapt the variability in the evaluation function. For example, a variable *v* is calculated from the fraction of tuners x_1 and x_2:

$$v = \frac{x_1}{x_2} \qquad (87)$$

where *v* has to be restricted to integer values. With the approach of (Besnerais et al., 2008), the preliminary tuner values have to be treated by a "repair algorithm" to get *v* as an integer:

$$v' = \frac{x_1 + \Delta_1}{x_2 + \Delta_2},$$
$$\begin{cases} \min_{\Delta} \sqrt{v^2 - v'^2} \\ subject\,to\,v' \in \mathbb{N} \end{cases} \qquad (88)$$

Examples for ν are the number of conductors per notch, where the number of turns and number of notches are independent tuner variables.

All tuner values were allowed to vary freely between minimum and maximum values, except the pole-pair number p.

The optimization problem is not convex, with discrete tuners and discontinuous tuner spaces (e.g. small variations of the preliminary tuners may not lead to variations of v). Gradient-based optimizers are not applicable but the algorithm must be capable to deal with the non-convex and partly discrete optimization. Therefore, this part of the study used an implementation of an evolutionary strategy algorithm, with self-adaptation of the mutation variation (Eiben and Smith, 2007).[5] The genetic algorithm search method is based on evolution principles, which guarantee the survival of the fittest individuals. Bounds on variables can be employed by penalty function techniques. Details on mutation and ranking schemes can be found in (Joos, 2017). The multi-objective optimization was implemented using the MATLAB-based DLR-SR optimization environment "MOPS" (Joos et al., 2002). A short background on the tool can be found in chapter A1.1.

3.3.2 Discussion of results

In the following, some characteristics of the optimized design are discussed qualitatively. Quantitative results are very specific to the design and are not of general interest, and may not be shared due to intellectual property limitations.

Figure 3.3 shows the optimization analysis window of the best weight result, at a pole-pair number of 3. In the plot, the mass of the machine (green) is scaled in relation to the original implementation (black line, "1"); the constraints (red) are scaled to their limits (black line, "1"). It appears, that the optimization is constraint by: 1) the thermal design (max_temperatures); the oil-spray cooling has to convey copper, iron and mechanical losses. 2) the maximum mechanical shear stress limits (sigma_rotoryoke1). High values are indicators of efficient designs. At the same time, the mechanical design has to withstand the stress. Some general values of shear stress are reported in (J. R. Hendershot and Miller, 1994) where aerospace machines are known to be in the region of 20 to 35 kPa, compared to 4 to 15 for standard industrial motors not smaller than one kW.

All limitations of the thermal design and from shear stress are in line with the expectations. Furthermore the design is constraint by 3) the maximum excitation current and 4) the minimum rotor tooth root. Both can be seen as tuner values. For the airgap, the minimum value is taken by the optimization. This is also in line with the expectations, since all these tuners are not necessarily constrained by analytic considerations; the limits are feasibility limits from manufacturing, material properties and design considerations.

---

[5]In the next chapter, an advanced study is proposed, based on a derivation of the genetic algorithm "NSGA2"
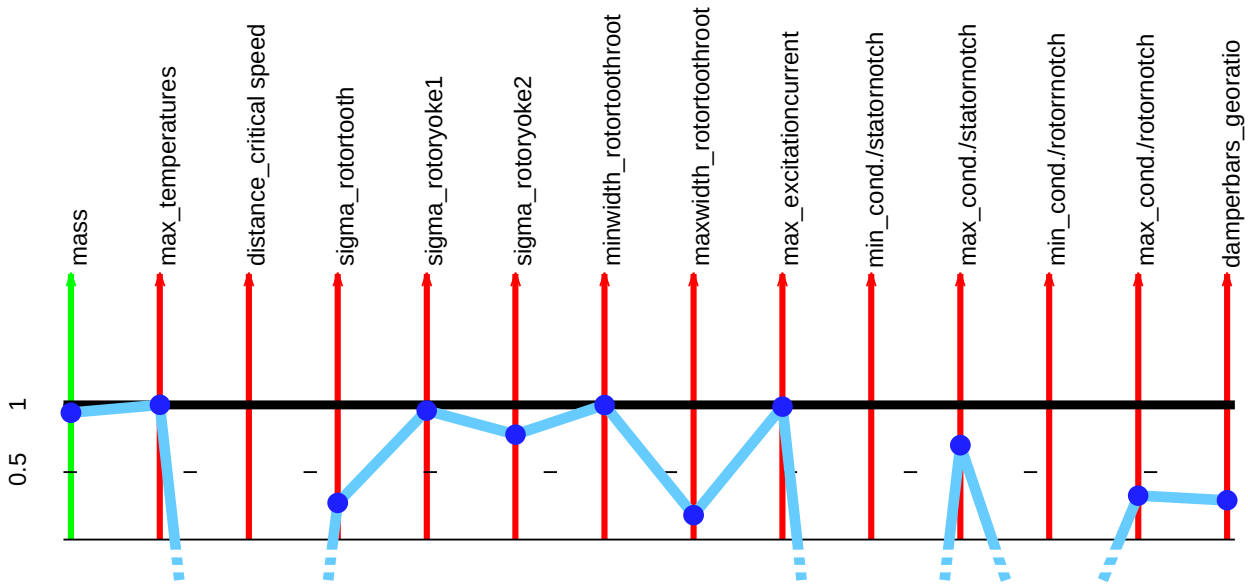
Figure 3.3: Optimization of generator for weight for p=3, result as displayed by MOPS
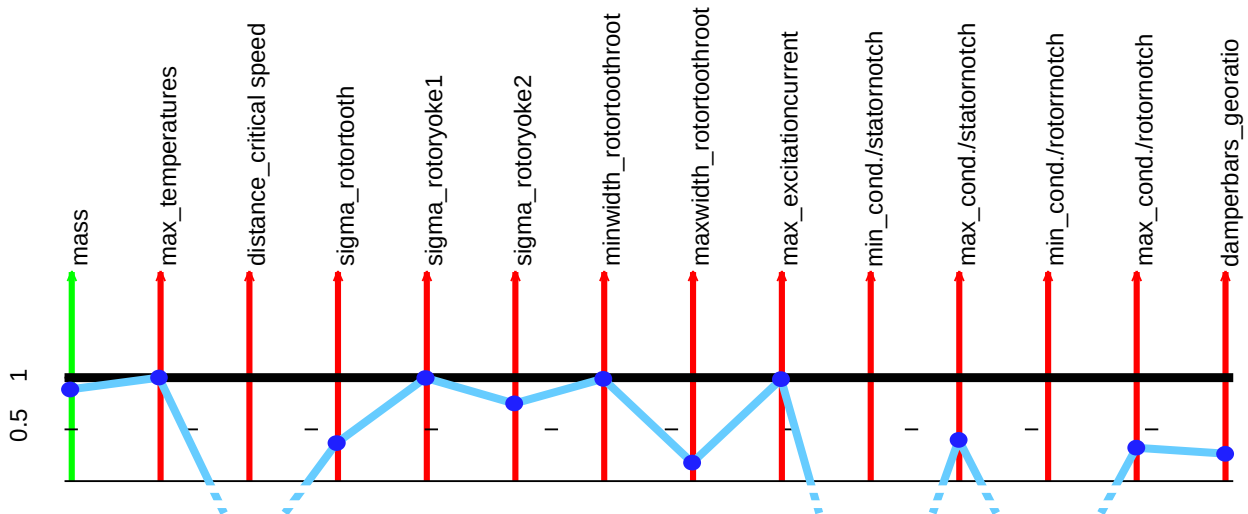
Figure 3.4: Optimization of generator for weight for p=4, result as displayed by MOPS

The results for a pole pair number of 4 can be seen in Figure 3.4. The result is feasible, with similar properties as the case p=3.

For a pole-pair number of 2, the mechanical speed is the highest of the three designs $(f_m = f_e / p)$. Figure 3.5 shows the final result of the optimization. The optimization result indicates a very compact design, which can not be realized due to the constraints. But some qualitative statements can be provided: the design demands excessive shear stress. It could be reduced by choosing smaller (rotor) diameters, with less electric loading (see relations in (Boglietti et al., 2010), "rotor diameter"). But the rotor's diameter has to be wide enough to have a first-order resonance frequency of the machine's shaft, well above the synchronous speed (see (Boglietti et al., 2010), Equation (1)) to avoid mechanical interaction. Furthermore, the rotor teeth would become too fragile.
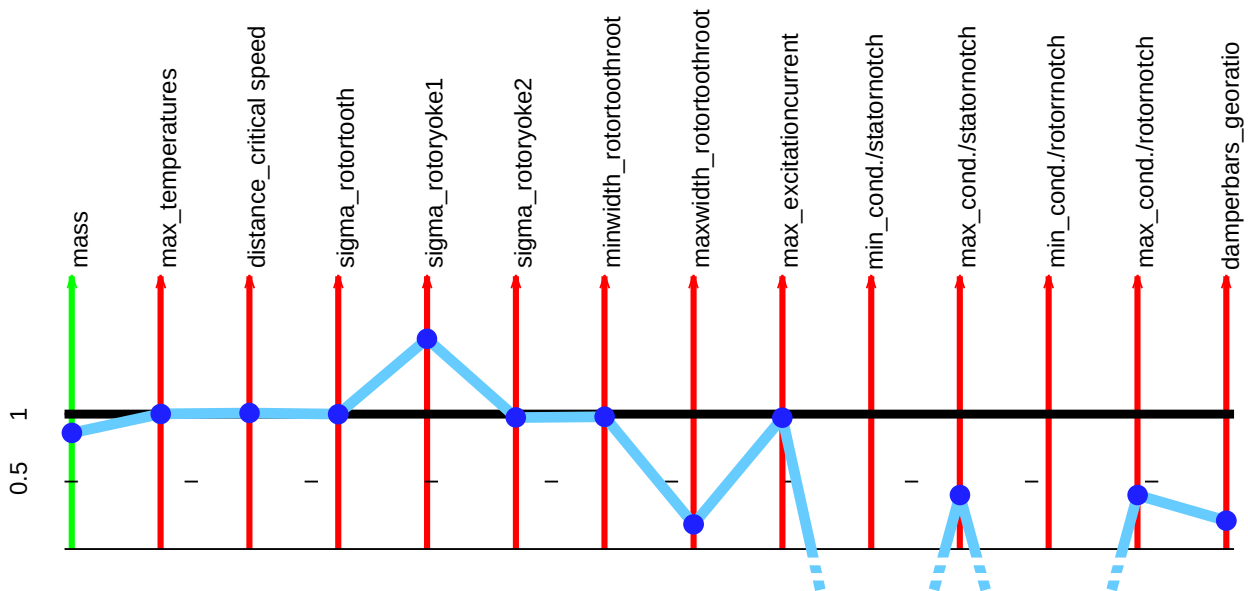
Figure 3.5: Optimization of generator for weight for p=2, result as displayed by MOPS

In Table 4 the weights, yoke heights, rotor excitation current, iron lengths and bore diameter are displayed in relation to the baseline (non-optimized) design.

	p=2 (constraint violation)	*p=3*	*p=4*	*p=3 (baseline)*
Total weight	(0.86)	0.89	0.94	1
Yoke stator height	1.00	0.89	0.82	1
Yoke rotor height	1.04	0.80	0.75	1
Rotor excitation current	1.30	1.31	1.32	1
Iron length	0.89	1.02	0.85	1
Bore diameter	0.88	1.01	1.25	1

Table 4:Results from multi-case optimization

The following conclusions can be drawn from the results:

1) It is known, that by increasing the number of poles, the stator and rotor yoke thickness hcs and rcs is reduced. Approximately, the yoke's thickness t_y is given by (Soong, 2008) with bore/rotor diameter D_r:

$$t_y \sim \frac{D_r}{p} \tag{89}$$

This relationship is verified by the results.

2) All optimized designs tend to use the maximum possible excitation current and minimum air-gap width.

3) Designs with a higher number of pole-pairs tend to have higher diameters at lower lengths.

The result with a pole pair number of 3 is the lightest of the feasible designs. Compared to the original, manually-tuned baseline implementation, there is mainly a reduction of the yoke widths.

The advanced setup with multi-objective optimization could reduce the weight of the generator layout by around 11%, compared to the original industrial design.

The designs are visualized by 3D sketches in Figure 3.6. The CATIA models (Dassault Systèmes, 2017) are built directly from the optimization environment, via a newly developed interface (Kuchar, 2012). Obviously, the design with p=4, has a much larger diameter. The interpretation of the manufacturing-specific aspects has to be left to specialists.
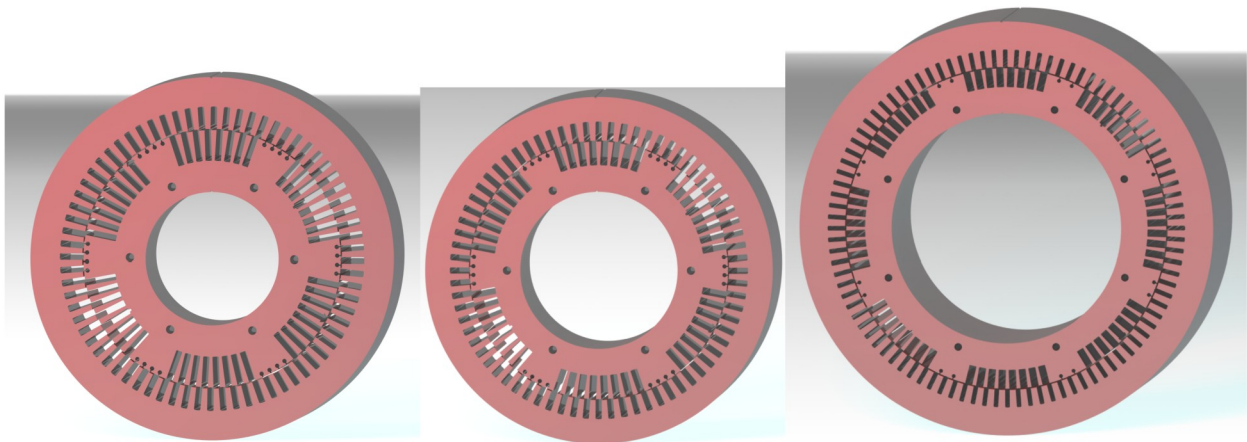
Figure 3.6: 3D sketches of generator designs; 1) baseline p=3, 2) optimized p=3, 3) optimized p=4

The design was validated with the manufacturer and was confirmed to be valid and superior to the old design in terms of weight. It was also stated that this optimization with single-objectives, gives little information to the designer in terms of trade-offs with other criteria and parameter influence. This limitation shall be overcome in the next chapter.

3.4 Generator design extension for power quality

The last chapter presented a multi-objective optimization setup for sizing of the on-board electrical generators. The results can be understood by an engineer with a strong background in machine design, but the degrees of freedom in the design may not be clear, and sensitivities of the results to the tuners are not visible. Furthermore the design does not consider criteria for power quality from generator-network interactions.

The following chapter deduces a novel extension for quantification of the impact of design choices to the power quality. At the same time, the optimization for Pareto-optimal solutions allows convenient visualizations, which clearly link the parameters, tuners and output results.

3.4.1 Design of AC power quality via negative sequence inductance

In the case of the rectifier load being the only load to the generator, the voltage waveform would be of little concern. In this case, the machine's output voltage may even be set by machine design to be

more square-like, rather than sinusoidal, for the purpose of smooth DC voltage. In case of a mixed-AC and passive rectifier load, the stringent standards for good power quality of the voltage wave-form apply. It was of high interest for the generator supplier, to get information on potential design choices in the generator design, which influence the propagation of harmonics in the AC distribution network.

For a better understanding of the problem, a typical waveform of the generator AC output voltage at rectified loading is displayed in Figure 3.7. It shows the simulation result of the output voltage of the Thales generator model, loaded with 25% six pulse rectified loading. Deviations from the ideal sinusoidal waveform are clearly visible. All measures on waveform distortions apply on the phase to neutral voltages.
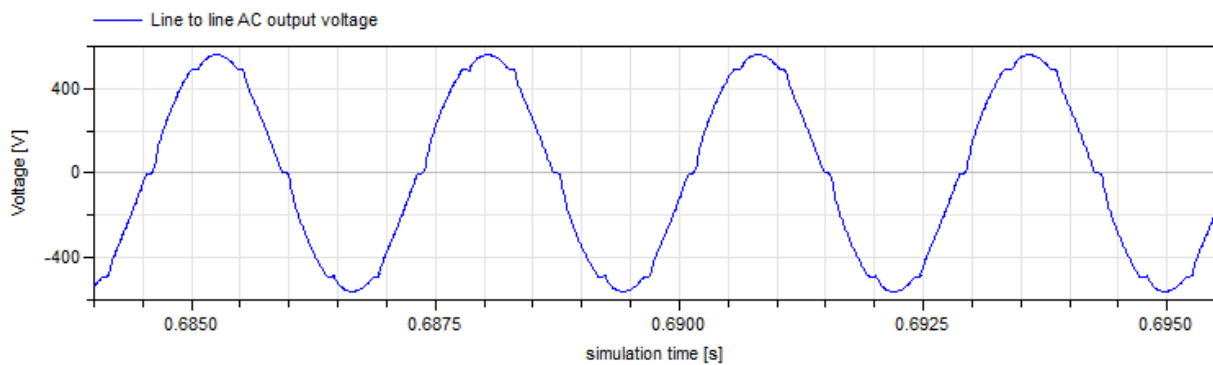
Figure 3.7: Example of line to line AC output voltage at rectified load

Improvements on the generator side may not only lead to better power quality, but may be directly related to it, to weight savings in a load's passive filters or prevention of expensive and reliability-decreasing electronic equipment. At the TEOS III forum in Barcelona 2009, Airbus representatives called filter weights the main show-stoppers for an all-DC electrical network.

Seizing for generator optimal weight and AC-power quality, could be implemented by a simultaneous optimization of the Thales design function and time domain simulation. The MATLAB based design function generates the necessary information of the machine's parameters for simulation. Measures for power quality could be extracted from the results of a behavioral simulation. While this is possible in theory, it is not feasible due to the amount of iterations needed for the MATLAB function, and disproportionately longer evaluation time for simulation. Typical characteristic values can be seen in Table 5.

Task execution time of MATLAB based design function of the generator	Dymola, simulation execution time for simulation of 0.5 s
0.5 s	100 s

Table 5: Characteristic values for calculation times

As can be seen, the calculation time between evaluating the MATLAB function of the analytic design rules and performing a simulation with Dymola, differs by two orders of magnitude. Generating the CAD model with CATIA would even take 180 seconds. The amount of iterations can be reduced, if only valid tuner combinations which lead to feasible results of the MATLAB function,

are further investigated by simulation. This would typically reduce the evaluations by roughly 80% (e.g. from 375000 evaluations to 70000 for p=3, leading to a minimum of 81 days total simulation time).

Alternatively, in literature, such as (Bonwick, 1980), theoretical and practical investigations on qualitative relations between harmonic content of passively-rectified AC circuits and generator parameters can be found. The study assumes a generator with zero saliency, and only rectified load. A high DC-side inductance is assumed, which causes continuous current to the DC load resistor r_L. In this case, the distortion of the AC line waveform can be analytically calculated, with the commutation angle γ:

$$distortion\,[\,per\,unit\,R.M.S\,]=\sqrt{\frac{3}{2\pi}\left(\gamma-\frac{\sin 2\gamma}{2}\right)} \tag{90}$$

(Bonwick, 1980). The commutation angle can be related to load ratio λ by

$$\gamma=acos\left(\frac{\lambda-1}{\lambda+1}\right) \tag{91}$$

The loadratio is the ratio of load resistance to the d-axis synchronous impedance

$$\lambda=\frac{r_L}{\frac{3}{\pi}\omega L_d^{'}} \tag{92}$$

The term d-axis "transient inductance" $L_d^{'}$, refers to lower frequent operational inductance, with frequencies up to the machine's characteristic frequency. The reduced-order transient equations are representative for electrical transient behavior of the machine during the early part of the transient period, assuming the field flux linkages remaining constant. $L_d^{'}$ is calculated by

$$L_d^{'}=L_d-\frac{L_{md}^2}{L_{fd}^{'}} \tag{93}$$

(Krause et al.(2002), 5.12); (for machine variables, see modeling section).

The plot of load ratio versus distortion is shown in Figure 3.8. As an important result it can be seen, the distortion can be decreased with the portion of the synchronous inductance. The result was validated experimentally in (Bonwick, 1980) and showed good congruence.
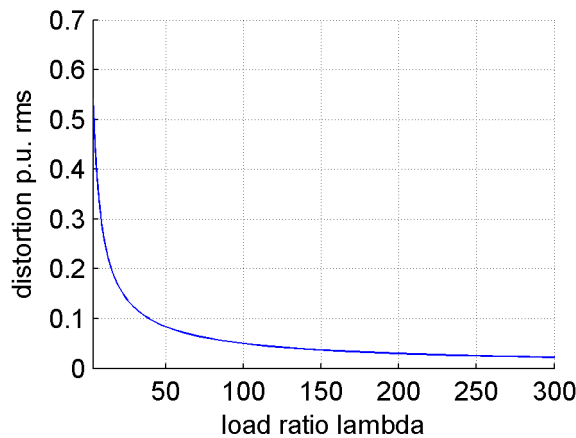
Figure 3.8: Voltage waveform distortion vs. load ratio

While (Bonwick, 1980) proposes to relate the distortion to the synchronous inductance, for machine with dampers the "subtransient inductances" are seen as more applicable. For the rectifier, in (Bing et al., 2009) the derivation of the spectrum and impedance of passively commutated six-pulse rectifiers can be found (see chapter 4.3.1). The rectifiers add significant positive sequence harmonics in the fifth harmonic and negative sequence harmonics in the seventh harmonic. For these high-frequency oscillations in the generator's terminals, well above the synchronous frequency, the operational impedance of the machine can be approximated by the subtransient inductances (or reactances $X = \omega_b \cdot L$):

$$
\begin{aligned}
L_q(\infty) &= L_q^{''} \\
L_d(\infty) &= L_d^{''}
\end{aligned}
\tag{94}
$$

with

$$
\begin{aligned}
L_q^{''} &= L_{ls} + \frac{L_{mq} L_{lkq1} L_{lkq2}}{L_{mq} L_{lkq1} + L_{mq} L_{lkq2} + L_{lkq1} L_{lkq2}} \\
L_d^{''} &= L_{ls} + \frac{L_{md} L_{lfd} L_{lkd}}{L_{md} L_{lfd} + L_{md} L_{lkd} + L_{lfd} L_{lkd}}
\end{aligned}
\tag{95}
$$

(Krause et al., 2002), 7.4-8/7.4-9), with two damper inductance in q axis L_{lkq1}, L_{lkq2} and one in d axis L_{lkd}.

In addition to the inductance (Bonwick, 1980) relates the voltage waveform destortion to the saliency in the machine. While the Thales machine was designed for low saliency, for higher frequencies the dampers do attenuate the saliency even more. Most machines are equipped with dedicated damper windings which limit high frequent voltage and torque distortions. Eddy currents in the iron core can also act as dampers. This parallel path is usually included in the damper inductance. Its analytical calculation in the machine design process stays ambitious, even with FEM calculation.

The high frequent noise interacts with both, d and q axis sub-transient impedances. In case $L_d^{''}$ and $L_q^{''}$ are similar, due to the turbo design with dampers, one can relate the high frequency noise to the mean of both. This is the so-called negative sequence inductance: $L_n = (L_d^{''} + L_q^{''})/2$. Therefore, it is assumed that current oscillations in the AC network coming from the rectifier, can be best damped by low L_n input impedance.

In any case, idealized modeling assumptions have to be treated with caution, since damper-winding time constants are fast and the error between approximation and detailed simulation might therefore be significant. While (Bonwick, 1980) derived many transient equations, some lack of accuracy was mentioned, as accurate simulation was not yet possible in the 1970s. Also (Krause et al., 2002) notes, that analytical calculation of transient behavior may be outnumbered by the possibility of detailed simulations.

Nevertheless, the basic conclusions stay valid:

- Saliency in the machine results in larger distortions.
- Dampers do attenuation on the saliency for higher frequencies.
- Low ratio of generator impedances in relation to load resistance lowers the distortion.
- From consideration of the rectifier it was found that the negative sequence inductance applies.

Therefore, for low saliency designs, the minimization of the power quality criterion "Total Harmonic Distortion" should give the same power quality optimal solution in the tuners X_q as the minimization of the negative sequence:

$$THD(X_q) = \begin{cases} \underset{x}{min} \, THD(X) \\ subject \; to \, \boldsymbol{constr}(X) \leq \boldsymbol{0} \end{cases} \Leftrightarrow \quad L_n(X_q) = \begin{cases} \underset{x}{min} \, L_n(X) \\ subject \; to \, \boldsymbol{constr}(X) \leq \boldsymbol{0} \end{cases} \tag{96}$$

The inductance/reactances in Equation (95) can be derived analytically from the machine parametrization at X_q. They are outputs of the Thales design function.

In the last chapter, a genetic algorithm-based optimization for the single objective "generator weight", with constraints was performed. But, a single-objective optimization for power quality or a combined criterion of power quality and weight is seen as not-informative. Instead, the dependencies of weight versus power quality are needed. This is the set of Pareto-optimal solutions of the antagonistic criteria, known as Pareto front.

A typical solution is shown in Figure 3.9. It is possible to generate the Pareto front by single-objective optimization and iterative change of a weighting ratio of the criteria. For a two-criteria optimization problem this is

$$crit_{new} = scale \cdot crit_1 + (1 - scale) \cdot crit_2 \tag{97}$$

with a weighting ratio *scale*.

Instead, multi-objective evolutionary algorithms are known to find multiple Pareto-optimal solutions in one single optimization run. All genetic algorithms are based on a "population" of solutions. This can be extended to maintain a diverse set of solutions. The individual solutions are ranked 1)
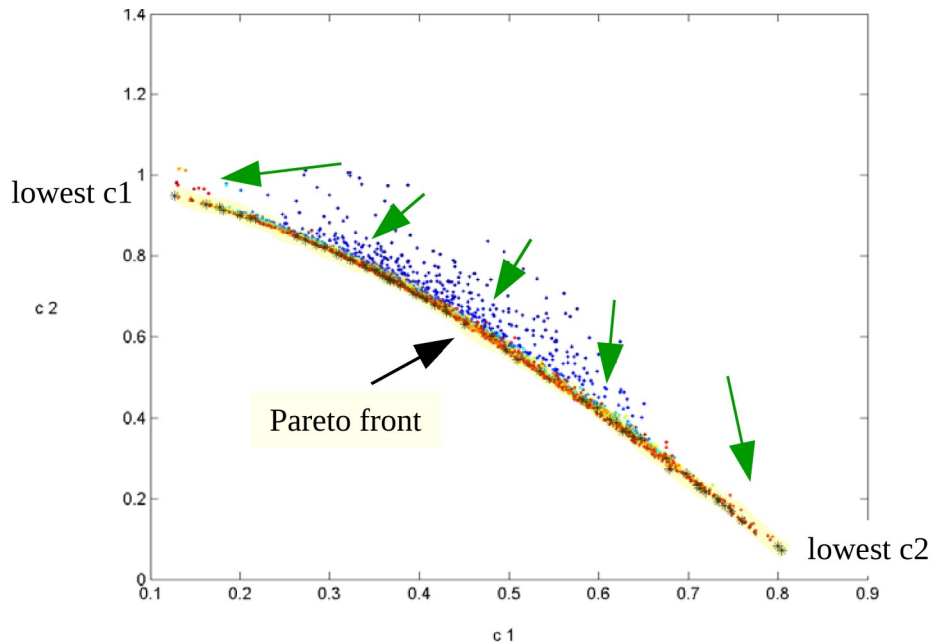
Figure 3.9: Typical solution of Pareto-optimal sorting algorithm; source: (Joos, 2017)

by their "fitness"; this means in relation to all criteria 2) and their diversity, which favors distant solutions of the equally ranked ones. By using this, it is possible to find multiple Pareto-optimal solutions in one single optimization run.

For the dependency analysis, the popular Non-dominated Sorting-based Multi-objective Genetic Algorithm "NSGA-II" (Deb et al., 2002), was selected. It is reported to be well suited for non-convex optimization problems and computational complexity was proven to be low in comparison to equivalent methods (see Deb et al.(2002)). Figure 3.9 shows typical results using this algorithm: Early scattered solutions (blue) tend to propagate to the Pareto front (yellow) after several iterations. Pareto fronts only exist in case the criteria rely on the same cost function, and an optimum of a criterion can only be found at the cost of another. For the details of the implementation, see (Joos, 2017) .

The Pareto-optimal set of tuner combinations $\{X\}_{pareto} \in \mathbf{X}$ within the space of feasible solutions $\mathbf{X}$ can be also expressed mathematically: With the objectives generator weight $w_i = wfunc(X_i)$ from a function *wfunc* of the tuners, and the negative sequence inductance $n_i = nfunc(X_i)$, as a function *nfunc* of the tuners, the set of Pareto-optimal tuner combinations is the solution of an optimization problem, such that

$$
\begin{aligned}
no\ solution\{\boldsymbol{X}\}_{\boldsymbol{Pareto2}}\ exists\ , such\ \ that\ \ \{w\}_{Pareto2}\ \ dominates\ \ \{n\}_{Pareto} \\
where\ dominate\ means \\
\forall\, i \in \{1,..,d\}: w_i(\boldsymbol{X}_i) \le n_i(\boldsymbol{X}_i) \wedge \\
\exists\, i \in \{1,..,d\}: w_i(\boldsymbol{X}_i) < n_i(\boldsymbol{X}_i)
\end{aligned}
\tag{98}
$$

Using Pareto-based optimization is new for the Thales design. In (Besnerais et al., 2008) a similar approach was proposed for an optimization of an induction machine.

3.4.2 Preliminary results and discussion

The optimization tool "MOPS" (Joos et al., 2002) was applied, again, to tune the input variables of the generator analytical design function. This work could benefit from and contribute to a parallel
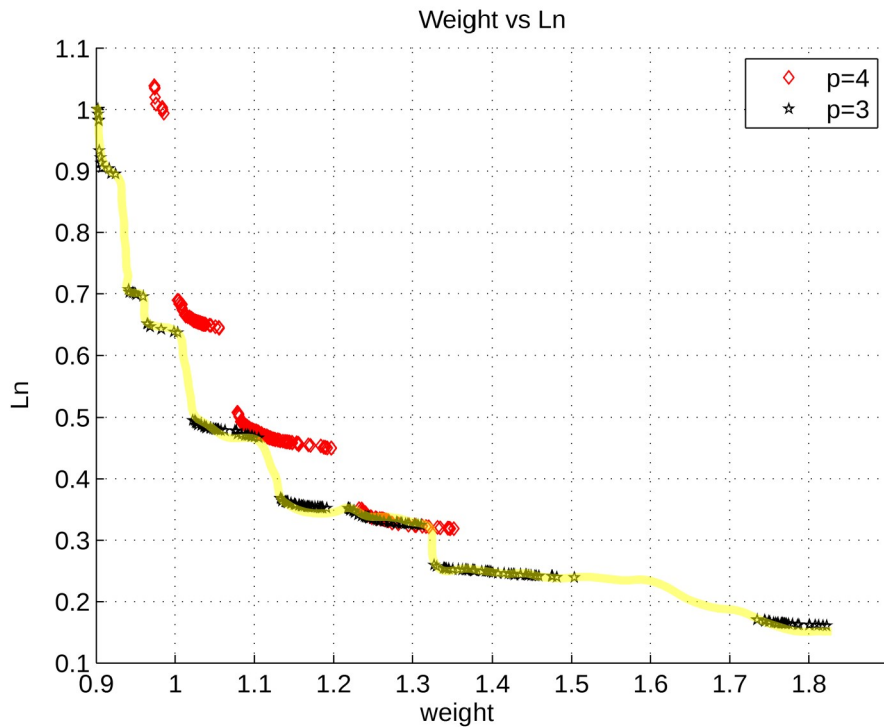
Figure 3.10: Pareto fronts of Weight vs. Ln (normalized by values of baseline design)

adaption activity of the NSGAII-adaption to MOPS. As design criteria, the generator's weight and negative sequence inductance L_n were taken, while constraints had to be maintained. Earlier, it was found that a pole-pair number of 2 does not give feasible results, p=3 gives the best weight designs and p=4 designs tend to be slightly heavier. Therefore, for the Pareto optimization, optimizations were only performed with a pole-pair number of three and four successively.

The results are displayed in Figure 3.10. Weight and L_n are normalized by the nominal values of the baseline design. The plot shows the Pareto-front of optimal solutions for low L_n and low weight for generators with a pole pair number of p=3 and p=4. Obviously, the two design targets are contradictory. Meaning, there are degrees of freedom in the design, to improve power quality by using lower L_n. This comes at the expense of more weight. Also, it can be seen that the design with the best weight can be realized with an equally good L_n as the baseline. The p=4 designs do not show any beneficial areas compared to p=3 designs.

In Figure 3.11 the negative sequence inductance versus some selected design variables are displayed. Again, all results are normalized to protect the intellectual property. In the upper-left sub-figure, from all feasible results, the weight versus L_n Pareto-optimal solutions are displayed in color. Those data points coincide with the colored points in the other sub-plots. Obvious correla-
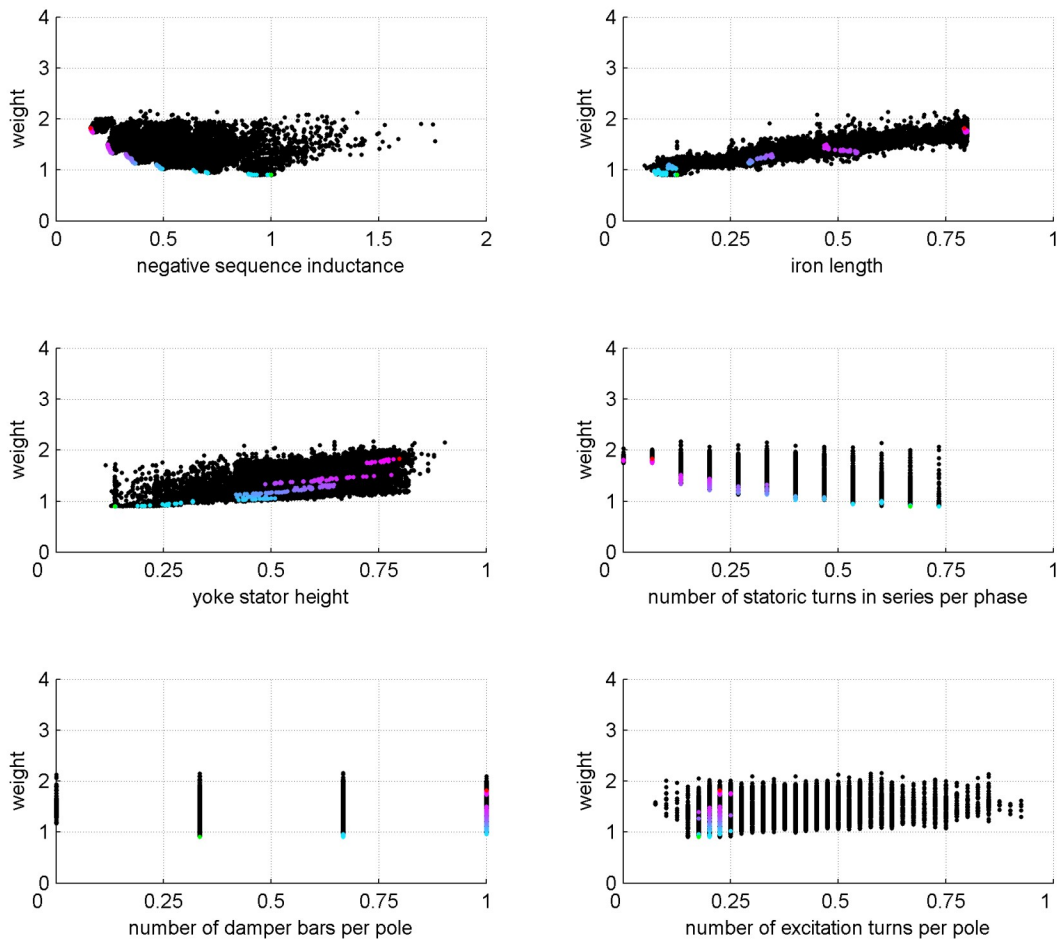
Figure 3.11: Optimization results (p=3, normalized and qualitative only results w/o unit, weight and Ln normalized by baseline results, other variables [0..1]); ♦ feasible design; ♦ lowest Ln-design; ♦ lowest weight design

tions between the Pareto data and tuning variables can be seen, for example, for the iron length and yoke stator height. Low weight machines tend to have a shorter iron core and lower height of the yoke, than low impedance machines. The lower inductance of the machine is gained by a reduced number of winding turns for each coil (number of statoric turns), while the area of the coil grows with the larger length. Also the strong damping (number of damper bars) has an effect. The plots show that the number of damper bars can not be varied arbitrarily (by design), but only in integral numbers. The last (bottom-right) plot, shows the number of excitation turns per pole in the rotor. This is selected for demonstration purposes, there do not necessarily exist clear and distinct relations between all tuners and the Pareto front of the criteria.

While not shown here, all insights are equally applicable to the designs with a pole-pair number of four. Some more relationships between machine characteristics and L_n vs. weight will be given in the next chapter.

In summary, by the method of optimization with Pareto-optimal solutions, design trade-offs can be visualized to support the design engineer. Freedoms in the design can be detected, which influence the negative sequence inductance; this is postulated to be correlated to AC power quality.

3.4.3 Extension for quantitative estimation of AC power quality

The consideration of the negative sequence impedance raises the awareness of power quality in the design, but can not deliver quantitative measures. Very good information can be added through extra time-domain simulation of the generator model in an electrical network. But, as pointed out before, the calculation time between evaluating the MATLAB function of the analytic design rules and performing a simulation with the behavioral model in Dymola, differs by two orders of magnitude. In a generator optimization study, the typical number of performed evaluations was found to be in the region of 375000. This inhibits the direct use of the long Dymola simulations in every optimization step.
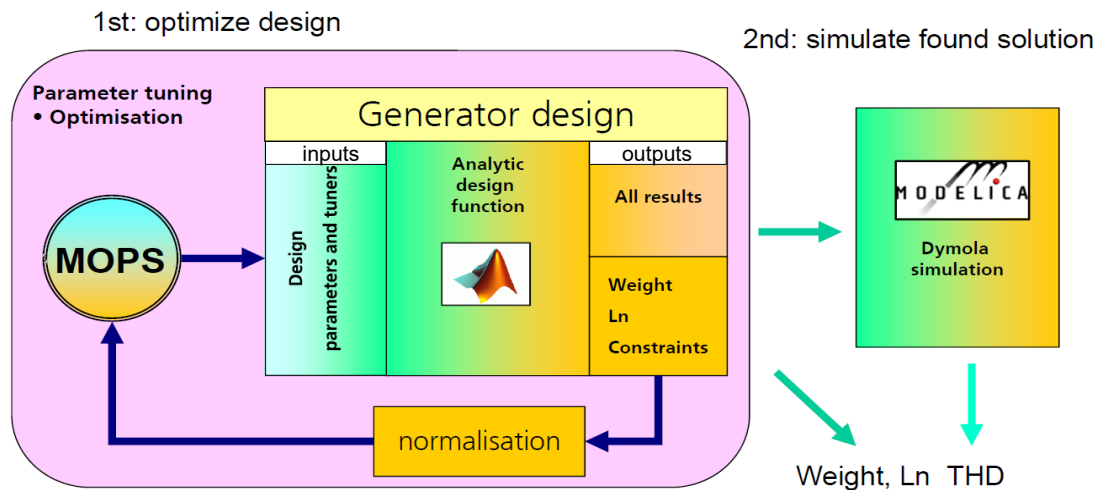
Figure 3.12: Optimization tool chain

Instead of performing optimizations with the criterion weight from the "fast" analytic function and power quality from the time-domain simulation simultaneously, the knowledge of relationships between power quality and some generator parameters can be utilized. The generator's saliency, as the main source of voltage distortions in conjunction with passively commutated rectifiers, can be limited by design choices. The other main drivers for voltage distortion are the generator's inductances, which are effective for higher frequencies. Since negative sequence inductance

$L_n = \left(L_d'' + L_q'' \right)/2$ is a good approximation of all sub-transient inductances, the qualitative relationship between L_n and power quality can be exploited to:

- optimize the design for
  - low L_n and
  - weight, while
  - adhering the constraints
- and find possible Pareto-optimal, qualitative relations between the criteria,
- add the quantitative relationship between L_n and power quality – here: total harmonic distortion-in a downstream process step.

The proposed extended optimization tool-chain is visualized in Figure 3.12, with the "Analytic design function" from Thales.

For the power quality investigation, a generator model with saturation, harmonic content and inclusion of damper circuits in both d and q-axis is established. The model equations are given in chapter 2.3.1. Generator parameters are inputs from the MATLAB design routine. The AC frequency was set to 360Hz by the mechanical shaft.

(Krause et al., 2002) note that for dynamic and transient stability considerations of solid iron rotor machines, at least two damper windings in q axis and two damper windings in d axis should be taken into account. They are associated to the transient inductance respectively sub-transient inductance, in d and q axes. Sometimes, the additional dampers are called "Canay-reactances", e.g. (Wamkeue-R et al., 1998). Those dampers take into account the damper bars, but also eddy currents in the rotor. It is not common to calculate more than one damper for each axis in early machine design. This requires detailed investigations through 2D-finite element electromagnetic calculations or measurements.

The combined electrical load to the AC network is 150kVA. This consists of 75% linear resistive load, and 25% rectifier non-linear switching load. No filters for common or differential-mode harmonics were taken into account. The share of non-linear load is in line with the consumption in classic airplane architectures. The demands on power quality were taken analogously to industrial standards (STD-704F, 2004) and (ABD100.1.8, 2002), see Table 6.

Limit name	Equation with Fourier coefficients A	Limit for voltage
Total Harmonic Distortion (THD) in relation to base harmonic content	$$THD = \sqrt{\frac{\sum_{h=2}^{M} A\left[h \cdot f_{base}\right]^2}{A\left[f_{base}\right]^2}}$$	11%
Individual Harmonic Content (IHC) in relation to base harmonic content	$$IHC = \max_{h \in 2..M} \left| \frac{A\left[h \cdot f_{base}\right]}{A\left[f_{base}\right]} \right|$$	7.5%

Table 6: Power Quality limits

For simulation, the electrical onboard network is strictly simplified with one concentrated rectified load and one concentrated resistive load. Only feeder impedances are taken into account, but no distribution lines. A screenshot of the simulation model is given in Figure 3.13. The parameterized generator model (left) feeds linear resistive/inductive AC load (top right), and non-linear switching
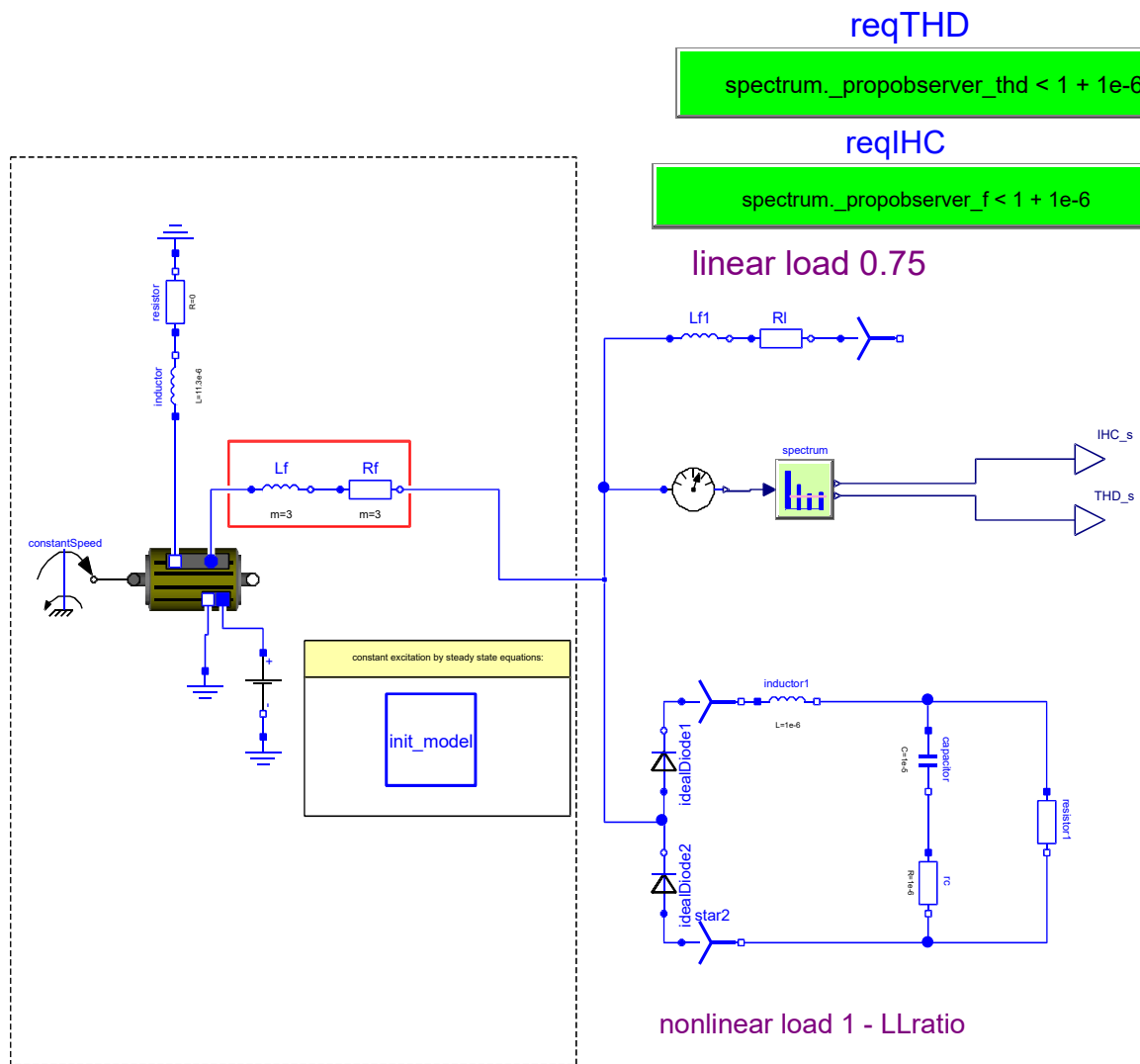
Figure 3.13: Simulation model for testing on power quality, with mixed AC/rectified load; in Dy-mola

rectified load (bottom right) via a feeder line (Lf/Rf). The "spectrum observer" block in-between the linear load and the rectifier DC load, checks the Total Harmonic Distortion (THD) and Individual Harmonic Content (IHC) of the AC line voltage against the industrial standards. The output information of the simulation are IHC and THD. Details on the efficient implementation of this non-standard block can be found in the appendix. The generator model is discussed in section 2.3.1. The original implementation of the generator includes equations for consideration of triple-space-harmonics, with parameters identified by hardware measurements. Since no methods were known to the research consortium to calculate the specific parameters in the analytic machine design phase, the effects are ignored in all proposed processing and simulation steps. This does not limit the validity of any of the newly developed methods and tool-chains, but motivates for research on finding of the parameters in early machine design stages.
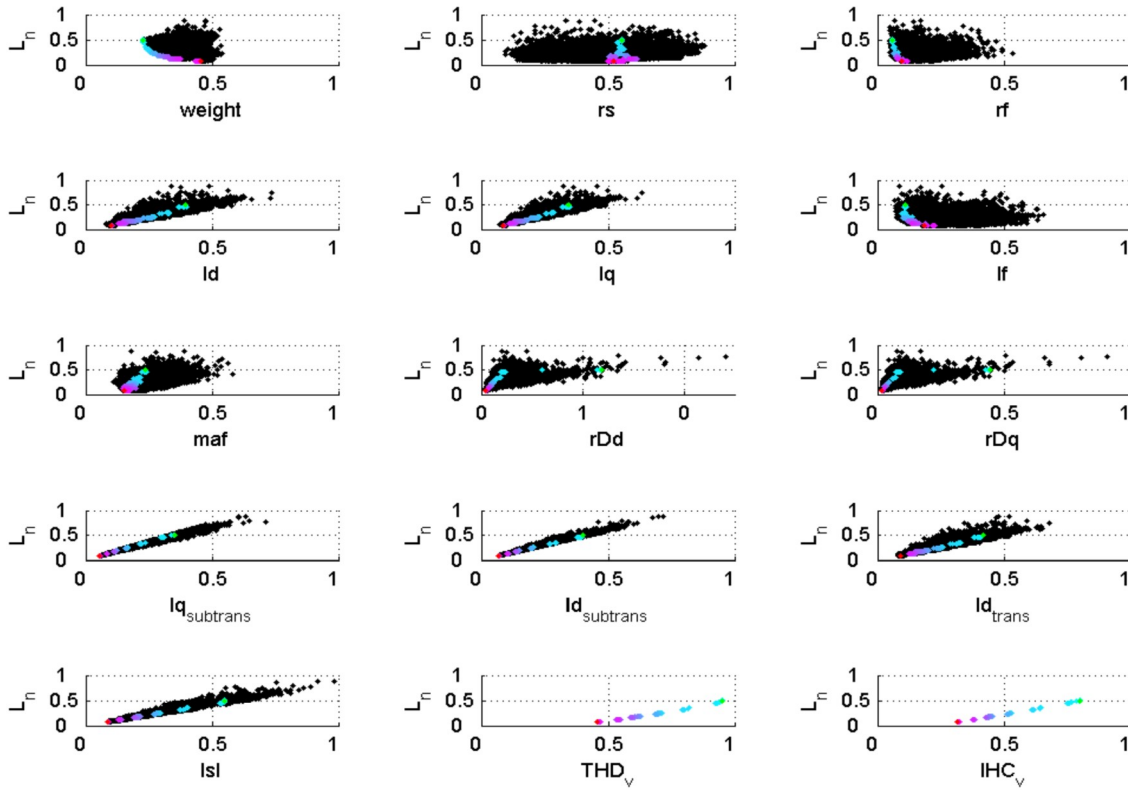
Figure 3.14: Optimization results (p=3, normalized results [0..1]); ♦ feasible design; ♦ lowest Ln-design; ♦ lowest weight design; [rs=phase stator resistance; rf= field resistance; ld= d axis synchronous inductance; lq= q axis synchronous inductance; lf= field inductance; maf= mutual inductance between the field and the armature windings; rDd= damper resistance d axis; rDq= damper resistance q axis; lq_subtrans= subtransient inductance q axis; ld_subtrans= subtransient inductance d axis; ld_trans= transient inductance d axis, lsl= stator leakage inductance, THD= total harmonic distortion (time domain simulation); IHC= individual harmonic distortion (time domain distortion)]; normalized and qualitative only results w/o unit

In a real aircraft electrical power network, the loads are not concentrated at the end of the feeder lines as linear and non-linear loads; they will be fragmented and distributed. The case of concentrated loads is seen as the most critical one: For example, (Wang and Liu, 2005) found that "the value of THD(%) and [IHC](%) decreases when the number of converters increases, regardless of the selected ranges for firing angle of the AC-to-DC power converters".

Typical calculation times of the MATLAB-based function and Dymola-based function were shown earlier in Table 5. The total simulated time in the time-domain model is 0.5 seconds. This splits into an initial transient phase for 0.45 seconds, to reach a periodic steady-state condition. The data of the following 0.05 seconds of simulated time, were taken as input data to the Fast Fourier Transformation (FFT) algorithm.

The approach for the two-step quantitative characterization of designs on power quality is demonstrated by the results in Figure 3.14. The Pareto-front is a set of roughly 200 elements. They can be seen in the top left weight vs. Ln-diagram. In a second step, every Pareto-front element was

related to a *THD* and *IHC* value by time domain simulations[6]. In Figure 3.14, in the bottom-middle and bottom-right plots, the relationship between voltage *THD* and *IHC* and negative sequence is plotted. Their tight, strictly linear relationship is clearly proven. This confirms the approach for *THD* versus weight investigations, by means of Ln versus weight Pareto optimization. The two-step approach is feasible in terms of a realistic duration of the optimization; the direct approach with parallel optimization of the analytic function and simulation is not.

Figure 3.14 also shows some relationships between generator characteristic parameters and L_n (and therefore power quality). Low L_n/THD designs tend to have lower direct and quadrature axis inductances, than lower weight designs (ld, lq, $lq_{subtrans}$, $ld_{subtrans}$, ld_{trans}, lsl). The magnetic network is optimized by less leakage inductance and more efficient magnetic circuits in the stator. The resistances of the rotor and damper circuits are kept small (rf, rDd, rDq), to get short time constants.

The results do coincide with the insights gained from the tuners-vs.-criteria studies.

In this fictitious example, no industrial standard was violated within a load share of 25% rectified load. But the setup can be used for investigations, to derive quantitative information about the weight cost needed to prevent harmonic over-voltages.

For the implementation of the FFT-based monitor of *THD* and *IHC* see appendix, chapter A3.2. The blocks were designed with special care on numerical efficiency, data storage and intuitive parameterization.

3.4.4 Investigation of maximum non-linear loads for generator designs

As described above, for future aircraft and in enhanced architectures, the installed electrical power tends to grow. At the same time, a trend towards a larger share of rectifier-fed DC loads can be observed, to feed brush-less DC drives and converters. This may have an impact on existing and future generators. Therefore, there is a necessity to know the relationships between the generator's weight, and the portion of non-linear load it can feed without violation of the standards for power quality. This is especially useful for network topology studies.

This information can be obtained with the tools developed above. Low L_n designs-which improve the power quality-can feed larger numbers of switching devices, without violating the standards. The exact number is found by further optimizations: The set of Pareto-optimal L_n versus weight generator candidates is examined, which is plotted in Figure 3.10 (p=3 only). For each Pareto-solution, the maximum proportion of the rectifier load *pload* is identified by simulations, which violates the standard on Total Harmonic Distortion $constr_{THD}$ of Table 6:

$$\left\{ \begin{array}{l} \underset{pload_i}{max} \\ subject\,to \\ constr_{THD}(\boldsymbol{X}_i)=0 \\ pload \in [0..0.9] \end{array} \right\}_{Pareto} \tag{99}$$

As before, it was assumed all rectifier loads in the network can be substituted by one concentrated element. The same applies for the AC loads.

The results of the optimization can be seen in Figure 3.15. Obviously, there is qualitative relation between the elements of the L_n versus weight plots and the maximum proportion of non-linear

---

[6]Optimization with NSGAII-algorithm, distributed computation on a 32 kernel Linux cluster took around 26 hours. Time domain simulation with the 200 Pareto-optimal results was performed on a single Windows PC, with 11 minutes per simulation (Dymola 2016); computations could have been parallelized as well
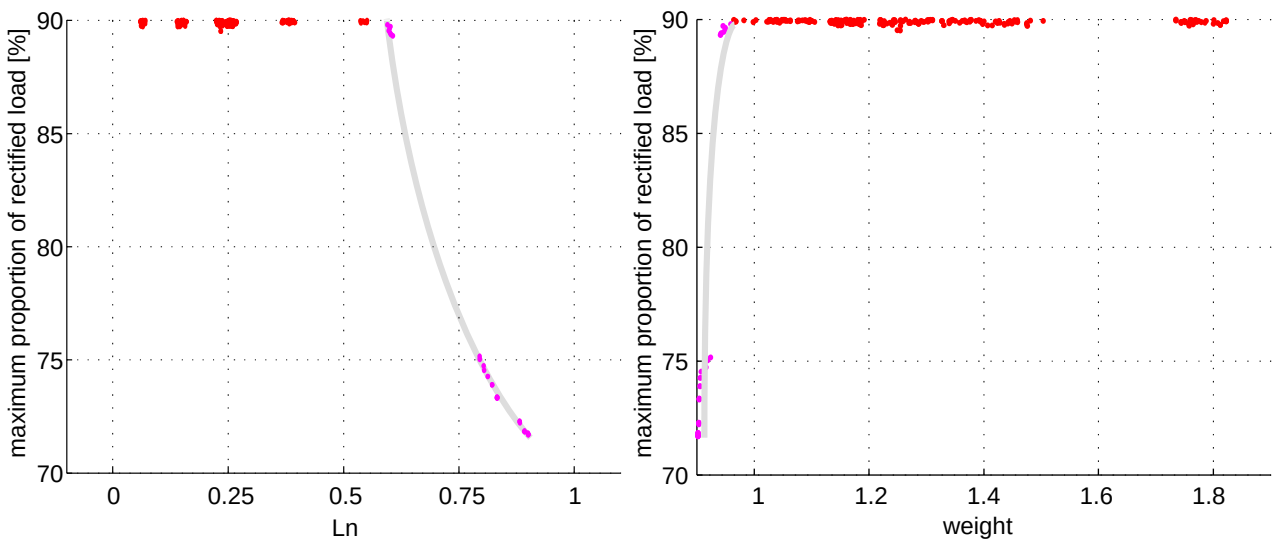
Figure 3.15: L_n versus maximum portion of nonlinear load (Ln normalized [0..1],weight normalized by nominal weight of baseline design); red dots: solution constrained in pload; grey line: trend

load. Again, this type of generator is quite robust against a higher ratio of rectified load which by far exceeds the demand.

3.5 Summary

In this chapter, a design tool-chain was elaborated for an externally-excited synchronous machine taking into account electrical, mechanical and thermal analytical models and finally, network power quality. The pre-existing original design relied on analytical design rules only with manual tuning. This work demonstrated the realization and potential of a multi-objective optimization. The results were analyzed in detail, with a background in machine design, but could not explain design trade-offs from the results. This could be overcome by using a state-of-the-art genetic algorithm. Design trade-offs can be easily explained by the Pareto-front of opposed criteria. Several convenient visualizations of the Pareto results are presented, which clearly link the parameters, tuners and output results.

The second part deals with the relationships of generator design and network power quality. The original generator was built for a classical airplane architecture, with little rectified load. Detailed information of the power quality, defined by industrial standards, can be found via time-domain simulation.

3.6 Contributions

It is not feasible to include the simulation in the optimization directly, because of lengthy simulation times. This work could solve this challenge of combined optimization for weight and power quality
   - *via an intermediate step, optimizing for low negative sequence inductance first and relate the result to power quality in a further simulation-based step.*

By this novel approach,
   - *information on the relationship between weight and power quality could be calculated and analyzed.*

As a further contribution a sophisticated simulation model was constructed with
   - *efficient monitors of power quality, based on Fast Fourier Transformation.*

The implementation of FFT-based blocks for calculation of THD and IHC is discussed in the appendix. There, the blocks are seen in a wider context, for the purpose of specification of demands of the aircraft manufacturer to the suppliers by "executable specifications". Contributions from the author include the transfer of methodology of (Becker and Giese, 2011) and (Otter et al., 2015) for requirements specification with Modelica, minor contributions in the development of Modelica Requirements library, and the concept and main implementation of the numerical efficient and easy-to-parameterize FFT-based property monitors.

Relevant Publications:
- *"Advanced generator design using Paretooptimization" (Kuhn, 2011)*
- *„Modelling and Use of an Aircraft Electrical Network Simulation for Harmonics Consideration in Generator Design" (Kuhn et al., 2012)*
- *"Model Based Specifications in Aircraft Systems Design" (Kuhn et al., 2015)*

4 Improved simulation performance by model simplification and direct steady-state initialization

In the simulation assisted optimization of the generator design, the model had to be simulated with a ramp up phase of 0.05 seconds of simulated time. This is followed by the generation of 0.45 seconds of data, which is later fed to the Fast Fourier Transformation algorithm for extraction of power quality criteria. Therefore, at least 10% of the simulation time is spent generating data which has no use. This share is relevant, if the simulation time is big in relation to the instantiation and processing of the simulation task.

The total time for the simulation is dependent upon

- the complexity of the model, in relation to
- the numerical integration algorithms and solvers,
- the amount of simulated data, consisting of the ramp-up phase and relevant time slot itself,

and, of course, the speed of the computer hardware; this can be a single processor, multi-processor or distributed computer system. Furthermore, the generation of the execution model and post-processing of data could take some time, especially if the pure simulation time is relatively short.

The following chapter deals with potential methods of speeding up the total simulation time through use of model specific simplifications, and initialization capabilities to reduce the ramp-up phase. State-of-the-art methods and a novel approach for model-based and automatic periodic steady-state initialization is discussed. Unless it is mentioned otherwise, single plots are always based upon the baseline parametrization of the machine.

The simulation of the generator was investigated as part of a study on simulation of large-scale electrical systems (Kuhn and Ji, 2014). Some tool specific guidelines for improvement of the simulation speed can be found in the appendix.

4.1 Types of Initialization

The behavioural level of a network model can be described by Differential Algebraic Equation system of the forml[7]:

$$0 = f(\dot{x}, x, y, u, t) \tag{100}$$

Simulation platforms do process this equation system from the (graphical) model. The equation system is of size m with

$$m = dim(x) + dim(y) \tag{101}$$

Where y are the algebraic variables. The equations map the space of variables with the inputs u and t and the (known) state variables x to the unknowns $\dot{x}$ and y:

$$f : \mathbb{R}^{dim(x)+dim(u)+1} \rightarrow \mathbb{R}^{dim(x)+dim(y)} \tag{102}$$

The initial conditions must be a solution of the equation system

$$0 = f(\dot{x}_{0}, x_0, y_0, u_{0,} t_0) \tag{103}$$

In addition to the input u_0 at time t_0, at most $dim(x)$ additional equations f_0 have to be provided since the initial vector x_0 is unknown:

---

[7]The variables are written in a simplified representation without the indication of the time dependency, where $x = x(t)$, $x_0 = x(t_0)$ and so forth.

$$0 = f\left(\dot{x}_{0,} x_0, y_0, u_{0,} t_0\right) \tag{104}$$

The initial value problem involves $2 \cdot dim(x) + dim(y)$ equations or assignments of the unknowns. This number could be smaller if the DAE has an index >1.

Finding consistent initial values for the underlying DAE, can be performed by solvers like Newton's method. In the case of the DAE involving non-linear equations, the solution may not be unique, but is dependent on the chosen start values. The solution is found via the manipulation of some chosen iteration values of the initial value problem. Setting of the iteration values to predicted guess values does improve the convergence speed, and the system will most likely converge to the nearby solution.[8]

Typical methods for setting of initial equations and conditions include:
1. initialization with states at zero with $x(t_0) = 0$,
2. initialization with derivatives at zero $\dot{x}(t_0) = 0$,
3. initialization with given start values $x(t_0) = x_0$ and
4. initialization with additional initial equations $0 = f_0\left(\dot{x}_{0,} x_0, y_0, u_{0,} t_0\right)$, f_0 of size dim(x).

For electrical systems, method 1 is equivalent to the ramp-up from the condition with no voltage. This corresponds to the physical experimentation, but demands the longest simulation time. Method 2 can initialize the steady-state solution of linear time-invariant systems directly, without the need for a simulation of the initial transient phase starting with $x(t_0) = 0$. However, for oscillating systems, such as electrical networks with alternating current (AC), no time-invariant solution for x exists. Method 3 is beneficial for systems, where state conditions or their educated guesses are known. In the initial equation system derived from Equation (100), the state derivatives may not be exactly zero for a non-perfect initial condition. This may effect initial transients in the simulation. Method 4 is the most generic case. Modelica also supports initial algebraic constraints which is a particular highlight of the language.

4.2 Analysis and adaptation of model to constant excitation

This chapter investigates the dynamics of the generator with GCU and possible speeding up of the simulation by constant excitation. Figure 4.1 shows a diagram of the basic simulation model of the AC and DC load connected generator, without the blocks for calculation of power quality standards and breaker circuits. The generator equations are given in the modeling section, chapter 2.3. For the demonstration, the model was simplified; the inductance of $Lfilt$ was set to zero, $Cfilt$ has a capacitance value of 100 μF, the filter resistance $Rfilt$ is set to 1 $\mu \Omega$.

The Generator Control Unit (GCU) has to maintain the 230 Volts AC RMS in the electrical network, independent of the shaft's variable speed and of the load. In aircraft electrical networks, the voltage is not measured at the generator output in the turbine nacelle directly, but at a distant point of regulation to compensate for the voltage drop in the feeder lines (see Figure 4.1, input of GCU). According to the relevant standards, the voltage control may not fail due to asymmetric load.

The control circuit excites the field winding based upon a dynamic control function

$$V_{fd} = F_{GCUdyn}\left(V_{ac}, t\right) \tag{105}$$

---

[8]Simulation environment Dymola does not allow the explicit selection of iteration variables but guess values of variables can be set, which are used in case of selection for iteration variables.
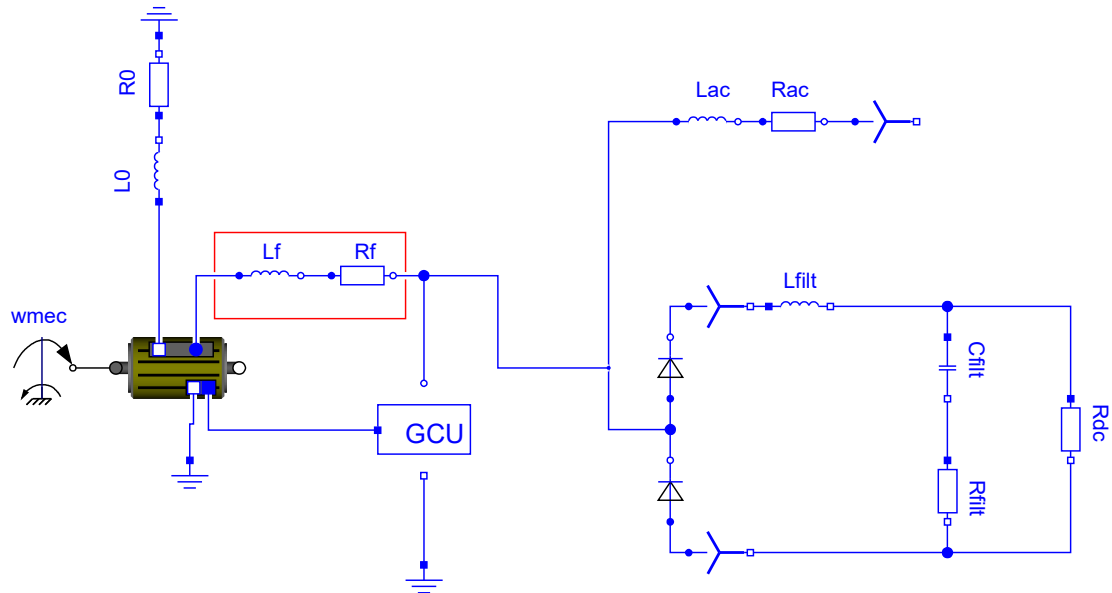
Figure 4.1: Simulation model for power quality, with GCU

Figure 4.2 shows a typical mixed analog/digital realization of the GCU, with analogue voltage sensing, filtering and PI controller. The voltage can be controlled more accurately if the dynamics of the excitation winding is compensated by a current control loop. This requires an additional current sensor.

The total simulation model of Figure 4.1 is processed to an equation system with

- 10 continuous time states (variables with time derivative):
  - 7 states in the generator: $i_{qs}, i_{kq}, i_{ds}, i_{fd}, i_{kd}, [B_{sat}], \varphi_{mec}$; ($B_{sat}$ is no real state, but breaks non-linear equation systems by a first order delay; φ_{mec} is the shaft's mechanical angle)
  - one state from the DC capacitor v_{cfilt}
  - two states in the controller (filter/corrector),
- one linear system with a size of 12 equations.
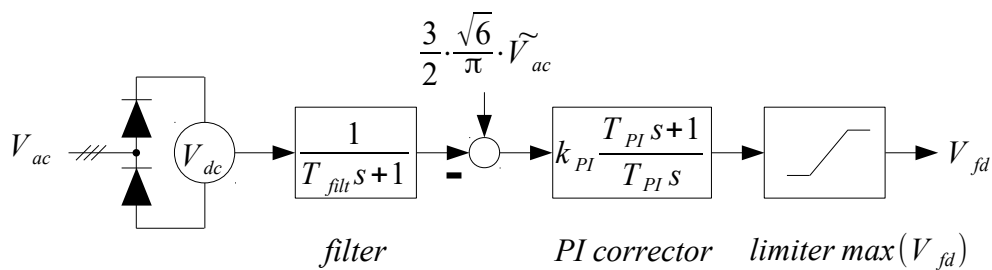
Figure 4.2: Generator Control Unit (realistic model, used for the testing

The model is initialized with all states set to zero. Finding consistent initial values for the detailed GCU is not a trivial task. Even in this case, the initial value problem relies on a 13th order non-linear system of equations and two mixed real/discrete conditions (rectifiers/limiter in GCU).

Figure 4.3 shows the transient plots of two selected variables of the full-scale model. The voltage output ramps up from zero and stabilizes at around 0.5 seconds. The ramp up can be seen even more clearly in the d-axis current.
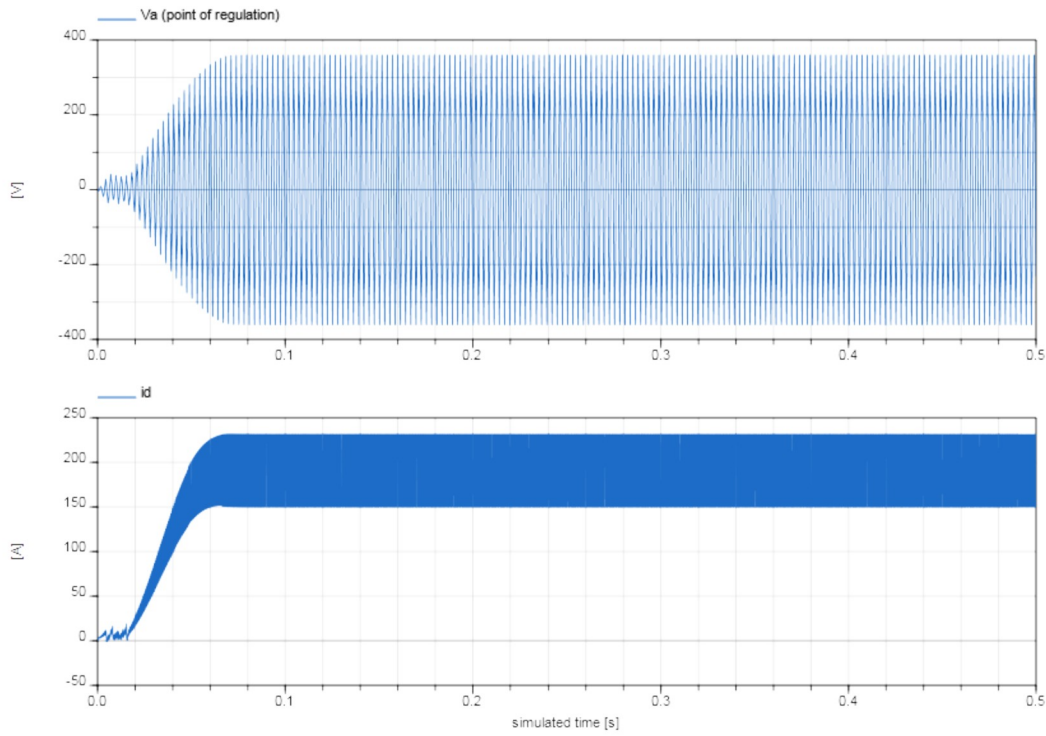
Figure 4.3: Simulation of full-scale model for power quality

Testing of the simulation model for harmonic content does not involve step loads or change of shaft frequency. Therefore, for speeding up the simulation, the replacement of the GCU in Equation (105) by a static input will simplify the closed-loop system equations into lower order open loop equations. Their steady-state results do coincide, if

- the GCU's transfer function shows a low-pass characteristic with a cut-off frequency well below the harmonic content $<1/5\cdot f_e$.
- and/or the transfer function of the rotor voltage to the output voltage or flux linkage shows the same low-pass behavior.

For this particular model, the GCU filter is known to damp this high frequency content sufficiently, without loss of generality. For a non-feedback-controlled machine, the system will converge to (periodic) steady-state conditions with the natural transient time constants. They can be approximated by the open-circuit transient time constants (Krause et al.(2002), table 7.6-1).

The influence of the excitation on the harmonic is analyzed in the following: The rotor's transfer function can be found analytically from Park's equations in operational form (Krause et al.(2002), 7.2-1pp). The equation in rotor reference variables, with field winding in d-axis and one damper winding in each axis, without zero system, is given by:

$$v_{qs}=-r\cdot i_q+\frac{\omega_r}{\omega_b}\cdot\psi_{ds}+\frac{s}{\omega_b}\cdot\psi_{qs}$$
$$v_{ds}=-r\cdot i_{ds}-\frac{\omega_r}{\omega_b}\cdot\psi_{qs}+\frac{s}{\omega_b}\cdot\psi_{ds}$$

(106)

and

$$\psi_{qs}=-X_q(s)\cdot i_{qs}$$
$$\psi_{ds}=(-X_d(s)\cdot i_{ds})|_{v_{fd}=0}+(G(s)\cdot v_{fd})|_{i_{ds}=0}$$

(107)

76

where the flux linkages per second $\psi_x = L_x \cdot \omega_b$ are the inductances normalized by the base frequency. $X_q(s)$ and $X_d(s)$ are the operational impedances. The direct axis voltage is targeted by the rectifier's phase-dependent impedance:

$$\frac{v_{ds}}{i_{ds}} = X_r(\theta(t))$$ (108)

For the voltage/current relationship, no true steady-state condition exists with all derivatives equal to zero, independent of the GCU.
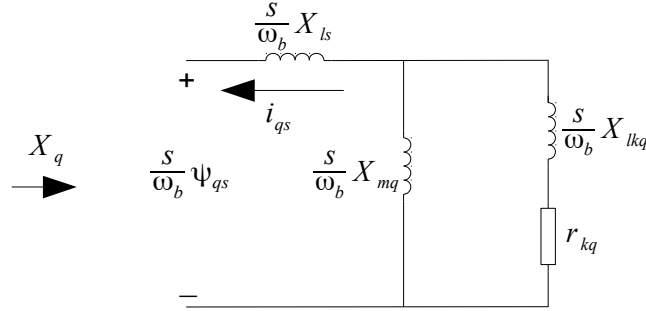
Figure 4.4: Equivalent circuit of operational impedance, q-axis
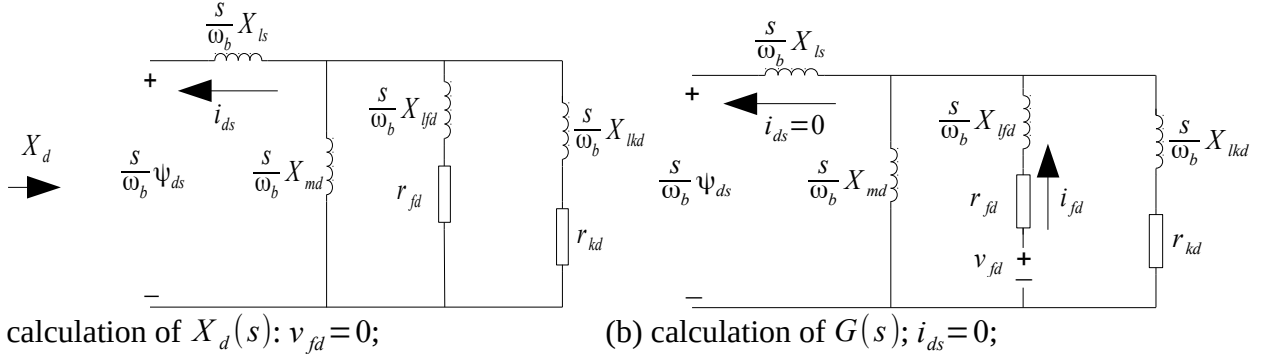
(a) calculation of $X_d(s)$: $v_{fd} = 0$;   (b) calculation of $G(s)$; $i_{ds} = 0$;

Figure 4.5: Equivalent circuit of operational impedance, d-axis

$G(s)$ is the dimensionless transfer function, relating the stator flux linkages per second to the field voltage $\psi_{ds}/v_{fd}|_{i_{ds}=0}$. The operational impedances are the input impedances of the equivalent circuits. $X_q(s)$, $X_d(s)$ and $G(s)$ can be calculated easily from Figures 4.4, 4.5(a) respectively 4.5(b).

With the intermediate variables

$$\tau_{db} = \frac{1}{\omega_b r_{fd}} X_{lfd}$$

$$\tau_{d1} = \frac{1}{\omega_b r_{fd}} (X_{lfd} + X_{md})$$

$$\tau_{d2} = \frac{1}{\omega_b r_{kd}} (X_{lkd} + X_{md})$$ (109)

$$\tau_{d3} = \frac{1}{\omega_b r_{kd}} \left(X_{lkd} + \frac{X_{md} X_{lfd}}{X_{lfd} + X_{md}} \right)$$

The transfer function is

$$G(s) = \frac{X_{md}}{r_{fd}} \frac{1 + \tau_{db} s}{1 + (\tau_{d1} + \tau_{d2})s + \tau_{d1} \tau_{d3} s^2}$$ (110)

It is not possible to make general valid assumptions on the time scales of the transfer function. With some manipulations, it can be assumed that the transfer function will have a lower cut-off frequency than

$$\widetilde{G}(s) \approx \frac{X_{md}}{r_{fd}} \frac{1}{1 + \tau_{d1}}$$ (111)

τ_{d1} is equivalent to the d-axis approximate open-circuit transient time constant (Krause et al. (2002), table 7.6-1). Therefore, the transfer function will probably not interact with sub-transient dynamics. A machine optimized for power generation is also unlikely to exhibit fast transient dynamics. However, the problem can be circumvented by a check done before simulation: all generator parameters are known, and using transfer function (110), the 3dB damping boundary can be evaluated.
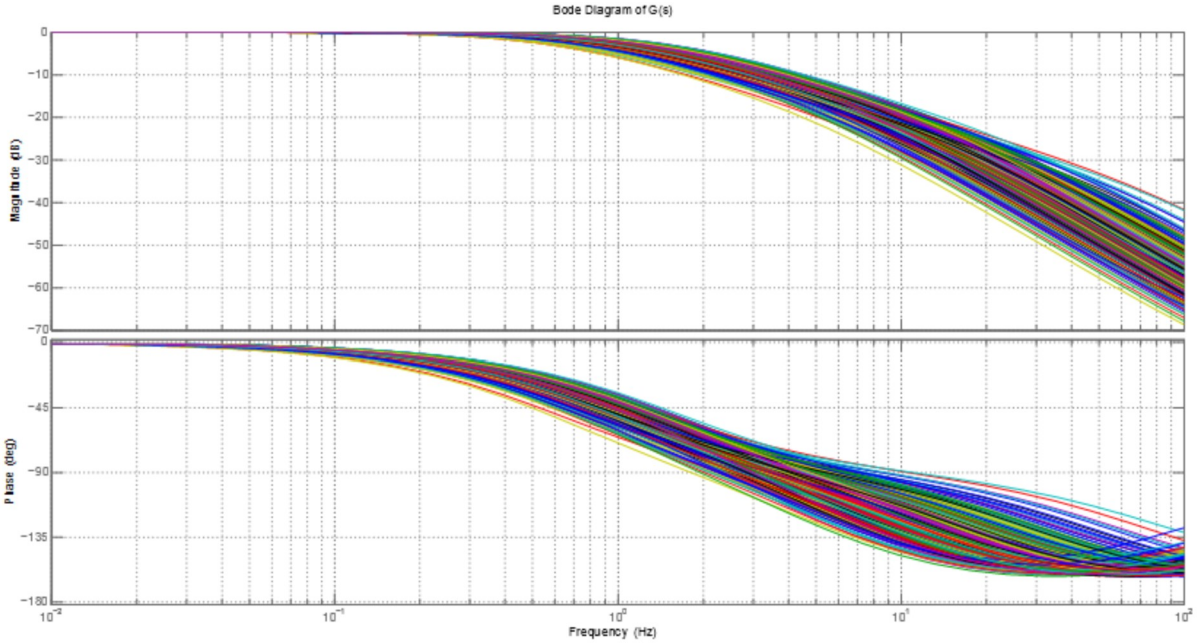
Figure 4.6: Bode diagrams of $G(s) \cdot r_{fd} / X_{md}$ of all Pareto-optimal machine designs (qualitative results, without allocation of colors to specific designs)

Figure 4.6 shows the bode plot of the normalized transfer function $G(s) \cdot r_{fd} / X_{md}$, of all weight versus negative sequence inductance Pareto-optimal machine designs, which were found in chapter 3.4.1. It can be seen, that the assumption of a slow transient behavior is clearly justified. The 3dB boundary is below 10 Hertz for all types of machines. The field voltage to flux transfer function is insensitive to the rectifier noise.

Therefore, in cases where the test on low-pass behavior is successful, the GCU can be replaced by a static excitation voltage:

$$v_{fd} = F_{GCUstatic}(p_{gen}, P_{load}, \omega_e)$$ (112)

It can be calculated analytically from: the generator parameters p_{gen}, the total load P_{load} and electrical frequency ω_e, such that V_{ac} equals 230 Volts RMS.
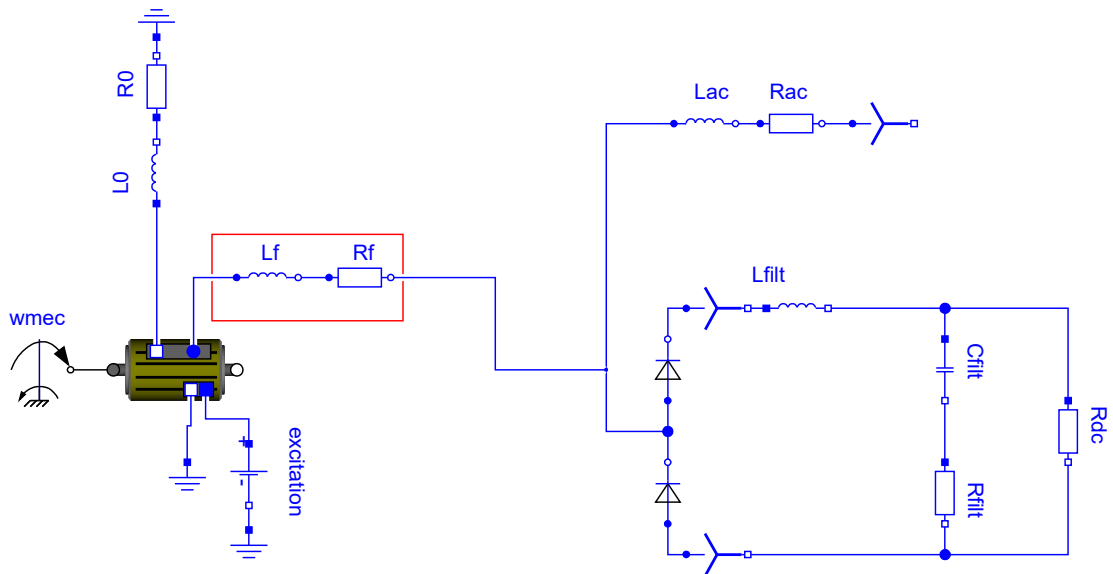
Figure 4.7: Simulation model for power quality, with initialization by steady-state equations

The Dymola simulation model with fixed excitation voltage is displayed in Figure 4.7. Similar to the full-scale model, the non-linear switching characteristics of the three-phase rectifier stage is kept.
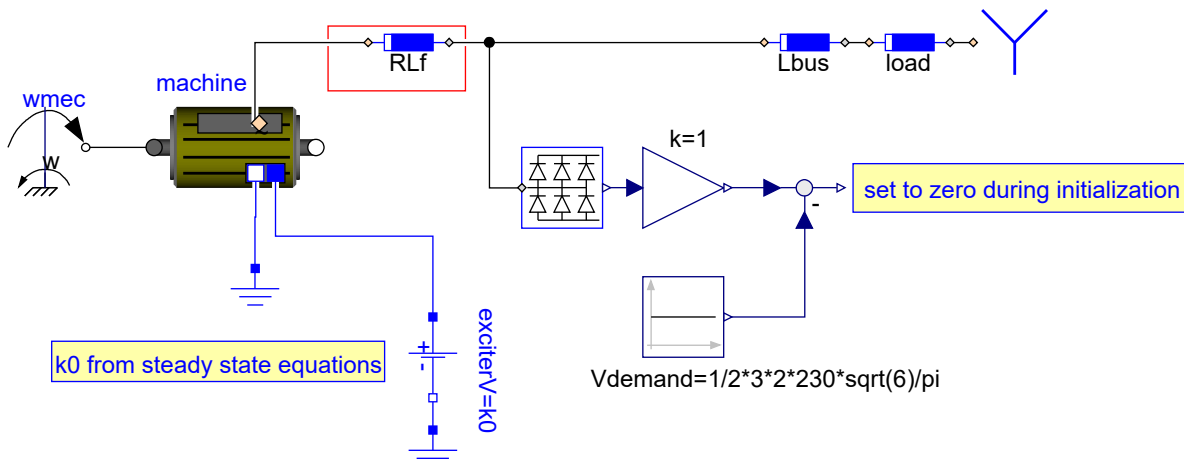
Figure 4.8: "Functional" model, for automatic calculation of excitation

The excitation current can be calculated from Equations (106) and (107) with additional equations for the mean load, such that the correct AC voltage is generated. Instead of error-prone, tedious calculation of the excitation current, this task is a good use case to demonstrate the efficiency of the multi-level modeling approach. The "functional" model in Figure 4.8 shows a non-switching, time average approximation of the full-scale simulation model. As only the steady-state value of the excitation has to be found and inductance in the network does not cause an essential shift in the voltage vector, it is sufficient to model the load by one concentrated resistive load, which is connected via the resistive/inductive substitute element of the bus-bars. Alternatively, the separated rectified *DC* and *AC* loads could be modeled in detail by the functional models of chapter 2.3.2. The functional model does not consider the losses from high frequency effects, which occur primarily in

the dampers. The losses can be neglected deliberately here, since their contribution in the power balance is of minor importance and the voltage level of the constant-excitation fed behavioral model is kept within the range of the industrial standards. The AC voltage sensing by the rectifiers can be approximated using the d/q voltages

$$V_{dc} = \frac{3\sqrt{3}}{\pi} \cdot \sqrt{v_d^2 + v_q^2} \tag{113}$$

Zero-sequence voltages are not influenced by the excitation (Dinh(1998), p62).

Both model levels are integrated in a joint simulation model, such that the detailed model's constant excitation $k0$ is taken from the excitation of the functional model. The non-linear equation system of the functional model is solved in the initialization phase, such that

$$\begin{aligned} \dot{x} &= 0 \\ V_{ac-sensed} - V_{demand} &= 0 \end{aligned} \tag{114}$$

The total simulation model of Figures 4.7 and 4.8 is processed to an equation system with
- 16 continuous time states (variables with time derivative):
  - 7 states in the generator: $i_{qs}, i_{kq}, i_{ds}, i_{fd}, i_{kd}, [B_{sat}], \varphi_{mec}$; ($B_{sat}$ is no real state, but breaks non-linear equation systems by a first order delay; φ_{mec} is the shaft's mechanical angle)
  - 1 state from the DC capacitor v_{cfilt}
  - 8 states in the functional model $i_{qs}^{func}, i_{kq}^{func}, i_{ds}^{func}, i_{fd}^{func}, i_{kd}^{func}, i_{0s}^{func}, [B_{sat}^{func}], \varphi_{mec}^{func}$,
- 3 independent linear systems of order 7, 5 and 5

Compared to the former model, the system grows by 7 states. However, the additional states of the functional model for excitation calculation are only of a theoretic nature. This sub-system is autonomous, with no type of excitation, and is separated at simulation time to a separate system without loss of numerical efficiency.

The behavioral model is initialized with the initial conditions $x=0$. The initial value problem which needs to be solved is non-linear, of size 5.
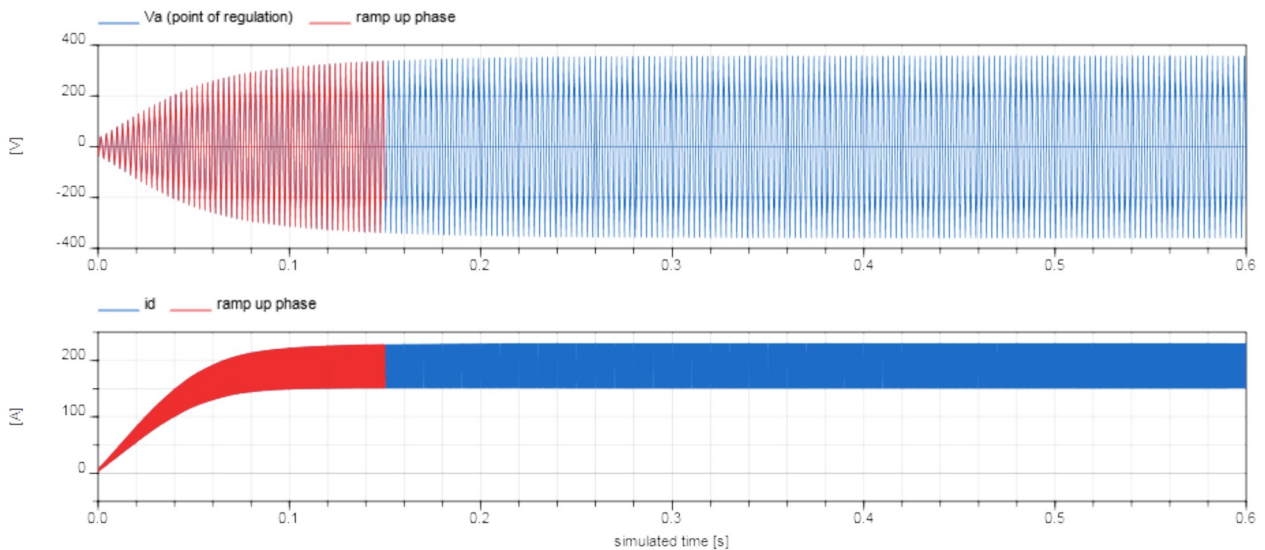
Figure 4.9: Simulation of open-loop model for power quality

Figure 4.9 shows transient plots of the model with constant field excitation, analogues to Figure 4.3. In both figures, voltage at regulation point (top) and generator d-axis current (bottom), a con-

siderably longer ramp-up phase of approximately 0.15 seconds can be seen. The longer ramp-up time has to be compensated for by a longer simulated time of 0.6 seconds.

The two approaches are compared in Table 7. The total simulation time for the simplified model is reduced by 48%, but the ramp up time is also considerably longer. The efficiency of the simplified model is dominant, compared to the delay by the worse transient behavior.

	Model with GCU	*Model without GCU*
Convergence to steady-state	by control	with internal transient dynamics (machines exhibit dissipative behavior, especially because of the dampers)
Size of equation systems	1 linear system, order {12}	3 linear systems, order {7,5,5}
Type of initialization	from zero	steady-state
Size of initialization system	non-linear, order {13}	non-linear, order {5}
Typical ramp up time (sim.)	0.05s	0.15s
Time for simulation of the models for 0.45 s data (normalized by time of Model with GCU)	100% (0..0.5s)	52% (0..0.6s)

Table 7:Comparison of properties of model with and w/o GCU
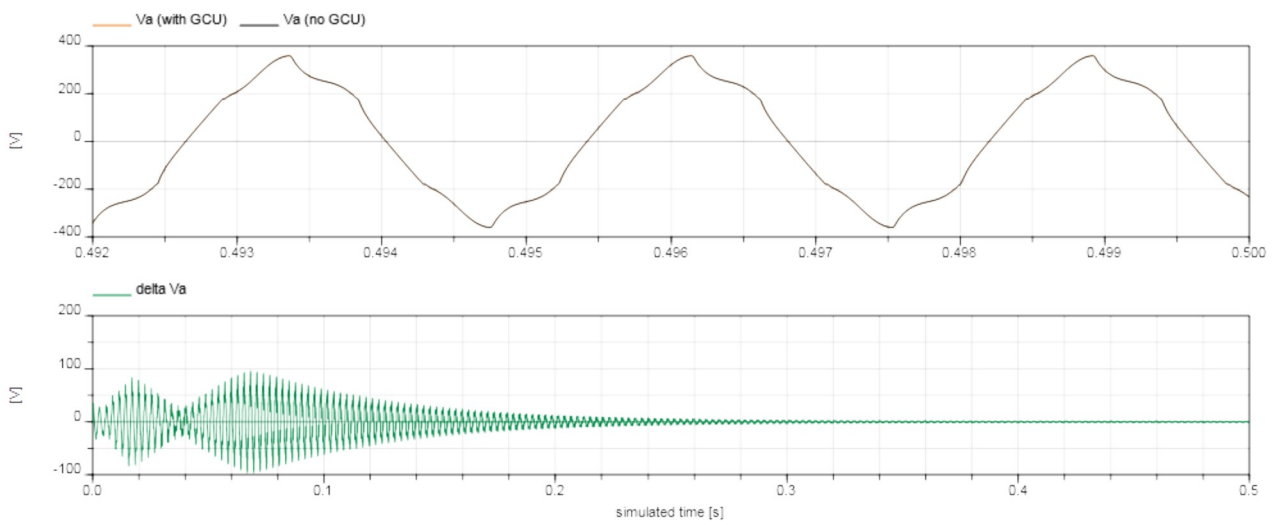
Figure 4.10: Direct comparison of Va for control by constant excitation and GCU

The replacement of the GCU by constant excitation is only valid, if the voltage quality is not affected. It is not affected, as can be seen in Figure 4.10. The upper plot shows the waveforms in de-

tail. The qualitative behavior is the same. The lower plot shows the absolute difference of the two waveforms for 0 to 0.5 seconds. After a transient time, the maximum of the difference is at most 0.4% in relation to the amplitude. This can be attributed to small deviations in the load assumption with slight underestimation of the excitation voltage. Since qualitative behavior is the same, the difference can be seen as negligible.

4.3 Direct initialization in Periodic Steady-State

4.3.1 Idea and demands

In the last chapter, the model complexity of the simulation model for harmonics consideration was reduced essentially, under the proven and checked assumption, that feedback control is not necessary in this case; at the same time, the initial ramp-up phase suffered from the uncontrolled, slower transient behavior to steady-state. This chapter deals with advanced initialization by harmonic modeling, to reduce or eliminate the ramp-up.

From theoretical considerations it is obvious, a direct initialization by setting the derivatives of the state variables to zero does not necessarily result in true steady-state conditions of the power network. In the example of Figure 4.7, each of the 3-phase feeder and load inductances, Lf and Lac, is fed by an AC voltage $v_{ac}(t) \approx \hat{V} \cdot \sin(2\pi f_e t + \phi_V)$, with arbitrary angles ϕ_V, and amplitudes $\hat{V}$. For a predominately resistive network, the inductor should have a sinusoidal shaped current $i_L(t) \approx \hat{I} \cdot \sin(2\pi f_e t + \phi_I)$. With the inductor equation $v_L = L \cdot \dot{i}_L$, the initial equation with zero-derivative would be $v_L = L \cdot 0$ instead of $v_L = \hat{V} \cdot \sin(2\phi f_e t + \phi_V)$.

For the "functional" models, direct initialization in steady-state is possible, since all of the state variables are represented in a non-phase-dependent rotor fixed reference system *qd 0*. But they do not consider the higher harmonics of interest. Alternatively, modeling in the Fourier domain gives good guess values independent of time: In case the system variables change periodically and the periodicity is known- which is the case for the synchronous generator fed network discussed in this thesis- the system equations may have an equivalent in a higher harmonic domain. While the use of frequency-domain models is standard for linear electrical network elements, there is ongoing research for frequency domain equivalents of non-linear and switching elements.

Periodic signals can be expanded into a Fourier series of the form

$$\chi(\tau) = \sum_{k=-\infty}^{\infty} X(k) \cdot e^{jk\omega_{base}\tau}$$
(115)

with the periodic time τ in the interval zero to period length T. ω_{base} is the base frequency while k times ω_{base} are harmonics of ω_{base}. The complex Fourier coefficients $X(k)$ are called phasors. Phasor representations can be time-variant itself, but for initialization from harmonic models, any time-variant behavior is not of interest after initialization, but a fast calculation of the full-scale behavioral model is preferred.

The Fourier-based method is generally not suitable for exact solutions. Fourier transformation shows poor convergence, especially for steep transients like square waveforms the (Gibbs' phenomenon). In contrast to this, the detailed time-domain model gave the exact solution, but was hard to initialize in general and hard to initialize in steady-state operation in particular.

Therefore this thesis proposes to set the initial values of the full-detailed switching non-linear models $x(t_0)$ from harmonic models $\chi(\tau_0)$, where both type of modeling are placed in the component models:

$$\boldsymbol{x}(t_0) = \chi(\tau_0) \tag{116}$$

The harmonic model assumes the phasor form of Equation (115) for all one-phase quantities, and harmonics in rotor fixed reference system for all three-phase quantities: The transformation converts the time-varying phase quantities χ_{abc} into a reference system χ_{qd0} which rotates synchronously with the generator's rotor (see chapter 2.1.2).

$$\begin{bmatrix} \chi_q(\tau) \\ \chi_d(\tau) \\ \chi_0(\tau) \end{bmatrix} = \boldsymbol{T} \cdot \begin{bmatrix} \chi_a(\tau) \\ \chi_b(\tau) \\ \chi_c(\tau) \end{bmatrix} \tag{117}$$

The Park transformation $\boldsymbol{T}$ is valid, independent of the electric variables waveform. The biggest benefit can be taken from considering "balanced" three-phase systems, changing periodically with the reference angular velocity $\omega_{base} = \dot{\theta}$. Balanced sets are generally defined as "a set of equal-amplitude sinusoidal quantities, that are displaced by 120°" (Krause et al., 1998). On balance, the requirement for the generator in this study is satisfied. Equations for asymmetrical lines in $qd0$ system are quite complex with harmonic terms, but greatly simplify for symmetrical RL lines where the same resistance value R and inductance value L applies for each of the three axes. Here, only symmetrical loads need to be taken into account. In order to consider the higher harmonics injected by the switching rectifier, the variables in $qd0$ system can be expanded into a Fourier series:

$$\chi_{qd0}(\tau) = \Re\left(\sum_{h=-\infty}^{\infty} X_{qd0}(h) \cdot e^{jh\omega_{base}\tau} \right) \tag{118}$$

This method should meet the following key demands to be of practical relevance in the simulation-assisted optimization:

- The time-domain model has to be designed robustly, to tolerate small errors in the guess values
- The initialization needs to be automated, where the model provides the correct number of equations for the initialization
- Modeling of both harmonic/time-domain models in one environment in an object-oriented way prevents duplicate work, mismatch of models and allows for easy reconfigurations of the network topology.

4.3.2 Alternative approaches and state-of-the-art in Multi-model-based initialization

Similar to the initialization study in this thesis, (Ji et al., 2010) uses an equivalent harmonic model of an actively-commutated one-phase DC/DC converter for a first initialization. Afterwards, numerical optimization is applied to fit the initial conditions of any transient model, to meet the time periodic constraint in Equation (138). The approach was demonstrated with one-phase loads. The harmonic model and time-domain simulation model were designed in two separate environments and without expansion to multi-phase systems.

Similarly, (Abel and Nähring, 2008) uses a harmonic balance type approach, to tune for the steady-state condition and record harmonic transfer functions fully-automated. Strong limitations exist for self-commutating converters.

While this thesis proposes a mixed frequency-/time-domain based approach, other publications propose to use frequency-domain models only. For example, in (Lian et al., 2008) the harmonic

modeling approach is justified as being more efficient concerning the computation time, compared to transient time-domain simulation. The proposed method directly calculates the steady-state solution without stepping through system transients, and can employ known waveform symmetry. While this approach is true from an academic point of view, limitations in the application exist: All publications in this area consider systems with a limited structure and size. For example, AC and DC line filters are often idealized to fit into the structure. Often, components are limited to the linear case or ideal case. For example, diodes and transistors are seen as ideal switching elements and inductors may not be driven into saturation. For the AC feeders, many models only support symmetric voltages and loads. In general, models of physical systems lose accuracy with every degree of abstraction. While abstracted models are designed to be more efficient in simulation or analysis, it has to be checked carefully, whether they are still valid in modes of operation, that they where not designed for. The check may be cumbersome, since errors may not be obvious while the model has to be validated against hardware or detailed simulation.

In terms of switching between reference systems, some publications on libraries can be found in literature, which can switch the reference frames and models of AC networks (for example Wiesmann(2007)), and initialize average models from models in the qd0 reference frame. However, there was no similar approach found for automatic initialization of switching systems by harmonic models.

4.4 Combined modeling in time and frequency domain

4.4.1 Layout of the components and initialization

In the following, the basic idea and structure of the electric network elements is discussed by means of the three-phase inductive element with resistive component (*RL*). Also, some practical considerations in the implementation with Modelica are given.

The "*RL*" model is instantiated three times for the demonstration network in Figure 4.15: as "feeder", "line1" and "acload1". Equations are based on Park theory, and can be found for example in Krause et al.(2002), with harmonic extension of chapters 2.1.2 and 2.1.3. From the Pseudo code (1) it can be seen, that both sets of equation for "abc system" and "harmonic system" are embedded in parallel in one model "*RL*". All equations of the "harmonic" section are time-invariant and state variables are complex. These are the $(m_{max}+1)$ dimensional variables $Vq, Vd, V0, Iq, Id, I0$, from non-harmonic content (0) to m_{max}-th harmonic content. All variables which are related to the abc system are real. These are the three-dimensional variables v and i. Parameters such as R and L and the angular velocity ω_{base} and multiples of it $\Omega[m]$ are also real.

```
model RL
// DECLARATION OF STATES AND INITIAL CONDITION
  ComplexCurrent Iq[mMax+1], Id[mMax+1], I0[mMax+1];
  ComplexVoltage Vq[mMax+1], Vd[mMax+1], V0[mMax+1];
  Current iI[3];
  Voltage vI[3];
  Current i[3](start=iI);
  Voltage v[3](start=vI);
// STATIC EQUATIONS QD0 HARMONIC SYSTEM
  for m∈0:mMax  loop
```

$$Vq[m]=R\cdot Iq[m]+\omega_{base}\cdot L\cdot Id[m]+j\cdot\Omega[m]\cdot L\cdot Iq[m]$$

$$Vd[m]=R\cdot Id[m]-\omega_{base}\cdot L\cdot Iq[m]+j\cdot\Omega[m]\cdot L\cdot Id[m]$$

$$V0[m]=R\cdot I0[m]+j\cdot\Omega[m]\cdot L\cdot I0[m]$$

```
  end for ;
// DYNAMIC EQUATIONS ABC SYSTEM
```

$$L\cdot der(i)+R\cdot i=v;$$

```
// RELATION QD0 TO ABC SYSTEM
```

$$iI=inversePark\left(\left\{\begin{matrix}Iq[0]\\Iq[1]\\..\end{matrix}\right\},\left\{\begin{matrix}Id[0]\\Id[1]\\..\end{matrix}\right\},\left\{\begin{matrix}I0[0]\\I0[1]\\..\end{matrix}\right\},t_{0,}\omega_{base},\left\{\begin{matrix}\Omega[0]\\\Omega[1]\\..\end{matrix}\right\}\right);$$

$$vI=inversePark\left(\left\{\begin{matrix}Vq[0]\\Vq[1]\\..\end{matrix}\right\},\left\{\begin{matrix}Vd[0]\\Vd[1]\\..\end{matrix}\right\},\left\{\begin{matrix}V0[0]\\V0[1]\\..\end{matrix}\right\},t_{0,}\omega_{base},\left\{\begin{matrix}\Omega[0]\\\Omega[1]\\..\end{matrix}\right\}\right);$$

Code 1: Pseudo code of RL element with combined time and harmonic domain equations; "start" means initial condition.

The "relation" section maps the static frequency domain variables to time domain (iI, vI), by back transformation from qd0 to abc system for all harmonic elements. The set of equations of the static and dynamic models are not linked after initialization but are independent of each other.

The input and output variables of each component are exchanged via connectors (see chapter 4.5), containing v and i for the abc system and $Vq, Vd, V0, Iq, Id, I0$ and Ω for the harmonic system, plus θ_{base}, where $\omega_{base}=der(\theta_{base})$.

All "harmonic" parts contribute to an algebraic equation system. The equations of the "ABC" sub-systems are translated into a Differential Algebraic Equation system.

The initialization is performed analogously to Equation (116). The time-domain variables are set to the periodic steady-state condition computed by the frequency-domain model. Thus, in the case where the frequency domain model gives the correct initial estimate for the periodic solution, the time-domain simulation starts without transient at near periodic steady-state condition.

In principle, the time domain quantities x could be constrained to initial variables xI by an additional initial equation, which eliminates one degree of freedom of Equation (103). In Modelica, additional start equations may be added in a separate initial equation code section. Since the number of freedom to initialize the Differential Algebraic Equations in Equation (103) is not necessarily known beforehand, a wrong number of additional equations would result in an under- or overdetermined set of Equations (103). For example, two inductors in series are coupled via the same current $i_{L1}=i_{L2}$. Only one independent state exists and one initialization variable or constraint need to be added for them. The initialization problem can be circumvented via an alternative Modelica lan-

guage construct. "Start" values of variables can be set in the variable declaration section. They are only applied in case the variable acts as initialization or iteration variable for the initialization. On the other hand, this demands that start values for all possible state and iteration variables are given. This type of initialization was applied in the Pseudo code example. In line seven and eight, the time varying quantities voltages v and currents i are declared. Their initial values are defined to be the solutions of the harmonic equation system, vI and iI by "start=".

Since the harmonic model does not contain derivatives and does not depend on time, the algebraic system of equations of the harmonic part need to be solved only once, during initialization. Dymola actually detects this feature and does not evaluate these equations anymore after initialization.

It is not possible to simplify the infrastructure and include the harmonic equations only in the initial equation section without additional variables in the connectors. The equation system of the harmonic models is built from all electrical components where the variables of the harmonic system and the abc system are not related by an orthogonal transformation.

4.4.2 One-phase elements

The layout of the other models follow the same principle. The time domain models of the standard components do not deviate from common modeling practice and are not listed here. In harmonic-domain, the single-phase impedance equations of inductors and capacitors can be taken, for example, from a pre-existing sub-library of the Modelica standard library, "Modelica.Electrical.QuasiStationary", see also (Haumer et al., 2008) (library only considers base harmonic).

For example, for the capacitance, for $m \in \{0.. m_{max}\}$ and $\Omega \in \{0.. m_{max} \cdot \omega_{base}\}$ the harmonic capacitor model is given by

$$I[m] = j \cdot \Omega[m] \cdot C \cdot V[m] \tag{119}$$

In case the capacitor is fed by a 6 pulse rectifier, the voltage harmonics $V[m]$ and current harmonics $I[m]$ are equal to zero except for $m = 6 \cdot z$, $z \in \mathbb{N}$.

4.4.3 Generator model

The model of the generator with temporal harmonics is derived from (Demiray, 2008). The original work also considered mechanical harmonics. In contrast to this, the model simplifies a lot if a rigid mechanical shaft is used with fixed speed and no torque-dependency:

$$\begin{aligned}
\phi_{qs}[m] &= -L_{ls} \cdot I_q[m] + L_{mq} \cdot (-I_q[m] + I_{kq}[m]) \\
\phi_{ds}[m] &= -L_{ls} \cdot I_d[m] + L_{md} \cdot (-I_d[m] + I_{fd}[m] + I_{kd}[m]) \\
\phi_{0s}[m] &= -L_{ls} \cdot I_0[m] \\
\phi_{kq}[m] &= L_{lkq} \cdot I_{kq}[m] + L_{mq} \cdot (I_{kq}[m] - I_q[m]) \\
\phi_{kd}[m] &= L_{lkd} \cdot I_{kd}[m] + L_{md} \cdot (I_{fd}[m] + I_{kd}[m] - I_d[m]) \\
\phi_{fd}[m] &= L_{lfd} \cdot I_{fd}[m] + L_{md} \cdot (I_{fd}[m] + I_{kd}[m] - I_d[m])
\end{aligned} \tag{120}$$

$$V_q[m] = -R_s \cdot I_q[m] + \omega_{base} \cdot \phi_{ds}[m] + j \cdot \Omega[m] \cdot \phi_{qs}[m]$$
$$V_d[m] = -R_s \cdot I_d[m] - \omega_{base} \cdot \phi_{qs}[m] + j \cdot \Omega[m] \cdot \phi_{ds}[m]$$
$$V_0[m] = -R_s \cdot I_0[m]$$
$$V_{fd}[m] = R_{fd} \cdot I_{fd}[m] + j \cdot \Omega[m] \cdot \phi_{fd}[m]$$
$$0 = R_{kq} \cdot I_{kq}[m] + j \cdot \Omega[m] \cdot \phi_{kq}[m]$$
$$0 = R_{kd} \cdot I_{kd}[m] + j \cdot \Omega[m] \cdot \phi_{kd}[m]$$

$$(121)$$

It was found earlier in this chapter that no dynamic control of the output voltage needs to be considered. The constant excitation voltage, generating the demanded generator output voltage, is set by $V_{fd}[0] = k_f$. The value of k_f can be computed automatically by an additional constraint of the output voltage in the initial equations:

$$\sqrt{Re(V_{qs}[0])^2 + Re(V_{ds}[0])^2} = 230 \cdot \sqrt{2}$$

$$(122)$$

or from the behavioral model depicted in 4.8. At other harmonics $V_{fd}[m]$ equals zero. k_f is also used for the excitation voltage of the time-domain model.

m denotes harmonics of the electrical base frequency ω_{base} from 0 to m_{max}. $\Omega[m]$ are harmonic angular velocities $\Omega = \{0, \omega_{base}, 2 \cdot \omega_{base}, .. m_{max} \cdot \omega_{base}\}$. The notation of the subscripts is identical to chapter 2.3.1: The subscripts qs and ds denote q-axis respectively d-axis quantities in the stator. $0 s$ stands for zero-axis and fd field winding in d-axis. kq and kd are related to the damper windings. $L_{m\_}$ denotes magnetizing inductances, while $L_{l\_}$ denotes leakage inductances. The magnetic fluxes are labeled by ϕ_X. Again, all variables denote complex quantities, while parameters and angular velocities are real.

The model of (Demiray, 2008) does not consider magnetic saturation. This effect can be implemented in analogy to the behavioral model of the generator in chapter 2.3.1 by scaling the magnetizing inductances in Equation (120) by a saturation factor k_{satP}:

$$\phi_{qs}[m] = -L_{ls} \cdot I_q[m] + k_{satP} \cdot L_{mq} \cdot (-I_q[m] + I_{kq}[m])$$
$$\phi_{ds}[m] = -L_{ls} \cdot I_d[m] + k_{satP} \cdot L_{md} \cdot (-I_d[m] + I_{fd}[m] + I_{kd}[m])$$
$$\phi_{0s}[m] = -L_{ls} \cdot I_0[m]$$
$$\phi_{kq}[m] = L_{lkq} \cdot I_{kq}[m] + k_{satP} \cdot L_{mq} \cdot (I_{kq}[m] - I_q[m])$$
$$\phi_{kd}[m] = L_{lkd} \cdot I_{kd}[m] + k_{satP} \cdot L_{md} \cdot (I_{fd}[m] + I_{kd}[m] - I_d[m])$$
$$\phi_{fd}[m] = L_{lfd} \cdot I_{fd}[m] + k_{satP} \cdot L_{md} \cdot (I_{fd}[m] + I_{kd}[m] - I_d[m])$$

$$(123)$$

For the behavioral model, the saturation coefficient k_{sat} is calculated as a function of all magnetizing currents. Applied to the harmonic system, this would mean an algebraic equation system which involves cross-coupling of all harmonic models. Since saturation is mostly affected by the offset of the magnetizing current the relationship is deliberately simplified by only taking the fundamental harmonics into account:

$$I_{md} = (-I_d[0] + I_{fd}[0] + I_{kd}[0]) / kfd$$
$$I_{mq} = (-I_q[0] + I_{kq}[0]) / kfd$$
$$I_m = \sqrt{(Re(I_{md})^2 + Re(I_{mq})^2)}$$
$$k_{satP} = f(I_m)$$

$$(124)$$

Where I_m, I_{mq} and I_{md} are the magnetizing current and magnetizing current in q- and d-axis respectively.[9] No space harmonics of the machine are taken into consideration. Also no magnetic remanence is considered, since this can be seen as an offset in the excitation current.

4.4.4 Alternative behavioral model of rectifier

For the "behavioral" rectifier model, it is proposed to replace the diode based implementation with a novel approach. As will be shown in this chapter, it has some benefits in initialization. It is inspired by the implementation in the SPOT library (Wiesmann, 2007), which was developed as part of the REALSIM project.

$$i = i_{ds}\left(e^{v/vt} - 1\right)$$
$$\left(vt = \frac{k\,T\,n}{q}\right)$$

$$v \quad = \quad V_{knee} + s \cdot \begin{cases} 1 & \text{if off} \\ R_{on} & \text{else} \end{cases}$$

$$i \quad = \quad Goff \cdot V_{knee} + s \cdot \begin{cases} G_{off} & \text{if off} \\ 1 & \text{else} \end{cases}$$

$$off \quad = \quad s < 0$$
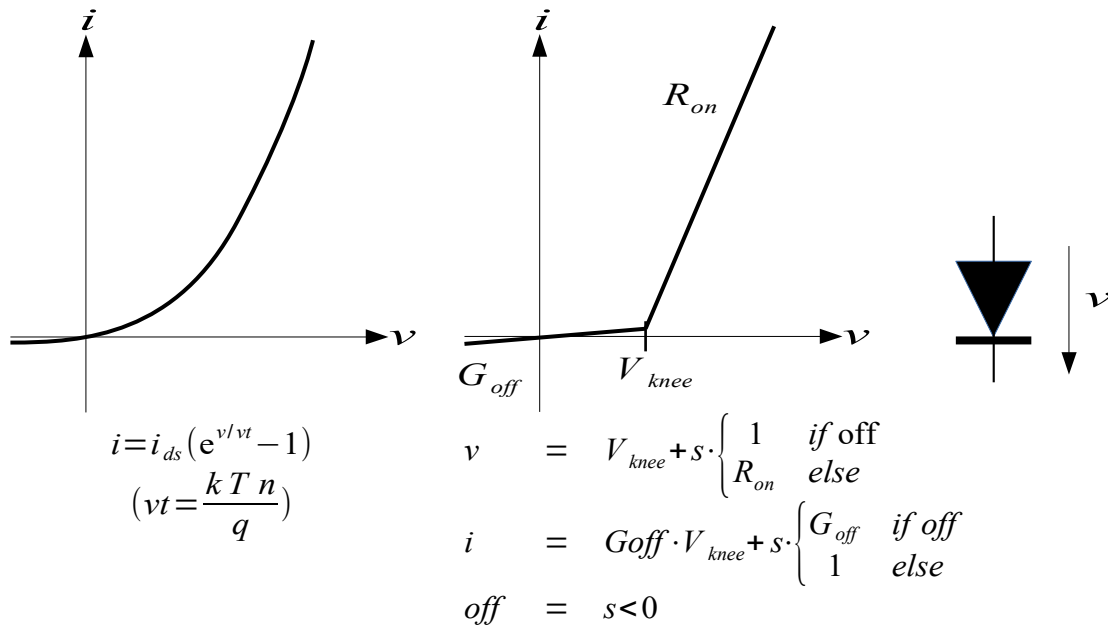
Figure 4.11: Illustration of coupling of voltages and currents in an idealized diode

The common approach for modeling passively commutated n-pulse rectifiers by interconnection of $n/2$ pairs of diodes was described in chapter 2.3.2. Characterization of the diodes by more precise equations, like Shockley-equations (Figure 4.11, left), exceeds the demands of network power quality studies. Instead, the diode models are simplified with idealized characteristics, for example $v = R_{on} \cdot i + V_{knee}$ for forward biased current. The model is superior in computation speed, since only linear relations are present. The right side of Figure 4.11, shows the s-parameterization model of Modelica's "IdealDiode". For a voltage controlled system, it is numerically efficient to set G_{off} to zero, with i=0 in reverse-biased operation rather than $i = v \cdot G_{off}$. In the onboard electrical network model, there is an inductor in the AC source. Setting i=0 would constrain the state i, which is no longer calculated by integration of di/dt any more. The chosen simulation platform can not handle systems with a changing number of state variables, and therefore this approach would not work.

Alternatively, for the SPOT library, a formulation was developed, which models the rectifier directly with pairs of diodes by one integrated equation system. The SPOT equations of the three-phase rectifier without internal losses, can be explained with the help of Figure 4.12, which visualizes the input/output relations. All equations with index κ denote to each phase: $\kappa = \{a, b, c\}$.

---

[9] Later on only half-sided spectra will be used but scaled by factor 2. This is already taken into account for calculation of Im, otherwise it must be scaled by factor ½

The DC quantities are separated into

$$v_{DC1} = 0.5 \cdot (v_{dc+} - v_{dc-}), v_{DC0} = 0.5 \cdot (v_{dc+} + v_{dc-})$$
$$i_{DC1} = i_{dc+} - i_{dc-}, i_{DC0} = i_{dc+} + i_{dc-} \tag{125}$$

where i_{DC0} and v_{DC0} are zero current and voltage quantities respectively.

Any common voltage component on the AC side is related to a shift in offset of the mean DC voltage (zero component):

$$v_{ac}[\kappa] = v_{sc}[\kappa] + v_{DC0} \tag{126}$$

For the currents, Kirchhoff's law always applies:

$$i_{DC0} + \sum \boldsymbol{i_{ac}} = 0 \tag{127}$$

The threshold voltage V is defined as the sum of the one-sided DC amplitude and the diode's knee voltage:

$$V = v_{dc1} + V_{knee} \tag{128}$$

The rectifier will conduct, if an AC input voltage is above the threshold voltage or below the negative threshold voltage.

The s-parametrization of the voltage and current relations assumes three areas for each phase: conduction to upper leg, no conduction, conduction to lower leg.

$$
\begin{cases}
v_{sc}[\kappa] = R_{on} \cdot s[\kappa] + (1 - R_{on}) \cdot V \\
i_{ac}[\kappa] = s[\kappa] - (1 - G_{off}) \cdot V
\end{cases} \quad \text{if } s[\kappa] > V
$$
$$
\begin{cases}
v_{sc}[\kappa] = R_{on} \cdot s[\kappa] - (1 - R_{on}) \cdot V \\
i_{ac}[\kappa] = s[\kappa] + (1 - G_{off}) \cdot V
\end{cases} \quad \text{if } s[\kappa] < -V \tag{129}
$$
$$
\begin{cases}
v_{sc}[\kappa] = s[\kappa] \\
i_{ac}[\kappa] = G_{off} \cdot s[\kappa]
\end{cases} \quad else
$$

The s-parametrization has the benefit that it can be reordered for voltage or current controlled systems and the switching can be related to the continuous variables s. G_{off} must not be zero if $i_{ac}[\kappa]$ is related to a state. Otherwise in "else" $i[\kappa] = 0$, which is not a valid constraint of a state variable.
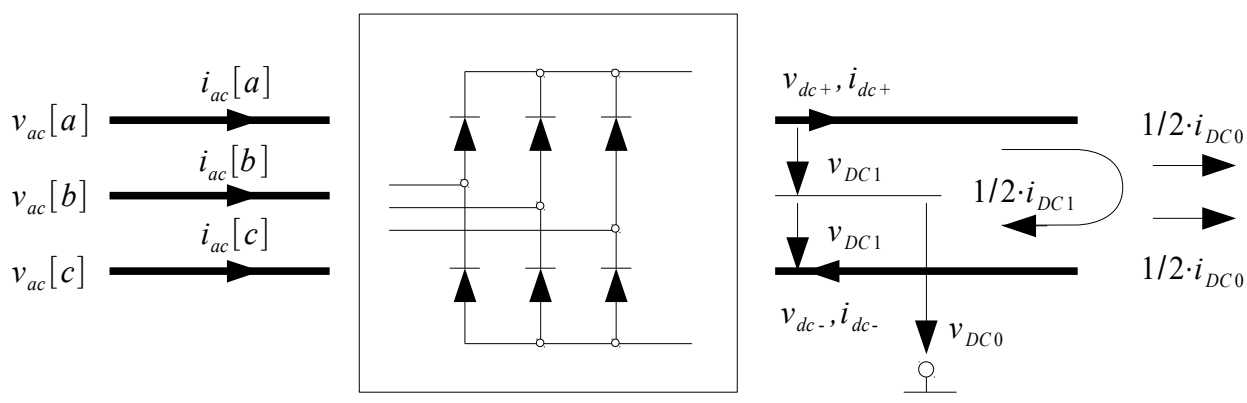
Figure 4.12: Rectifier model, voltages and currents flow diagram

89

For better understanding of the Equations (129), "s" can be eliminated:

$$
\begin{aligned}
v_{sc}[\kappa] &= R_{on} \cdot i_{sc} - G_{off} \cdot R_{on} \cdot V + V \quad &&\forall\, i_{sc}[\kappa] \;>\; G_{off} \cdot V \quad &&\text{or } v_{sc}[\kappa] \;>\; V \\
v_{sc}[\kappa] &= R_{on} \cdot i_{sc} + G_{off} \cdot R_{on} \cdot V - V \quad &&\forall\, i_{sc}[\kappa] \;<\; -G_{off} \cdot V \quad &&\text{or } v_{sc}[\kappa] \;<\; -V \\
v_{sc}[\kappa] &= 1/G_{off} \cdot i_{ac}[\kappa] \quad &&else
\end{aligned}
\tag{130}
$$

The relationship of the current input to output is given by

$$
i_{DC1} + \boldsymbol{switch} \cdot \boldsymbol{i}_{ac} = 0
\tag{131}
$$

where

$$
switch[\kappa] = sgn(s[\kappa])
\tag{132}
$$

Equation (131) may trigger errors in the case of inductive elements in the AC and DC connection, since dynamic switching of state variables is a non-trivial problem for the integration algorithm. In Modelica, state variables may not be set to values directly, since no finite derivatives for non-continuous values exist. The model itself is not more efficient than the implementation with the six single diodes with s-parametrization.

Instead of Equations (129), (131), and (132), the adaption to Equations (133) and (134) is proposed:

$$
\begin{cases}
\begin{aligned}
v_{sc}[\kappa] &= R_{on} \cdot s[\kappa] + (1 - R_{on}) \cdot V \\
i_{ac}[\kappa] &= s[\kappa] - V \qquad &&if\ s[\kappa] \;>\; V \\
switch[\kappa] &= +1
\end{aligned} \\
\begin{aligned}
v_{sc}[\kappa] &= R_{on} \cdot s[\kappa] - (1 - R_{on}) \cdot V \\
i_{ac}[\kappa] &= s[\kappa] + V \qquad &&if\ s[\kappa] \;<\; -V \\
switch[\kappa] &= -1
\end{aligned} \\
\begin{aligned}
v_{sc}[\kappa] &= s[\kappa] \\
\dot{i}_{ac}[\kappa] &= 0 \qquad &&else \\
switch[\kappa] &= \;0
\end{aligned}
\end{cases}
\tag{133}
$$

$$
\dot{i}_{DC1} = \boldsymbol{switch} \cdot \dot{\boldsymbol{i}}_{ac} - k_i \cdot (i_{DC1} - \boldsymbol{switch} \cdot \boldsymbol{i}_{ac})
\tag{134}
$$

In the same way as before, the variables $s[\kappa]$ act as continuous decision variables. The conductance G_{off} for reverse-biased mode is neglected, since physical meaning is questionable and it will be seen that it is not needed from a modeling point of view. For better understanding, $s[\kappa]$ is eliminated in Equation (133):

$$
\begin{cases}
\begin{aligned}
v_{sc}[\kappa] &= R_{on} \cdot i_{ac}[\kappa] + V \\
switch[\kappa] &= +1
\end{aligned} \quad &&\forall\, i_{ac}[\kappa] \;>\; 0 \quad &&\text{or } v_{sc}[\kappa] \;>\; V \\
\begin{aligned}
v_{sc}[\kappa] &= R_{on} \cdot i_{ac}[\kappa] - V \\
switch[\kappa] &= -1
\end{aligned} \quad &&\forall\, i_{ac}[\kappa] \;<\; 0 \quad &&\text{or } v_{sc}[\kappa] \;<\; -V \\
\begin{aligned}
\dot{i}_{ac}[\kappa] &= 0 \\
switch[\kappa] &= \;0
\end{aligned} \quad &&else
\end{cases}
\tag{135}
$$

The equations can be interpreted as:

1. When $v_{vsc}[\kappa]$ exceeds the threshold voltage, current conduction from AC to DC is enabled. $s[\kappa]$ may follow $v_{vsc}[\kappa]$, if the input is related to a state of a voltage, or $i_{ac}[\kappa]$, if the input is related to a state of a current, and will switch to the "else" part if $\dot{i}_{ac}[\kappa]=0$ or $v_{sc}[\kappa]=V$. The same applies for conduction to the lower leg. The equations are valid even if $R_{on}=0$ for a resistive source. If the source exhibits an inductive behavior then $R_{on}=0$ would eliminate the commutation interval (see chapter 2.3.2).

2. if $v_{vsc}[\kappa]$ is not higher than the threshold voltage, or lower than the negative threshold voltage, there is no change of the current $d\,i_{ac}/dt=0$ ("else" section). The decision variable $s[\kappa]$ follows $v_{vsc}[\kappa]$ (the original formulation links currents in place of current derivatives)

This formulation is of particular benefit for an inductive source. The formulation links the time derivative $d\,i/dt$ of the AC currents rather than i. For non-inductive sources the linkage of currents is more beneficial, but it will not have the benefits shown hereafter. Non-inductive sources can be adapted by addition of tiny inductances in the source connection. This is in agreement with physical reality since every connection line exhibits at least tiny inductive behavior. It has to be admitted that an approach using different models depending on the environment, is not truly object-oriented.

The $k_i(..)$ term in Equation (134) with parameter k_i is introduced to prevent two resultant modeling deficiencies: The coupling of the currents is modeled similar to a transformer-based isolated AC/DC rectifier. During initialization, there is a degree of freedom for circular currents through the DC side. During simulation, all current state derivatives on the DC side are tightly linked to the AC side's current derivatives and there is no decay of these circular currents. Second, coupling of derivatives is problematic for long simulations. In numerical simulation, the derivatives are calculated with user-specified tolerances σ, thus $(\dot{i}_{DC1}+\sigma_{DC1})+\boldsymbol{switch}\cdot(\dot{\boldsymbol{i}}+\sigma)=0$.

Small numerical deviations in the derivatives will integrate in time to small offsets of the coupled states:

$$i_{DC1}+\boldsymbol{switch}\cdot\boldsymbol{i}=\int \Delta\,\sigma\,dt \tag{136}$$

The $k_i()$ term acts as a feedback control, to consolidate initial mismatches in the AC and DC side currents and compensate drifts. While exact initialization prevents the circular current, the initialization by approximations can take advantage of this initial degree of freedom: a non-conducting phase may be loaded with an initial current, to compensate for smaller current mismatches. In the original Equations (130), this would result in high voltages $v_{sc}[\kappa]=1/G_{off}\cdot i_{ac}[\kappa]$.

With the parameter k_i a decay rate can be defined.

In simulation, at the transient to the non-conduction interval, the equation system switches to the "else" branch with $\dot{i}_{sc}=0$ at zero-current crossing. Therefore $\dot{i}_{sc}=0$ is preserved in the case of correct detection of the crossing point. Non-zero-currents, for example from an approximate initialization, decay exponentially: If we split the current derivative $\dot{i}_{DC1}$ of Equation (134) to $\dot{i}_{DC1}=\dot{i}_{DC1,\,coupled}+\dot{i}_{DC1,\,mismatch}$, with

$$\begin{aligned}\dot{i}_{DC1,\,coupled}&=\boldsymbol{switch}\cdot\boldsymbol{i}_{ac}\\ \dot{i}_{DC1,\,mismatch}&=-k_i\cdot(i_{DC1}-\boldsymbol{switch}\cdot\boldsymbol{i}_{ac})\end{aligned} \tag{137}$$

then any deviation of $i_{DC1}-(switch[a]\cdot i_{ac}[a]+switch[b]\cdot i_{ac}[b]+switch[c]\cdot i_{ac}[c])$ to zero induces a repelling term on i_{DC1}.

This rectifier model relaxes the coupling of currents to allow the initialization of currents from the harmonic model and shift any initial unbalance to a relaxation term. For harmonic sources with

voltage harmonics, the relaxation term must be introduced in the relations of the derivatives of the potential-variables.
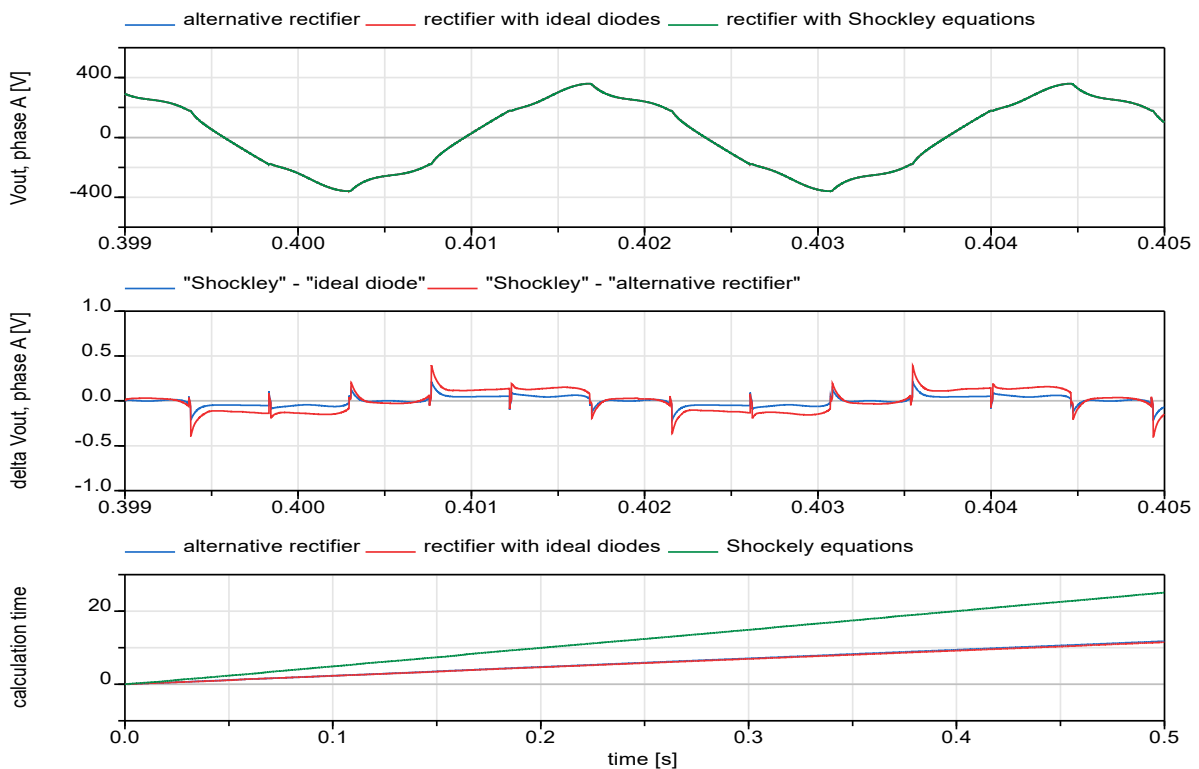
Figure 4.13: Comparison of rectifiers

The alternative rectifier model is demonstrated in Figure 4.13. The plots show the results of the three rectifier types: The rectifier with the detailed Shockley equations is compared to the rectifier based on ideal switching diodes, and to the new alternative rectifier model. All three rectifiers are tested with the small electric network-arrangement which was shown in Figure 4.7. The alternative rectifier works best with an inductive source. Therefore a small-but physically justified- line inductance of 1nF was introduced between the rectifier and the branch point. The voltage Vout is sensed at the branch point. The upper plot shows Vout for the three types of rectifiers. No difference can be seen by inspection. The differences of the detailed model to the idealized rectifiers are plotted separately in the middle chart. The deviation in relation to the base signal is in the per mil region, with slightly better results of the rectifier based on ideal diodes. This benefit can be attributed to the conductance of the diodes in the "closed" region. For this simulation model the detailed rectifier showed the worst performance, while the rectifiers with ideal characteristics showed similar performance.

Note, the equations of the alternative rectifier model can be used also for modeling of an active power module if "switch" is commanded externally. The DCCU, see chapter 2, could be only initialized in combination with this model, since the equations can handle inductive loads (here: transformer of DCCU).

In summary, the benefits of the alternative implementation in comparison to the standard approach are

1. Relaxation of the initial conditions: the non-conducting phase may be initialized with an approximate current, where the offset to the correct solution will vanish with time exponentially.

2. Efficiency: idealized switching is possible, even for inductive sources. For Dymola, this effect is of minor importance.

4.4.5 Rectifier model in harmonic system

The harmonic model of the rectifier model can be seen as the most critical component, due to its non-linear and switching behavior. Under the assumption of ideal switching, the differential equation system of electrical circuits with line-commutated converters, such as passively commutated rectifier systems, switches between different state space representations. While there exist operation modes with undamped oscillations or chaotic behavior, all well designed circuits tend to a time periodic steady-state solution. In the case of self-commutating rectifiers, the repetition rate is proportional to the net frequency ω_{base}. A system is in exact periodic steady-state condition, if all model variables repeat exactly:

$$\boldsymbol{x}(t) = \boldsymbol{x}(t + T) \tag{138}$$

with and within the cycle duration $T = 2\pi/\omega_{base}$. The state space matrices and may-be even the number of state-derivatives, switch at commutation instants $t_{1..n}$ or phase angles $\theta_{1..n}$ where $\theta_\rho = \omega_{base} \cdot t_\rho$. The commutation instants are determined by the DAE system and may be calculated analytically and even symbolically, by solving the DAE with the time periodic constraints of equation (138) at all commutation instants. The knowledge of the commutation instants can be used for time averaged state-space modeling of the type

$$\widetilde{x} = \frac{1}{2\pi}\left[\int_{\theta_0}^{\theta_1} F_1(\theta)\,d(\omega_{base}t) + .. + \int_{\theta_{n-1}}^{\theta_n = \theta_0} F_n(\theta)\,d(\omega_{base}t)\right] \tag{139}$$

or can be used to develop harmonic state space representations in the Fourier domain, where

$$x(\theta) = \sum_k X_k \cdot \sin(k\theta + \phi_k), \theta \in [0..2\pi], \omega_{base}t = \theta \tag{140}$$

Numerous papers exist on average models and harmonic modeling. To give some examples, some early sources of parametric analytic solutions of the Differential Algebraic System for the purpose of average modeling are documented in (Krause et al., 1998). This is the base of the average rectifier model in chapter 2.3.2. A system, like in Figure 4.7, but with AC voltage sources with distorted waveforms, was analyzed in detail in some more recent papers with the intention of building harmonic models. Both continuous conduction mode and discontinuous conduction mode are addressed. (Carpinelli et al., 2004) solves the DAE system using inverse Laplace transformation. Alternatively, in (Lian et al., 2008) the DAE system is brought into explicit form and some numerical iteration algorithm was formulated in order to find the switching angles. An overview on average models is given in the thesis (Chiniforoosh, 2012).

(Bing et al., 2009) pursue a different approach, as it is focused mainly on impedance models. For aircraft electrical systems, the requirements on the power quality of the AC lines are very stringent. Thus, the switching pattern is determined by the base harmonic, but may be distorted by voltage perturbations with small amplitudes at frequencies around base frequency. The paper derives frequency-dependent transfer functions of the rectifier at harmonic and inter-harmonic frequencies. The model is limited:

*   It only considers continuous conduction mode. This is critical if only limited power is drawn from the AC side and the DC voltage is filtered by the capacitance.

- • The commutation intervals are neglected on the grounds that for six-pulse rectifiers, they are small compared to the conduction phase and the source impedance is considerably lower than for auto-transformer rectifier units. For onboard electrical networks, this is also a reasonable assumption, since distribution lines are relatively short with low inductance.

Due to its simplicity, the equations of (Bing et al., 2009) were used as the basis of the harmonic rectifier model for the system studied in this thesis. The validity outside continuous conduction mode has to be questioned critically and improved models may be needed for future applications. Since the harmonic model is used for initialization only, the error may be seen as negligible in this context.

The rectifier models assumes sinusoidal AC source voltages v_x at base frequency f_1. The distortion is assumed to be small and therefore is neglected for the current transmission to DC and the determination of the switching angle. A balanced three-phase voltage source is assumed. No commutation interval is considered. The input AC voltage is assumed as

$$v_a(t)=v_1\cdot\sin(2\pi f_1 t)\multimap j\pi[V_1\cdot\delta(\omega+f_1)-V_1\cdot\delta(\omega-f_1)] \tag{141}$$

If the rectifier is fed by an electric network, the real rectifier's phase-shifted input voltage $v_{a,real}(t)=v_1\cdot\sin(\theta_r-\theta_0-\phi)$ has to be transformed into Equation (141) by a rotatory transformation first. θ_0 is the (known) initial angle of the rotor, in case the generator's position is taken for phase information. The shift angle by the source impedance can be calculated from the qd voltage: $\phi=atan2(\Re(V_q(0)),\Re(V_d(0)))$.

The DC side voltage can be be calculated by a convolution of an ideal rectangular shaped switching function and the AC voltage:

$$V_{dc}(i)=\sum_{l=-\infty}^{\infty} \boldsymbol{S}_{abc}(l)\cdot\boldsymbol{V}_{abc}(i-l) \tag{142}$$

Variables in capital letters are complex phasors which are related to time quantities by $x(t)=\sum_{\omega}\left(X(\omega)\cdot e^{j\omega t}\right)$. The index (i) indicates the i-th multiple (harmonic) of the base frequency f_1. The subindex abc denotes three-phase quantities $\boldsymbol{S}_{abc}(i)=[S_a(i),S_b(i),S_c(i)]$, $\boldsymbol{V}_{abc}(i)=[V_a(i),V_b(i),V_c(i)]^T$.

The switching window is given by

$$S_a(l)=-\frac{(-1)^k j\sqrt{3}}{\pi(6k\pm1)} \qquad \forall\ l=(6k\pm1)f_1. \tag{143}$$

V_b and S_b share the amplitudes of V_a and S_a but are time shifted backwards by $-2\pi/3$ of a period. V_c and S_c are shifted forward by $2\pi/3$. In the three-phase system, the convolution in (142) is only non-zero at frequencies

$$V_{dc}(6m f_1)=\frac{(-1)^m 3\sqrt{3}V_1}{\pi(1-36m^2)} \tag{144}$$

Similarly, the AC current can be calculated as a convolution of switching function and DC current:

$$I_a(i)=\sum_{k=-\infty}^{\infty} S_a(i)\cdot I_{dc}(i-k). \tag{145}$$

Since the DC side equation system is just excited by the rectifier harmonics, the spectrum is non zero for

$$I_{DC}(i) \neq 0 \; \forall \; i = 6 \cdot m \cdot f_1 \tag{146}$$

To transform the harmonic current in the *abc* system to the harmonic system in *qd*0 the transformation equations in chapter 2.1.2 are used with

$$\boldsymbol{X}_{qd0}(m) = \boldsymbol{P}_1 \cdot \boldsymbol{X}_{abc}(m-1) + \boldsymbol{P}_2 \cdot \boldsymbol{X}_{abc}(m+1) + \boldsymbol{P}_0 \cdot \boldsymbol{X}_{abc}(m), \; m \in \{0 .. \, m_{max}\} \tag{147}$$

with the Park transformation matrices $\boldsymbol{P}$ in complex domain. While the method is very general, only time-invariant phasors are needed here. With some knowledge of symmetrical component frames from (Chen et al., 1999), the elements in equation (145) are only non-zero for $n = 6 \cdot m$, where $n \in [0 .. \, n_{max}]$. Therefore, in the rectifier AC connector, only the vector of $n_{max} + 1$ non-zero quantities for voltage and current need to be exchanged. Furthermore, since all variables in the qd0 spectrum represent real values, it can make use of the relationship

$$X(-\omega) = X^*(\omega) \tag{148}$$

The negative side of the spectrum does not give additional information and only the right-hand-side quantities of the spectrum need to be transferred. With the inverse Park transformation in the complex domain in Equation (43) and a limited choice of AC harmonics "*ach*" at angular velocity $h[ach] \cdot \omega_e$ in qd0 domain, the time varying three-phase variables $\boldsymbol{x}_{abc}$ can be calculated by:

$$
\begin{aligned}
\boldsymbol{x}_{abc} = \sum_{o=1}^{ach} \{ \quad & \boldsymbol{PT}_1 \cdot \boldsymbol{X}_{qd0}[o] \cdot e^{j(h[o]+1)\omega t} & + \boldsymbol{PT}_2 \cdot \{\boldsymbol{X}_{qd0}[o]\}^* \cdot e^{-j(h[o]+1)\omega t} \\
+ & \boldsymbol{PT}_2 \cdot \boldsymbol{X}_{qd0}[o] \cdot e^{j(h[o]-1)\omega t} & + \boldsymbol{PT}_1 \cdot \{\boldsymbol{X}_{qd0}[o]\}^* \cdot e^{-j(h[o]-1)\omega t} \\
+ & \boldsymbol{PT}_0 \cdot \boldsymbol{X}_{qd0}[o] \cdot e^{jh[o]\omega t} & + \boldsymbol{PT}_0 \cdot \{\boldsymbol{X}_{qd0}[o]\}^* \cdot e^{-jh[o]\omega t} \}
\end{aligned}
\tag{149}
$$

For example, for a passive rectifier the *qd*0 system has a non-zero content at $6 \cdot (o-1)$ multiples of $\omega_e. = \{0,6,...\}$. With a choice of $ach = 2$ the *abc* variables can have content at $\{0,1,5,6,7\} \cdot \omega_e$.

4.5   *Special Infrastructure for harmonic initialization*

The general layout of the combined behavioral/harmonic modeling was proposed earlier. In the following, details on the Modelica-specific implementation is shown, which is necessary for the automatic code generation.[10]

All **AC components** are based on the same **interface** definition in "`Acplug`":

---

[10]Indices [ ] in Modelica start with "1" while harmonics were labeled by ( )

```
connector Acplug "Plug for 3-phase interface"
  outer parameter Integer ach;
  AC_Angle AC_base[1];
  AC_Angle AC_angle[ach];

  flow ComplexCurrent iq[ach];
  flow ComplexCurrent id[ach];
  flow ComplexCurrent i0[ach];
  ComplexVoltage vq[ach];
  ComplexVoltage vd[ach];
  ComplexVoltage v0[ach];

  flow Current i[3];
  Voltage v[3];
end Acplug;
```


acplug
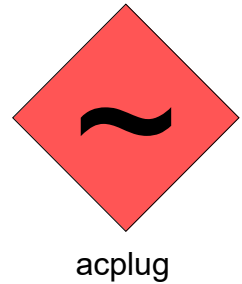
In the plug, the interface variables for AC 3-phase quantities (`i`,`v`) and of the harmonic system (`iqd0`,`vqd0`) are defined. The phase angles of electrical base frequency, AC_base, and of the harmonics, AC_angle, could be set globally on the top-level. Instead, the transfer of this information via the connectors allows to simulate independent systems with different net frequencies in parallel in a top-level model. The source of the net frequency and source of the harmonic content are not necessarily the same. Also, for efficiency reasons, only a limited number of harmonics should be treated in the model and simulation. This number of AC harmonics "`ach`" is defined on the top-layer ("`outer`"). For the electrical network under consideration, the generator feeds in the net frequency. w_{base} can be calculated from $der\left(AC_{base}\right)$ The harmonic frequencies of interest are defined by the harmonic source: On the DC side and AC side in qd0 system, the 6-pulse rectifier excites distortions in relation to the net frequency at zero frequency, plus multiples of the 6th harmonic[11]. The harmonic source can easily be replaced by other kinds of rectifiers, like 12-pulse, 18-pulse or active-switching inverters. The infrastructure does not support several harmonic sources with different orders of harmonics fed to the same line.

The **one-phase plug** is very similar to the Acplug:

```
connector Dcplug " Plug for a 1-phase interface"
  outer parameter Integer dch;
  DC_AngularVelocity omega[integer(2*dch+1)];
  ComplexVoltage vcx[integer(2*dch+1)];
  flow ComplexCurrent icx[integer(2*dch+1)];

  flow Current i;
  Voltage v;

end Dcplug;
```


dcplug
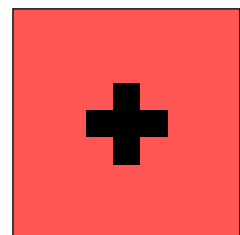
Interface variables are the 1-phase quantities i and v, plus harmonics `vcx`, `icx` and their angular velocities `omega`. It is assumed that the definition of the base-frequency comes from the AC side. Therefore, no kind of base DC harmonic is foreseen. The number of one-sided DC harmonics is defined globally by dch. The quantities are of index $dch\cdot2+1$, with positive and negative side harmonics $\{[-dch],..,[0],..,[dch]\}$[12]. The exact representation of the behavioral model in the harmonic domain would demand an infinite number of harmonics. Obviously, only a limited number of DC and

---

[11] In ABC system harmonics $\{(1),\{(5),(7)\},\{(n\cdot6-1),(n\cdot6+1)\}\}$ would occur.

[12] Further reduction of information to only right-half side spectrum would be possible, but complicates the implementation of the rectifier equations; since only little elements on DC side are treated the full spectrum considered

AC harmonics has to be selected for the frequency convolutions in (142) and (143). `acplug` and `dcplug` exist in the versions "positive" and "negative", to indicate the direction of flow.

The **generator equations** were already introduced earlier. For the behavioral model, the saturation factor was smoothed by a first order filter

$$\dot{k}_{sat} = \left(k_{sat} - f\left(i_m, vars_2 \right) \right) \cdot 1 / T_1 \tag{150}$$

with certain benefits for symbolic processing. This is also helpful for the harmonic initialization: Here, k_{sat} is a state, rather than a direct result of a function. Therefore it may be initialized to k_{satP} of the harmonic model.

As written above, the electrical angles must be defined by a "root" in one of the components. The generator equations link the mechanical shaft speed to the synchronous speed of the electrical network. Therefore, the electrical base angle `AC_base` is defined by this component.

In case there are several electrical machines in the network, with the same synchronized frequency, the base angle `AC_base` would be set by each component. This would result in over-determined equations for `AC_base`. The language construct "root" allows parallel operation of multiple generators in the same network with the same operating frequency. It will be shown later, that each electrical component can split the information-network of each "root" variable into autonomous parts by the "branch" operator. For details, see chapter 9.4 in the Modelica language specification (Modelica, 2010).

```
...
Connections.root(Plug_a.AC_base);
Plug_a.AC_base[1]=theta_e;
..
Modelica.Blocks.Continuous.FirstOrder
 firstOrder(T=1e-6,y(start=KsatP));
...
```
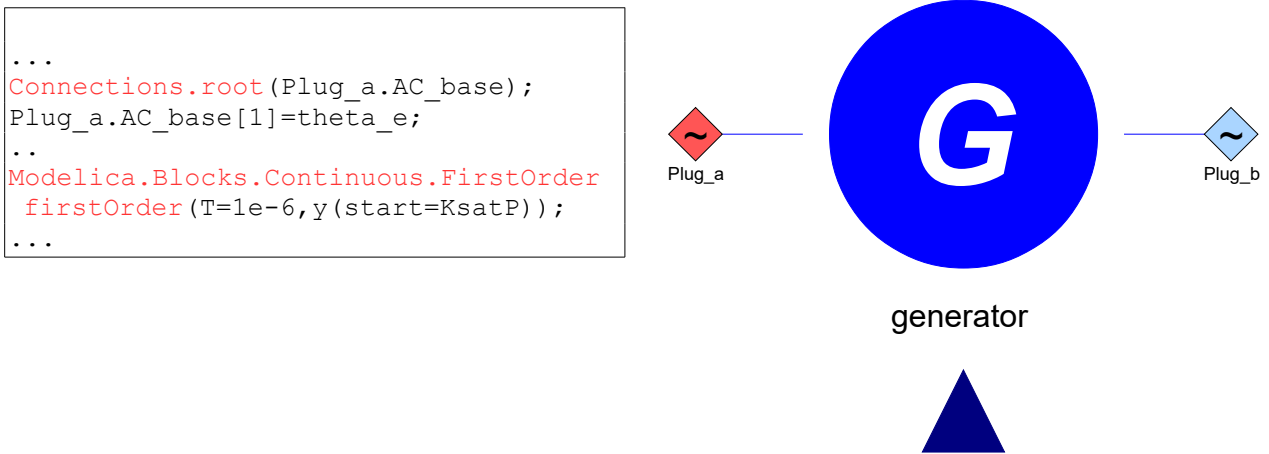

generator

Also, the **rectifier's equation** were already studied in detail. The rectifier is the base for the harmonic frequencies on AC side `plug_ac.ac_angle` and on DC side `pin_p.omega`. While the base frequency is the synchronous frequency of the generators, the number of harmonics is specific to the type of rectifier and must be set here.

```
...
Connections.root(pin_p.omega);
Connections.root(plug_ac.ac_angle);
...
```


rectifier
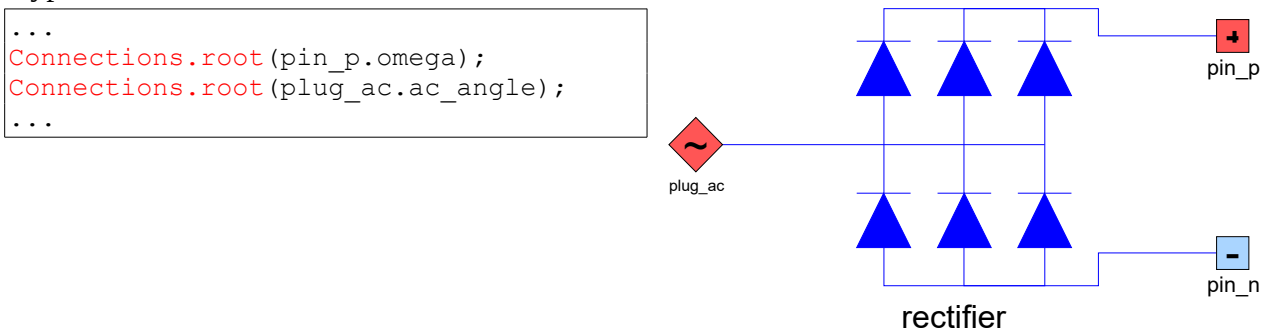
The **RL-element** was discussed in section 4.4.1 with its pseudo-code.

97

```
model RlPhasor
 extends twoplugPhasor(v(start=vI),i(start=iI);
 parameter Resistance R;
 parameter Inductance L;
 parameter Resistance R_qd[3,3]=diagonal(fill(R,3));
 parameter Inductance L_qd[3,3]=[L,0,0;0,L,0;0,0,L];
 parameter Resistance R_abc[3,3]=diagonal(fill(R,3));
 parameter Inductance L_abc[3, 3]=[L,0,0;0,L,0;0,0,L];
 parameter Real yL_qd[3, 3]= y*L_qd;
 constant Integer y[3, 3]=[0, 1, 0; -1, 0, 0; 0, 0, 0];
equation

//EQUATIONS HARMONIC SYSTEM
for o in 1:ach loop
   wac_base*yL_qd*iqd0[o] + j*wac[o]*L_qd*iqd0[o]+
   R_qd*iqd0[o] = vqd0[o];
 end for;

//EQUATIONS ABC SYSTEM
  L_abc*der(i) + (R_abc)*i = v;
end RlPhasor;
```

The model contains equations for harmonic domain and ABC system. All relationships which are common by **two-port elements** (R,L,C,…) are shifted to the sub-model "TwoplugPhasor".

```
model TwoplugPhasor
  outer parameter Integer ach;

//SECTION FOR DEFINITION OF VARIABLES EXCLUDED
..

//CONNCECTION OF ANGLES
for o in 1:ach loop
  theta[o]= Plug_a.AC_angle[o];
  Plug_a.AC_base=Plug_b.AC_base;
  Plug_a.AC_angle[o]=Plug_b.AC_angle[o];
  wac[o] = der(theta[o])
 end for;
  Connections.branch(Plug_a.AC_angle,Plug_b.AC_angle);
  Connections.branch(Plug_a.AC_base,Plug_b.AC_base);

//TWO-PORT EQUATIONS ABC
  v=Plug_a.v-Plug_b.v;
  i=Plug_a.i;
  Plug_a.i = -Plug_b.i

//TWO-PORT EQUATIONS HARMONIC
for o in 1:ach loop
  vqd0[o]= Plug_a.vqd0[o] - Plug_b.vqd0[o];
  iqd0[o]= Plug_a.iqd0[o];
  Plug_a.iqd0=-Plug_b.iqd0[o];
  iI=PI(iqd0[o],wac[o],time)
  vI=PI(vqd0[o],wac[o],time)
 end for;
...
```

The angular velocities are calculated from the angle information.

The "connections.branch"-operator is part of the "root" concept. Internally, a spanning-tree-structure for each "root"-type-variable is generated, based on the geometric propagation of the in-

formation of the variable via the components and connections. In case the angle information is set by several sources, and available on both interface sides of an element (positive plug and negative plug), only the information from one side is taken. Otherwise the information of the variable is "connected" to the other side. The multiple information could come from multiple generators or multiple rectifiers in the same network.

The relationship `iI=PI(iqd0[x],wac[x],time)` calculates the time domain solution from the static harmonic phasor representation, using the inverse Park transformation in Equation (149). The same holds for vI. These variables are the estimated periodic steady-state values, which are indicated as possible start values for the time-domain value. For the RL-element, this is:

```
model rlPhasor
  extends twoplugPhasor(v(start=vI),i(start=iI);
```

The transformation of the static phasor variables in qd0 domain to time domain is only necessary for the calculation of the estimates for initialization. In simulation, it is still helpful, since the simulation of the behavioral model can be compared easily to the harmonic model's periodic steady-state solution. For slightly better numerical performance, all transformations of Equation (149) may be evaluated at initialization time t_{start} only. For this, in "`TwoplugPhasor`" iI and vI are calculated from the static t_{start} instead of the variable "time".

The propagation of the angle information is visualized in (4.14). The only generator propagates the base angle information through the AC network to all AC components (greenish). The upper rectifier is a root for the angles of the harmonics back to the AC network (blue-green). Also, it is a root of the DC harmonics to its network (orange). The lower rectifier is a root of harmonic angles, only to a part of the AC network (warm green). The propagation of the harmonic angles is interrupted in the "ACbusbar" component. However, this rectifier is a root of DC harmonic angles to the separate DC network (red).
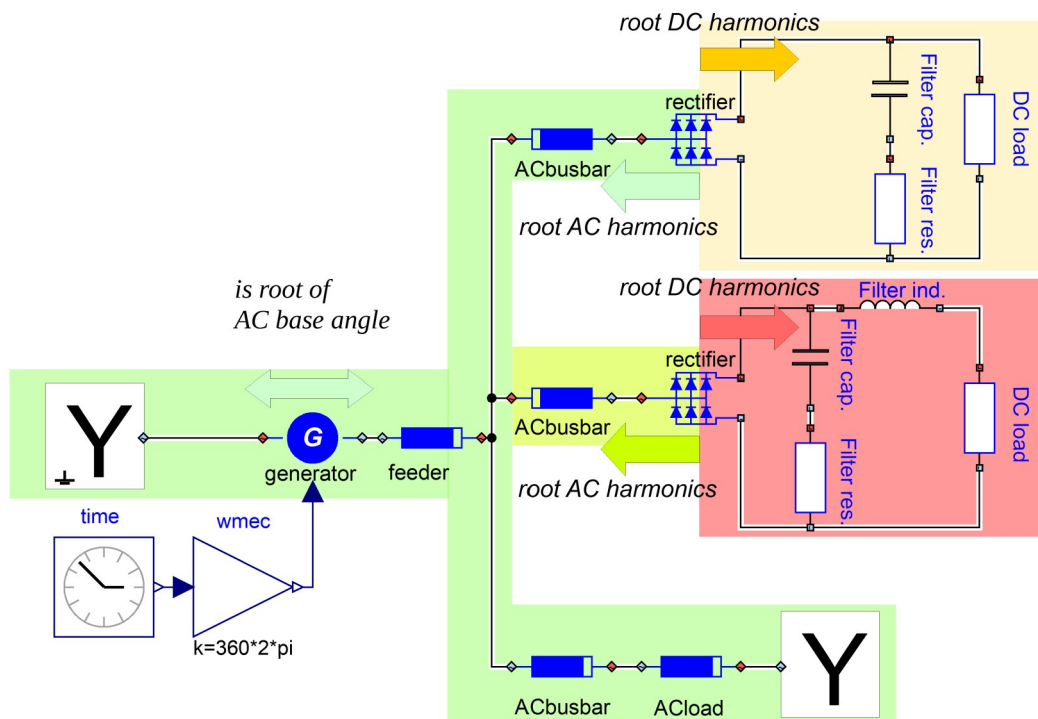
Figure 4.14: Propagation of angle information

4.6 Demonstration and results

Figure 4.15 shows an equivalent model structure to the prior simulation model for the power quality study. The generator is driven by a fixed-speed input. The generator, feeder, line and acload are three-phase quantities. The rectifier labeled with "AC/DC", feeds the DC circuit to the right. All components contain both a frequency-domain model and the time-domain model. For the AC side, 3 harmonics in qd system are treated ($f = \{(0),(6),(12)\} \cdot f_{base}$); (the abc variables at $1 \cdot f_{base}$ are re-
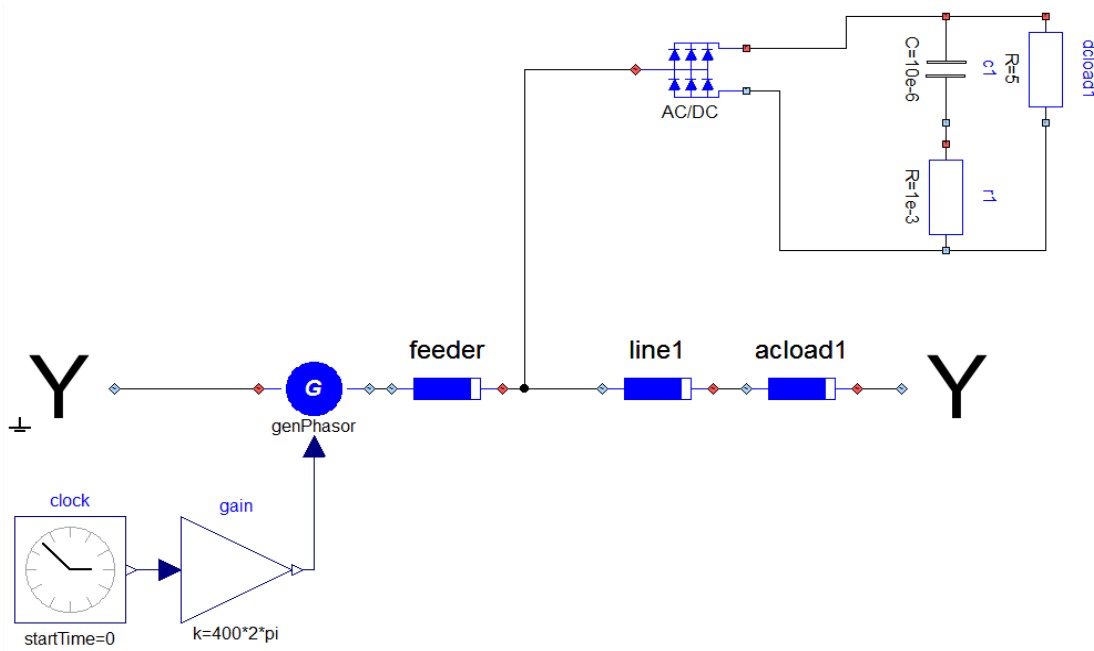
Figure 4.15: View of alternative simulation model with parallel harmonic/behavioral modeling
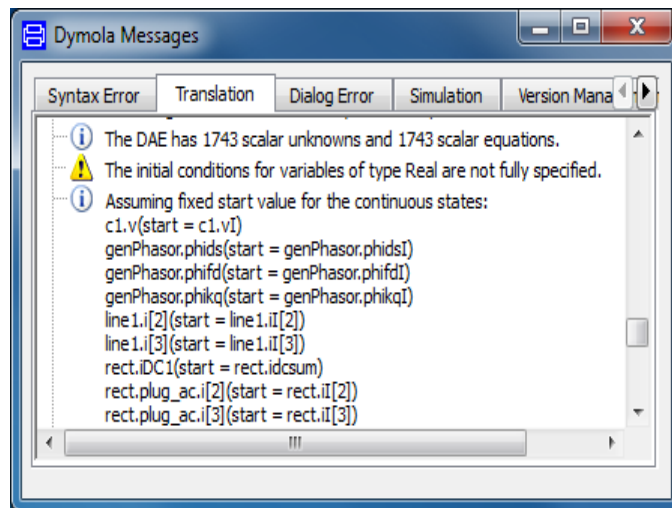
Figure 4.16: Translation transcript

lated to the qd system at $0 \cdot f_{base}$). For the DC side, two side harmonics are considered ($(f = \{(-7), (-5), (0), (5), (7)\} \cdot f_{base})$.

The harmonic models served as a start value for the detailed models. The correct choice of the initial conditions can be seen in the simulator's translation transcript window in Figure 4.16. All state variables are set by their equivalent harmonic variables. The initial equation system is quite complex. A non-linear equation system of order 12 has to be solved. This high complexity meets the expectations, since the harmonic relations are of high order and the behavioral model has to be initialized with it.

In Figure 4.17 a plot of the AC line current, phase A, can be seen. "Harmonic steady-state model" means the approximation model in frequency domain transferred to time-domain while "behavioral" is the result of the full-scale behavioral model's simulation in time-domain.
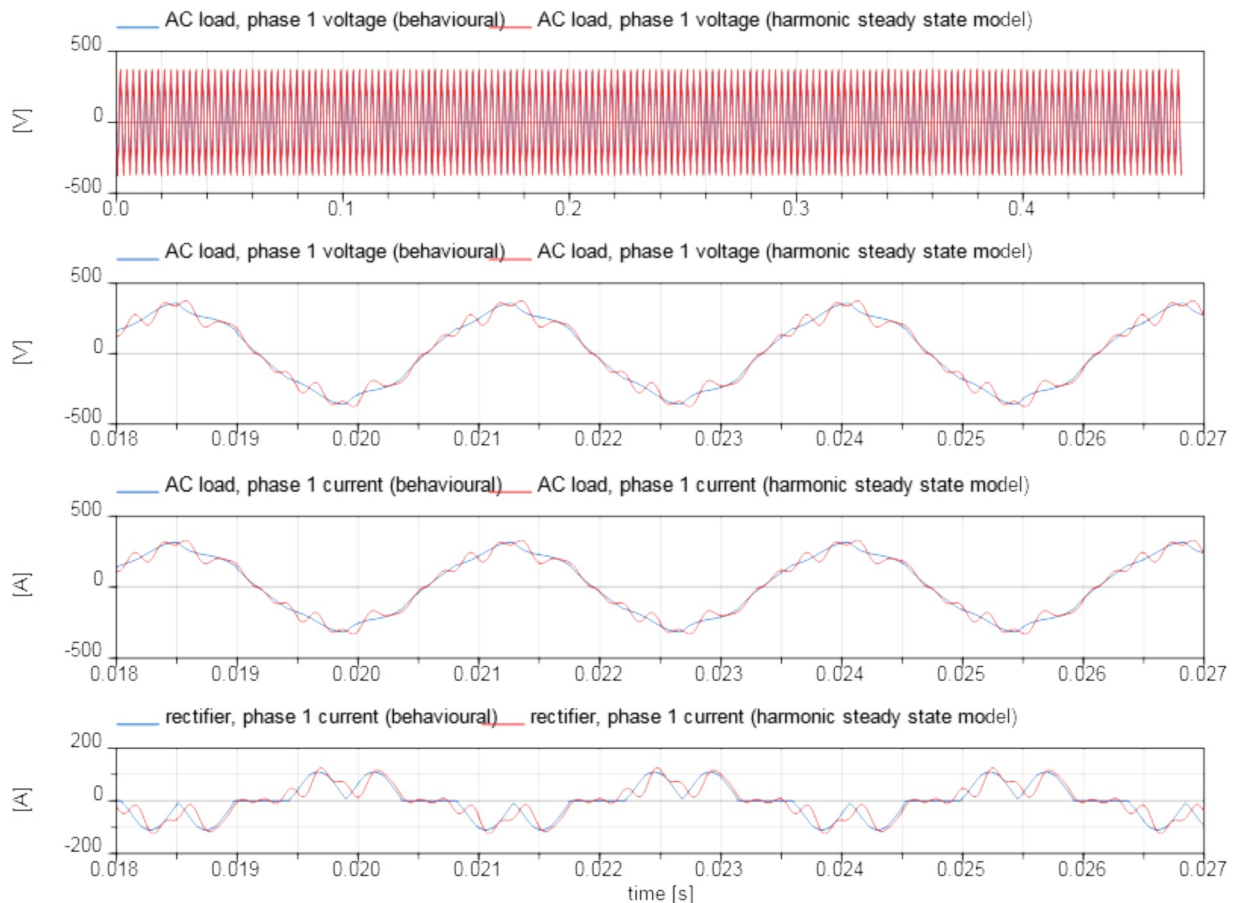
Figure 4.17: Simulation result, behavioral model vs. harmonic model

The currents' behaviors coincide quite well. Since the simple harmonic rectifier model does not consider the discontinuous current mode, the harmonic model slightly exceeds the validity domain. Similarly, if the DC load is made larger, then the rectifier is operated in continuous current mode. In this mode, the generator and feeder lines exhibit inductive behavior in the order of 50 µH, which will induce a commutation interval. This also exceeds the validity-domain of the harmonic model. Therefore the red plots of the harmonic solution show some unexpected deviation from the blue behavioral plots. Nevertheless, it is not necessary to match the waveforms exactly, but to find an initialization which is close enough to the real solution to achieve robust initialization. This was found for all operation modes.

The "periodic steady-state" condition of the ACload phase 1 voltage in the upper plot can be seen easily by inspection. But, as can be seen from Figure 4.18, there exists internal states which are not in periodic steady-state but where model deficiencies results in an initial transient. The model converges to periodic steady-state within no more than 0.15 seconds. Therefore, it is a question of definition, whether periodic steady-state condition means periodic steady-state of all variables of the system, or only in the output variables.

The periodic steady-state condition in the output variable is tested more precisely, by a test of
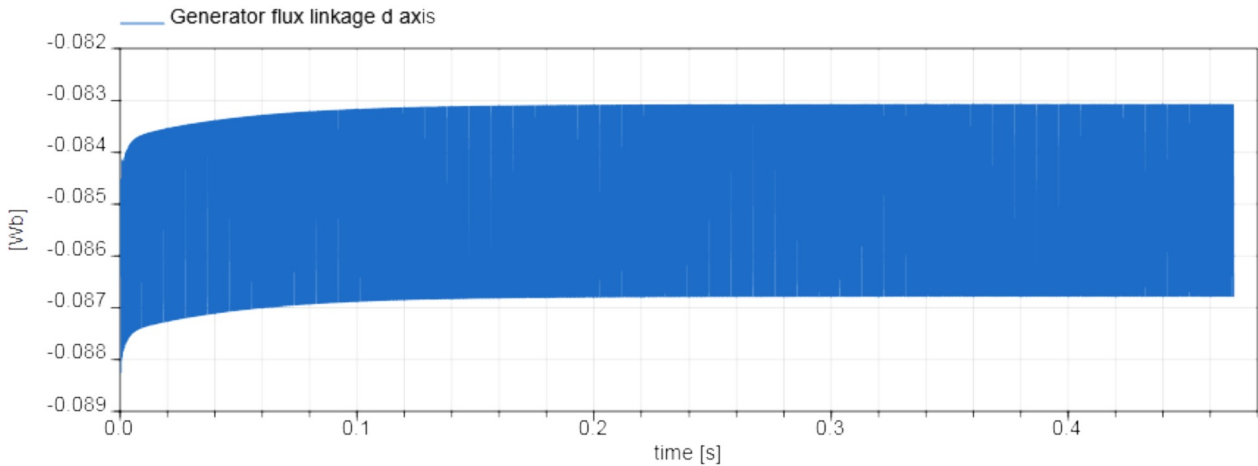
Figure 4.18: Simulation result- flux q axis
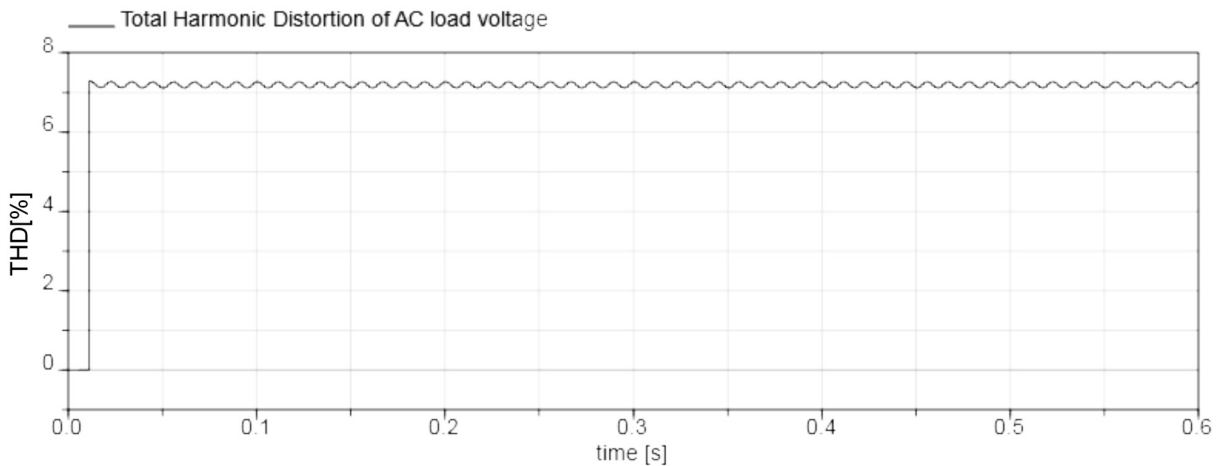
Figure 4.19: THD of Va of AC load

the change of total harmonic. Instead of the data samples of 0.45 seconds, the signal is checked at a lower internal frequency resolution, with a data vector of 0.0110833seconds of simulated time. The THD is plotted in Figure 4.19. The first evaluation is performed after simulation of the first data vector length. Oscillations of THD are an inherent phenomena of the FFT calculation without spectra averaging and are not related to the real value. The local mean value of THD stays at 7.19% from the beginning, which confirms that a periodic steady-state is found almost instantly in the output variable.

In terms of simulation speed, the simulation model behaves similar to the model without GCU. Small benefits can be traced back to the alternative ideal switching rectifier.

For the ramp-up phase, a time of 0.02 seconds is estimated. With generation of 0.45 seconds of data, the total simulation time is reduced by 59% compared to the original model with GCU. Details can be found in Table (8)[13].

	Model with GCU	Model without GCU	Model with harmonic initialization w/o GCU
Convergence to steady-state	by control	transient dynamics of system	transient dynamics of system
Size of equation system	1 linear, order {12}	3 linear, order {7,5,5}	1 linear, order {10}
Type of initialization	from zero	From zero with const. excitation	start values from harmonic
Size of initialization system	non-linear, {13}	non-linear, {5}	2 Linear {7,7}, 1 non-linear, {12}
Typical ramp up time (sim.)	0.05s	0.15s	0.02s
Scaled time for simulation of the models for 0.45 s data	100% (0..0.5s)	52% (0..0.6s)	41% (0..47s)

Table 8: Comparison of properties of model with GCU, w/o GCU, with harmonic initialization and alternative rectifier modeling

4.7 Summary

In the original study the simulation model was shown to be slow. This chapter concentrated on simulation efficiency and found potentials in the simplification of the generator control unit. At the same time, the open loop system showed a considerably longer ramp-up phase to the operating point. Therefore, in the second part, an alternative initialization was proposed which approximates the model by the harmonic periodic steady state solution and maps the initial solution to the detailed simulation model. One of the basic ideas is to couple the derivative of states, rather than the states, in the harmonic sources and introduce an additional relaxation term. For the rectifier with current harmonics, this enabled the initialization of the flow variables by the harmonic model, even with a little deviation of the input/output current-relations to the ideal-switching model. The relaxation term decays by it self in simulation. Algebraic loops involving multiplications of state-variables- like the magnetic saturation- can be relaxed by introduction of dummy-derivatives. The potential benefit of the advanced initialization of time-domain simulation models by harmonic models was demonstrated.

Apart from the missing implementation of the triple-space harmonics and the idealization of the rectifier, the behavioral model is unrestrictedly valid, independent of the harmonic model. Incorrect

---

[13] Time without calculation of time-domain equivalent of phasor system; with calculation, for better comparison with behavioral model: 48% in relation to model with GCU

estimates of the harmonic model do affect the correct initialization of the periodic steady-state, but do not affect the validity of the simulation itself.

The actual implementation of the harmonic model is known to lack generality for the following aspects:

- No asymmetrical AC feeders are considered. This was not a limitation, since only symmetrical lines were demanded for the tests according to the industrial standards.
- No periodic common mode current is considered. This assumption is valid for this test case, since the relevant industrial standard defines no impedance to ground.
- For the rectifier harmonic model, a continuous current mode with no commutation interval is considered and the switching angle is calculated from the phase of the fundamental wave only. The authors of (Bing et al., 2009) point out for six-pulse rectifiers with reasonable load, this is a valid assumption. They propose alternative models with other operation modes which may be implemented easily.
- No dynamics of the mechanics is taken into account. This assumption is valid for aircraft turbines with high inertia.
- The generator model can only consider magnetic saturation in dependency of the base-magnetizing current, which results in a static pre-factor of the magnetizing inductance. Saturation in higher harmonics may need advanced models and proper verification against hardware.

The success of the initialization method was shown but can not be proven mathematically. Also the convergence to periodic steady-state was checked only by inspection. It was shown that internal states may have transients, which are not visible in the output variables. The correct identification of the periodic steady-state condition is subject to chapter 5.[14]

4.8 Contributions

In this chapter a detailed analysis of the simulation model for consideration of power quality was performed, with focus on initialization and reduction of unnecessary system dynamics.
The study confirmed

- *the usefulness of a multi-level based modeling approach, which is used here for automatic calculation of steady-state values.*

While a lot of research is spent on alternative models, there is no literature known for systematic initialization of high fidelity switching, AC driven models by harmonic models. This thesis

- *analyzed the needs of the benchmark example for the infrastructure and models.*
- *For the rectifier, a novel detailed simulation model was developed further, which suits very well for the automatic initialization.*
- *The extended infrastructure allows a fully-automated graphical-based modeling of the network, where information on the specific harmonics is shared automatically among the components via the connectors.*

Relevant publication:
„Modeling and Use of an Aircraft Electrical Network Simulation for Harmonics Consideration in Generator Design" (Kuhn et al., 2012)

---

[14]The DC side shows low damping because of the low resistance. The filter values are taken constant throughout this thesis and the values do not limit the validity of the method and models. For real trade-off studies of the generator and DC load a higher ratio of DC filter resistance to filter capacitance might be taken.

5 Identification of Periodic Steady State condition

The following section focuses on methods for stationary Steady State Identification (SSI) of systems. An overview is given and a method suitable for an AC-connected electrical on-board network is proposed.

5.1 Introduction

Testing of power quality criteria of electrical components and networks according to industrial standards, as (STD-704F, 2004), often demands testing in settled condition. When the data is generated from a simulation of the physical system, at best, the system might be initialized in steady-state condition already. For non-linear switching and periodic systems this condition might not be found easily or only approximately from alternative representations, as in 4.3.1. In this case, the time-domain simulation of the system may converge to the exact periodic steady-state condition from a start condition, if the system is internally stable and well damped. The correct estimation of the convergence time becomes crucial if the evaluation of the quality criterion is part of a closed-loop optimization of the system itself. Then the time for simulation to reach steady-state condition, may affect the total time for the optimization process significantly. While the convergence rate may be known analytically for simple systems, generally this is not the case for arbitrary systems. This chapter shows practical methods for testing on the periodic steady-state condition of AC electrical circuits to reduce unnecessary simulation time. Input signals can be simulation results or measurements. It is assumed that the differential algebraic equation system or the loosely coupled subsystem of interest is completely observable via the chosen output.
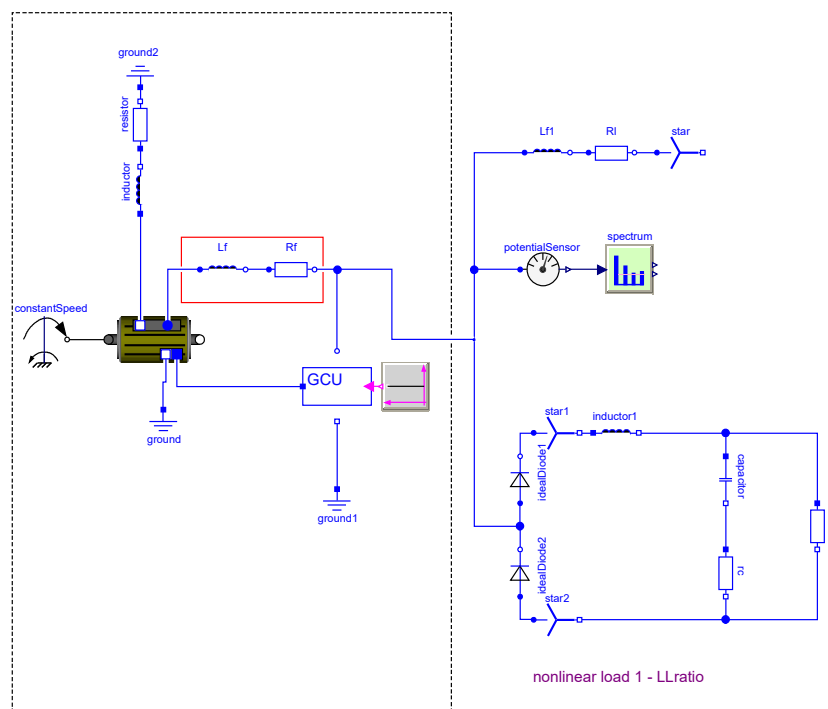
Figure 5.1: Simulation model for power quality of a small aircraft electrical network (components in Modelica layout: 3phase elements with circular connector, 1phase elements with rectangular connector)

To demonstrate the requirement, the already presented example of a small aircraft electrical network in Figure 5.1 is used. The generator feeds a mixed AC resistive and DC 6-pulse switching load. The model simulates through an initial transient phase, till it reaches periodic steady-state. The design is then tested for conformance with industrial standards on power quality in the AC distribution line, which is found between the generator on the left and loads on the right. Power quality is tested via a Fast Fourier Transformation (FFT) Routine block.

The fast identification of periodic steady-state is of wider interest in simulation technique; for example for the non-linear transfer analysis in the simulation software Saber[®][15] or a similar Modelica-based tool (Bünte, 2011). Both record the input/output behavior of a system, where the input is a frequency sweep signal. Its rate of change is limited in order to arrive -hopefully- in steady-state at the output. The sweep rate may need manual tuning for the specific condition, which may be circumvented by an automatic steady-state detection.

This work focuses purely on the detection of the periodic steady-state of systems with output $x(t)$, which can be represented by a superposition of band-restricted time-varying harmonic phasors $X_k(t)$. with base angular velocity ω_{base}.[16]

$$x(t) \approx \sum_{k \in K} X_k(t) \cdot e^{j k \omega_{base} t}, K \in \mathbb{Z}, X \in \mathbb{C}, x \in \mathbb{R} \tag{151}$$

The time variant complex variable $X_k(t)$ is called dynamic phasor

$$X_k(t) = \frac{1}{T} \int_{t-T}^{t} x(\zeta) e^{-j k \omega_e \zeta} d\zeta \tag{152}$$
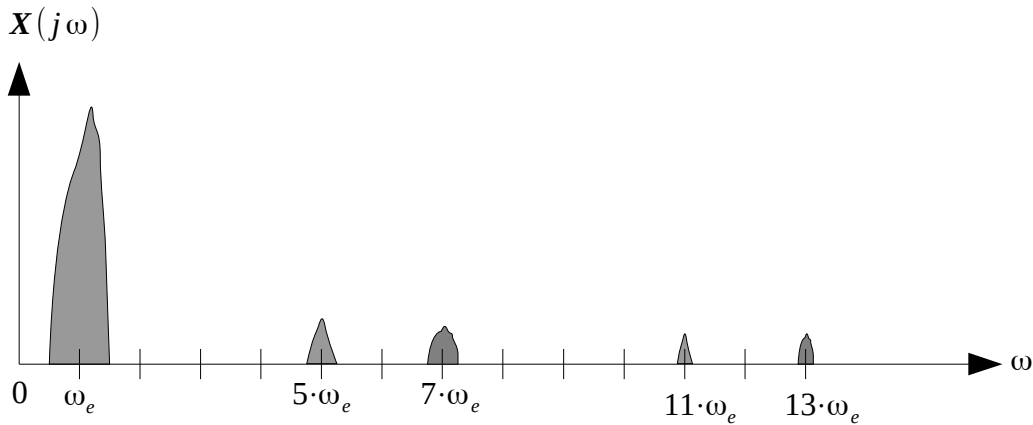
Figure 5.2: Fourier spectrum of nonstationary signal, with spectral content around $\sin(\omega_e)$, $\sin(\omega_e \cdot (6 \pm 1))$, $\sin(\omega_e \cdot (12 \pm 1))$

The mathematics can be found for example in (Demiray, 2008). An example of such a system with time-varying content around distinct frequencies is displayed in Figure 5.2.

It is called a non-steady state condition, where any content $X_k(t)$ is changing in the interval of interest. Once periodic steady-state condition is found by the steady state monitor, the system may be analyzed further.

---

[15]Synopsys, Inc. "Saber", https://www.synopsys.com/verification/virtual-prototyping/saber.html

[16]For analysis of periodic systems and initialization of models one may look for methods like harmonic balance or shooting method (Föllinger, 1993). For modeling of periodic systems also some Modelica libraries exist such as Modelica.Electrical.QuasiStationary.

The section is structured as follows: First, the difference between steady-state and periodic steady-state is highlighted. An overview on applicable methods for Steady State Identification is given in section 5.3. Section 5.4 discusses the transformation from periodic to non-periodic domain by pre-operators. The main theory of three selected methods for steady-state detection is presented and tested in section 5.5. This is followed by a conclusion. A derivation on parametrization of Discrete Fourier Transformation (DFT) for the purpose of Total Harmonic Distortion (THD)-based steady-state detection is given in section 5.7.

5.2 Steady State versus Periodic Steady State Identification

In general, a time-variant system $F(x,\dot{x},u)=0$, excited by input u or autonomous, may show stable-stationary, unstable-stationary, stable-periodic, unstable-periodic or chaotic behavior of the state variables and possibly of the outputs. For non-linear systems, the system may bifurcate into several possible periodic steady-state solutions (Schupp, 2003). For linear differential algebraic systems, a steady-state detection mechanism may search for the condition

$$x(t)-x(t-\Delta t)=0 \text{ or } \dot{x}=0 \tag{153}$$

In practical applications only the detection of a minimum convergence rate $\dot{x}<\alpha_1$ may be feasible, since a longer duration of $\dot{x}=0$ may not appear because of asymptotic convergence and/or additive noise. In the case of periodic systems, the steady-state definition has to be adapted. It is called a periodic steady-state condition, where consecutive cycles do not deviate, which means they have an auto-correlation of 1. This can be expressed by

$$x(\tau)-x(\tau-T)=0 \,\forall\, \tau\in[t-T..t] \tag{154}$$

where the periodicity time constant T replaces the infinitesimal Δt in equation 153.

To display the difference between steady-state and periodic steady-state, Figure 5.3 shows the output of a very basic first-order lowpass (PT_1) system with a time constant T, excited by a unit step at t=0. The system is asymptotically internal stable and converges to 1. An amplitude of 0.95 may be seen as quasi steady-state condition, appearing after $t=3\cdot T$.
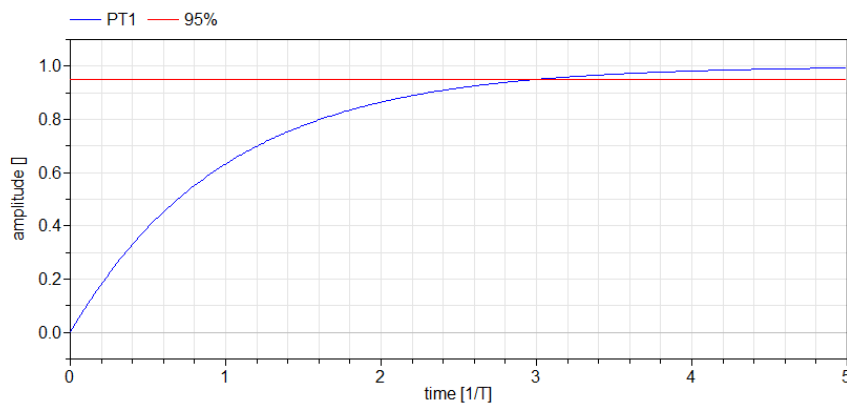
Figure 5.3: Transient of PT_1 system

In contrast to this, the transient of phase A of a three-phase AC voltage of the aircraft electrical network example is plotted in Figure 5.4. While it is oscillating, at the same time, it shows a first-order like transient behavior of the envelope.
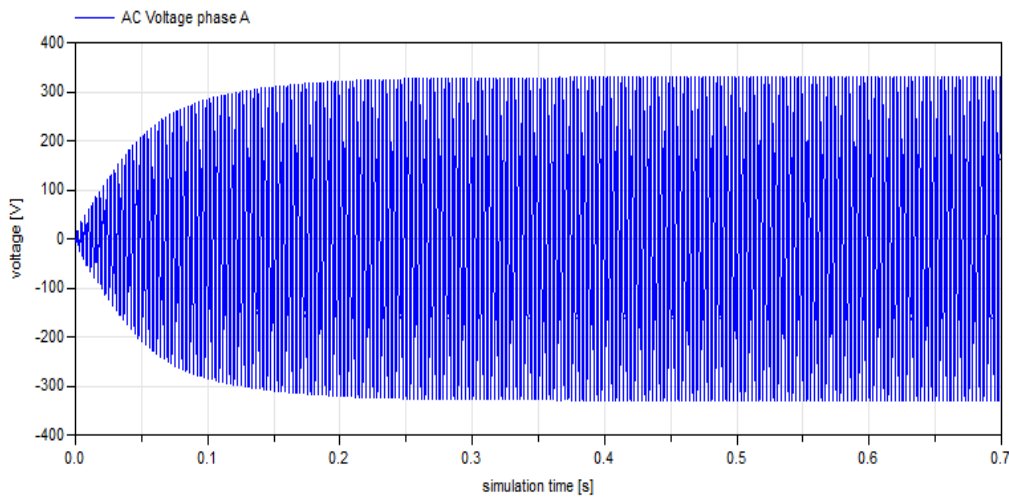
Figure 5.4: Transient of AC voltage of small aircraft electrical network example (original data)

5.3 Overview of methods

The process of signal-based steady-state detection has remarkable analogies with the theory of fault detection. The signal-based fault detection observes the behavior of a system on the change from its nominal (dynamic) behavior. Steady-state detection basically observes the behavior of a system on its change from past behavior. They differ, as fault detectors generally are designed offline with specific fault data and models; absolute values on nominal or faulty conditions are known. Steady-state observers do not necessarily rely on detailed knowledge of the system. Isermann (Isermann, 2006) classifies methods for single signal fault-detection into methods with "limit or trend checking", and methods with "signal models". "Limit and trend checking" methods are applicable for measurable absolute values or measures from statistical observers. Detection by "signal models" include correlation methods, spectrum analysis and wavelet analysis. Isermann defines the basic steps of a scheme for fault detection with signal models, as preparation and transformation into "signal model", extraction of relevant measures by "feature generation" and detection of faults, or by comparison to the nominal behavior in "change detection".

Similar to it, steady-state detection can be separated into the steps:

- "Signal model" preparation, for periodic systems with removal of oscillation by an operator: The prepared signal can be any property in time domain, frequency domain or stochastic property.
- Application of a test on steady-state: The test itself is based on the signal model.
- Decision making: the steady-state decision has to be made. It is very specific to the system, where noise and additional dynamics superpose the potential periodic system and the threshold has to be set based on prior knowledge.

(Additive high-frequency noise is not correlated by definition, and should be filtered out from the original signal beforehand, by low pass filtering)

For the steady-state detection, the following methods attracted attention in research in recent years:

The F-like test developed first by Cao and Rhinehart (Cao and Rhinehart, 1995) belongs to the class of index-based change-detection methods[17]. It relies on statistical methods to identify steady-state in noisy processes. It was tested and expanded on afterwards (Brown and Rhinehart, 2000).

---

[17]A "F-Test" is a detector of the change in variance

Applications included different processes, especially in chemical engineering. Other works by Kelly and Hedengren (Kelly and Hedengren, 2013) concentrated on slow varying drifts in non-stationary processes with application to a windowed signal.

Wavelet transformation can be used to analyze characteristics of a specific system and match its specific output patterns. Based on this, Jiang (Jiang et al., 2000) developed a method for identification of steps, peaks, noises, abnormal sudden changes and similar for chemical processes and reciprocally steady-state. The technique is not adapted to on-line steady-state detection. However, in an independent work, Korbel (Korbel et al., 2014) developed a steady-state identification for on-line reconciliation, based on wavelet transform and filtering for real-time data.

THD is a quality criterion, which is a measure of the distortion of a base oscillation through its harmonics (multiples). In case where industrial standards demand testing for a specific maximum THD, the criterion needs to be evaluated at periodic steady-state condition. When THD is evaluated repeatedly, observation of convergence of ΔTHD can be used as a direct indicator of the steady-state condition. This definition is industrially sufficient for the purpose of testing of THD. It was proposed in (Kuhn et al., 2015).

A further method for detecting steady-state is to use auto-regressive exogenous models with exogenous inputs (ARX). This method allows the SSI by system identification, where an auto-regressive model is tuned from the results of simulation or measurements. It is not based on detailed knowledge of the system equations. The identifiability of the system is checked where singularities in the model matrices appear in case of steady-state. Based on this singularity an index is proposed (Rincón et al., 2015).

From these methods, the "F-like test", wavelet-based test, THD-based test, and an adaptation of the THD-based test in frequency domain will be discussed in detail in the next sections. The first, due to its popularity and simplicity. The second, as a promising approach and to test the new Modelica Wavelet library. The THD criterion and the adapted frequency-based criterion is chosen, since it relies on the objective criterion directly. An overview is shown in Figure 5.5.
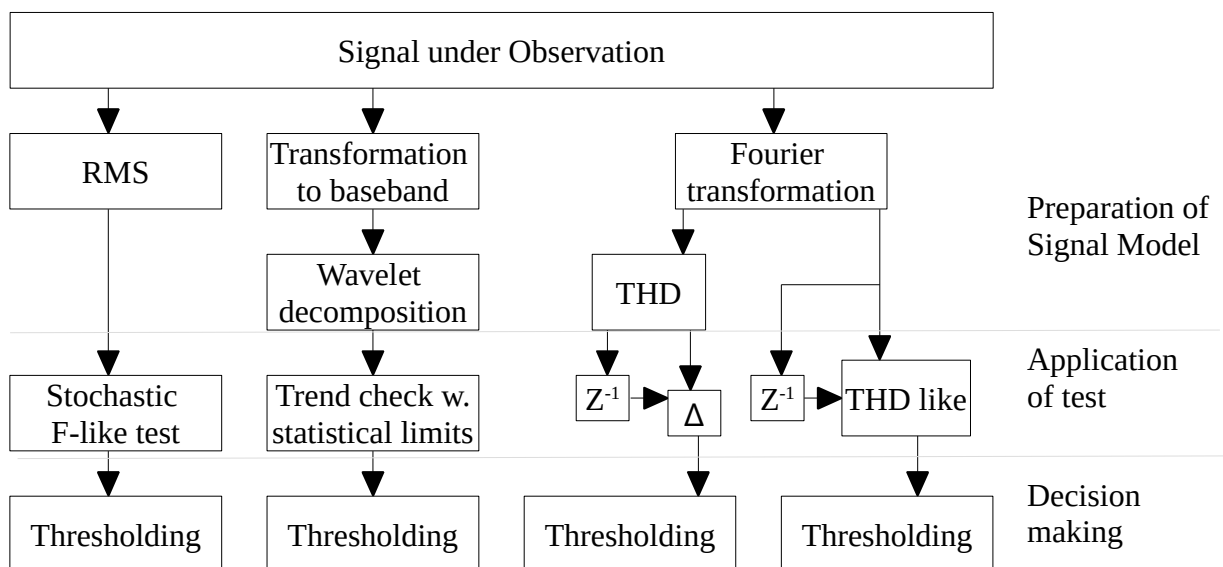
Figure 5.5: Overview on methods for steady-state detection

All methods are tested for detection of steady-state on the small electric on-board network example of the introduction of this chapter.

5.4 *Mapping of periodic to non-periodic variables*

For AC circuits, the method for steady-state testing has to be capable of detecting periodic steady-state. Either by itself, or the signal model preparation has to transform it to an oscillation-free measure. The problem can be overcome by mapping of the periodic signal to a non-cyclic equivalent and identification with standard methods. For a system of type (151), knowledge of a dominating, excited oscillation can be exploited, to identify the steady-state condition of the AC voltage signal. The signals main content is a modulation of a baseband signal x_{bb} and forced oscillation as

$$x(t) = \Re\{x_{bb}(t)e^{j\omega_{base}t}\} \tag{155}$$

plus harmonic content at $k \cdot \omega_{base}$, plus uncorrelated noise. The minimum periodic cycle is the forced oscillation's time constant $T_{osc} = 2\pi/\omega_{base}$, $2 \cdot T_{osc}$ in case of additive odd harmonics, or arbitrary in case of non-harmonic content.

Detection by Equation (154) is not useful to implement, since the condition is only fulfilled for perfect congruence. Instead, it can be simplified by using a norm $\breve{x}(t)$. The steady-state condition can be identified directly via $\dot{\breve{x}}(t) < \epsilon$ or via some more advanced methods on $\breve{x}(t)$, listed next.

The test on steady-state can be seen as testing of the auto-regression of the signal, separated in intervals of length T. And it is similar to regression testing of two signals by the use of norms (e.g. (Pollok and Bender, 2014)). The **maximum error norm** of consecutive periods generates a periodic sampled one-dimensional output:

$$\breve{x}_{me}[t] = max\left(\frac{\|x(\tau) - x(\tau - T)\|}{\|x(\tau)\|}\right) \forall \tau \in [t-T..t] \tag{156}$$

The norm is quite efficient, due to its simplicity. Since it is a norm on signal amplitude rather than energy, it will penalize sharp discontinuities and noise.

Similar to this and even more easy to implement, by a rough knowledge of the period, only peak values within consecutive periods can be selected. The signal corresponds to sample-and-hold of the peak values with sample period T. In aeronautical standards, this is often called the **"envelope"**:

$$\breve{x}_e[t] = \frac{\hat{x}(t-T..t) - \hat{x}(t-2T..t-T)}{\hat{x}(t-T..t)} \tag{157}$$

Only one sample is gained within one interval at maximum or in case of application to the absolute value, an additional sample at minimum. Peak values may be prone to noise as some electronics, as rectifiers, add high portions of distortion to the high amplitude part of a voltage wave.

The **temporal** (time limited) **auto-correlation** treats not only minimum and maximum values, but all data of a period. It normalizes the signal to

$$\breve{x}_{auto}[t] = \frac{\int\limits_{t-T}^{t} x(\tau-T)x^*(\tau)d\tau}{\left(\int\limits_{t-2T}^{t-T} |x(\tau)|^2 d\tau\right)^{1/2}\left(\int\limits_{t-T}^{t} |x(\tau)|^2 d\tau\right)^{1/2}} = \frac{\int\limits_{t-T}^{t} x(\tau-T)x^*(\tau)d\tau}{\left(\int\limits_{t-2T}^{t} |x(\tau)|^2 d\tau\right)^{1/2}} \tag{158}$$

This norm is tolerant to noise and time shifts but highly prone to incorrect estimation on the length of period T. The temporal auto-correlation measure is similar to the temporal auto-co-variance γ_{yy} of stochastic signals. It is common to treat complex or unmodeled processes as stochastic

processes (Oppenheim, 1999), which opens the field of stochastic data analysis for the problem. Other coherency metrics on spectrum, energy and time or phase-shift are listed in (Marple and Marino, 2004).

Alternatively the steady-state condition can be seen as the steady-state condition of the baseband signal. When the condition of a cycle is known exactly, the steady state condition can be identified by one of the following methods:

AC coupled **RMS** (Root Mean Square): This method is best known for power supply networks at a fixed frequency of 50 or 60 Hz. It can be calculated as by MIL 704f, where RMS is the "value for one half-cycle measured between consecutive zero crossings of the fundamental frequency component". Information on harmonic contents is lost by the integration.

$$X_{RMS} = \sqrt{\frac{1}{T} \int_0^T x(t)^2 \cdot dt} \tag{159}$$

When the phase angle θ is known, mathematical transformations to **phase-fixed reference system** can be applied (e.g. dq0/Park system or Fortescue transformation): For simulation, the phase angle is known. For real electrical systems, with single synchronous generator fed networks, it can be obtained by measuring a machines angular position. Without position measurement, the phase can be derived from the AC voltage by Phase Locked Loops (PLL). A PLL is a control circuit which generates an output signal in proportion to the phase difference of a reference signal to a measured signal. It can be used to adapt the frequency and phase of an observer to the measured signal. For equations, see section 2.1.2.

Alternatively, the base band and harmonics can also be identified by **frequency selective filtering**: Signals can be analyzed in the spectral domain, where the base frequency is usually associated with the spectral content of maximum amplitude. The frequency spectrum can be computed as the correlation of the signal with theoretically infinite sinusoidal waves at certain frequencies (Fourier transformation) or the correlation to finite wave packages at prevailing base frequencies (wavelet transformation (Mallat, 2008)). For wavelet transform, one has to distinguish between direct application on sinusoidal signals and application on the pre-processed oscillation-free signal. For finite signals, the Fourier transformation is called Short Time Fourier Transformation, which can be implemented efficiently using Fast Fourier Transformation (FFT) (Cooley and Tukey, 1965)

detail

→ sample-and-hold of the **peak values**
  (industrial: "envelope")

→ testing of the **auto-regression** of the signal,
  e.g. maximum error norm

→ AC coupled **RMS** (Root Mean Square)
  (period from measurement, calculation, zero crossing,…)

→ **temporal** (time limited) **auto-correlation**

→ mathematical transformations to **phase-fixed reference system**
  (e.g. dq0/Park system or Fortescue transformation)

→ frequency selective filtering (incl. Fourier transform)

No harmonics

harmonics

Figure 5.6: Overview of mappings of oscillatory signals to baseband

The methods are listed in Figure 5.6, to show the level of detail. Only the transformations to reference system and the frequency selective filtering methods preserve information of the harmonic content.

5.5 Implementation and validation of tests

In the following section, the selected theories of Steady State Identification are summarised and the steady-state monitors are tested through experiments.

5.5.1 F-like test

The F-like test, by Cao and Rhinehart (Cao and Rhinehart, 1995) is based on statistical measures. The algorithm tests a signal on showing settled distribution at an associated level of significance. Possible distributions are uniform and Gaussian distribution. Measures are variance between data, moving average value and variance in the data itself. This method relies on sampled data.

The following steps can be implemented at low computational effort: First, the sampling vector is filtered by a filter factor of λ_1.

$$X_f[i] = \lambda_1 X[i] + (1-\lambda_1) \cdot X_f[i-1] \tag{160}$$

Where $X[i]$ are sampled data, $X_f[i]$ are filtered values and λ_1 is a filter factor. In the second step, a measure of the variance v_f^2 is computed with a moving average filter factor of λ_2:

$$v_f[i]^2 = \lambda_2(X[i] - X_f[i-1])^2 + (1-\lambda_2)v_f[i-1]^2 \tag{161}$$

The unbiased estimate of the variance based on the filtered squared deviation from previous filtered values var_1 is given by:

$$var_1[i] = (2-\lambda_1)\frac{v_f[i]^2}{2} \tag{162}$$

A measure on the second filtered variance estimate δ_f^2 is calculated based on the filtered square differences of successive data:

$$\delta_f[i]^2 = \lambda_3(X[i] - X[i-1])^2 + (1-\lambda_3)\delta_f[i-1]^2 \tag{163}$$

The formula includes a moving average filter with factor λ_3. This second variance var_2 is given by:

$$var_2[i] = \frac{\delta_f[i]^2}{2} \tag{164}$$

Finally, the Steady State Identification index R is obtained as the ratio of the two variances:

$$R = \frac{(2-\lambda_1)v_f[i]^2}{\delta_f[i]^2} \tag{165}$$

While R is a continuous measure, decision making needs tuning of a threshold R_t to distinguish between steady-state $R<R_t$ and non steady-state $R>R_t$. Filter values have to be tuned to match the time constants of the system under observation. Some more theoretical considerations on correct

and incorrect identification of steady-state are given in (Cao and Rhinehart, 1995), with respect to different types of error signals.

In a first trial, the F-like test was applied directly on the sinusoidal phase voltage. No useful results could be gained (not plotted), which can be explained by the strong correlation of the sinusoidal shaped signal. Therefore, isolation of the signal of interest had to be conducted first. For this example, simulation results did not show significant difference between several methods of RMS detection. Those are transformation by phase angle, integration over one period with start and end conditions identified by zero crossing detection, and peak-value detection. Figure 5.7 (top plot) shows the source signal of the test. The AC voltage is mostly settled after 0.1 seconds simulation time with an additional step of 10% at 0.3 seconds.
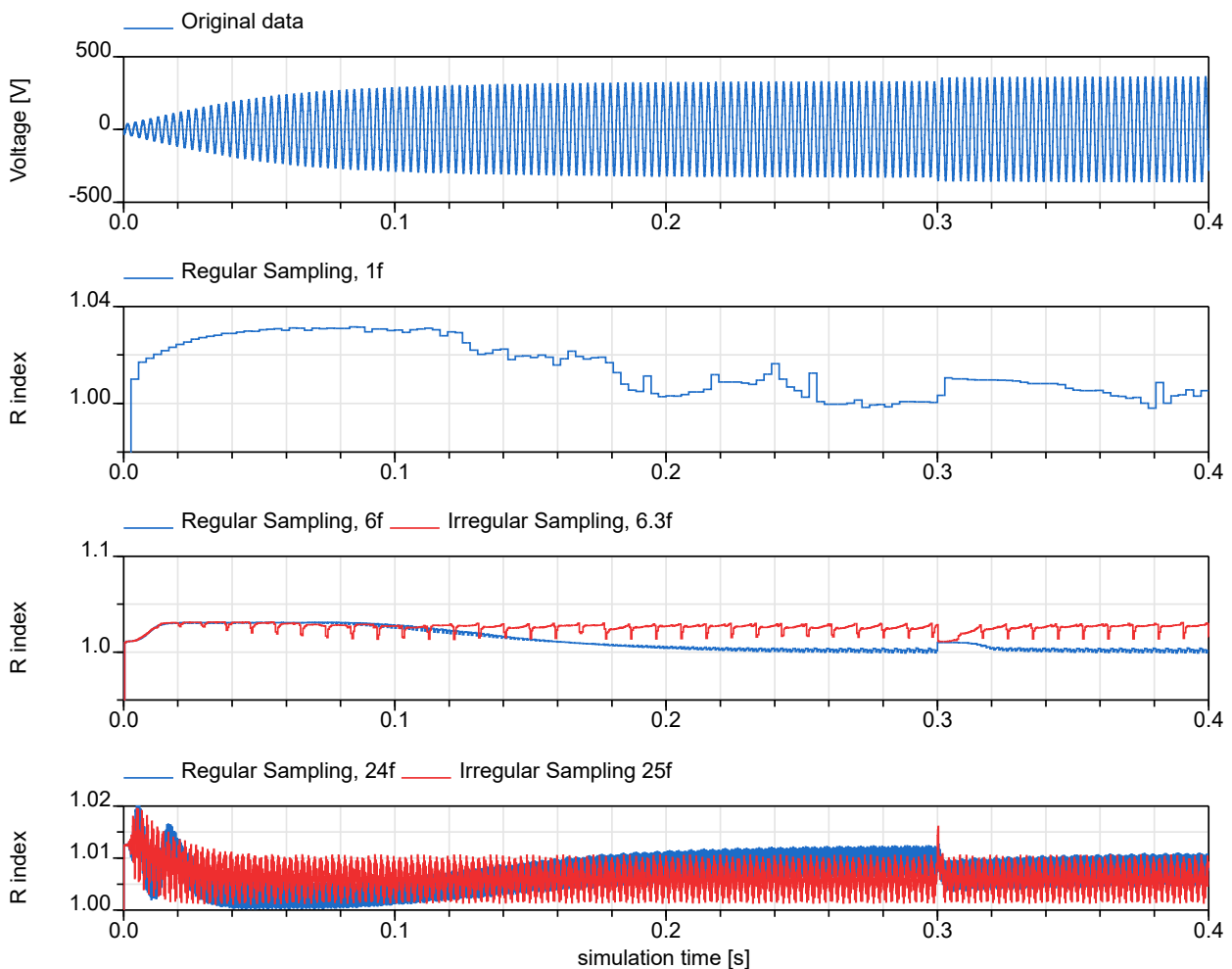
Figure 5.7: "R" index of F-like test for several sampling rates

The influence of different types of sampling, and therefore different dominating noise on identification index R, can be seen in Figure 5.7. The plots present the results of the F-like test, applied on the same source data. Regular sampling intervals with multiples of the rectifier's distortion at 6 times f are: 6f and 24f. Irregular sampling is shown at 6.3f and 25f. The lambda factors were tuned manually. It can be clearly seen the quality of the results diverge on a big scale. The results based on the sampling at 1f show some slow transient behavior, which is hard to interpret. In contrast, 6f and 24f sampling identify changes better. Deeper analysis shows, the method can not detect a significant change in the statistic behavior for this signal but only detects the change of mean.

The R statistics show low pass behavior at steps of the input signal. A decision value on steady-state can be set but needs to deal with the chattering around the boundary value R_t.

5.5.2 Wavelet test

In wavelet analysis, the one-dimensional time variant input signal is decomposed into time variant subspaces with bandpass characteristics. By iterative wavelet multi-level decomposition, the original signal $f(t)$ is projected into a sequence of nested subspaces; each subspace is characteristic for a spectral content, similar to the indices of the Discrete Fourier Spectrum:

$$f(t) = \sum_{i \in I_j} c_{J,i} \varphi_{J,i} + \sum_{j=1}^{J} \sum_{k \in k_1} d_{j,k} \psi_{j,k} \tag{166}$$

The first sum represents low frequency content, while the right part represents higher frequency content. The wavelet spectrum originates from iterative bisection of the high-frequency signal up to scale J. $\psi_j(t)$ are scaled mother wavelets which define orthogonal spaces. Filtering of a signal corresponds to variation and limiting of its wavelet coefficients $c_{j,i}$ and $d_{j,i}$. Adaptive methods for filtering of Gaussian noise exist in many wavelet toolboxes. The filtered signal in the time domain can be restored by inverse transformation of the conditioned data. Formulas for discrete wavelet transformation are similar.[18]

Similar to the F-like test, this method needs separation of the fundamental of the amplitude-modulated wave first. While this can theoretically be done by an additional wavelet transformation, there is no benefit compared to the RMS method presented before. Next, the signal can be de-noised if necessary. Jiang (Jiang et al., 2003) proposes to separate the baseband signal into the desired process trend T(t) and process noise N(t), by wavelet multi-level decomposition, filtering and reconstruction. Any other type of continuous or discrete filters may be used equivalently. Although the signal will suffer from a frequency dependent group delay by the filter, for steady-state detection, this can be seen as negligible compared to the typical time scales.

The wavelet-based detection itself uses the fact, a wavelet transform $Wf(t)$ of a signal $f(t)$ is proportional to the time derivative of the signal smoothed by the scaling function φ (see wavelet theory for details):

$$W f(t) = 2 \frac{d}{dt} (f * \varphi)(t) \tag{167}$$

Furthermore, by the wavelet transform of the wavelet transform $WWf(t)$ one gets an analogon to the second-order derivative. Analogue to assumption of a steady-state condition as a local extremum where first and second time derivative being zero, single and double wavelet transform can be applied. At a (local) minimum, the conditions

$$Wf(t) < \alpha_{w1}, \; d(Wf(t))/dt < \alpha_{w2}. \tag{168}$$

must hold true. Similarly, for steady-state detection in the time domain, specific scaling of the α would be necessary. Where an ideal temporal derivative function is unspecific of the frequency and a Fast Fourier Transformation based spectral decomposition lacks information on the temporal variation, a wavelet can be adapted to the "characteristic scale". This means, the frequency of the wavelet is chosen close to the characteristic response time τ of a system which acts as a kind of a bandpass filter. This can be realized by the sampling frequency directly, or iteratively by fragmentation

---

[18]For background on wavelet analysis, see (Debnath and Shah, 2002) section "Wavelet bases and Multiresolution Analysis".

into a wavelet spectrum with narrower bands of equation (166) which is called multi-resolution representation or alternatively (Jiang et al., 2000) calls it multi-scale process data analysis.

The steady-state index $\beta(t)$ is calculated from equations (169-171) (Jiang et al., 2003), where $\theta(t)$ is a factor of combined contributions from the first and second order wavelet and $\gamma(t)$ is an amplitude-limiting signal operator on the second order wavelet transform.

$$\theta(t) = |Wf(t)| + \gamma(WWf(t)) \tag{169}$$

$$\gamma(WWf(t)) = \begin{cases} 0 & , |WWf| \leq T_w \\ (|WWf| - T_w)/2 \cdot T_W & , |WWf| \in \{T_w, 3 \cdot T_w\} \\ 1 & , |WWf| \geq 3 \cdot T_W \end{cases} \tag{170}$$

β itself calculates as a threshold comparator from the contributions factor $\theta(t)$, with smoothed transient from 0 to 1.

$$\beta(t) = \begin{cases} 0 & , \theta(t) \geq T_u \\ \frac{1}{2}\left[\cos\left(\frac{\theta(t) - T_s}{T_u - T_s} \cdot \pi\right) + 1\right] & , T_s < \theta(t) < T_u \\ 1 & , \theta(t) \leq T_s \end{cases} \tag{171}$$

Where T_s=standard deviation of Wf, $T_u = 3 \cdot T_s$, T_w=median (WWf). In β, "zero" indicates unstable status and "one" steady-state condition. For details, see (Jiang et al., 2003) and for advanced end-of-steady-state-detection see (Korbel et al., 2014).

(Jiang et al., 2003) demonstrates steady-state detection but does not focus on online implementation. It may look straightforward to perform the analysis continuously on a window of past samples. Practical implementations for this thesis showed the correct choice of the limits T_s, T_u and T_w often fails when considering only one window. The median especially moves quite arbitrarily. Therefore, limits are calculated non-causally by using the full data set. This confirms the considerations of (Korbel et al., 2014) who proposes to choose the limits from past measurements.

To implement the wavelet test, the Modelica wavelet library (Gao et al., 2014) was used[19].

The test makes use of the interpolation routine, definition of a wavelet function and the discrete wavelet transform:

```
Wavelet.General.interpL()
Wavelet.Families.wavFunc(Wavelet.Records.wavletDefinition());
Wavelet.Transform.dwt());
```

Results of the test are displayed in Figure 5.8: From the original signal, the RMS value is calculated via Park transformation using generator angular information. The RMS value is processed by first and second order wavelet transformation. The transforms show a clear relationship to the temporal derivatives. β is calculated via Equations (169-171). The first steady-state condition is detected at around 0.05 seconds. This assumption is based on the limits T_s, T_u and T_w and may be changed by different settings.

---

[19]The library is similar to MATLAB's wavelet toolbox. Since the Modelica wavelet library does not support online computation yet, this study is an offline demonstration only. The library can be developed further for online computation, if issues regarding the initialization of buffers, data storage and allocation of vector sizes of intermediate variables are solved. Furthermore, the plotting relies on Dymola-specific Modelica scripting.
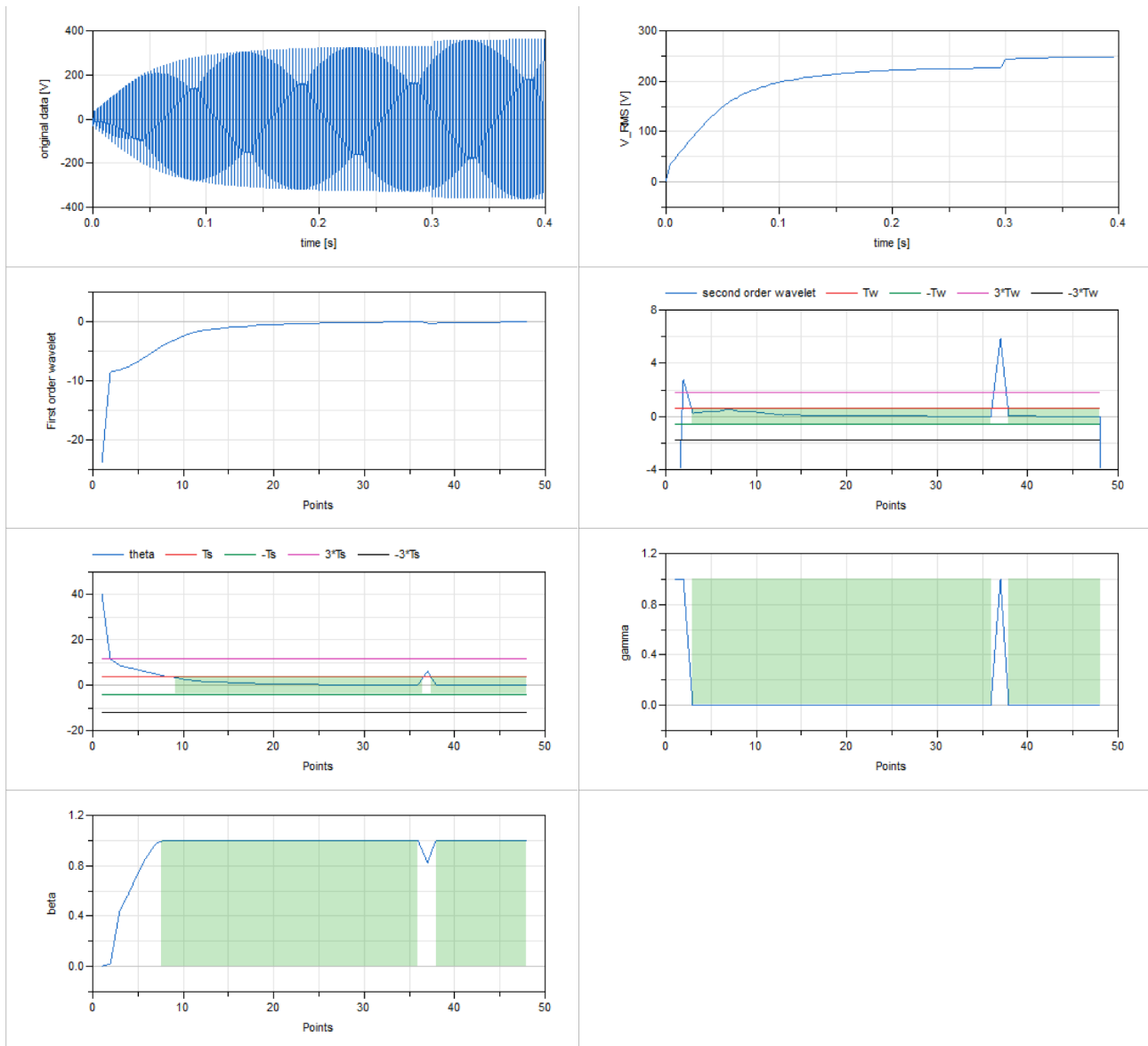
Figure 5.8: Wavelet based test, results; greenish: indication of steady state of individual measure (final selection by "beta")

In summary, the wavelet-based method identifies the steady-state condition of the base harmonic well for the example. The signal can not be processed directly but has to be transformed to a non-periodic representation (RMS). The time scale for the wavelet transform and the limits need to be adapted to the model, based on known prior results.

The computational efficiency can not be tested since the wavelet library is for post-processing only. The tests with this implementation indicate slow performance while the actual performance is highly linked to the number of wavelet coefficients, see (Fan et al., 2004) for a numerical comparison of some techniques. Future Modelica wavelet libraries may be adapted for in-simulation evaluation with state-of-the-art algorithms like fast wavelet transform.

5.5.3 Discrete Fourier transformation based THD criterion

In (Kuhn et al., 2015) a Total Harmonic Distortion based steady-state detector was proposed. Its "signal model" relies on the Fourier spectrum. According to (Isermann, 2006), Fourier spectra are well suited for identification of periodic, stochastic, and non-stationary properties, and therefore for periodic Steady State Identification.

In a first step, a vector of sampled data of the input signal is decomposed into a discrete amplitude-frequency spectrum by a short time Discrete Fourier Transform algorithm. THD is calculated from the spectrum by [20]

$$THD = \sqrt{\frac{\sum_{h=2}^{M} A[h \cdot f_{base}]^2}{A[f_{base}]^2}} \tag{172}$$

It is a one-dimensional norm on the $M-1$ amplitudes of the harmonics, which is normalized by the amplitude of the base frequency. The phase information and DC component is not considered.

Finally, the steady-state test is designed as a normalized "trend checking", based on ΔTHD:

$$y_{THD} = \frac{|THD(t_x) - THD(t_x - \Delta T)|}{max(THD(t_x), \epsilon)} \tag{173}$$

$$y_{THD} \overset{?}{<} \delta \Rightarrow steady\ state$$

ϵ prevents division by zero and influence of noise at small values of THD. The criterion relies on consecutive evaluations of the spectra at times t_x and $t_x + \Delta T$. Each evaluation is based on data sets of length $N[s]$. The time delay between the two THD windows is defined in proportion pr of the data set length, where an overlap of 50% is proposed for the data sets. Theoretical consideration are derived in section 5.7. While THD could be evaluated at every sampling interval, for efficiency reasons, the Modelica algorithm is only evaluated every $\Delta T = N \cdot pr$. When the frequency resolution is set to $1/r \cdot f_{base}$, the total data set length is $(1 + pr) \cdot r \cdot T_{base}$ and evaluated no later than $pr \cdot r \cdot baseperiod$ after an event. For example: $r = 4m$, $pr = 1/2 \rightarrow$ criterion evaluation not later than in $2 \cdot T_{base}$, based on data set length=$6 \cdot T_{base}$.

The main features of the implementation by the Modelica block "WithinAbsoluteFFTdomain_THD" are already discussed in chapter 3. It is a big advantage of this method, that the AC signal can be taken directly as an input. There is no need for pre-processing as RMS or transformation to base band. While the expected base frequency should be given roughly, the algorithm was implemented to tune itself to the dominating peak in the nearby-spectrum. Also, the block features the option to use the criterion as an indicator for termination of simulation; the THD is delivered as a final result at this steady-state condition. No extra FFT computation is necessary for this, as the computation of THD and THD-based steady-state criterion rely on the same FFT data.

The THD-based criterion was tested with the small grid example. Here, the criterion could NOT identify steady-state condition. This shortcoming can be better understood from the plot of the THD in relation to V_{rms} in Figure 5.9, rather than the criterion itself.

As can be seen in the upper plot, the THD is not correlated with the main trend in the bottom graph, even at steps. This is a special property of the small grid example. There exist higher harmonics because of the rectifier, but they are in fixed proportion to the base harmonic with fast and

---

[20]e.g., IEEE Standard 519-2014 (IEEE, 2014)
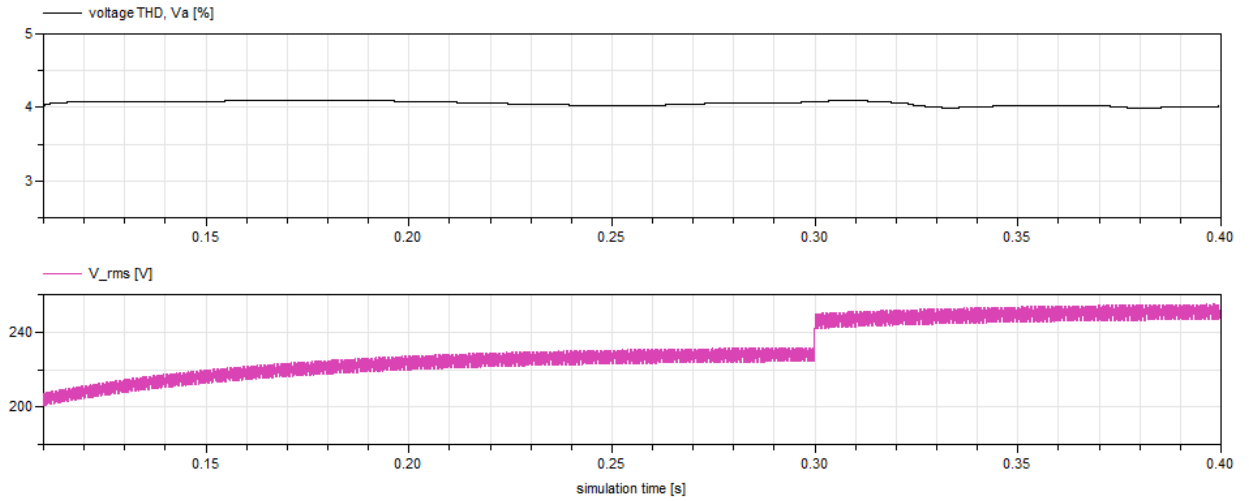
Figure 5.9: Investigation on spectrum: THD vs. signal (FFT window 0.017s)

well damped filter dynamics on the DC side. Therefore, normalization of THD by the base amplitude prevents a change of the criterion in this case. Strictly speaking, for the THD identification according to industrial standards, no "real" steady-state condition would be necessary here, as the THD does not change. But since it is not a proper indicator, it is not generally recommended. But it can be adapted to overcome the obstacles as shown next.

5.5.4 Adapted THD-similar criterion

In order to overcome the problems of the THD-based steady-state monitor, the new "THD-similar" criterion is proposed:

$$y_{THD-similar} = max \left(\frac{\left|A\left[h \cdot f_{base}[t_x]\right]\right|^2 - \left|A\left[h \cdot f_{base}[t_x - \Delta T]\right]\right|^2}{\left|A\left[f_{base}(t_x)\right]\right|^2 + \epsilon \cdot \left|A_{nom}\right|^2} \right) \forall h \in [1..M]$$

$$y_{THD-similar} \overset{?}{<} \delta \Rightarrow steady \ state$$

(174)

It is also based on the DFT spectrum and is inspired by the THD criterion, maximum error norm and variation in base amplitude. In contrast to THD, also the first (=base) harmonic is considered. An educated guess of a factor ϵ of the nominal base amplitude A_{nom} prevents division by zero and smooths the result. The decision threshold δ has to be set based on knowledge from past results.

The discussion of the criterion and the parameterization of FFT is shifted to section 5.7. It is shown, that this criterion is well suited for identification of steady-state of dynamic systems (151), where unmodeled dynamics are treated as uniform noise.

In summary, the difference between Equation (173) and Equation (174) are:

- The $\Delta-THD$-test is a criterion on the change of the THD-factor where THD is a H^2-norm on the higher harmonics of the signal normalized by the base amplitude.
- The $THD-like$-test is a criterion based on the H^∞-norm of the individual differences of all harmonic contents, including the base amplitude. It is normalized by the base amplitude.

The implementation of the function is based on WithinAbsoluteFFTdomain_THD, with the same parameters unless stated otherwise. It shares the benefits with the THD approach, with little simulation overhead through the efficient FFT algorithm. As soon as steady-state is detected, the
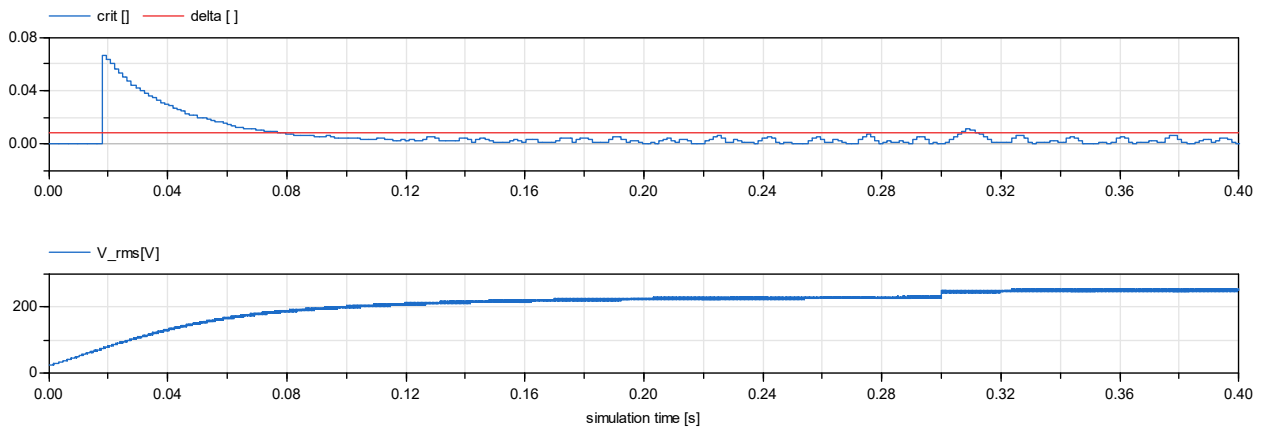
Figure 5.10: Investigation on new steady-state criterion vs. signal (FFT window 0.017s)

test on conformance with the standards on THD can be performed. The quality test is based on the same FFT data without need for an additional FFT calculation. Results analogue to Figure 5.9 are shown in Figure 5.10.

It can be seen that the steady-state condition is found reliably, with proper detection of the initial transient period. The change in amplitude at 0.3 seconds is detected shortly after the event.

Lastly, all methods are tested with an example based on hardware tests. The top plot in Figure 5.11 shows the measurement data of a generator connected to an electrical-driven Wing Ice Protection System (WIPS), see chapter 2.3.3. The load is increased at 0.15seconds. It can be seen that the F-like criterion detects the event, but the output is noisy although care was taken for proper parameterization. In contrast to this, the beta parameter of wavelet-based test and THD and THD-similar criterion detect the event reliably, with high signal-to-noise ratio.
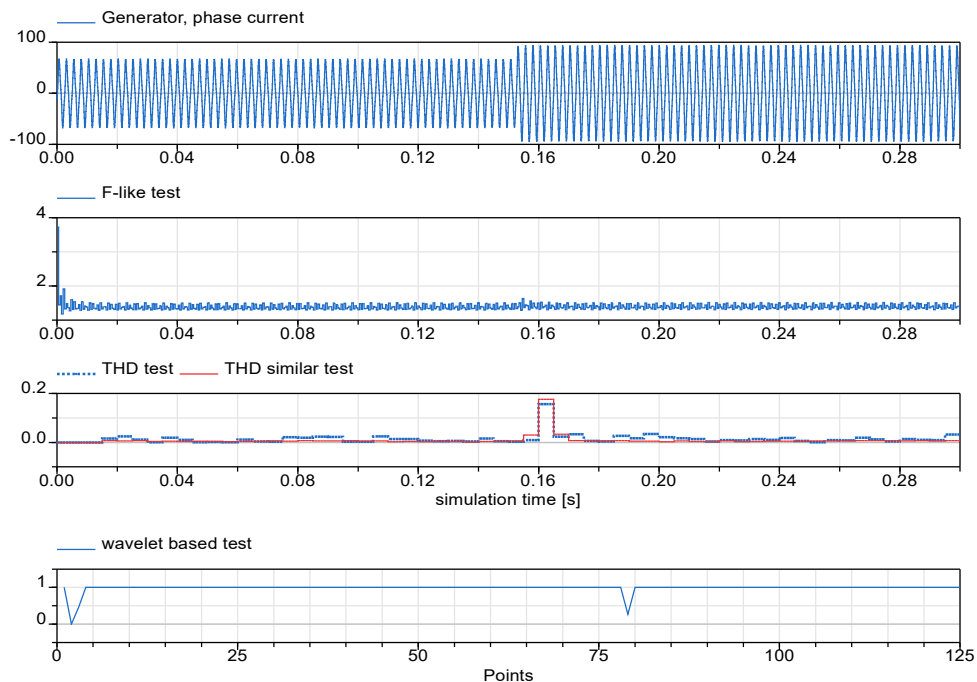
Figure 5.11: Identification of steady-state, based on real test data

5.6 Summary

In this section, procedures for Steady State Identification were tested with an AC electrical circuit, with dominant main amplitude and harmonic distortion, and a second example. Both methods from literature require a mapping of the periodic to non-periodic signals. The F-like test showed good performance and short delays. However, it was difficult to parameterize, and detection was weak. The wavelet-based test was very successful, but computational overhead and delay is high. Alternatively, an experiment based on a variation of THD was tested. The monitor can treat the periodic signal directly, at medium computational overhead. The delay is high but it can be seen as not critical, since evaluation of THD in steady state is requested. This criterion was not able to detect a transient period, where the signal had a fixed ratio of the base amplitude and harmonics. The THD-similar criterion was designed to also consider the base. Tests were very promising, at medium efficiency and medium delay. Due to its generality and efficiency, the last method is proposed as the best choice for the application. The results are summarized in Table 9.

Test	Quality of SSI for the examples	Pre-operator needed for AC	Delay	Computation Efficiency
F-like	bad	yes	Short	High
Wavelet based	Very good	yes	medium-high	(Low)[21]
THD criterion	Only partial	no	high	Medium, high if THD is needed
THD-similar criterion	good	no	high	Medium, high if THD is needed

Table 9: Evaluation matrix of proposed methods

5.7 Implementation of monitors for detection of steady-state condition

The following section builds on the FFT based property monitors results in section 3.[22] Computation of FFT might sound numerically demanding, but efficient routines are available as public domain software, or as proprietary software down to chip-optimized routines from Intel and AMD. Cyclic FFT can evaluate the FFT at each sampling step, where results from earlier computations can be reused rather than freshly computated. For practical reasons, one may not evaluate the FFT and THD at every sample, since the convergence of the signal may happen within some AC periods, but not within some sampling intervals.

5.7.1 Properties of Short Time Fourier Transformation

The FFT algorithm for use by THD calculation is well parameterized by

---

[21]Only tested by offline-algorithm

[22] In the meantime the underlying FFT algorithm found its way into the Modelica standard library 3.2.2 as tool independent implementation "Modelica.Math.FastFourierTransform.realFFT()"

- The expected base frequency f_{base} and number of harmonics demanded $n_{harmonics}$; the maximum frequency in the spectrum $f_{max,FFT}$ needs to be well above the highest treated harmonic: $f_{max,FFT} > n_{harmonics} \cdot f_{base}$, where sample frequency $f_s = 1/T_s = 2 \cdot f_{max,FFT}$.
- The type of window function, (e.g. rectangular, Hamming or Butterworth).
- The window length $N = n_s \cdot T_s = 1/f_{resolution}$, with the spectral resolution $f_{resolution}$ and the number of sample points n_s.

(proper anti-aliasing by a low-pass filter is assumed).

"Windows" transfer the theoretical unlimited data set to finite length by selection of N samples, where the signal is multiplied by the window function before applying DFT. Such a window function starts near or at zero, then increases smoothly to a maximum at the center of the time series and decreases again (see Figure 5.12 for a Hamming window). The theory of DFT implicitly postulates that the input is periodic, where any waveform must repeat itself after the window of sampled signals. This means, for signals with sinusoidal content, the Fourier spectra of temporal consecutive windows coincide: if the windows are of length $l_n \cdot T_n$, and time shifted by $pr_n \cdot T_n$; with arbitrary integer numbers l_n and r_n, and wavelength T_n for each sinusoidal content n.
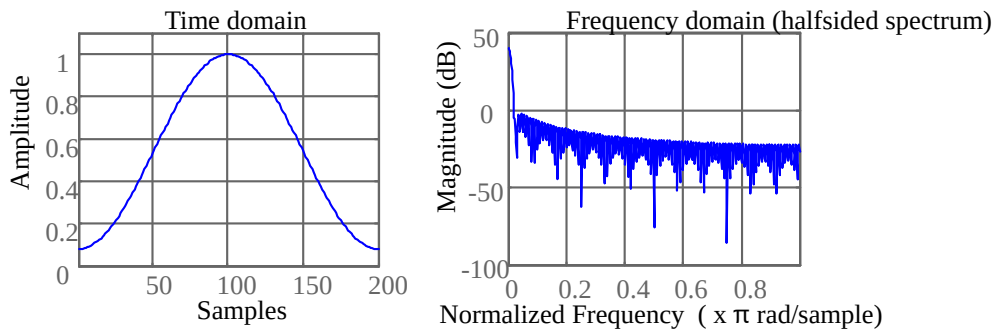
Figure 5.12: Hamming window

5.7.2 Discussion of effects of non-steady state condition

In the following, the properties of the spectral analysis are discussed with the purpose of steady-state identification. For better understanding, Figure 5.13 shows two spectra of the voltage transient of the small aircraft electrical network example: The amplitudes spectrum on the initial transient phase (red) differs from the spectrum of the settled phase (blue) in amplitude and distinctiveness of the peak (a sinusoidal oscillation of infinite length would result in a distinct Dirac impulse). The example shows that the spectra clearly differ and can be used for distinction of steady-state and non steady-state.

The spectrum can be affected by:
a) Smearing of peaks, from non-periodicity (energy conservation by Parseval's theorem) or mismatch of period by window length,
b) spectral leakage, from convolution of the spectrum X by the window's spectrum W,
c) band restricted variation and smearing of peaks, from unmodeled dynamics.
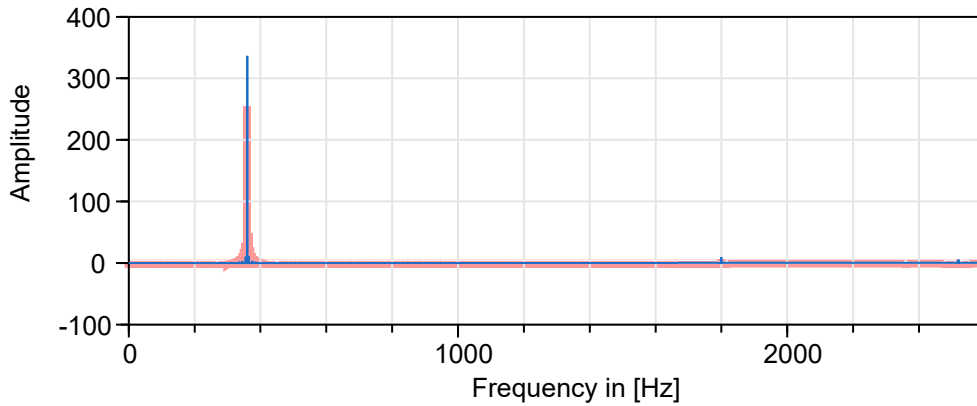
Figure 5.13: Voltage spectrum of a transient of the small aircraft electrical network example, with dominant signal $\sin(2 \cdot pi \cdot 360\,Hz)$; blue: spectrum of period [0..0.2s], red: spectrum of period [0.2..0.4s],

Case a) might be used as an indicator for the variation of the wavelengths, where non-integer l_n distort the spectrum. This is not recommended. The exact finding of the wavelength or phase information is highly prone to errors. Instead, the discontinuity can be removed by application of a non-rectangular window (Henning etc.)

Case b) can be seen as a requirement on the shape and length of the window function. For better understanding, the effect of windowing is demonstrated in Figure 5.14. It shows the windowing of the input signal X (grey peaks) by "rectangular" window (blue) and a "flattop" window (green). The width of the window in frequency domain is indirectly proportional to its length in time domain. The window type itself is characterized by the peak flatness (3dB bandwidth) and peak level of the sidelobes (see overview of window types in (Heinzel et al., 2002)).
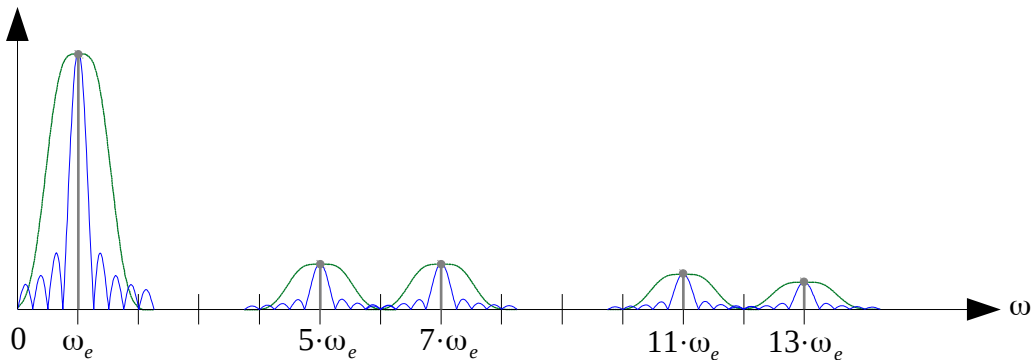
Figure 5.14: Influence of windowing and sampling ; $\mathbf{X}(j\omega)$ (grey): Dirac peaks in continuous Fourier domain, e.g. from sine and cosine; $\mathbf{Y}(j\omega)$ (blue): convolution of "rectangular" window with $\mathbf{X}(j\omega)$; $\mathbf{Y}(j\omega)$ (green): convolution of "flattop" window with $\mathbf{X}(j\omega)$

The convolution of the window with the signal in frequency domain is:

$$Y(e^{j\omega}) = \frac{1}{2\pi} \int_{-\pi}^{\pi} X(e^{j\theta}) W(e^{j(\omega-\theta)}) d\theta \tag{175}$$

The following requirements result, to distinguish tight steady-state and wider non steady-state spectra X of a signal of type (151):

1) The DFT has to resolve the individual baseband signals of the spectrum, without overlapping caused by the window; (e.g. in Figure 5.14, the adjacent blue wave packs shall not merge). The window type and length $n_s \cdot T_s$ have to be chosen with focus on their broadening and height of sidelobes.

2) The steady-state and non-steady-state condition in the basebands of X, need to have distinguishable amplitudes in discrete Y as well: The discretization of (175) at a given sampling rate f_s results in

$$Y[k] = Y\left(e^{j\omega}\right)\Big|_{\omega_k = (2\pi/N)k} = \frac{1}{2\pi} \int_{-\pi}^{\pi} X\left(e^{j\theta}\right) W\left(e^{j(\omega-\theta)}\right) d\theta \Big|_{\omega_k = (2\pi/N)k}, \quad k = 0..N-1 \tag{176}$$

2) is similar to 1), but includes a further demand: $Y[k]$ may not be undifferentiated for the shapes of X with the same local area c:

$$\int_{(2\pi/N)(k-1/2)}^{(2\pi/N)(k+1/2)} X\left(e^{j\omega}\right) d\omega = c \tag{177}$$

This can be the case with flat top windows which makes them not favourable for the purpose of identification of band restricted disturbances: They exhibit broad peaks, with 3dB widths starting from 2.9 bins (see next). This gives them an approximate characteristics of $W\left(e^{j\omega}\right) = 1$ in the interval around a discretized angular velocity $\omega_k = (2\pi/N)k \pm 1/2$ (called "bin"). This certainly has benefits for the correct identification of amplitudes, in case of a frequency mismatch of signal and discretized frequency; but overlapping and visibility of narrow banded effects had to be prevented by high spectral resolution and therefore be paid by large window lengths.

Case c) is the most interesting effect. Steady-state identification can be based on prior knowledge, with measures from a single spectrum. Measures are the amplitudes of the main peaks, or their (3dB) widths, or their amplitude to width ratio, or the ratios of the main peaks. Or it can also be based on the temporal change of these measures. For this work, we assume there is little information on the spectrum given. Furthermore, there is no need to tune the algorithm for a special spectral shape, since any distinct change is seen as non-periodic condition. Instead, **a measure is proposed based on the variation of the noise from unmodeled dynamics**.

5.7.3 Construction of criterion by change-of-spectrum operator

In the 1970s a method called "Welch's method of averaging modified periodograms" was developed to improve the accuracy of periodograms. Periodograms are estimates of the spectral density of a signal. In this context, "modified" means the window is not of type "rectangular". According to (Oppenheim and Schafer, 1998), the estimate r, of a sequence of K periodograms is given by

$$I_r(\omega) = \frac{1}{NU} \left| Y_r\left(e^{j\omega}\right) \right|^2 \tag{178}$$

where estimates are based on non-overlapping data segments of length N, which are taken from a total data set length Q by a window. The correction factor U normalizes the amplitudes of the windows (if not already included in Y_r):

$$U = \frac{1}{L} \sum_{n=0}^{N-1} \left(w[n]\right)^2 \tag{179}$$

Averaging of the K estimates results in the averaged periodogram

$$\bar{I}(\omega) = \frac{1}{K} \sum_{r=0}^{K-1} I_r(\omega) \tag{180}$$

respectively

$$\bar{I}[k] = \frac{1}{K} \sum_{r=0}^{K-1} \frac{1}{NU} |Y_r[k]|^2 \tag{181}$$

of a discrete spectrum. In case the properties of the signal remain stationary, and noise is additional and uniformly distributed, the variance of $\bar{I}(\omega)$ is reduced by a factor of $1/K$ (Heinzel et al., 2002). Welch (Welch, 1967) proofed that other types of windows may be used with similar reduction in variance (modified periodogram). Also he found, with a fixed length of data, that HALF-overlapped windows (see Figure 5.15) reduce the variation in the spectral components approximately by an additional factor of 2. More than 50% overlap usually gives no additional benefit, since the cross-correlation of the windows grows. Detailed considerations on the optimal usage of the information in relation to window overlap, are summarized in (Heinzel et al., 2002). The author lists 33 types of windows with amplitude flatness and power flatness in relation to overlap correlation. Results clearly show, that an overlap of 50% is a good choice for all windows except the "flat top" windows.
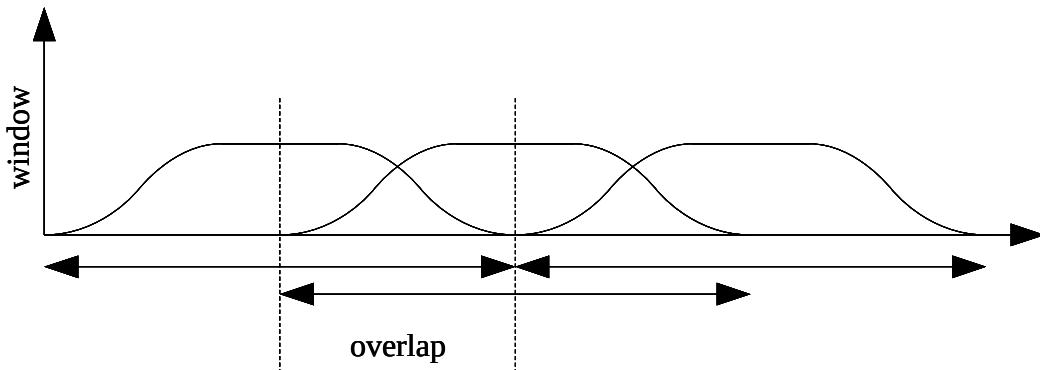
Figure 5.15: Segmented signal, with three windows and 50% overlap

By Welch's method it is possible to get better, unbiased estimates of the spectrum, and therefore better inputs for THD calculation. Additionally, with the data of the periodogram (181), the standard deviation of the estimate can be computed with little extra effort. It is possible to construct an F-like test upon these measures, where transition to steady state can be associated with decreasing noise, and therefore decreasing standard deviation. This is not recommended since the large data vector with several evaluations of the periodogram would lead to substantial delay in the steady state detection. Instead, a test based on the indicator named `randomness' (Heinzel et al., 2002) is proposed and more applicable. It is the ratio of the standard deviation σ to the averaged estimate of the signal E, that dominates the frequency bin under consideration. "Randomness" is near unity for stochastic signals such as noise, and small for coherent signals such as a sinusoidal wave:

$$' randomness' = \frac{\sigma(\bar{I}[k])}{E(\bar{I}[k])} \tag{182}$$

This "randomness" criterion is proposed as base of the THD-similar steady-state detector. Since reduction of delay is of highest interest, the set of input data must be kept short. This directly results in a number of 2 windows, with an overlap of 50% (more windows might be used to filter noise). The choice of only two windows transforms the $\sigma(\overline{I}[k])$ operator into a $\Delta(I[k])$ operator. $\Delta(I[k])$ is evaluated per "bin" $[k]$. Since any variation can be seen as "non steady-state", it is sufficient to map the data vector to a single value by a maximum norm. (Euclidean norm might work as well, with smoother output). The criterion can be made less prone to noise if the variances [k] are normalized by the expectation value of the main amplitude, rather than the expectation value [k]. This results in:

$$y_{randomness} = max\left(\frac{\left|A[k[t_x]]\right|^2 - \left|A[k[t_x - \Delta T]]\right|^2}{\left|A[k_{base}(t_x)]\right|^2}\right) \forall\, k \tag{183}$$

The SSI delay needs to be kept to a minimum, where delay is proportional to the window length, which in turn is proportional to the resolution of the DFT spectrum. The minimum delay is attained, when each band restricted variation is included by one bin each, but the window is not "flat top" whilst the resolution is high enough to prevent overlap with the adjacent harmonic by the window. Since we assume that all non-steady-state-caused distortion is centered around the base-frequency and the harmonics, the set of all k in criterion (183) can be limited to all bins which represent a harmonic of f_{base}. With the usual notation of expressing the number of the bins by their equivalent frequency, the ks in (183) are replaced by $k = h \cdot f_{base}$, with $h = [1..M]$. Inserting an additional ϵ in the denominator to prevent division by zero and influence of noise directly results in the final proposal:

$$y_{THD-similar} = max\left(\frac{\left|A[h \cdot f_{base}[t_x]]\right|^2 - \left|A[h \cdot f_{base}[t_x - \Delta T]]\right|^2}{\left|A[f_{base}(t_x)]\right|^2 + \epsilon \cdot \left|A_{nom}\right|^2}\right) \forall\, h \in [1..M] \tag{184}$$

The windows of type
- Bartlett, Hamming or Hanning

are especially recommended due to their small 3dB peak width of 1.2736,1.3008 and 1.4382 bins. For these windows the resolution of the spectrum should be at least $1/3 \cdot f_{base}$ to prevent overlap.

5.8 Contributions

Analysis of dynamic systems is often carried out at steady state condition. For cyclic systems like rotating machinery, it is not possible to detect this condition by simply monitoring the change rate of their variables, due to their periodicity. This section focused on methods for stationary periodic steady state identification of AC electrical systems. The study was motivated by the need to identify the steady state condition of an aircraft electrical network for power quality checks.

- *An overview of relevant methods is given and mappings of periodic variables to equivalent stationary variables are discussed.*
- *Two new periodic steady state monitors based on Short Time Fourier Transformation are proposed with analysis of the signal processing*
- *A novel criterion, called "THD-similar" showed the best results for this application*

- *An implementation of all methods is demonstrated.*

Relevant Publications:

"Periodic Steady State Identification of electrical circuits" (Kuhn, 2017) [23]

---

[23] Some preliminary studies were performed together with Mr. Mohamed Jmari, who did an internship at DLR as part of his studies at ENSMM, Besançon, France.

6 Stability analysis

The following chapter addresses the stability of the generator-fed network. Design of the electrical network and system integration is one of the main challenges in aircraft design. It is kept as a core competence at the airframer.

The design starts early in the "concept phase" of the aircraft development process, where the global system architecture is assessed and optimized in terms of performance and weight. The architecture is broken down to system-level in the "system specification" phase. In both phases, the aircraft manufacturer is still in discussion with more than one supplier for the same system. And at this stage there is no global purchaser-supplier contract available, which secures the economic exploitation of the supplier's components (Schlabe et al., 2015). For these reasons, the competition among the manufacturers prevents a deep insight into the technologies among them, and partially with the airframer. This lack of information could lead to sub-optimal electrical networks, and costly demands on single components. Therefore, it is essential for the supplier to perform their own integration studies, and then support the aircraft manufacturer with their findings.

Besides reliability figures, the suppliers provide the following (Giese et al., 2010):

- system architecture proposals,
- scalable performance and weight models,
- preliminary geometric models,
- and preliminary cost figures.

The power quality and the network stability are dealt with late in the system's specification phase. They have an influence on all of the topics in the list, by means of filter design and the electrical impedance of the components. Therefore, the generator manufacturer should participate actively in the network design process through its own pre-studies, to avert network stability driven design decision, at its expense.

The objective of this work was to

- compare relevant methods for the assessment of stability,
- adapt them to the problem formulation,
- discuss their implementation in a model based design process and develop methods for automated evaluation from the standard models.

Chapter 6.1 explains the motivation and the system interactions which have to be considered. An overview of the state-of-the-art in industrial based stability investigation is presented in chapter 6.2, and alternative methods from academia are addressed. All methods are implemented, including software tool-chains, and are analyzed in-depth in the chapters 6.2.2, 6.2.3, and 6.2.4. They are demonstraed in chapter 6.3. Their benefits and drawbacks for pre-studies are discussed in chapter 6.4.

6.1 Motivation

The electric network tends towards instability, because the system load can change swiftly and without warning. This is due to a large range of duty cycles and unpredictable spikes (Louganski, 1999), especially for modern power-optimized architectures using large high voltage DC networks (Schallert et al., 2006). Therefore, it is necessary to investigate the stability of the whole electric network, both at small signal level for steady-state conditions and large signal level for transients, impacts and network reconfiguration. The applied methods must be capable of handling systems becoming more and more extensive for future aircraft. One key problem is to find when and how the
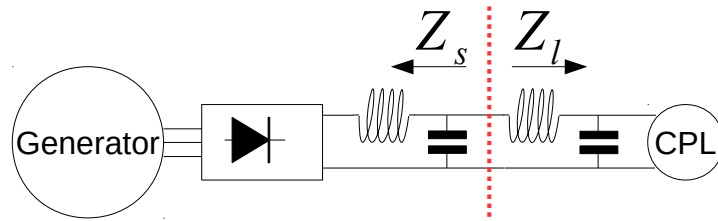
Figure 6.1: Motivation for stability investigation

electric on-board system could become unstable. It is already recognized that the regulated DC/DC converter, e. g. the buck converter, is one of the most critical components in on-board electric networks (Barruel et al., 2005). Switching-mode regulators have a negative input resistance at low frequencies, well below switching frequency and may become unstable by the addition of an input filter (Middlebrook, 1976). This includes all types of AC/DC, DC/AC, AC/AC or DC/DC converters. For the design of aircraft power transmission networks, this means any converter interacts with its power source. For an AC transmission-based system, a DC/DC converter may interact with its source, consisting of the rectifier, distribution lines and the generator itself. This means the generator's parametrization is essential for stability of the subsystems. A typical setup is depicted in Figure 6.1. The generator´s AC voltage on the left of the dotted line is rectified and filtered. On the right side, a constant power load draws a current via an input filter.

6.2 Overview of methods

In control theory, stability is often defined as the property of a system to stay at an equilibrium or return to it from a disturbance. For internal stability of linear systems, state stability can be proved by methods of eigenvalue analysis, root locus or Bode plots. Due to this inherent character of converters, these methods for the investigation of stability were adapted with special emphasis on DC converters. Till now, the "Middlebrook criterion" (Middlebrook, 1976), which examines small signal stability of state space averaged (=non switching) models, is one of the standard methods in aircraft electrical systems design, because of its simplicity. Only the input impedance of the load subsystem, the output impedance of the source subsystem and their Bode diagrams are needed. It is the origin of the so-called impedance-based stability criteria. The Middlebrook criterion is originally intended for investigating the stability of a power converter system, which includes two subsystems.

Alternatively, the "Modal Analysis" gives proof of stability via the region of the eigenvalues and uses participation factors and eigenvalue sensitivities ((Kundur, 1994) (Barruel et al., 2005) (Han et al., 2006a)) to retrieve dependencies between system modes and elements of the state matrix $\widetilde{A}$ of a Linear Time -Invariant (LTI) system. The linear time invariant representation needed, is calculated by numerical linearization of the system at an equilibrium point. It is easy to see that non-linear impacts on the steady-state condition cannot be analyzed with the Modal Analysis approach. For example, the system load has a non-linear influence and must be treated as constant at linearization which limits the validity of the model to a special loading case. Additionally, the Modal Analysis approach is not appropriate for finding the critical component, which is the most fragile and likely to destabilize the system.

The drawbacks of Modal Analysis is supposed to be avoided by "μ-Analysis". The Structured Singular Value μ is an indicator for the system robustness, applicable to the class of linear time invariant systems with parametric uncertainties. It enables identification of the critical parameters (Zhou and Doyle, 1998).

In contrast to mathematical stability, an industrial applicable definition of stability is the ability of a system to keep a specific system variable of interest within desired limits. The requirements of the standards must be fulfilled for any combination of parametric uncertainties and over the whole operation range. This problem may be solved using "anti-optimization" or "worst-case search" as improvement of the verification process. The basic idea is to reformulate a stability criterion as a minimum distance problem, which is minimized to determine worst-case parameter combinations and operation conditions leading to worst-case performance. Optimization-driven worst-case search based on Non-Linear Programming (NLP) techniques, was first proposed in (Bals et al., 1996). It was previously used on the clearance of flight control laws (Varga, 2002) and developed further in (Menon et al., 2007). Within the GARTEUR Action Group, it was the most successful method for the use case of "military aircraft1".

In the following section, the classic impedance-based methods and Modal Analysis are analyzed. They are compared with μ-Analysis suitable for linearized models. In contrast to the analytic methods, the optimization-driven worst-case search is investigated. It is applicable for industrial demands and suitable for simulation-based stability investigation of large non-linear systems.

All of the methods are demonstrated by means of a power source and a single buck converter. The generator, converter and DC line source filter are represented by a low-order, equivalent source impedance; whereas the load consists of a 350V to 28V DC/DC buck converter with input filter. A DC/DC converter is usually a critical component for system stability in an electric on-board network due to its inherent character: if the source voltage decreases, the converter keeps the power constant by drawing higher currents. In combination with an unsuitable input filter, the DC/DC converter begins to oscillate and becomes unstable (Middlebrook, 1976).

6.2.1 Impedance-based methods

Impedance-based methods like Middlebrook criterion investigate local, small-signal stability at a nodal point between a source and a load part. The electrical network is modelled by "voltages behind impedances", which are called Thévenin equivalents. Figure 6.2 shows this basic architecture. The source voltage v_o[24] is connected to the nodal point via the impedance Z_o, and the load voltage v_l is connected via the load impedance Z_l. The impedance-based stability is explained hereafter, following the summary in (Sudhoff et al., 2000a).
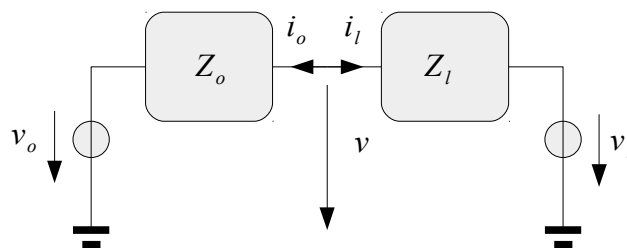
Figure 6.2: Thévenin equivalent source and load

The DC link voltage can be calculated by

$$v = \frac{Z_l}{Z_o + Z_l} v_s + \frac{Z_o}{Z_o + Z_l} v_l \tag{185}$$

Splitting the impedances into numerator and denominator gives

---

[24]The nomenclatures output voltage v_o and source voltage v_s are used equivalent in literature. This also applies for the impedances and currents.

$$Z_o = \frac{N_o}{D_o} \tag{186}$$

and

$$Z_l = \frac{N_l}{D_l}. \tag{187}$$

Substitution yields

$$v = \frac{N_l D_o v_o + N_o D_l v_l}{N_l D_o + N_o D_l} \tag{188}$$

Two ideal cases can be considered for Equation (188): If the load is connected to an ideal constant voltage source, with no source impedance Z_o, then the load current is proportional to the inverse of the load impedance. The system is stable, iff the roots of the impedance's nominator N_l are located in the complex left half plane. Similar for the source: a system with an ideal constant current load, and no load impedance Z_l, is stable, iff all roots in the source's denominator D_o are non-positive.

Transforming Equation (188) with $Y_l = 1/Z_l$ gives

$$v = \frac{N_l D_o v_o + N_o D_l v_l}{N_l D_o (1 + Z_o Y_l)} \tag{189}$$

With the assumptions made on N_l and D_o, the system is stable in case $1 + Z_o Y_l$ has just negative poles. Or, in other words: the system is stable if the amplitude of the output impedance Z_o is considerably smaller than the amplitude of the input impedance Z_i, within the studied frequency range. In Nyquist plots, this is equivalent to the Nyquist contour of $Z_o Y_l$ encircling the critical point -1 anticlockwise.

This design guideline not only ensures small-signal stability, but also dynamic decoupling between the converter and its input filter. Further developments reduce conservatism, since stability is not just a function of the impedance magnitude, but also the phase. The Middlebrook criterion preserves infinite phase margin. Later publications extended the approach to multiple-module DC power systems. Here, the stability margin of the load impedance has to be adapted to consider the impedance of parallel-connected DC/DC power modules. The first impedance criteria for multiple loads were difficult to apply, as individual impedance specifications for all of the load impedances had to be provided. (Sudhoff et al., 2000) aims on relaxing unnecessary limitations and incorporating uncertainty, the wide range of operating points and reconfiguration. The design rule of (Feng et al., 2002) defines a forbidden region of the impedance ratios for each of the k subsystems in the s-region in relation to the power:

$$\Re\left\{\frac{Z_o}{Z_{lk}}\right\} \geq -\frac{1}{2}\frac{P_{load\,k}}{P_{source}}, \text{ where } P_{source} \geq P_{load\,1} + P_{load\,2} + ... + P_{load\,n} \tag{190}$$

This means, the larger the consumer of power, the larger the "consumed" stability reserve. With this, the following small-signal stability theorem can be posted:

> *Theorem 1: A system consisting of k loads, designed with Equation (190), circles the (-1,0) point in the s-plane with a gain margin of 6dB and a phase margin of 60 dB.*

The proof is quite simple:
For a system with parallel loads with input impedances $Z_{i1}..Z_{in}$, the total input impedance is

$$Z_l = Z_{l1} \| Z_{l2} \| ... \| Z_{ln} = \left(\frac{1}{Z_{l1}} + \frac{1}{Z_{l2}} + ... + \frac{1}{Z_{ln}} \right)^{-1} \tag{191}$$

And thus

$$\frac{Z_o}{Z_l} = \frac{Z_o}{Z_{l1}} + \frac{Z_o}{Z_{l2}} + ... + \frac{Z_o}{Z_{ln}} \tag{192}$$

And with Equation (190):

$$\Re\left(\frac{Z_o}{Z_l} \right) = \Re\left(\sum_{k=1}^{n} \frac{Z_o}{Z_{lk}} \right) = \sum_{k=1}^{n} \Re\left(\frac{Z_o}{Z_{lk}} \right) \geq -\frac{1}{2} \cdot \sum_{k=1}^{n} \frac{P_{loadk}}{P_{source}} \tag{193}$$

Alternatively, the condition can be formulated using the Bode diagram. For stability, the following condition should hold:

$$|Z_{lk}| > |Z_o| + 6\,dB + 20\log\left(P_{source}/P_{load\,k} \right) \tag{194}$$

If condition (194) is not satisfied, Z_{l_k} needs to satisfy the phase-limitation

$$-90\,° - \Phi_k < phase\left(Z_0 \right) - phase\left(Z_{l_k} \right) < 90\,° + \Phi_k$$
$$where \; \Phi_k = \arcsin | \frac{1}{2} \frac{Z_{lk}}{Z_0} \frac{P_{load\,k}}{P_{source}} | \tag{195}$$

The condition is only necessary, but not sufficient for a well damped system. The total damping has to be checked again in the integration phase. Real systems tend to have a better damping than theoretically calculated values, due to parasitic resistances.

For a graphical interpretation, see Figure 6.3. This condition gives some decoupling of the load filters. Loads in regeneration mode acting as power sources are not treated.

(Florez-Lizarraga and Witulski, 1996) uses two-port theory to specify filter impedance demands in order to guarantee stability for the load/filter, filter/source and multi-load interaction for converters. (Feng et al., 2002) interprets a parallel connection of the loads as destabilizing. (Florez-Lizarraga and Witulski, 1996), on the other hand, assumes this may stabilize the system since the input impedance of the combined loads decreases. For each load, the other loads act as additional output impedances: "The more converters are present, the more the individual converter performance is improved". This presumes a p*ositive input impedance of the filters with load*. (Florez-Lizarraga and Witulski, 1996) gives design rules for the impedances of the filters for stable filter/load, source/filter and multi-modules interaction for converters. Applying both preserves stability and prevents degradation of the control loops. Nevertheless, it can be stated that the approach of (Feng et al., 2002) will essentially limit the filter/filter interactions, while (Florez-Lizarraga and Witulski, 1996) does not. Since (Feng et al., 2002) interprets the source with the maximum amount of identical, worst-case consumers as the most critical case, and (Florez-Lizarraga and Witulski,
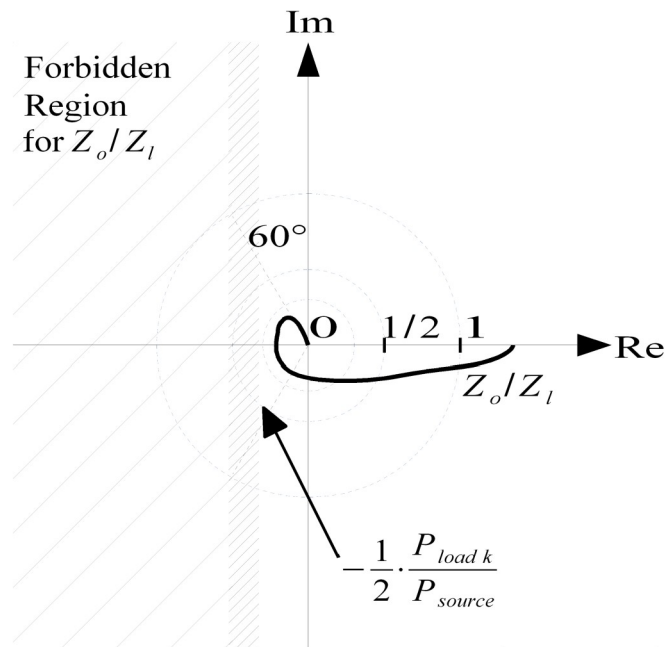
Figure 6.3: Individual load impedance specification for $Z_{ik}(k=1,2,..,n)$ (sparse cross-hatched area: 60° margin; dense cross-hatched area: additional margin of individual load)

1996) interprets the single-load case as the most critical, the following new adapted general design rule takes both approaches into account:

> A load L is designed well in the context of impedance-based small-signal stability, if
>
> - the requirement (190) is met, with a given source impedance
> - and the single load case is stable
> - and a system consisting of n loads of type L is stable, with the nominal power of the source equals n times the load power.

The impedance-based stability approach has strong benefits for the interaction of the suppliers in the aircraft design process. Only black-box models of the systems need to be exchanged or the impedances can be assumed. In the design process, the generator supplier is privileged, since in the impedance criterion (190), the source impedance is defined, and the loads are tested with it. The analytic calculation of the input/output impedances itself is quite convenient, if a linearisable model exists. Using Dymola, it is easy to calculate the impedance automatically. Figure 6.4 shows a model for the automated calculation of the impedance of a Constant Power Load (CPL) with an input filter. The operating point has to be set by appropriate sources (here: voltage supply of 540VDC). Inputs and outputs of voltages and currents have to be defined, where the impedance is calculated as the transfer function from a voltage input to a current output (here: voltage *vin* and current *iin*). By automatic, numeric linearization of the model, a linear state-space representation is derived, and the transfer function can then be computed from it. Also, a hardware measurement approach for the impedance criterion (Feng et al., 2002) was shown.

On the other hand, all impedance-based design rules are restrictive and not appropriate for design and optimization goals (Barruel et al., 2005). There is no information on the sensitivity of the impedances to parameter variations available for a hardware measurement approach (Feng et al., 2002). Also the impedance-based methods can not guarantee internal stability of the sub-systems. As a result, electric on-board systems are increasingly analysed by other methods for small-signal stability.
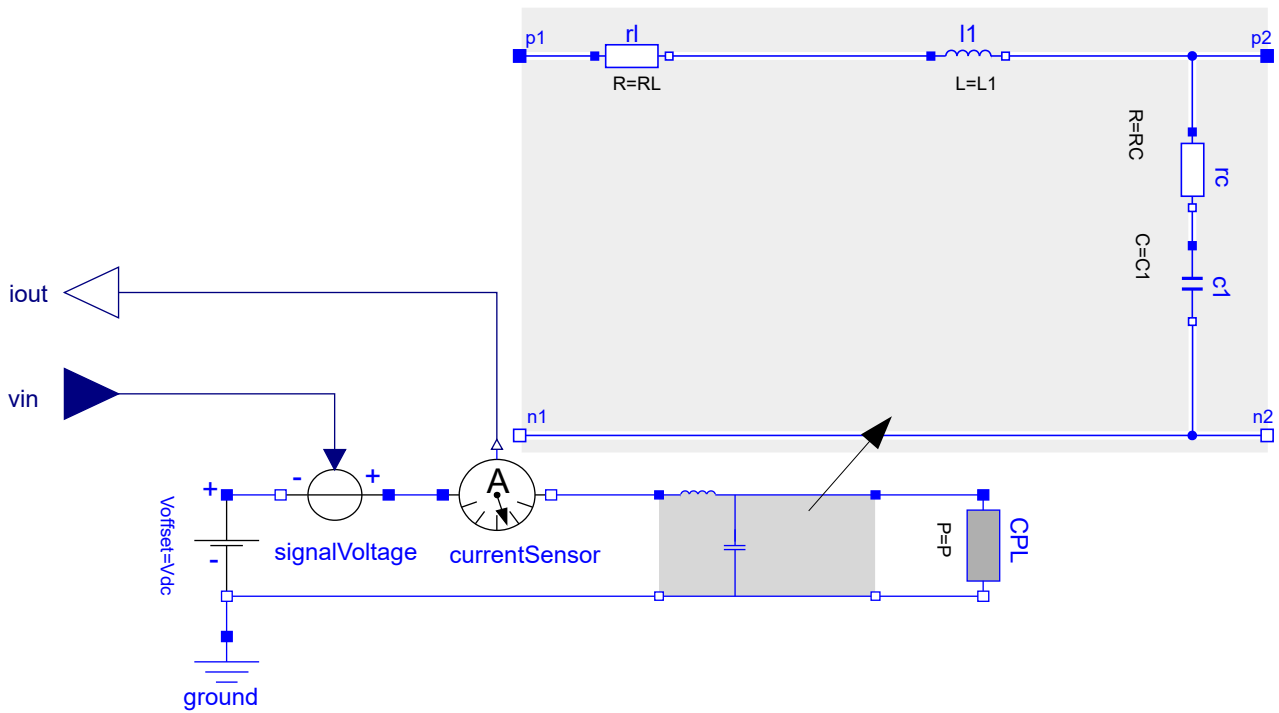
Figure 6.4: Example of Modelica test circuit, for automatic impedance determination

6.2.2 Modal Analysis

Modal Analysis is an extension to the LTI state-space stability criterion. It was used in (Barruel et al., 2005) and (Han et al., 2006b) for design and stability studies of More Electric Aircraft architectures. For a LTI system with a state matrix $\widetilde{A}^{n \times n}$, ϕ_i and ψ_i are the right and left eigenvector and λ_i is the corresponding eigenvalue. The sensitivity of the eigenvalue λ_i to the element $\widetilde{a}_{kj}$ of the state matrix $\widetilde{A}$ is calculated by

$$\frac{\partial \lambda_i}{\partial \widetilde{a}_{kj}} = \Psi_{ik} \Phi_{ji} \tag{196}$$

with $\Phi = [\phi_1 \ \phi_2 \dots \ \phi_n]$ and $\Psi = [\psi_1 \ \psi_2 \dots \psi_n]$.

The correlation between the kth state variable and the ith eigenvalue can be found by calculating the participation factor p_{ki}. It is actually equal to the sensitivity of the eigenvalue λ_i to the diagonal element $\widetilde{a}_{kj}$ of the state matrix $\widetilde{A}$

$$p_{ki} = \frac{\partial \lambda_i}{\partial \widetilde{a}_{kk}} \tag{197}$$

The matrix $P = [p_1 \ p_2 \dots p_n]$ is called participation matrix (Kundur, 1994) with

$$p_i = \begin{bmatrix} p_{1i} \\ p_{2i} \\ \vdots \\ p_{ni} \end{bmatrix} = \begin{bmatrix} \Phi_{1i} \Psi_{i1} \\ \Phi_{2i} \Psi_{i2} \\ \vdots \\ \Phi_{ni} \Psi_{ni} \end{bmatrix} \tag{198}$$

133

The method is based on the knowledge of the LTI state-space representation, which includes internal stability. All system equations of the load-models and source-models have to be available to the control engineer. But the models do not have to be built by one design environment, as long as model equations are exchanged. The FMI is a valuable interface format for integration of systems from many suppliers (Schlabe et al., 2012). The intellectual property can be protected through the use of obfuscation and binary code.

For Modal Analysis with Dymola, a ready-to-use automation tool exists (Modelica_LinearSystems2.ModelAnalysis.FullAnalysis). For the theory and implementation, the reader is referred to (Baur et al., 2009).

6.2.3 Robust stability by μ-Analysis

6.2.3.a Theoretical background

The Linear Fractional Representation of uncertain systems is often used as the basis for stability analysis and controller synthesis in Robust Control. The structured singular value μ , the skewed-structured singular value ν and μ-sensitivity are some of the most important definitions for robust stability analysis and robust controller design. In this section, these basic concepts are briefly reviewed.

(a) lower LFT   *(b) upper LFT*
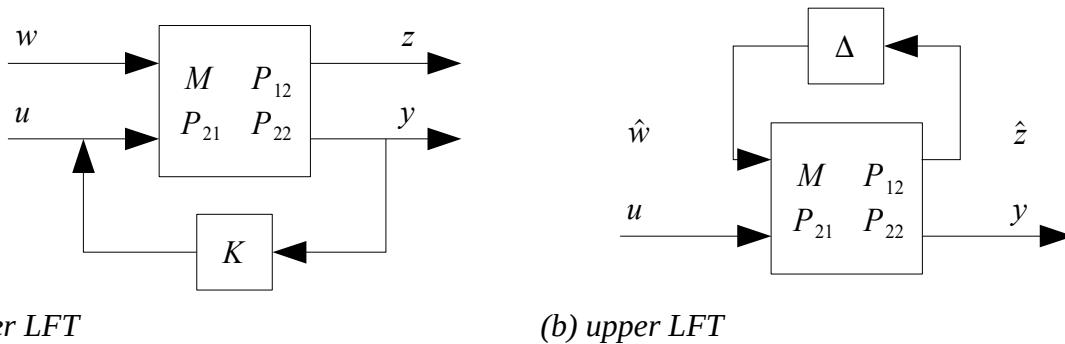
Figure 6.5: Linear Fractional Transformation Framework

A. Linear Fractional Transformation (LFT)

Suppose P is the transfer matrix of a nominal system with $P = [M \, P_{12} ; P_{21} P_{22}]$. K and Δ represent the controller and system uncertainties of the parameters, respectively. The lower Linear Fractional Transformation $F_l(P , K)$ of P and K is defined as

$$F_l(P , K) = M + P_{12} K (I - P_{22} K)^{-1} P_{21} \tag{199}$$

The lower LFT represents the transfer function from signal *w* to *z* when closing the lower loop. In general, *w* can represent all uncontrollable signals, e.g. disturbance and noise and *z* denotes the signal that allows characterizing whether a controller has certain desired properties. *z* is called the controlled variable e.g. *z* equals the control error (Scherer, April 2001) (see Figure 6.5.a). *u* and *y* include the controller inputs and the system outputs respectively.

Similarly, the upper LFT $F_u(\Delta , P)$ is defined as

$$F_u(\Delta , P) = P_{22} + P_{21} \Delta (I - M \Delta)^{-1} P_{12} \tag{200}$$

134

(see Figure 6.5.b). The upper LFT is the transfer function from $\hat{w}$ to $\hat{z}$, which defines all uncertainty outputs and inputs in the system when closing the upper loop. All system uncertainties are normalized to ±1 and pulled out into the Δ matrix. The row dimension of Δ is called the order of the Linear Fractional Representation (LFR) model. The two Linear Fractional Transformations defined above, play a very important role in Robust Control. The LFR-toolbox (Hecker, 2006) for Matlab can build the LFR models '$\Delta - P$' (Figure 6.5) automatically.

Low order LFT-based uncertainty models can be obtained, for example, with the LFR-toolbox for Matlab using symbolic pre-processing and numeric reduction techniques (Hecker and Varga, 2005). This allows the utilization of the LFT-based stability analysis, for industrial-relevant complex systems (Hecker, 2006). For simple systems, the parametric state-space representation can be generated from the Modelica-model by automatic symbolic code-generation. Then, the LFR-toolbox uses several symbolic approaches to convert the parametric state-space representation into special decomposed forms which allow to immediately obtain a low order LFT-representation (Hecker et al., 2004). The uncertainties may be multivariate rational and polynomial functions and matrices.

B. Structured and skewed-structured singular value

Let the Δ matrix in terms of a '$\Delta - P$' model in Figure 6.5 be diagonal or block-diagonal. It includes all system uncertainties and its norm remains less than 1. Then the structured singular value $\mu_\Delta(M)$ of P with respect to the structured uncertainty matrix Δ is defined as:

$$\mu_\Delta(M) = \frac{1}{min_\Delta\{\bar{\sigma}(\Delta) : det(I - M\Delta) = 0\}} \tag{201}$$

where $\bar{\sigma}(\Delta)$ is the largest singular value of matrix Δ i.e. $\|\Delta\|_\infty$ and $\mu_\Delta(M) = 0$ if there is no Δ that satisfies the determinant condition. The structured singular value defines the reciprocal of the minimal H_∞ norm of the uncertainty matrix, which makes the term $I - M\Delta$ singular.

The nominal system M must be stable. Then the linear formulation of an uncertain system given by (200) can only be unstable if the term $I - M\Delta$ is singular.

Therefore,

- $\mu_\Delta(M) \leq 1$ implies that $I - M\Delta$ is non-singular for all uncertainties which satisfy $\|\Delta\|_\infty \leq 1$
- $\mu_\Delta(M) \geq 1$ implies that a system uncertainty exists which makes $I - M\Delta$ singular

Robust Stability: The system described by Figure 6.5.b is robustly stable against all uncertainties in the specified uncertainty range iff

$$\mu_\Delta(M) < 1 \ for \ \|\Delta\|_\infty \leq 1 \tag{202}$$

A system tends to become more unstable as the structured singular value increases (Zhou and Doyle, 1998). The structured singular value is usually determined by calculating its upper and lower bounds because the exact computing of $\mu_\Delta(M)$ is in general NP-hard (Braatz et al., 1994). The upper bound is used to calculate the μ-sensitivity, which will be introduced in the following section. The lower bound of μ is suitable for determination of the worst-case combination of the uncertain parameters. It is calculated by algorithms using local optimization. Numerous methods for computing bounds of μ are introduced in (Balas et al., 1998) and (Ferreres, 1999).

If a subset Δ_f of Δ (in Figure 6.6.b) may not vary freely and $\|\Delta_f\| < 1$ when computing the μ, while the norm of another subset Δ_v in matrix Δ may increase without restriction, then it is called the skewed Structured Singular Value $\nu_{\Delta s}(M)$ of matrix M with respect to the uncertainty matrix $\Delta_s = diag(\Delta_v, \Delta_f)$. It is defined as:

$$v_{\Delta s}(M) = \frac{1}{min_\Delta \{\overline{\sigma}(\Delta_v) : det(I - M \Delta_s) = 0\}} \tag{203}$$

where $\|\Delta_f\| \leq 1$. $v_{\Delta s}(M)$ is zero if no Δ_s exists that makes $det(I - M \Delta_s) = 0$ (Ferreres, 1999). The skewed Structured Singular Value gives a solution for determining the maximum allowable range for a subset of uncertain parameters, while other parameters are fixed in a specified range. $\mu_\Delta(M)$ is a special case of $v_{\Delta s}(M)$.

C. μ-sensitivity

In the last subsection, the relationship between the stability degree of a system against uncertainties and μ was defined. Also important is the identification of the most critical parameters of a system. This is equivalent to the uncertain parameters which are most sensitive with respect to μ. The most sensitive parameters are those parameters which lead to the greatest increase of μ by a variation of their normalized range. Consider there is a Δ with two parametric uncertainties $\Delta = [\Delta_1 0; 0 \Delta_2]$ of the nominal system M, $\delta\beta$ represents the perturbation of the first uncertain parameter (see Figure 6.6.a) with $\beta = 1 + \delta\beta$. The uncertainty matrix Δ_β perturbed with $\delta\beta$ becomes

$$\Delta_\beta = \begin{bmatrix} \Delta_1 & 0 \\ 0 & \Delta_2 \end{bmatrix} \begin{bmatrix} \beta I & 0 \\ 0 & I \end{bmatrix} \tag{204}$$

It is easy to see that Figure 6.6.b is equivalent to Figure 6.6.a. The perturbation in the uncertainty matrix Δ can be absorbed into M_β with Figure 6.6.a, so that the original uncertain matrix Δ remains. The new system matrix with absorbed perturbation $\beta\Delta_1$ becomes

(a) *(b)*
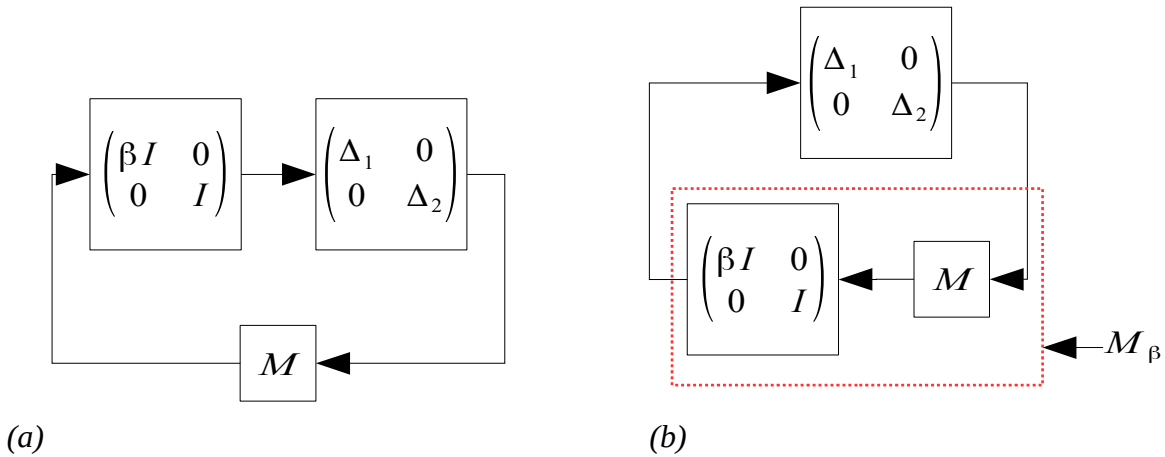
Figure 6.6: Transformation of parametric perturbation into system matrix

$$M_\beta = \begin{bmatrix} \beta I & 0 \\ 0 & I \end{bmatrix} \cdot M = \begin{bmatrix} \beta M_{11} & \beta M_{12} \\ M_{21} & M_{22} \end{bmatrix} \tag{205}$$

The μ-sensitivity with respect to the jth uncertainty parameter in Δ_1 can be defined as:

$$Sen^{\mu}_{p_j} = \frac{\lim\limits_{\delta\beta_j \to 0} \mu_\Delta(M(\beta_j)) - \mu(M(\beta_j - \delta\beta_j))}{\delta\beta_j} \tag{206}$$

with $j \in 1 \ldots n$. It is proven that the skewed μ is equivalent to μ-sensitivity (Marcos et al., 2005). Thus, the μ-sensitivity can be calculated easily in two ways. In the first way, the parametric perturbation is absorbed into the system matrix. μ-sensitivity is computed using definition (206) by computation of the Structured Singular Value μ. The μ-sensitivity can also be calculated with the help of skewed μ. Both can be done with the Skew μ Toolbox (Ferreres and Biannic, 2003).

6.2.4 Determination of worst-case parameter combinations by Anti-optimization

The requirements of industry-defined standards must be fulfilled for any combination of parametric uncertainties and over the whole operation range. Using only analytical methods, from classic control theory for industry-defined criteria may therefore not be straightforward, conservative or may just be impossible. For large power networks, it might be impracticable to prove stability and rely only on simulation. This it due to the usually high, non-linear and wide ranging dynamics coming from very fast switching. For example, a state could be oscillating at low damping. The eigenvalues could be in the stable area ,while the industry-defined limits of overshoot, steady-state limits and permitted frequencies are violated. Therefore, for aircraft electrical systems, the current industry verification process basically relies on repeatedly checking the limits for the parameter range and operation envelope, often by running a regression of simulations. The limits are given by general aviation standards and airframers' directives. Parameter combinations are chosen by gridding or Monte-Carlo simulation for a few parameters. This demands extensive computation and no guarantees can be given for hitting the worst-case combination.

This problem may be solved using anti-optimization or worst-case search, as an improvement of the verification process. The basic idea is to reformulate a stability criterion as a minimum distance problem, which is minimized to determine worst-case parameter combinations and operation conditions, leading to worst performance. This is the reason why it is also called anti-optimization. Since the search is directed, it is likely to be much faster and more accurate than gridding or Monte-Carlo analysis. Now, the theory shall be transferred to the network stability problem.

Chapter 6.2.4.a is about the theory. Next, some criteria suitable for stability investigations are designed; first generally, and focused on industrial design. The method is tested with the DC/DC converter, and compared to the results of the other methods under consideration, in section 6.6.

6.2.4.a Theory of anti-optimization

With the theory of (Varga, 2002), let p be the parameters vector and OC the operating condition. The clearance problem for a given performance criterion $c(p, OC)$ can be formulated as a distance-minimization problem to find the worst-case parameter combination/operation condition leading to the worst performance. With c_0 being the limiting acceptable value of $c(p, OC)$ as defined in a requirements specification, the difference

$$d(p, OC) = c(p, OC) - c_0 \tag{207}$$

is to be minimized by variation of p within the parameter space at all possible operating conditions OC. The minimum distance

$$d(OC) = \min_p d(p, OC) \tag{208}$$

can be interpreted as the robustness measure of how far the system is away from the limiting acceptable performance c_0. For flight control, this optimization-based approach was used with parametric non-linear aircraft models, which were linearized for eigenvalue based analysis. But the approach is general, being able to address all kinds of mathematically formulated criteria for linear, non-linear and switching models. This is necessary for industry-defined stability criteria, since they are mixed criteria for network stability, power quality and performance for complex models, which can not necessarily be treated with linear systems control theory.

It is applicable to:

- simulation-based stability studies with behavioral systems for large signal stability, by applying the industry stability criteria,
- stability studies, by testing non-switching functional systems with linearised equations for small signal stability,
- robust stability for parameter variations in a predefined range,
- design by determination of maximum parameter variations, which are tolerable for a nominal system to still be stable (for multiple parameters, the ratio must be weighted by a cost function),
- and design by iterative optimization of design parameters (e.g. controller), optimized for worst operating conditions identified by anti-optimization (see Bals et al.(1996).

The evaluation of criteria based on linearized models, involves trimming, linearization and frequency response or eigenvalue computation. The evaluation of criteria based on non-linear models usually involves simulations, preceded by trimming or periodic steady-state determination.

For this work, the anti-optimization is transferred to electrical network design, and demonstrated with a design problem. The aim is to find the maximum range for a design parameter not violating a stability, performance or quality criterion. The optimization problem is proposed to be as follows:

$$\min_{\bar{P}} \{ f(\bar{P}) \}$$
$$\min_{k,\bar{p}} \{ d_k(\bar{p}, \bar{P}, OC) \} \overset{!}{\leqslant} 0 \tag{209}$$
$$c_i(\bar{p}, \bar{P}) \geqslant 0$$
$$l_j \leqslant p_j \leqslant u_j$$

In words: We assume there is a range in the design parameters $\bar{P}$ where the defined stability criteria can not be violated within the system variation $\bar{p}$ or Operation Conditions range OC. The optimization problem is to size $\bar{P}$ to find the minimum solution of $f(\bar{P})$ which will make the distance to instability $d_k(\bar{p}, \bar{P}, OC)$ to zero for the criterion which is "easiest" to violate. The vector of uncertain system parameters lies within the limits $l_j \leqslant p_j \leqslant u_j$. Additional constraints to exclude certain parameter combinations $c_i(\bar{p}, \bar{P}) \geqslant 0$ may be stated (e.g. combinations not occurring for the real system or exclusion of areas where stability already is known).

Considerations about the optimization method and problem formulation are stated in an extra paragraph. For several design parameters the problem is non trivial since $f(\bar{P})$ has to be formulated to destabilize the system just in case of growing. Non-convex problems will prevent good solutions. Therefore as much analytic information should be inserted in the problem formulation as possible.

6.2.4.b Criteria formulation

It is advantageous for a single evaluation or in hardware certification tests, to have binary indicators such as "criterion fulfilled/ not fulfilled". For use in optimization, algorithms can usually not handle discrete indicators. Even for algorithms which are capable of handling non-convex optimization problems, such as genetic algorithms or particle swarm optimization, those indicators should be continuous. This requires a thorough formulation of the objectives, by means of smooth optimization criteria. In this section, it is considered how to formulate the optimization criteria for the investigation of system stability. First, by means of methods aiming for internal stability, based on eigenvalues. Second, by means of methods aiming for limits from industrial standards, based on output stability. The criteria are similar to the model-based specifications in (Kuhn et al., 2015).

Statespace criteria

The **eigenvalues** give information about small-signal stability and settlement of a linear time-invariant representation. In the case that the largest eigenvalue of a system passes the imaginary axis of the complex plain to the right half side, the system is unstable. With the l eigenvalues λ_l, calculated from the linearised functional model, the distance criterion can be defined as:

$$d_{ev} = \min_l \left(\frac{\epsilon - \mathrm{Re}(\lambda_l)}{\epsilon - \mathrm{Re}(\lambda_{l0})} \right) \tag{210}$$

where ϵ is an additional stability margin which can be used to limit the maximum settling time. λ_{l0} are the initial values of the eigenvalues, which are used for normalization of the criterion. From the practical point of view, one might mainly be interested in the behaviour of a monitored state. This may not be dependent upon all eigenvalues. The correlation between the k states of a linear system and its l eigenvalues can be determined by the participation factor:

$$p_{kl} = \frac{\delta \lambda_l}{\delta a_{kk}} \tag{211}$$

In any case, one can say the states $\bar{x}$ of a linear asymptotically-stable system will return to the equilibrium point $\bar{x}^*$ of the *OC* exponentially, with at least the convergence rate of the largest eigenvalue:

$$\|\bar{x} - \bar{x}^*\| \leq k\, e^{\gamma t}, k > 0, \max_l(\lambda_l) < \gamma < 0 \tag{212}$$

This information could be used to transfer the demands of the industry standards for settlement to the eigenvalue criterion.

The **damping** of the eigenvalues is important for the attenuation of oscillations. The distance criterion can be defined as the minimum damping distance of the eigenvalue to the accepted damping value:

$$d_D = \min_l \left(\frac{D - \zeta}{D - \zeta_{l0}} \right), \zeta_l = damp\,(\lambda_l) \tag{213}$$

Again, the initial damping value ζ_{l0} is used for normalization

Output stability criteria

In this section, initially some typical requirements are defined; then it is discussed how to convert them for the optimization problem formulation. For demonstration of the methodology, the limits are inspired by the often-applied Military Standard 704F. See (STD-704F, 2004) for specification of the 28 Volts DC network. Since this work treats the network design from a generator manufacturer perspective, the focus is on the limits for the system, not on the tests at equipment level.

The following relevant **limits** were identified:

- *Case 1*/ Steady State: For steady state, maximum and minimum voltages are given. Upper and lower boundaries are not necessarily equidistant from nominal value.
- *Case 2*/ Transient characteristics: For transients, the voltage of the DC network must remain within time-variable limits after a displacement. After the settling time, steady state limits apply. As for the steady state case, upper and lower boundary envelopes may differ in extent, but also in the shape. Figure 6.19 shows a typical operation envelope, the permitted range is highlighted. Standards often provide scenarios to test the system for the transient limits. Typical changes are power-up or power-down, network reconfiguration, load variation and short circuits.

All steady-state and transient-state limits may be superposed by a ripple.

- *Case 3*/Ripple: The distortion has to be bounded to a maximum voltage amplitude (time domain).
- *Case 4*/Frequency domain limitations: For the frequencies spectrum of the network voltage, limits in the amplitudes are given.
- *Case 5*/Frequency domain limitations: The total distortion may not exceed a certain ratio of the DC signal. For special conditions such as over-voltage or power-up, other limits may apply. They are not treated here since they are variations of the mentioned cases.

6.2.4.c   Design of criteria from limits

The cases may be re-formulated into optimization criteria formulations as follows:

For *case 1*: Since this is a performance criterion for steady-state condition of the base voltage, both functional and behavioral models apply.

For the functional model, trimming the model at steady-state already gives the network voltage. Using the Dymola simulation environment, steady-state initialization at zero and fixed value initialization (e.g. $\dot{\varphi}=400Hz$) can be mixed easily. Since the initialization problem may be non-linear, it is advantageous to set estimated values for the iteration variables, close to the actual values. The result of a previous simulation run with similar parameters, can be used to set the estimated values. Using just the steady-state solution for the functional model is equivalent to using architectural models.

For behavioral models, the mean voltage does not change at stationary operation, but it is superposed by the alternating voltages of case 3. The mean component can be separated from the DC component of the Fourier-transformed result of a simulation run. As stability distance criterion, the distance between the actual net voltage V and the upper or lower boundaries V_u/V_l shall be defined, normalized by the distance between the nominal value V_0 and the bounds. If the criterion is below 0 the standard is violated.

$$d_{DC} = \begin{cases} \left(\dfrac{V - V_u}{V_0 - V_u}\right), V \geqslant V_0 \\ \left(\dfrac{V - V_l}{V_0 - V_l}\right), V < V_0 \end{cases} \tag{214}$$

An optimizer, which is just gradient based, is not applicable for this criterion since the sign of the function changes at V_0.

For *case 2*: This limit can be tested most effectively when simulating an operation scenario with some sort of induced transition, e.g. step response on a load change. Some typical scenarios are given by the standards such as power-up or power-down, network reconfiguration, load variation and short circuits. In practice, often the scenario most critical to stability is not known a priori, but fixed scenarios without guarantee in targeting worst-case violations are applied. The scenarios must be processed consecutively. Alternatively, it is possible to include parameters defining the operating condition in the unknown parameters vector and anti-optimize for the most critical condition. In (Menon et al., 2007), the flexibility of global optimization methods was exploited to show how continuous regions of the flight envelope could be cleared in a single analysis. Furthermore, for time-dependant inputs, a scheme was proposed for the computation of worst-case inputs. The idea was to represent the discretized switching times and amplitudes for switching as "genes", which are varied by a genetic algorithm.

The distance criterion for the limit itself can be formulated similar to Equation (214). With the discrete time steps i, the criterion is the maximum value of Equation (214), evaluated at all i's. If it is below 0 the standard is violated.

$$d_{trans1} = \min_{i \in 0..n} \left\{ \begin{cases} \left(\dfrac{V_i - V_{u\,i}}{V_{0\,i} - V_{u\,i}}\right), \forall\, V_i \geqslant V_{0\,i} \\ \left(\dfrac{V_i - V_{l\,i}}{V_{0\,i} - V_{l\,i}}\right), \forall\, V_I < V_{0\,i} \end{cases} \right\} \tag{215}$$

Filtering can also be achieved by calculation of the mean value by using integration:

$$d_{trans2} = \min_{j \in 0..m} \left\{ \frac{1}{T_{j+1} - T_j} \int_{T_j}^{T_{j+1}} \begin{cases} \dfrac{V(t) - V_u(t)}{V_0(t) - V_u(t)}, \forall\, V(t) \geqslant V_0(t) \\ \dfrac{V(t) - V_l(t)}{V_0(t) - V_l(t)}, \forall\, V(t) < V_0(t) \end{cases} dt \right\} \tag{216}$$

Care must be taken to choose the intervals j long enough to limit the frequencies' content, but not to hide local overshoots. It is convenient to use the integration algorithm of the simulation program for evaluation of this criterion.

For *case 3*: The voltage ripple can be seen as the opposite problem to the former limits cases. For the behavioral model constant operation, and both modeling levels transients simulation, the ripple superposes the slowly varying section. The ripple can be separated by high-pass filtering, subtraction of the low-pass filtered or averaged signal from the simulation result.

For *case 4*: This limit resembles case 2 but for the frequency domain. The criterion for optimization can be formulated as the minimum of the distances of the amplitudes $A(f_k)$ at frequencies f_k to their applicable limits $\lim(f_k)$:

$$d_{fs} = \min_k \left\{ \lim(f_k) - A(f_k) \right\}, \quad k = 1..l \tag{217}$$

For the Discrete Fourier Transformation (DFT), the sampling time has to be chosen low enough to cover the highest frequencies appearing in the simulation or specified in the standards. The number of sampling points determines the spectral resolution and therefore must be chosen high enough not to mask peaks of neighbouring frequencies. For heavy-switching systems, the results of the DFT could be wrong, since the algorithm demands a fixed sampling rate. To cover the events generated by switching, it might be noteworthy to use the Lomb periodogram, which allows frequency analysis for potentially non-uniformly sampled data. More considerations on the use of FFT can be found in chapter 5.7.

For **case 5**: The criterion for the total distortion factor (TD) is quite straightforward. With the TD calculated as the RMS value of the alternating voltage component, divided by the DC voltage and the limit TD_{lim}:

$$d_{TD} = TD_{\mathrm{lim}} - TD \tag{218}$$

The implementation of the distance criteria with Modelica, is in parts identical with the property monitors in chapter A3. For details about the implementation, the reader is referred to this chapter.

6.2.4.d   *Implementation and optimization algorithm*

For stability analysis, it is sufficient to find one solution in the parameter range which will result in a boundary violation. For design, it is essential to find the global solution of the optimization problem, otherwise the design limit is over-estimated. It is quite easy to see that the optimization problem (209) is very affine for local minima, as only the worst criterion has to be minimized. Local optimization algorithms, such as gradient based optimization, will minimize just one criterion with the minimum located next, neglecting other solutions in the parameter space for this criterion at all other criteria in general. It is essential to normalize the criteria at the starting conditions. As a basis, one could perform a first evaluation run for the nominal model and scale the criteria by the nominal values.

For global optimization, there exist stochastic and deterministic solvers such as the well known stochastic genetic algorithm, particle swarm optimization or the deterministic differential evolution algorithm. The possibility to parallelize the computation is seen as being essential for efficient computation. Therefore, as one promising solution, the particle swarm optimization (PSO) is used.

For tools, the object-oriented simulation environment, Dymola, and the DLR-developed Matlab-based multi-objective optimization tool, MOPS, is used.

The implementation in the DLR optimizer of PSO in MOPS is extended for constraint optimization problems. It also has additional hybrid (combined local/global) optimization features, to overcome slow convergence of stochastic search methods to some extent (Joos, 2017). The particle swarm optimization tries to simulate the social behaviour of a population (swarm), for example a swarm of birds. This is a successful application of the philosophy of bounded rationality and decentralized decision-making to solve the global optimization problems (Simon, 1982) (Bauer, 2004) (Fleischer, 2005). A swarm of birds or insects searches for food, protection, etc. in a very typical manner. If one of the members in the swarm finds a desirable path e.g. nearest to the goal, the rest of the swarm will follow quickly. Each member of the swarm searches for the best in its vicinity

and learns from its own experience. Simultaneously, it learns from the others, typically from the best performer among them. PSO has been extended to many variants after it's introduction in (Kennedy and Eberhart, 1995) e.g. the repulsive particle swarm, for finding the global optimum more effectively (Urfalioglu, 2004) and other variants using dynamic schemes (Liang and Suganthan, 2005) (Huang et al., 2006). The basic algorithm is easy to implement. A given problem (tuner) space is firstly explored randomly. In iteration k, for each particle (tuner vector) $x^i(k)$ in the population a new candidate $c^i(k+1)$ is computed as

$$
\begin{aligned}
c^i(k+1) &= x^i(k) + v^i(k+1) \\
v^i(k+1) &= I(k) v^i(k) + \alpha \omega_1(k)(\bar{x}^i(k) - x^i(k)) + \beta \omega_2(k)(\bar{\bar{x}}(k) - x^i(k))
\end{aligned}
\tag{219}
$$

Where

- $I(k)$ is a weighting factor (called inertial parameter) linearly interpolated between initial and final value after maximum iterations.
- $\bar{x}^i(k)$ is the best solution on position i of the population so far.
- $\bar{\bar{x}}(k)$ is the overall best solution at iteration k.
- α, β are weighting factors (called cognition and social parameters respectively).
- $\omega_j(k)$ is a random number uniformly drawn from (0,1).

In the terminology of PSO v is also called velocity. A candidate is then taken as new particle in population $k+1$ if it outperforms the corresponding particle of the iteration before. The implementation of POS in MOPS is instrumented to deal with mixed continuous/discrete optimization problems and it is extended by a hybrid (combined global/local) optimization feature (Joos, 2017).

As written above, the methodology relies on fast and robust simulation. While the capability to conveniently model complex physical systems with Modelica is generally accepted, the capability to perform large-scale electrical system simulation in an optimization process remained unproven. In the large scale benchmark which is treated in chapter (7.1) it is shown that Dymola simulations can be designed robustly for model integration and analysis, as part of a validation and verification process. The same procedure can be used to design the anti-optimization setup. For the technical implementation, the reader is referred to the conference publication.

6.3 Demonstration

In this section, the approaches for stability analysis are demonstrated and compared, by means of a buck converter. As pointed out before, a DC/DC converter is usually a critical component for system stability in an electric on-board network due to its inherent character: its controller exhibits a negative input impedance Z_i (see Figure 6.7). In combination with an unsuitable input filter, the DC/DC converter begins to oscillate and becomes unstable (Middlebrook, 1976). The converter transforms the 350 Volts input voltage to 28 Volts DC output voltage. Input filter inductances (R_f, L_f, C_f) prevent propagation of switching ripples to the voltage source. The input filter components can also be seen as an equivalent Thévenin model of a more complex input network. This could be the generator with rectifier and feeders. While the parameters and equations for the filter parameterization are known in this case, it would not be so straightforward for several loads and the AC source. Therefore, all parameters are treated as independent, uncertain ones.
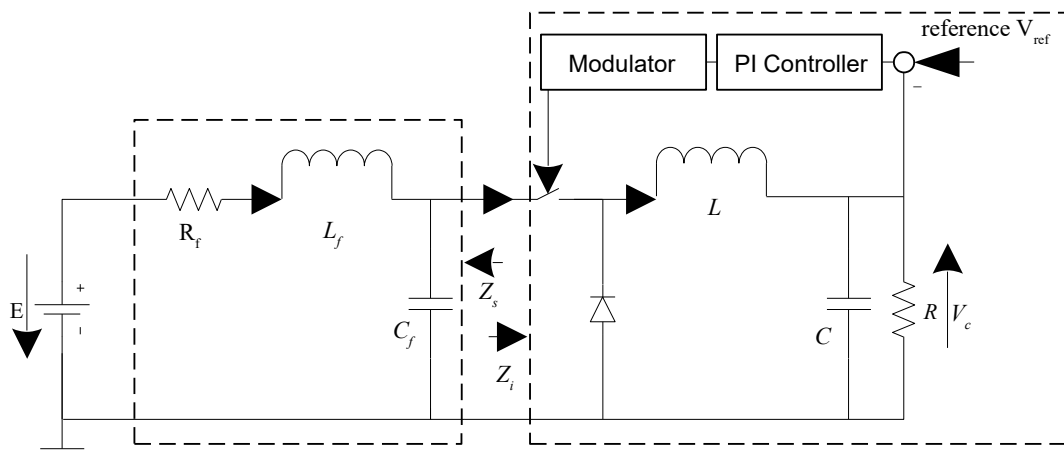
Figure 6.7: Time discrete buck converter with PWM controller block diagram

6.3.1 Demonstration model

The methods demand models with different levels of complexity. The layers are chosen analogue to the definitions in chapter 2.1: *Behavioural models* are complex models including switching and HF injection behaviour. They are representative, even for network power quality studies, but simulation speed is low. *Functional models* are averaged models, valid for steady-state power consumption and mean-value transient behaviour. Equations related to net frequency have to be transformed to a net-frequency fixed system, which gives a time-independent steady-state solution for stationary operation. Linearization can be applied on the functional models for network stability investigations and network logic is studied via them.

6.3.1.a Behavioural model of buck converter

The behavioral model can be seen in Figure 6.8. All nominal parameters except for the controller of the buck converter model are taken from (Barruel et al., 2005). The parameters, including the PI controller parameter, are given in Table 10.
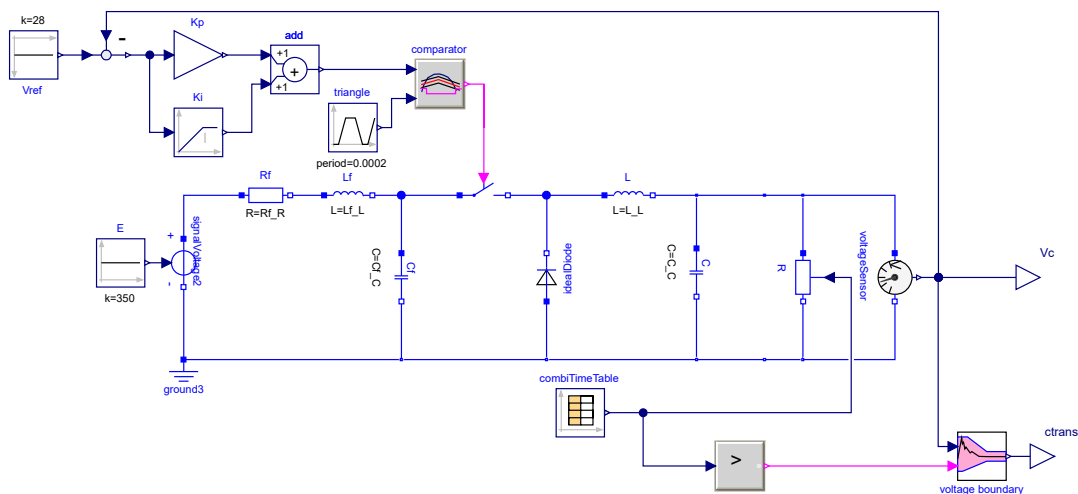
Figure 6.8: "Behavioural" Modelica model of DC/DC buck converter

For analytical and steady-state conditions, several load conditions are studied, where the output resistance is varied around its nominal value. For the behavioral model, instead of a variable load parameter, a load step is used and the limits are checked according to industrial criterion 2). In the behavioral model for transients simulation in Figure 6.8, the load resistance changes, where the con-

144

ditions are set in the "combiTimeTable". The transient response of the low voltage side is monitored by the "voltageboundary" element.

Parameter	Value	Unit		Parameter	Value	Unit
voltage source E	350	Volts		resistance of input filter R_f	250e-3	Ohms
reference output voltage V_{ref}	28	Volts		inductance of input filter L_f	100e-6	Henrys
output power P	5000	Watts		capacitance of input filter C_f	100e-6	Farads
output resistance R	0.1568	Ohms		gain of I controller K_i	5	-
inductance L	290e-6	Henrys		gain of P controller K_p	0.05	-
capacitance C	399e-6	Farads				

Table 10: Nominal parameters of buck converter

6.3.1.b Average model of buck converter

The differential equations of the state space, averaged buck converter are

$$
\begin{aligned}
\frac{d}{dt}i_{Lf} &= \frac{1}{L_F}\left(E - R_f \cdot i_{Lf} - V_c\right) \\
\frac{d}{dt}V_{Cf} &= \frac{1}{C_f}\left(i_{Lf} - \alpha \cdot i_L\right) \\
\frac{d}{dt}i_L &= \frac{1}{L_h}\left(\alpha \cdot V_{Cf} - V_c\right) \\
\frac{d}{dt}V_C &= \frac{1}{C}\left(i_L - \frac{V_c}{R}\right) \\
\frac{d}{dt}\alpha &= -\frac{K_p}{C}\left(i_L - \frac{V_c}{R}\right) + K_i\left(V_{ref} - V_c\right)
\end{aligned}
\tag{220}
$$

$X = \left(x_{1,}\,x_{2,}\,x_{3,}\,x_4,\,x_5\right) = \left(i_{Lf},\,V_{Cf},\,i_L,\,V_C,\,\alpha\right)$ represent the five states of the buck converter system, where α is the duty circle. u includes all system inputs. The implementation of the functional model in Modelica can be seen in Figure 6.9.

6.3.2 Analysis of buck converter

6.3.2.a Analysis with μ-sensitivity

μ-Analysis is only suitable for LTI systems. The buck converter with time-discrete parts in Figure 6.7, must be first transformed into a time-continuous model using the average modeling technique (Louganski, 1999) (see Figure 6.9). For small signal analysis with μ-sensitivity, the system must be linearised around equilibria points. The linear state space system
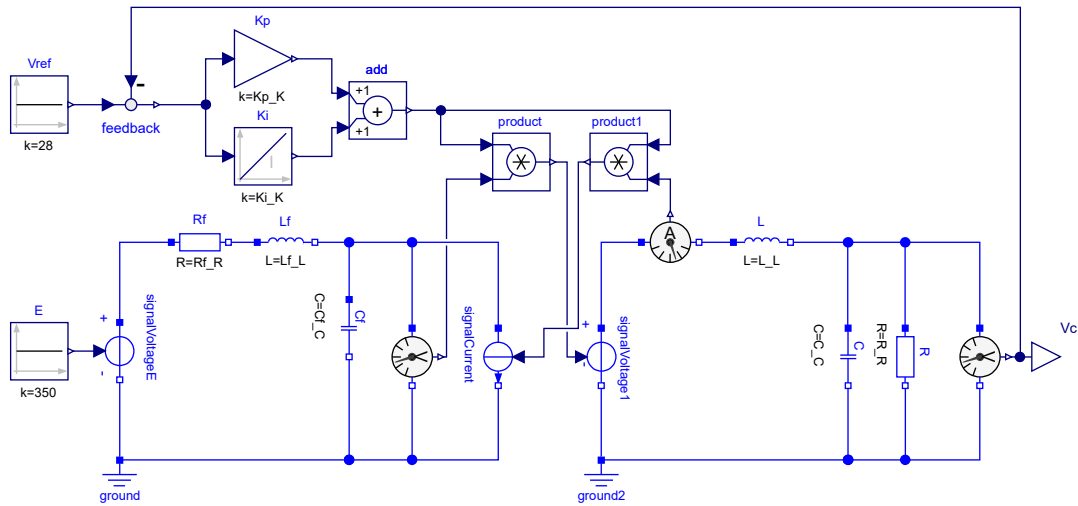
Figure 6.9: "Functional" Modelica model derived manually from "behavioral" model of DC/DC buck converter

$$
\begin{aligned}
\Delta \dot{X} &= A \Delta X + B \Delta u \\
\Delta Y &= C \Delta X + D \Delta u
\end{aligned}
\tag{221}
$$

of the buck converter is obtained by symbolic linearization for all equilibria points

$$
\begin{bmatrix}
x_{1,eq} \\
x_{2,eq} \\
x_{3,eq} \\
x_{4,eq} \\
x_{5,eq}
\end{bmatrix}
=
\begin{bmatrix}
\dfrac{350 - \sqrt{350^2 - \dfrac{4 \cdot 28^2}{R} \cdot R_f}}{2 R_f} & [A] \\[3mm]
\dfrac{28^2}{R} \cdot \dfrac{1}{x_{1,eq}} & [V] \\[3mm]
\dfrac{28}{R} & [A] \\[2mm]
28 & [V] \\[2mm]
\dfrac{28}{x_{2,eq}} & [\,]
\end{bmatrix}
\tag{222}
$$

The resulting state space matrices in (221) are

$$
A =
\begin{bmatrix}
-\dfrac{R_f}{L_f} & -\dfrac{1}{L_f} & 0 & 0 & 0 \\[3mm]
\dfrac{1}{C_f} & 0 & -\dfrac{x_{5,eq}}{C_f} & 0 & -\dfrac{x_{3,eq}}{C_f} \\[3mm]
0 & \dfrac{x_{5,eq}}{L} & 0 & \dfrac{1}{-L} & \dfrac{x_{2,eq}}{L} \\[3mm]
0 & 0 & \dfrac{1}{C} & -\dfrac{1}{RC} & 0 \\[3mm]
0 & 0 & -\dfrac{K_p}{C} & \dfrac{K_p}{RC} - K_i & 0
\end{bmatrix}
\tag{223}
$$

$$
B =
\begin{bmatrix}
1/L_f & 0 \\
0 & 0 \\
0 & 0 \\
0 & 0 \\
0 & K_i
\end{bmatrix}, \quad
C = [0\,0\,0\,1\,0], \quad D = [0\,0]
$$

The model was symbolically constructed with object-oriented modeling and the simulation tool Dymola.

All elements in the state-space matrix must be constant or of polynomial type in order to use the LFR Toolbox for generating an LFR. As seen in (223), there are some items which are not polynomials because of the root in the first system equilibrium point $x_{1,eq} = \left(350 - \sqrt{350^2 - 4 \cdot 28^2 / R \cdot R_f}\right)/2\, R_f$.

Thus, this expression has to be approximated. Utilizing a first-order Taylor series expansion (Ansorge and Oberle, 2000) at the point $x_{1,eq} = 14.27\, A$, the first equilibrium point becomes

$$\hat{x}_{1,eq} = \frac{89.304 - 7.29\,e - 4 \cdot \left(350^2 - \dfrac{4 \cdot 28^2 \cdot R_f}{R}\right)}{R_f} \tag{224}$$
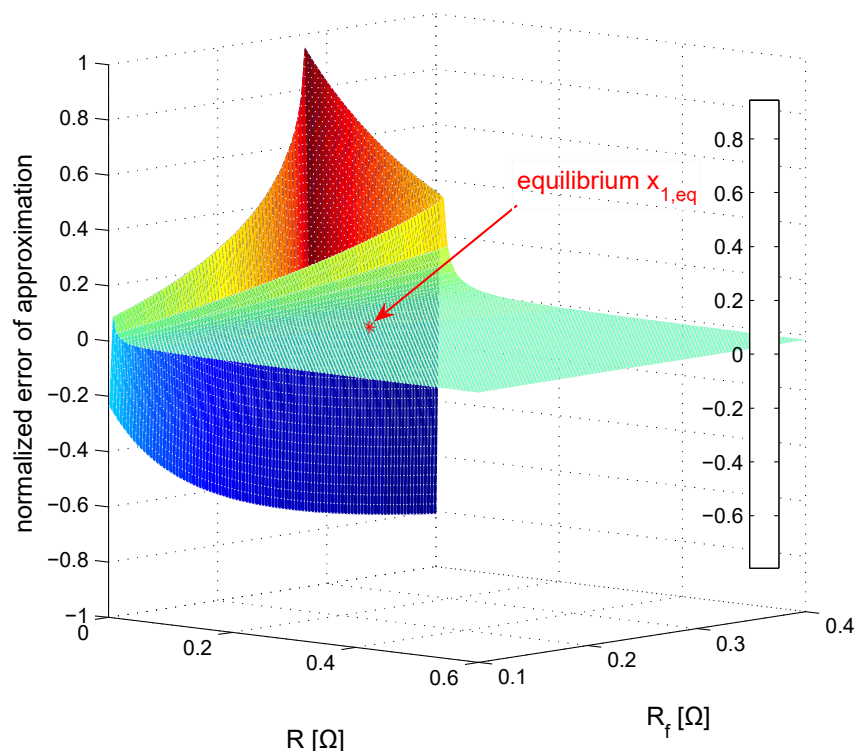
Figure 6.10: Error of approximation $\left(x_{1,eq} - \hat{x}_{1,eq}\right)/x_{1,eq}$
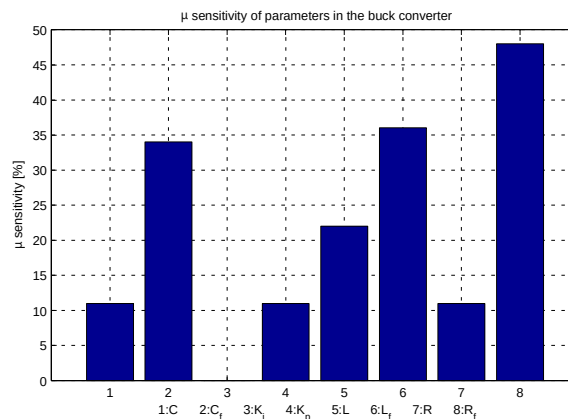
Figure 6.11: μ sensitivity analysis

The reliability of the approximation is analysed by plotting the error of the approximation $(x_{1,eq} - \hat{x}_{1,eq})/x_{1,eq}$ with respect to R and R_f. Figure 6.10 shows that a first-order Taylor series expansion is surely valid when $0.086\,\Omega \leq R \leq 0.24\,\Omega$ and $R_f \geq 0.14\,\Omega$ (error of approximation $\leq 1\%$). Otherwise, an approximation by higher-order Taylor series or a rationale function should be used.

Inserting the approximation of the equilibrium point into the system matrix of the average-value buck converter (223), yields the symbolic linearized model which is compatible with the LFR Toolbox 2.0.

Figure 6.11 shows the variation of μ with regards to identical small perturbations of all parameters in the buck converter in percent. According to the figure, the four most critical parameters of the buck converter are determined. They are R_f, L_f, C_f in the input filter and L in the load system of the buck converter, with decreasing effect for the system stability. This is a very important result, since the input impedance seems to be crucial. In a real application, this impedance could vary due to the source impedance; this may consist of DC line feeders, rectifier, AC distribution network and generator. Thus, the variation of those most critical parameters e.g. R_f and L_f has to be considered with very high accuracy in the design and operation of the buck converter. The restrictions for the relative insensitive parameters e.g. C in the load system could be relaxed. This means that for a design or study or control, the exact identification or a guaranteed range of a parameter is not crucial. The maximum uncertainty range for each uncertain parameter or for a group of uncertain parameters, can be calculated by the skew μ toolbox (Ferreres and Biannic, 2003). The details for computing the maximum uncertainty range can be found in (Ferreres and Biannic, 2003).

6.3.2.b   Analysis with Impedance-based Criterion

In the Middlebrook criterion, the system is stable if the amplitude of the (source) output impedance Z_s is smaller than the amplitude of the (load) input impedance Z_i within the studied frequency range. Instead of the Middlebrook criterion, the similar criterion of theorem 1 is applied. The original model was displayed in Figure 6.4. Figure 6.12 shows the Dymola model for automatic impedance calculation. For impedance calculation, the original model is split into input and output systems. Coupling terms are replaced by constant offsets (Iin0, vin0), and adapted with input and output interfaces (Iout, Vout, Iin, Vin). For the buck converter in Figure 6.12, the output impedance of the input filter is
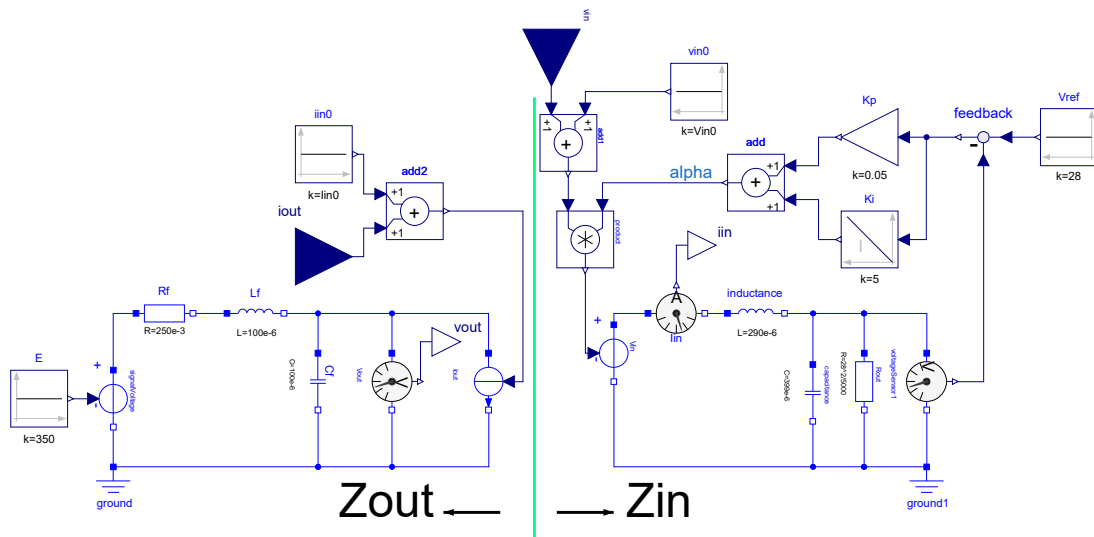
Figure 6.12: Modelica model of buck converter, for input/output impedance analysis

$$Z_s = \frac{R_f + s\,L_f}{s^2\,L_f\,C_f + s\,R_f\,C_f + 1} \tag{225}$$

The peak Z_{smax} (in Figure 6.13) magnitude of the output impedance of the input filter is $L_f/C_f R_f$. The frequency ω_o at which the maximum output impedance Z_{omax} appears equals $1/\sqrt{L_f C_f}$. Compared to the result of the μ-sensitivity approach, the impedance based criterion shows a similar result. Varying an input filter for a given regulated buck converter, the system could become unstable in two ways:

- the peak Z_{smax} crosses over the input impedance of the buck converter Z_i mostly due to the variations of R_f
- the frequency ω_s moves to the left, so that the peak Z_{smax} crosses over the input impedance Z_i (L_f and C_f are most responsible)
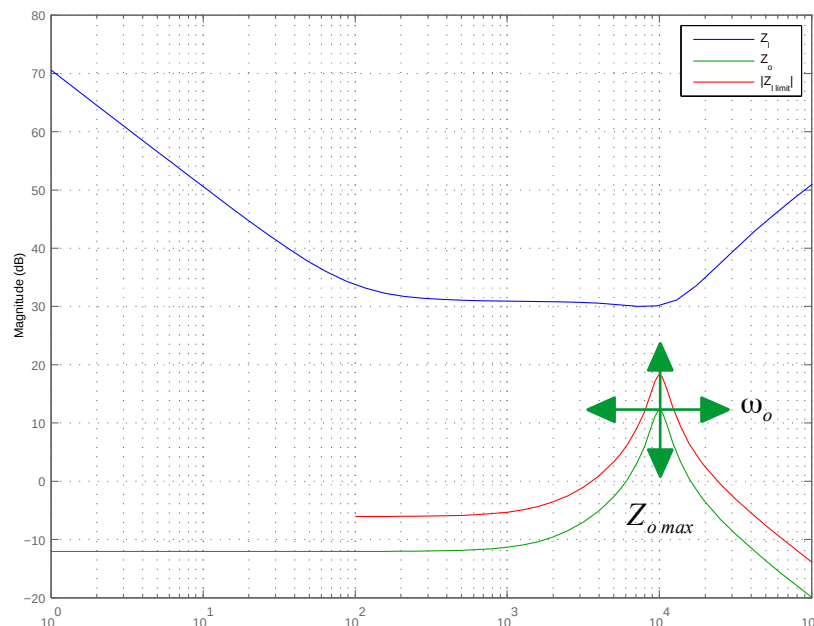
Figure 6.13: Bode diagram of output impedance of source Z_s and input impedance of load Z_i

The assessment of the critical parameters is very similar to the μ-Analysis. In the determination of the critical parameter combination or the allowed range, the impedance-criterion is not very useful. The system engineer has to be well aware of the interpretation of the bode plot. The standard way to assess the stability bound is a time- consuming parameter variation. The impedance criterion has to be repeatedly evaluated for all components of a network, with special considerations for parallel circuits. The impedance-criterion cannot give a quantitative analysis for the critical level of uncertain parameters.

6.3.2.c Analysis with Modal Analysis

Figure 6.14 shows all eigenvalues and the corresponding states for the buck converter. With the results from (Barruel et al., 2005):

- λ_1 is mostly sensitive to K_p, K_i and R
- $\lambda_{2,3}$ are mostly sensitive to L_f and C_f
- $\lambda_{4,5}$ are mostly sensitive to L, C and K_p
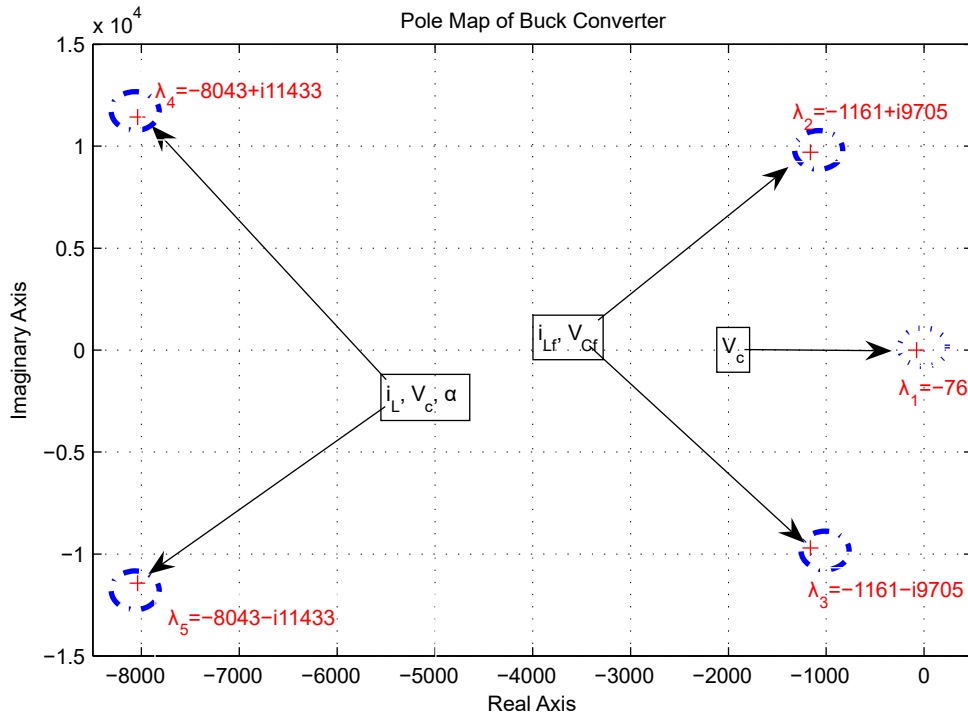
Figure 6.14: Poles and their corresponding state variables of the buck converter

The combined information from the participation factors and the eigenvalue sensitivity can be used by a system designer to detect suitable parameters for pole displacement e.g. for a higher stability margin or better dynamic performance. For example, the state variables i_{Lf} and V_{Cf} can be significantly influenced by changing the parameter L_f and C_f because of the great participation factor of the state variables i_{Lf} and V_{Cf} to the eigenvalues $\lambda_{2,3}$ and the great sensitivity from L_f and C_f to the eigenvalues $\lambda_{2,3}$. Although the Modal Analysis is very suitable in design, it is not reliable to look for the most critical parameters with respect to system stability. It is easy to see in Figure 6.14, that the most critical eigenvalue for stability in the nominal system is now the first eigenvalue λ_1, which is the nearest to the imaginary axis. However, an equal perturbation of all parameters will first let the eigenvalues $\lambda_{4,5}$ cross over the imaginary axis, although the eigenvalues $\lambda_{4,5}$ are the least critical ones in the nominal system. The Modal Analysis cannot explain the phenomenon at all. Once again, the standard way for doing global stability analysis is exhaustive iterative parameter variation, e.g. by the Monte Carlo method, linearization at equilibrium and calculation of the eigenvalues. There is no guarantee to find all critical parameter variations.

6.3.2.d Analysis with Anti-Optimization

For demonstration of the approach with the buck converter, three distance criteria are used. These are the eigenvalue criterion (212), the eigenvalue damping criterion (213) and the transient limits criterion (218). The former two are evaluated with the functional model, while the latter is checked with the behavioral model. The optimization criterion (here: "LXdist"), which makes use of the former three criteria, was implemented as proposed in Equation (209). The minimum damping was set to 0.1, the maximum eigenvalue to -1. Here, the "LXdist" criterion weighs the L^2-norm of distance of the eight tuning parameters (Cf, Rf, Lf, C, R, L, Ki, and Kp) to their nominal values. The nominal system has an "LXdist" of "1". The anti-optimization brings the "stab" criterion to the stability threshold, with a minimum of the "LXdist" criterion.

With a population size of 40, the optimization converges after 45 iterations. The results can be seen in the results window of the optimization environment MOPS in Figure 6.15. On the left, the three intermediate results for minimal damping "Dstable", eigenvalue stability "Estable" and transient criterion "Tstable" can be seen (here: stable, if >1). The optimization criterion "LXdist" is based on the most critical of the three values.

As can be seen in Figure 6.15, the damping criterion was found to be the most critical criterion (stability limit "1" of "stab" and "Dstable"). The damping criterion can be brought to the stability limit with the lowest square sum of the parameters. In Figure 6.16 the L^2 minimal parameter variation is shown, which results in the criterion violation. Here, the most critical parameters are the filter resistance Rf (-16.9%), filter capacitance (-4.8%) and capacitance C (-2,2%). Figures 6.17 to 6.19 show the results of the single distance criteria at this most critical parameter combination.
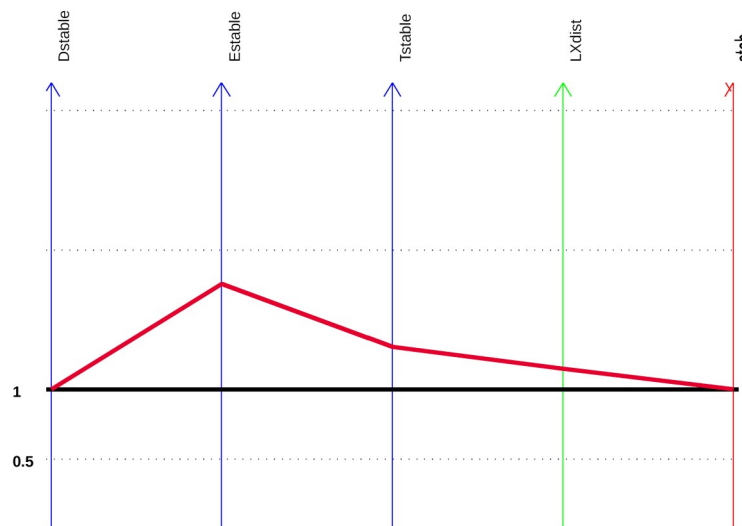
Figure 6.15: Criteria and results of the iteration steps, displayed by MOPS
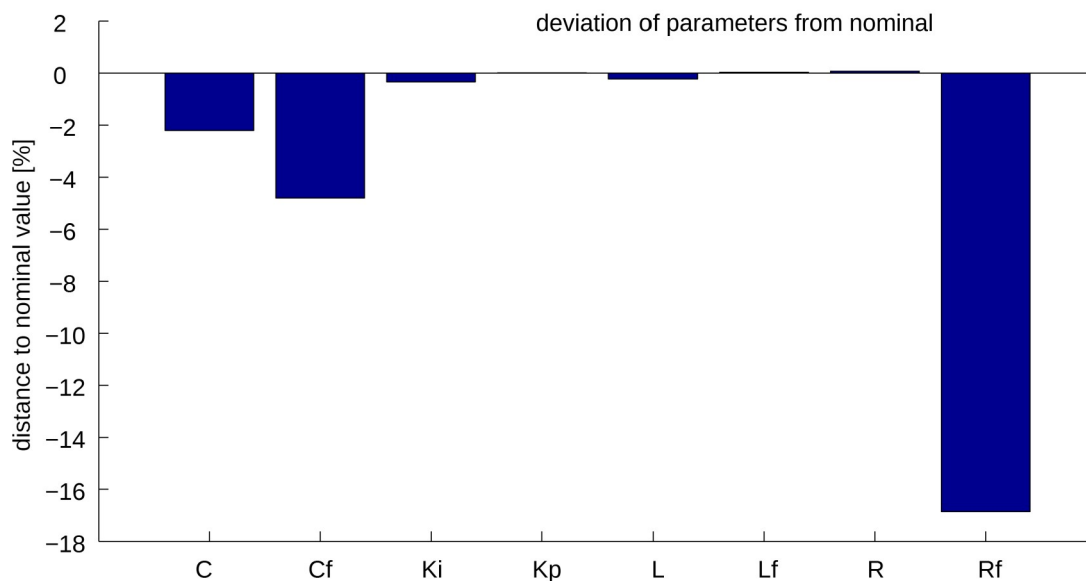
Figure 6.16: Minimum distance of parameters at stability limit (L^2-norm), most critical: damping limit

151

In conclusion, one can say: for the design in Figure 6.7, with the nominal values in Table 10, any variation of the parameters not exceeding more than 17.67% in the Euclidean norm, will not result in a violation of one of the three criteria: eigenvalue stability, minimum damping and limitation to the transient envelope. Such a system is considered as transient and eigenvalue stable and well damped. Also, no variation of a combined parameter variation within a quadratic norm of 11.1% will lead to this violation.

The example considered three criteria, whereas the alternative methods for stability investigation were focused on the eigenvalue stability. To have more comparable results with impedance-based methods, Modal Analysis and μ-Analysis, the anti-optimization based approach was performed with only the eigenvalue criterion activated. The limit of the real part of the eigenvalues was set to zero. For the minimum distance criterion, a L^{∞}-norm (maximum) was taken.

In Figure 6.20 one can see the determined worst-case parameter combination. The most critical parameter is the filter resistance R_f (-78%), and L (-33.6%), L_f (33.1%), C_f (-26%) and K_p (16.3%). The distance is far above the limit of the damping criterion of the last example. Based upon the result, the following statement can be made: Any parameter variation from the nominal values below 78% does not violate the eigenvalue stability requirement. The system is most sensitive to R_f.

The eigenvalues at the most critical parameter combination, at lowest distance, can bee seen in Figure 6.21. For the nominal system, a single eigenvalue at -95+0I was closest to the stability limit. Here, the stability limit system was violated by a couple of pole-pairs. This confirms the results of the sensitivity analysis in Figure 6.14.
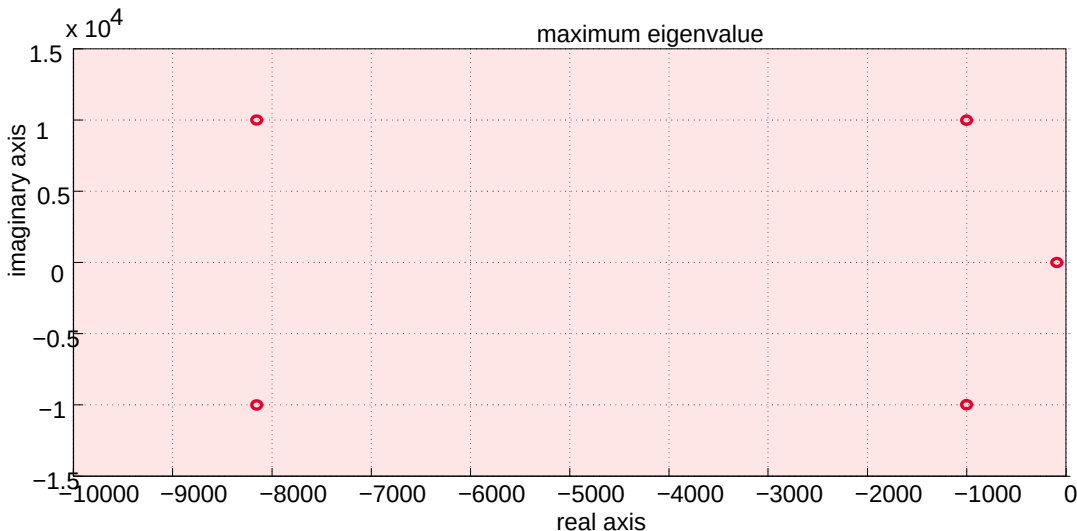
Figure 6.17: Eigenvalue criterion (complex plane); red area: tolerated
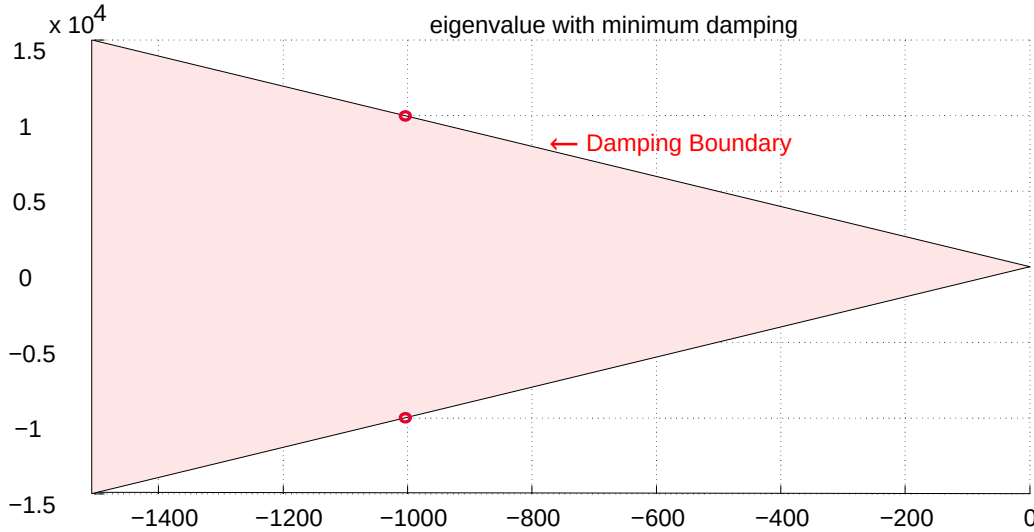
Figure 6.18: Damping criterion (only most critical pair of eigenvalues)
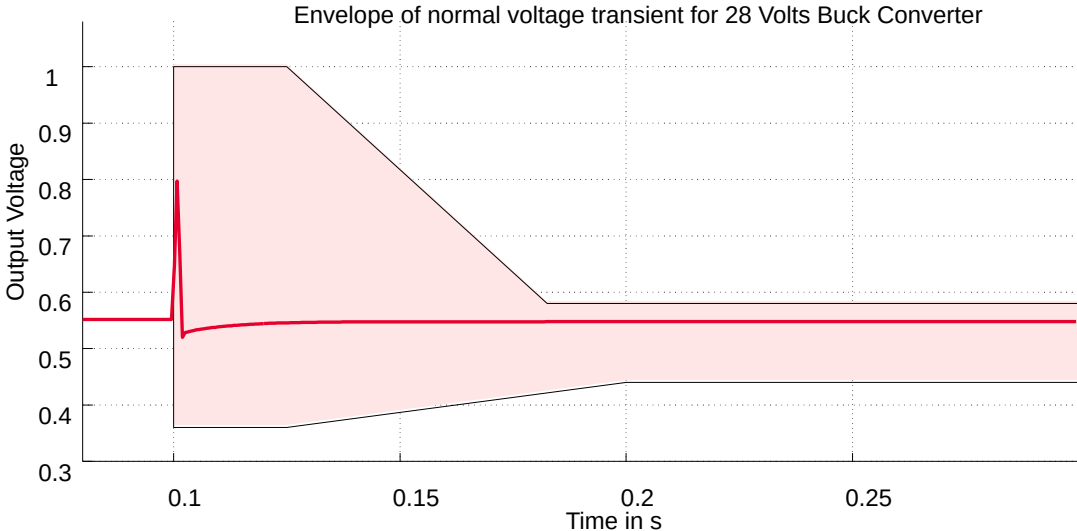
Figure 6.19: Transient criterion

153
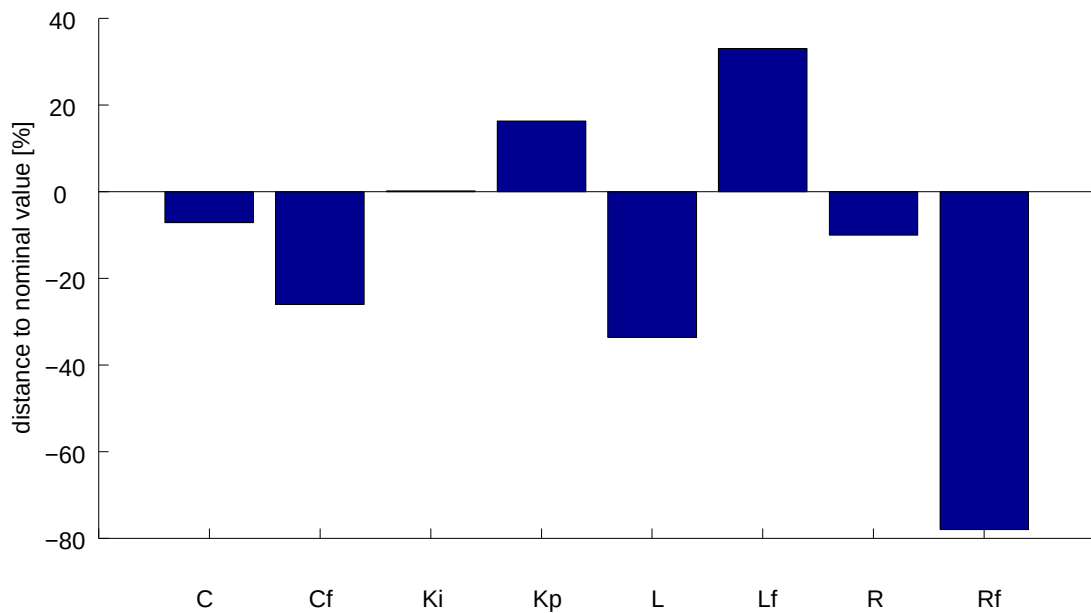
Figure 6.20: Minimum distance of parameters at stability limit (L^∞ norm), eigenvalue criterion only, norm of parameters
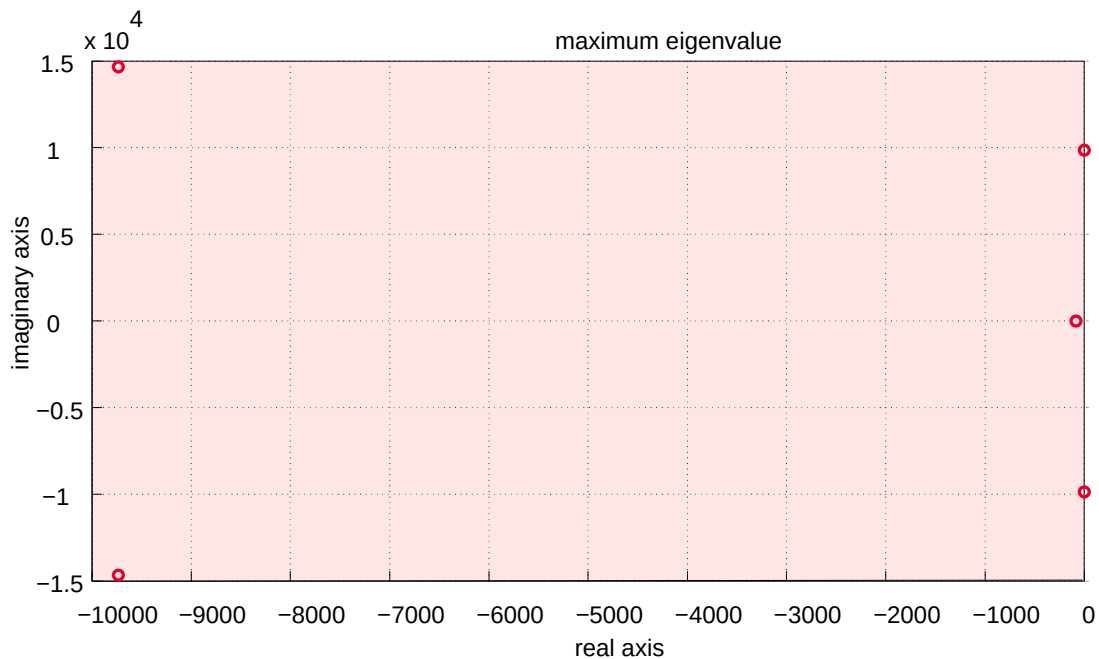
Figure 6.21: Eigenvalue criterion only ; red area: tolerated

6.4 Summary

The standard way for doing global-stability analysis is exhaustive, iterative parameter variation, e.g. by the Monte Carlo method, linearization at equilibrium and calculation of the eigenvalues. There is no guarantee to find all critical parameter variations. In an industrial driven design process of the electrical power supply network, it is not only necessary to asses the stability, but the designer should be able to assess tolerable design parameters and uncertainty ranges.

Four typical and suitable methods for the stability investigation of the electrical network were investigated and adapted to the problem formulation. The μ-Analysis was shown to be suitable in

the characterization of the robustness level and identification of the critical parameters. It is very reliable for a broader range of operating points, due to the symbolic linearization. The good finding of tolerable uncertainty ranges makes it a good candidate for definition of uncertain loads. On the other hand, the model preparation and computation of μ is far more complex than, for example the Modal Analysis. In practical applications, the method is limited to problems with approximately 10 parameters or less. The method relies on detailed knowledge of the system, which has to be modelled by a linear parameter varying representation.

The assessment of the critical parameters by impedance-based methods, can be performed via easy-to-apply model modifications and standard tools for impedance calculation. In the determination of the critical parameter combination or the allowed range, the impedance-criterion is not very useful. The system engineer has to be well aware of the interpretation of the Bode and Nyquist plot. The standard way to assess the stability bound is a time-consuming parameter variation. The impedance criterion has to be repeatedly evaluated for all components of a network, with special considerations for parallel circuits. The impedance-criterion cannot give a quantitative analysis for the critical level of uncertain parameters. The method relies on state-space averaged models, but can include impedance measurements from real hardware tests.

The Modal Analysis is very suitable in design, since the method assists an engineer by indication of parametric dependencies to certain eigenvalues. For example, the designer can see the dependencies of eigenvalue damping and resistances. Also, the method is very convenient to use, since automated tools can assist the designer. But it is not reliable to look quantitatively for the most critical parameter combinations with respect to system stability. The method relies on state-space averaged models.

In contrast to this, the optimization based approach for stability analysis of electrical networks can include any stability criteria, and assess the most critical parameter combination. A norm on the parameter deviation to the nominal values has to be chosen (L^1, L^2, L^∞), which can be used for definition of the maximum tolerable design and uncertainty range. The method is applicable for linear, non-linear and also for non-linear switching models without the necessity of any averaging technique and linearization. The approach seems to be a good solution for the stability analysis with industrial specified standards since for a well-conditioned setup the worst case condition is found without additional uncertainties induced by the analysis method. Furthermore the maximum design range can be estimated. The method strongly relies on suitable optimization algorithms which are capable to solve the mixed optimization problem of minimization with constraints. The PSO algorithm was very robust and efficient in this case, even compared to genetic algorithms. For practical application, the main demand is to deal with long computation times and be able to initialize complex models without a time consuming simulation start-up. Those issues are addressed in other chapters of this thesis.

Lastly, it should be mentioned, the critical parameter conditions found by the methods do vary to some extent; even if the models were the same. The direct comparison of the critical parameter variations in μ-sensitivity analysis in Figure 6.11, impedance analysis in Figure 6.13 and anti-optimization in Figure 6.16 show some similarities: All do identify the critical parameters R_f, L_f and C_f. But the order is slightly different, as are the amplitudes. The meaning of the statements of the methods is slightly different: Impedance methods give more qualitative results. μ-Analysis investigates stability of a pre-defined uncertainty range, while μ-sensitivity indicates the sensitivity to the change of the single parameters. Anti-optimization shows the worst-case parameter combination; the distance of the parameters is weighted by a norm. No other parameter variation within this "distance" value should lead to instability.

Table 11 gives an overview of the investigated methods. They are rated with respect to effort, expressiveness and capability to handle design and uncertainty ranges.

It was demonstrated, that impedance-based methods and Modal Analysis are beneficial due to their simplicity and can give the designer some information on the stability and influencing parameters. It is not possible to define maximum design ranges by them. In contrast to it, µ-Analysis is a substantial more complex method. Design ranges can be defined which ensure necessary stability. The method is restricted to LTI parameter varying systems. Transient limits can be mapped to time constants of eigenvalues; but they are not representative in terms of industry-defined stability definitions or non-linear characteristics. The anti-optimization method is the most flexible. Any type of constraint and analysis can be embedded. This comes at cost of heavy computational effort, where the optimization algorithm must be capable to cover the full range of parameter combinations. Nevertheless, the flexibility and scalability makes it the recommended candidate for definition of maximum design ranges or parameter uncertainties.

	Impedance	Modal Analysis	µ-Analysis	Anti-optimization
Abstractness of model building and implementation	low	low	high	low
Computational effort	low	low	medium	high
Conservatism	high	high	medium	low
Validity	LTI	LTI	LTI, with uncertainties	only restricted by optimization alg.
Treats design or uncertainty range	qualitative	no, just gridding possible	yes, influence to design range	yes, quantitative limits

Table 11: Rating of tested methods

6.5 Contributions

In this chapter, four methods for stability assessment of electrical systems are investigated. The focus was on investigation of stability and definition of design and uncertainty ranges, for the distributed design of aircraft electrical networks. Modal Analysis and impedance-based methods are generally accepted methods used in network design. The theory is shown and the state-of-the-art is extended by considerations on the definition of design and uncertainty ranges for the impedance-based method.

Alternatively, an approach based on the µ-Analysis is presented. This method was able to define the critical components in an electrical network and define design and uncertainty ranges. While µ-Analysis has been known for years, this thesis contributes by

- *the first systematic comparison of methods for definition of electrical networks design ranges. The feasibility of µ-Analysis for electrical system design is demonstrated.*

The fourth method, an anti-optimization based approach, based on determination of worst case parameter combination is derived. This is the only method, which can test on industrial standards of output signals directly.

- *The work lists typical stability criteria for the electrical network and develops the equivalent constraints as part of a multi criteria optimization.*

Anti-optimization is demonstrated to be the most flexible and capable of the compared methods. All approaches were demonstrated using the same small electrical network example, which is representative for the load/generation interaction.

The relevant results were published together with Mr. Yang Ji. His PhD-thesis (Ji, 2016) focuses on the use of the models of the large scale test in a model-based V&V process. His implementation in the thesis is focused on the airframer perspective while this thesis is more oriented to the perspective of the generator supplier.

Relevant publications:

"Stability Studies of Critical DC Power System Component for More Electric Aircraft using µ-sensitivity" (Kuhn et al., 2007)

"An Approach for Stability Analysis of Nonlinear Electrical Network using Anti-optimization" (Kuhn et al., 2008)

7 Framework for model based system studies

7.1 The Modelica benchmark and state of the art

The aircraft electrical network validation and verification process strongly relies on software for modeling, simulation and analysis of network components and systems. Substantial efforts are made to reach platform independence and link simulation tools each with special strengths and dedicated for specific domains. Especially the FMI standard[25] was a major step forward and was verified to improve an aircraft systems design process. Nevertheless, for the sake of performance and transparency, industrial processes often rely on a single common tool. The software used in an aircraft project for the systems integration validation and verification (V&V) process is defined by the airframer for all model suppliers and contributors.

The software "Dymola" has demonstrated its maturity with all major automotive OEMs, some smaller aircraft manufacturers and for environmental control systems and special electrical systems at some larger aircraft manufacturers. Comparable software products for simulation of electrical systems include Easy5 (MSC Software Corporation, 2017) (originally developed by Boeing), Simplorer (ANSYS, Inc., 2017), FastSim (PC Krause and Associates, 2017), Simscape (The MathWorks, Inc., 2017) and Saber (Synopsys Inc., 2017).

In order to evaluate the potential and performance of Dymola and Modelica in relation to the proven solutions, a study was undertaken in the framework of the project Cleansky JTI WP2.1. The main focus and main highlight was the simulative verification of a large scale electrical network of an aircraft. For an industrial process, the capability of the modeling and simulation environment itself is only one of the relevant aspects. The study considered the aspects:

- **Modeling of the system**, by the modeling language (here: Modelica).
- **Numerical efficiency of the simulation**, through dedicated solver.
- **Post processing of data**, through advanced analysis tools.
- **Display and record data**.
- Business aspects.

The highlighted items will be explained below. The Thales starter-generator model and measurement data are among the core elements of the V&V study. A combination of traditional generator design tools, and testing of the design by network studies, can extend the scope of the design extensively. This demands the availability of reliable models and test environments. In the study, a dedicated library was developed, for the simulation of the onboard electrical network of an aircraft. The following chapter gives an overview of the virtual testing process of the electric power network of MEA. It shows the necessities of the infrastructure which had to be developed and the required modeling level of the components. Necessary tools are addressed and lessons learned from the study are documented[26].

7.2 Modeling requirements of aircraft power systems

A key-factor for the success of developing the MEA is to incorporate high quality system models in the complete aircraft design process (Bals et al., 2009), which briefly can be divided into 4 major phases: concept phase, system specification phase, system development/validation phase and system verification phase (Giese et al., 2010).

---

[25]http://fmi-standard.org/

[26]This chapter shows the main concepts and challenges of the V&V study. Further details of the models, tests and scripts were subject to confidentiality agreements.

Today, the aircraft industry utilizes a multi-level approach for the design of the aircraft system, see chapter 2.1 or (AE-7M, 2016). For the V&V study only functional and behavioral models have been considered. The modeling of functional models followed the industrial definition where AC networks are represented by an equivalent one-phase DC network rather than in the equivalent qd0 system (see chapter 2.1).

7.3 Modeling of MEA power systems
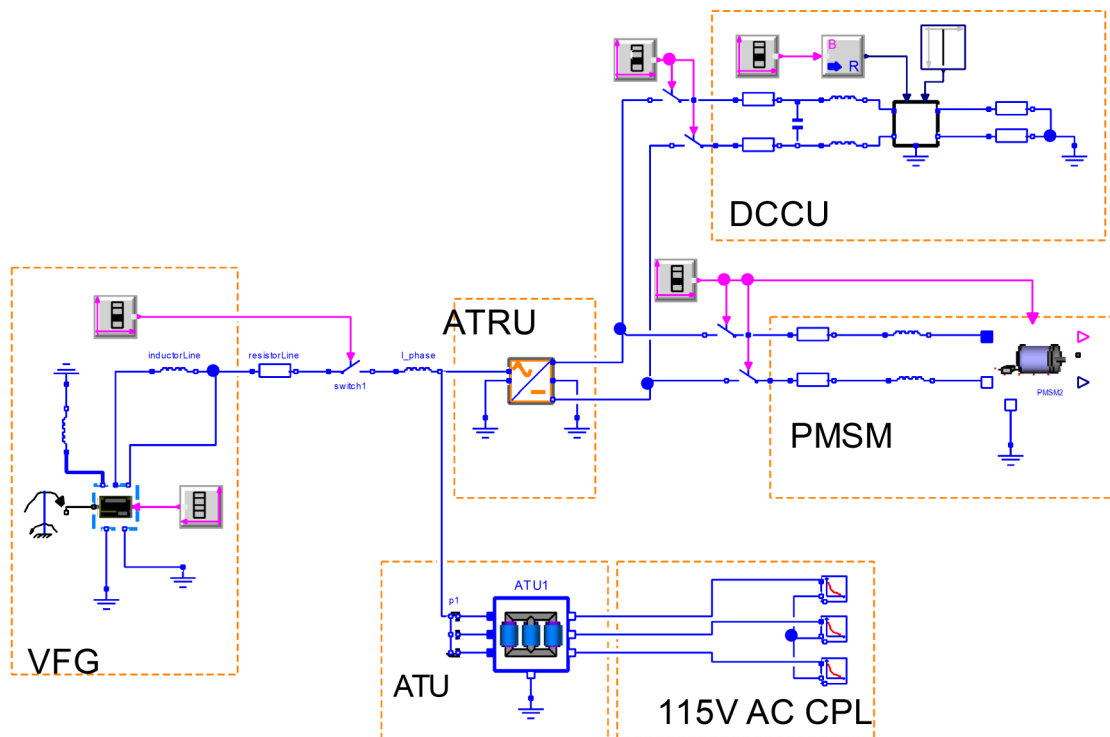
Figure 7.1: An integrated electrical power network for MEA

High quality modeling of the components and the integrated power network, is a precondition for the virtual testing process in the aircraft system verification phase. An electric power network in the MEA typically covers several physical domains such as electrical systems, magnetic systems, mechanical systems and control. Therefore, a modeling language to be selected for virtual testing process, has to be capable for modeling multi-domain systems. Furthermore, powerful solvers which can deal well with complex dynamic systems, including switching actions, are needed. An electric power network is often a very complex large scale system. For instance, the proposed aircraft power network in Figure 7.1 contains a Variable Frequency Generator (VFG), a high power 18-pulses Auto-Transformer Rectifier Unit (ATRU), a 3 phase Auto-Transformer Unit (ATU), a DC/DC Power Converter Unit (DCCU), a Permanent Magnet Synchronous Machine (PMSM) and a 115V AC Constant Power Load (CPL). In total, it has more than 100 dynamic state variables.

The behavioral model of the **generator** can be found in chapter 2.3.1. The functional model of the study uses a 3 phase RMS equivalent rather than "qd" representation.

The topological model of a 6/18-pulse bridge **Rectifier Unit** (RU) can be implemented very easily using the diode model of the Modelica standard library. Detailed parameters in diodes, such as forward state-on resistance and forward threshold voltage, can be tuned to match the real performance of physical components (see also chapter 2.3.2). For large systems, the diode based represen-
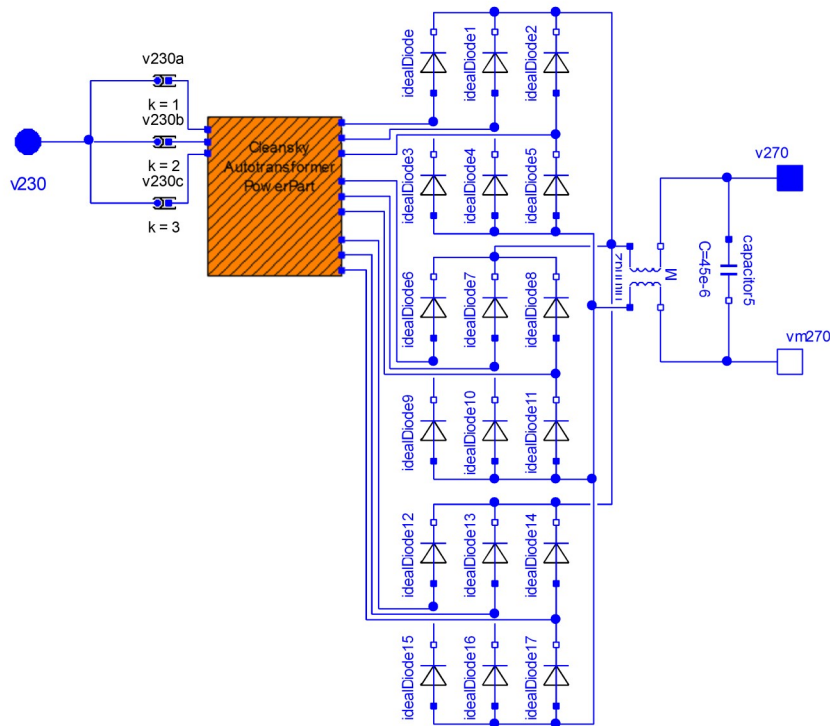
Figure 7.2: Scheme diagram of an 18 pulses auto-transformer rectifier unit

tation was partly replaced by the time-domain formulation of the advanced rectifier with ideal switching which was proposed in chapter 4.4.5.

For higher power, the **18-pulse auto-transformer rectifier unit** has advantages over a 6-pulse rectifier unit in terms of power quality. These power transformers are essential components in future aircraft but they are susceptible to transient inrush currents, which are several times of the rated value. Therefore, inrush current tests are becoming an indispensable task in the validation/verification phase of the More Electric Aircraft design process.

The ATRU model is displayed in Figure 7.2. The magnetic core of the auto-transformer is built with the Modelica magnetic library (Ziske and Bödrich, 2012), that allows to model electro-magnetic components with magnetic hysteresis effects leading to inrush currents. The functional model of the ATRU ignores the diodes switching but considers the inrush current effect. A physical modeling approach to describe the inrush current characteristics of power transformers has been proposed in (Ji and Kuhn, 2013).

The 3-phase **auto-transformer unit** with 230V AC input voltage and 115V AC output voltage is also modeled by the Modelica magnetic library. The geometry parameters of the magnetic circuit, such as area and length of magnet core as well as the characteristics of magnetic hysteresis loop, e.g. coercive field and permanent-magnetic field, can be conveniently set by users.

The full bridge isolated **DC/DC buck converter** unit contains a full bridge inverter, magnetic transformer, input filter and control of the phase-shift. The DCCU typically supplies 28V DC low voltage loads in the electric power network. The scheme of the modeled DC/DC buck converter is depicted in Figure 7.3. Modeling and simulation of DC/DC converter units is very challenging, since the pulse-width-modulation of this component inherently works with a very high frequency in the order of kilohertz. This high frequency switching operation could lead to a great amount of time- and state-events which will significantly slow down or harm the simulation process. The synchronous feature of Modelica (Otter et al., 2012) can improve issues with the time events. State-
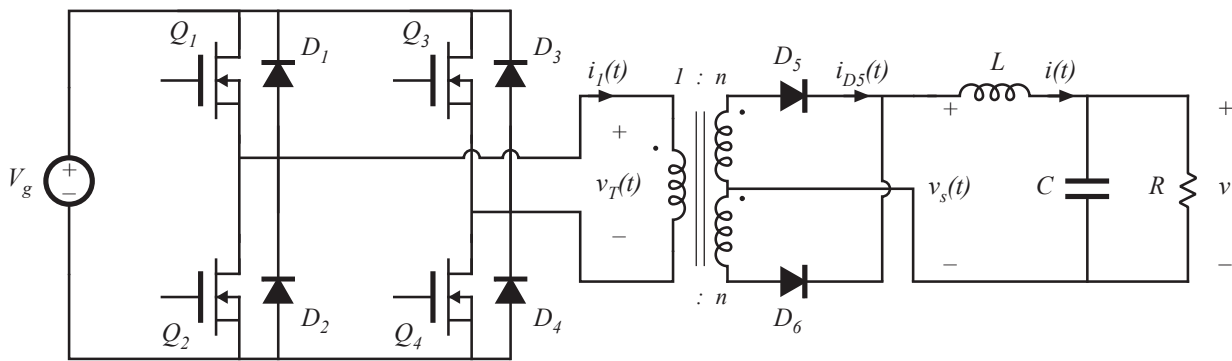
Figure 7.3: Scheme diagram of a DC/DC converter unit

events should be transferred to time-events, where possible. For the implementation of the functional model of the DC/DC buck converter, a classical averaging technique has been utilized.

Permanent-magnet synchronous motors are essential components for replacement of classical non-electric architectures. They are used for a wide range of applications, from fuel pumps to secondary flight controls (Cao et al., 2012). The newly developed PMSM models address all important components of an electro-mechanical actuator unit. This includes the machine itself, the input filter, the power inverter with dead-time, protections for over/under voltage, the pre-charger, the motor control unit and mechanical friction in the bearing system. The functional PMSM models were derived by replacing the power inverters by continuous transfer functions and replacing the 3-phase values by RMS values.

An integrated model of the electric power network, including the behavioral models of a VFG, an ATRU, an ATU, a DCCU, a PMSM and a 115V AC constant power load (CPL), are shown in Figure 7.1.

7.4 Virtual testing

By a virtual integration platform of the energy system, integration issues can be found prior to the physical integration on the test rigs and the test coverage can be extended. Today, virtual testing of the integrated aircraft energy system is becoming an indispensable task in the system verification design phase.

7.4.1 Process of virtual testing

The process of virtual testing can be briefly divided into two steps. Before the simulation and test of the integrated system model, each subsystem or component model shall be firstly evaluated by so-called component standalone test. A standalone test usually consists of a set of tests such as

- Power connection,
- Power disconnection,
- Power consumption at steady state,
- Current harmonic analysis,

etc. for one component. Standalone tests are required for both functional and behavioral models. As soon as the standalone tests for all components and subsystems are successfully finished, the simulations of integrated system model can be done. Finally, specific analysis and post-treatment tasks can be performed, based on the simulation results of the integrated models.

7.4.2 Requirements of virtual testing for More Electric Aircraft

For virtual testing, special requirements in terms of methods and tools have to be fulfilled. First of all, component and system models shall be built at both, functional and behavioral, levels. Furthermore, to simulate complete aircraft electrical power systems- which tend to have stiff dynamics and are suffering from huge amount of event handling actions, due to switching components- the performance and robustness of the solver(s) has to be ensured. For the various analysis tasks, such as harmonic analysis in frequency domain and stability analysis in time domain, tools for analysis and post-processing (Ji and Bals, 2010) are required. Finally, it has to be possible to customize different test scenarios by scripting tools.

7.4.3 Standalone tests for electric components
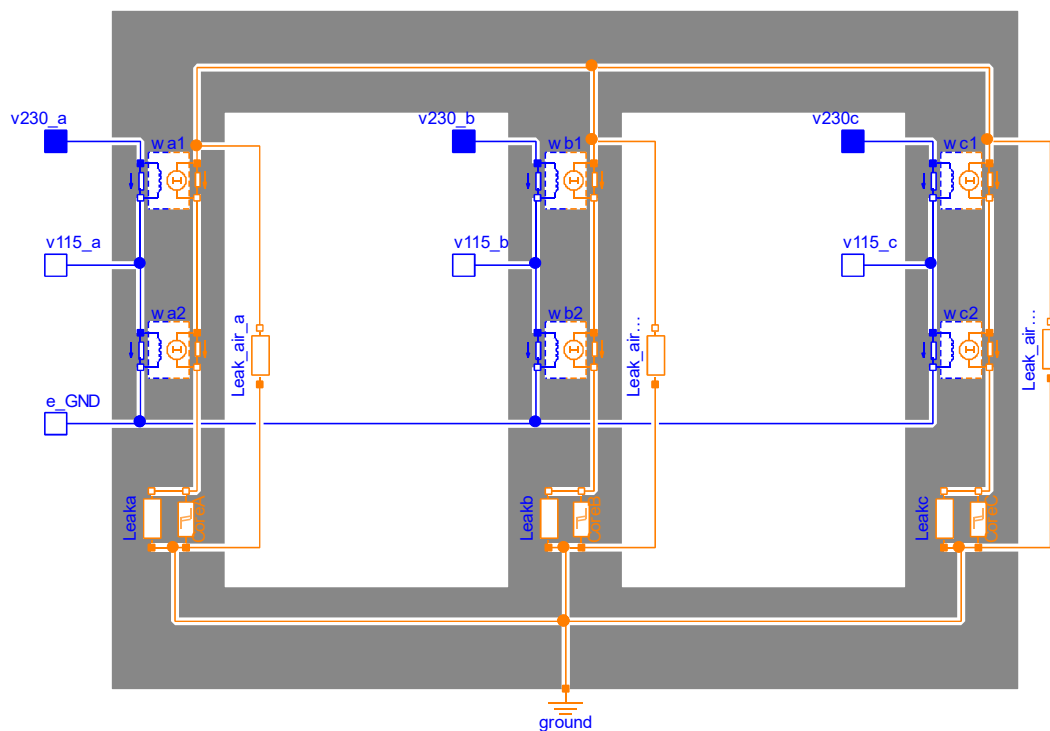
Figure 7.4: Modelica model of AC/AC auto-transformer

The standalone tests for components are demonstrated by the 230VAC/115VAC auto-transformer model which is depicted in Figure 7.4. The tests which are considered, are harmonic current test, inrush current test, power connection and power disconnection test.

The harmonic current analysis checks the harmonic distortion, which is injected to the source by the equipment, at several base frequencies of the power supply. The distortion is checked by FFT, once the simulation of the ATU model reaches (periodic) steady state.

The results of the harmonic current analysis, with a source voltage of 230V and frequency of 720Hz, is depicted in Figure 7.5.
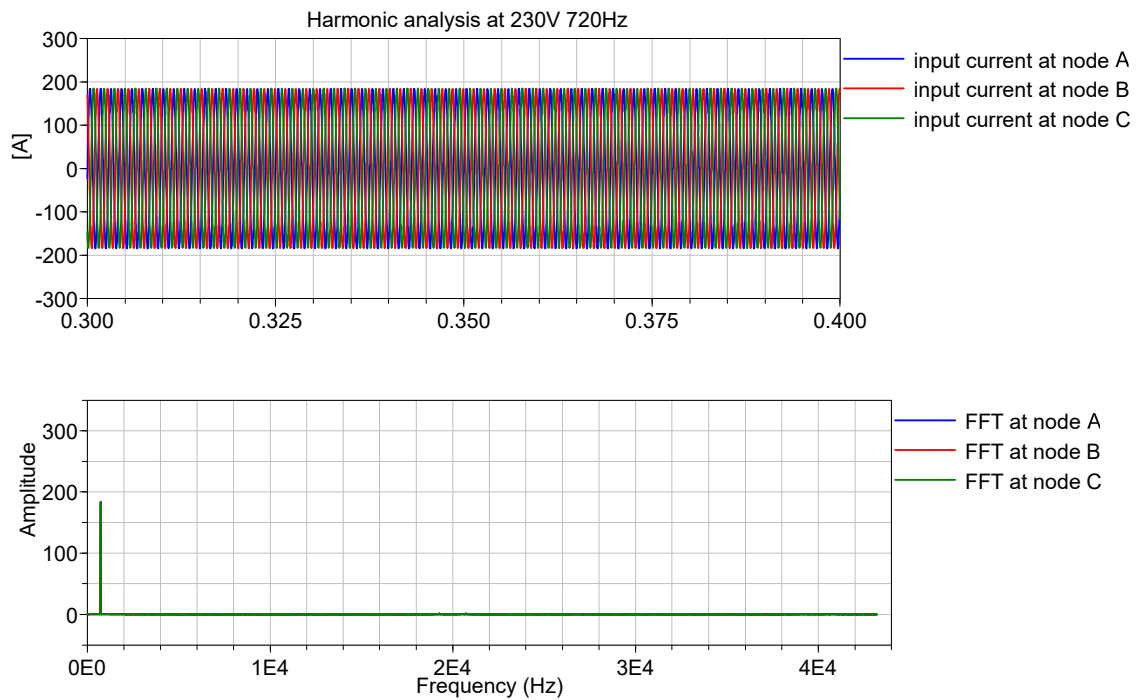
Figure 7.5: Current harmonic analysis of ATU at 230V and 720Hz input voltage; upper chart: transient simulation, lower chart: spectrum
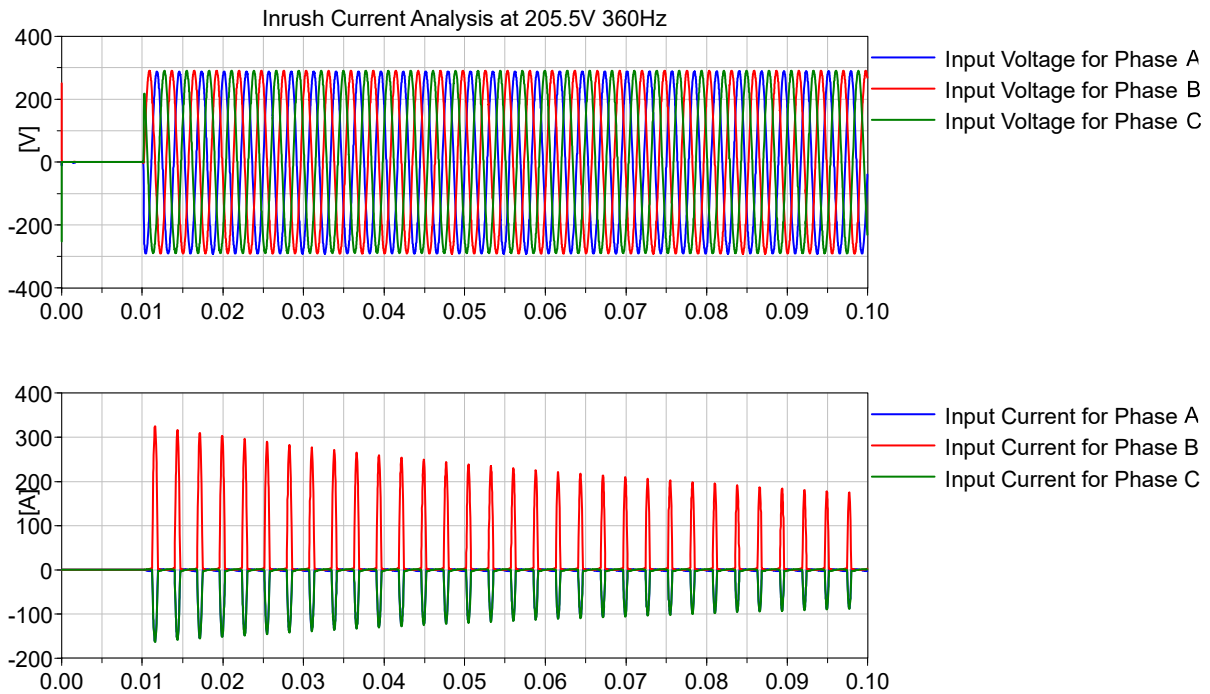
Figure 7.6: Inrush current analysis at 205V and 360Hz input voltage; upper chart: voltages, lower chart: currents

The inrush current test studies, if the ATU may cause inadvertent trip at power up. The result is presented in Figure 7.6.

Electrical power consumers may initially draw large currents from the network after connection. For larger loads, this current has to be limited by pre-chargers or other appropriate measures. The
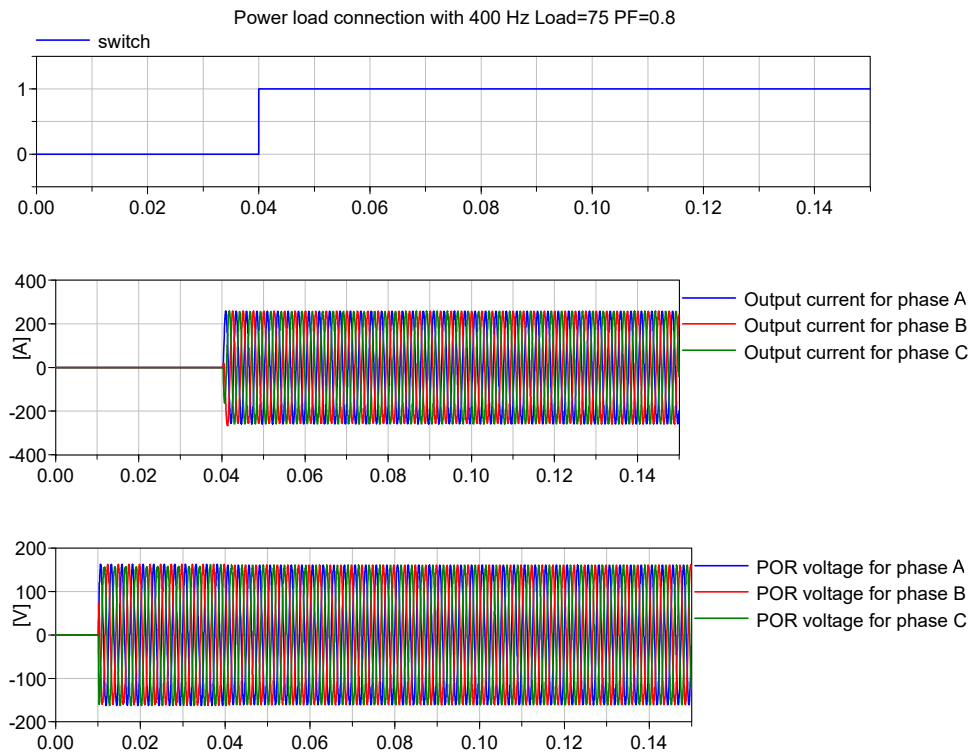
Figure 7.7: Power load connection test of ATU with 75% load and 0.8 power factor; upper graph: connection profile, middle graph: currents drawn by load, lower graph: source voltages
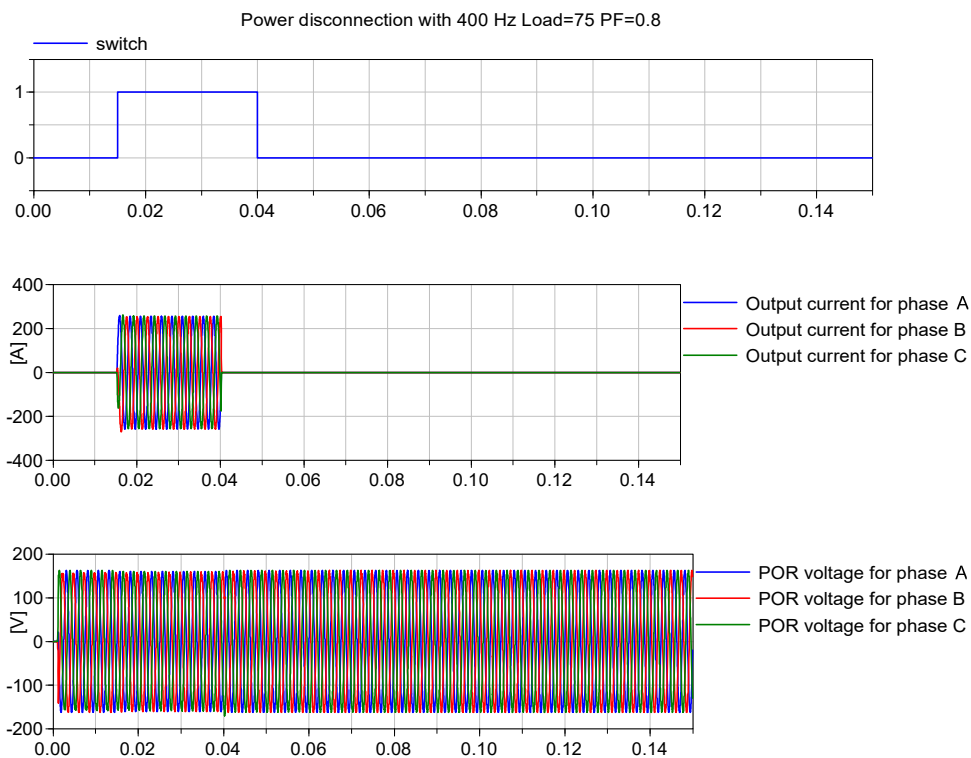
Figure 7.8: Power disconnection test of ATU with 75% load and 0.8 power factor; upper graph: connection profile, middle graph: currents drawn by load, lower graph: source voltages

165

power load connection and disconnection tests validate the behavior. Test results of load connection are depicted in Figure 7.7.

Figure 7.8 shows the compliance test at load disconnection.
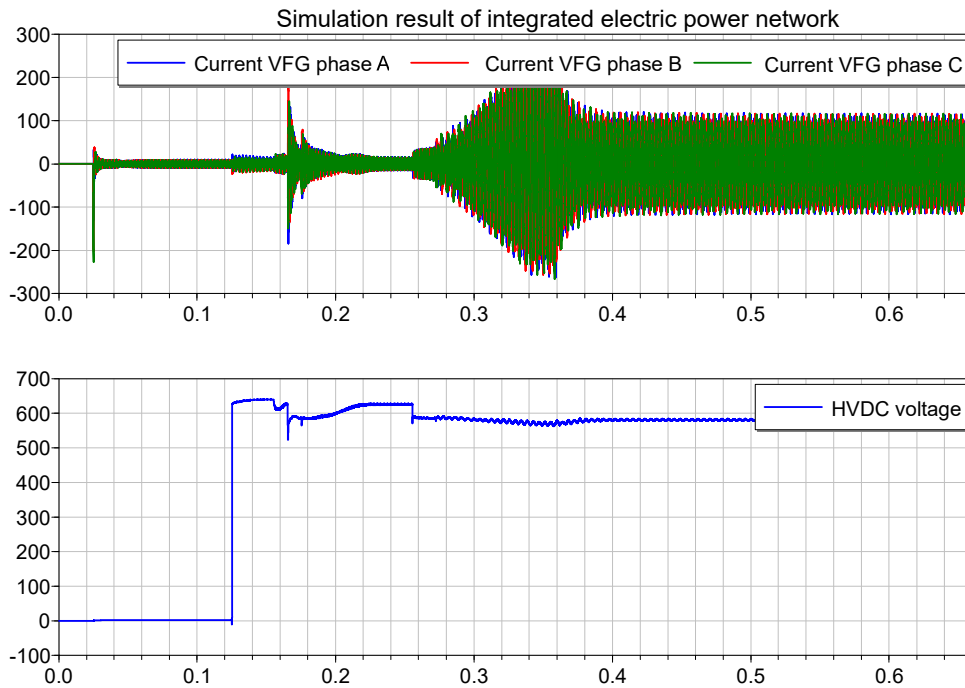
Figure 7.9: Simulation result of the integrated electric power network: VFG current and HVDC voltage (behavioral level)
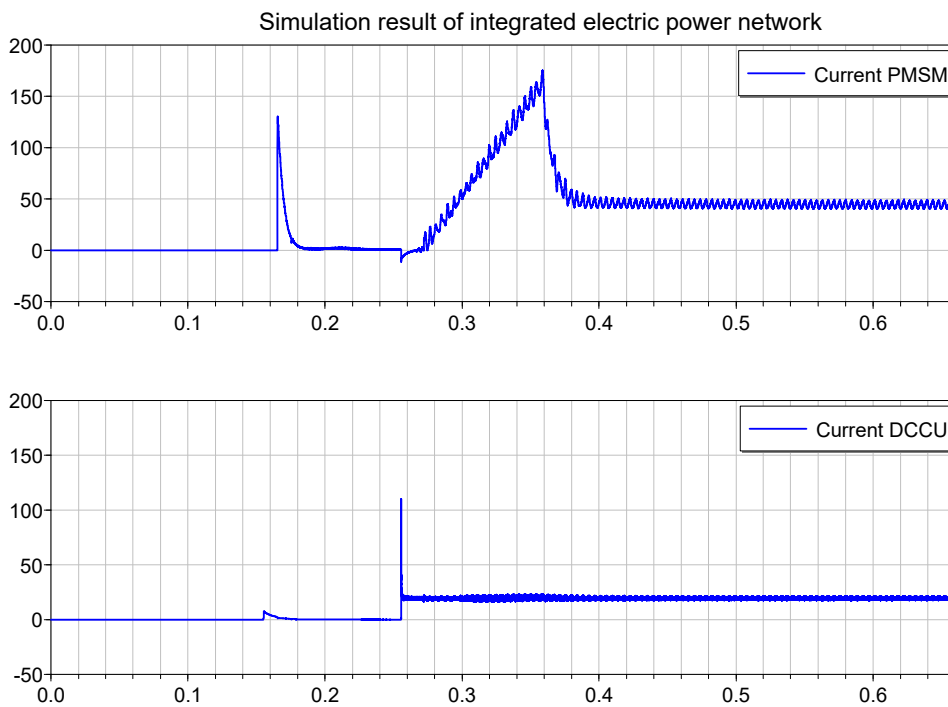
Figure 7.10: Simulation result of the integrated electric power network: current of PMSM and DCCU (behavioral level)

7.4.4 Testing of the integrated aircraft power system

As soon as all components have passed the stand-alone tests successfully, various scenarios for testing of the integrated electric power network can be started. The capability of Modelica/Dymola, to deal with large scale power systems, is demonstrated by simulation of the electric power network depicted in Figure 7.1. The system is simulated at both behavioral and functional levels. In this electric power network, the ATRU is connected to the grid at 0.0025 seconds. After pre-charging the ATRU for 25 milliseconds, the DC output of the ATRU is connected to the HVDC network. The PMSM has a built-in pre-charging time of 20 milliseconds. It is connected to the HVDC network at 0.055 seconds. After the power inverter in the PMSM is activated, the PMSM receives a constant speed command. The mechanical shaft is retarded by a constant load independent of speed. Figures 7.9 and 7.10 show the process of the speed ramp-up of the PMSM, at behavioral level. The plotted variables are: the AC currents of the VFG, the DC voltage in the output of the ATRU, the input currents of the PMSM, and the currents drawn by the DCCU.

The results of the same test, at functional level, are depicted in Figure 7.11 and Figure 7.12. One can clearly see the inrush currents and the DC ripple in the ATRU output, when the ATRU is switched on. These values are important indicators in a stability test of the electric power network of a MEA.

More tests and models can be found in (Ji, 2016). An extended study of physical modeling and simulation of inrush current in the power transformer was subject of the publication (Ji and Kuhn, 2013a).

7.5 Summary

The research proposed a Modelica-based solution for the virtual testing process of large scale power systems in MEA. Typical components of the power network are electrical generators, power con-
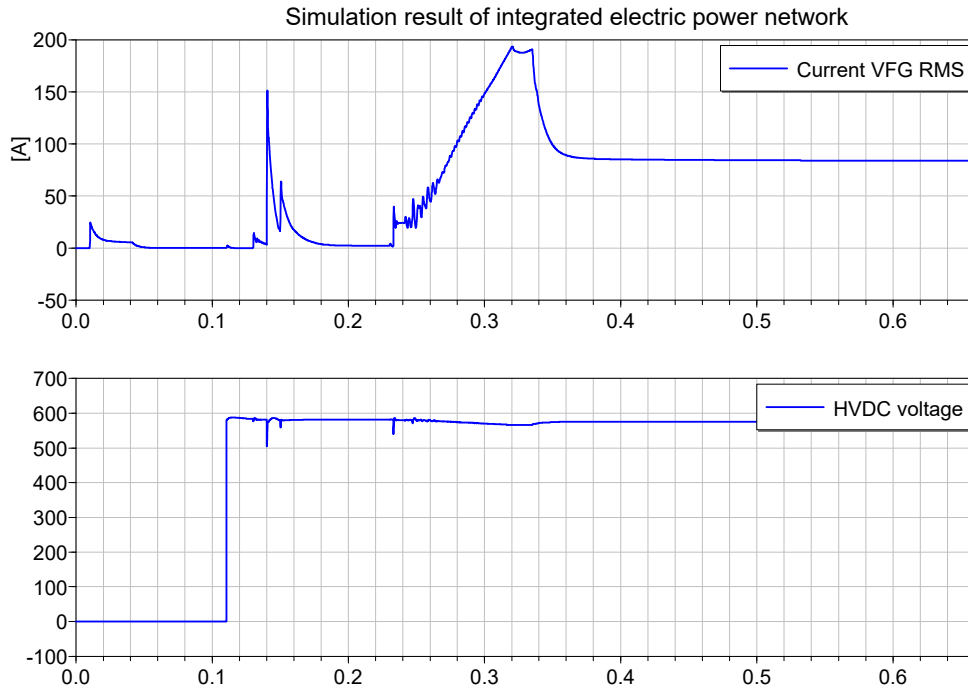
Figure 7.11: Simulation result of integrated electric power network: VFG current and HVDC voltage (functional level)
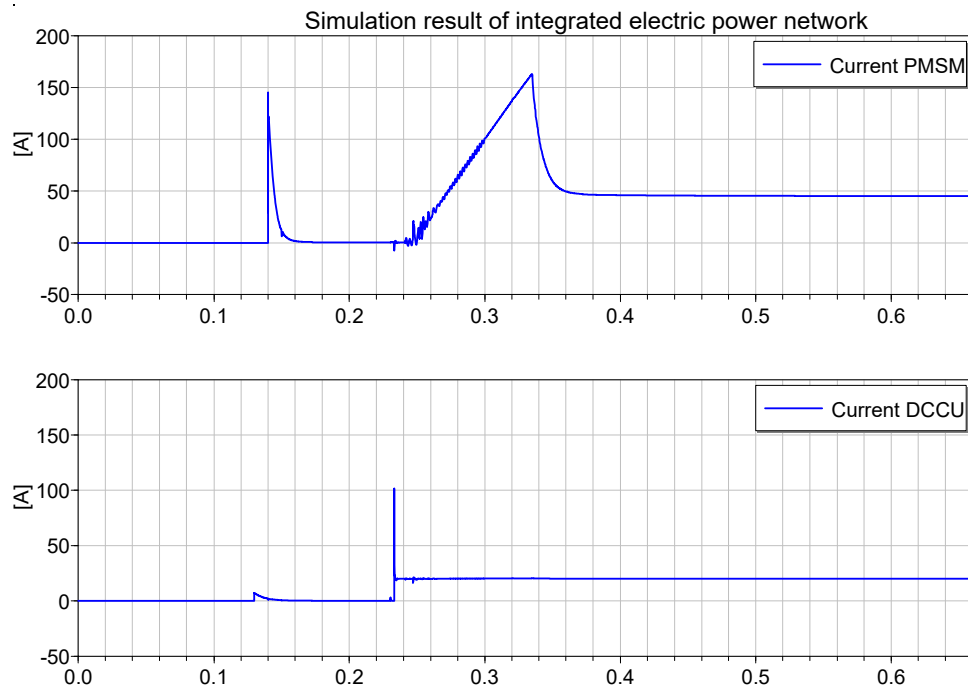
Figure 7.12: Simulation result of integrated electric power network: VFG current and HVDC voltage (functional level)

verts (AC/DC, DC/DC, AC/AC) and various electric power loads such as permanent-magnet syn-

chronous machine and constant power loads. All components have been considered at both, functional and behavioral level to fulfill all modeling requirements of diverse design tasks. The successful implementation and demonstration of the component stand-alone tests, as well as the tests of an integrated aircraft power network, prove the suitability of the library in particular and Modelica in general for testing and analysis of complex energy systems in the future MEA. With additional powerful post-processing and scripting features provided by the Modelica platform Dymola, a successful virtual testing process is possible. It was shown, that some of the integrated tests involve several of the components. For example for the ATU inrush test, the generator and transformer are both affected. The library and procedures can support the component manufacturers in their design studies prior to system integration, based on generic models.

The appendix, chapter A2, gives an overview of the models and library structure. Also the lessons learned from building and simulation of large scale electrical systems are documented.

7.6 Contributions

In this chapter, the modeling, simulation and testing of the electric power network of MEA is addressed. The implementation exceeds by far the scale of former published Modelica based network simulations.

Contributions of the author includes the modeling of all major components of the library and robust setup of the large test cases. Especially the formulation of the modeling equations of the components was of importance. They are modeled such that they can be transformed into low order differential-algebraic equation systems. This includes the generator and rectifier models. Furthermore, the proposal on the choice of interface-variables of the magnetic system and the implementation of the circuit transformer's magnet equation was essential for the implementation of the large scale tests.

The V&V study was implemented and published together with Mr. Yang Ji. His PhD-thesis (Ji, 2016) focuses on the use of the models of the large scale test in a model-based V&V process.

The chapter quoted from the relevant publications:
(Ji and Kuhn, 2013a) "Physical modeling and simulation of inrush current in power transformers of more electric aircraft"
(Ji and Kuhn, 2013b) "Modeling and Simulation of large scale Power Systems in More Electric Aircraft"
(Kuhn and Ji, 2014a) "Next generation design framework for the aircraft electric power"
(Ji and Kuhn, 2014) "Model Based System Level Studies of More Electric Aircraft"
(Kuhn and Ji, 2014b) "Modelica for large scale aircraft electrical network V&V"

8 Summary

This thesis contributes to the field of model-based methods for design and analysis of the electrical network systems of modern aircraft, with focus from the perspective of the manufacturer of the generators. Model-based methods are used for the optimization of a generator design, taking into consideration the power quality, network stability, and network interactions. Various model-based methods and tools have been developed and adapted, which support the design of the electrical components and systems. The methods expand the recent scope of the component design, to the effect that interactions of the integrated network can be already investigated in earlier design phases.

8.1 Contributions in modeling

Models may occur in different layers of abstraction for different kinds of studies. This work gives an overview of the choice and implementation of models, as well as the simulation infrastructure, partially in multi-levels. For the detailed behavioral simulation, contributions include a numerical-efficient generator model, an improved 6-pulse rectifier stage and a library of components for large-scale electrical systems simulation of the electric power network of a more electric aircraft. For the abstracted functional-layer, contributions include the implementation of a 6-pulse rectifier model and an infrastructure for modeling in qd0(Park)-transformed system. For the simulation in an abstracted layer with harmonic content - the harmonic functional-models - contributions include the implementation of a novel infrastructure for the parallel-simulation of behavioral and harmonic functional models. By using a combination of adapted behavioral-models and the harmonic functional-models, a method for direct initialization in periodic steady-state has been invented.

8.2 Contributions in simulation-assisted generator optimization

Starting with a given design routine for an externally-excited synchronous-generator, the work demonstrates how the design can be improved using multi-objective optimization. The conventional design criteria include analytical constraints on electrical, mechanical and thermal properties. Around 10% savings in weight are possible compared to the original design. The optimization is extended by measures of the power quality, which evaluate the performance of the generator when feeding a partial-rectified AC load. A straight approach using simulation of the system and extraction of the criteria, is too slow for practical implementation. Instead, good results are possible via a novel two-stage setup, first optimizing the negative-sequence inductance of the generator, and quantification of the measure for power quality by simulation in a downstream process. The optimization for Pareto-optimal solutions enables the determination of relationships between power quality, generator weight and the aspect ratio of non-linear loads.

The simulation is a time-critical part of the optimization process. This thesis provides three significant improvements that also can be applied in combination:

1) The system is modeled by numerical-efficient models and the network model is analyzed for possible simplifications. A generator model without voltage control but constant excitation, which is calculated by a functional model, showed better performance without loss of accuracy.

The analysis of the power quality is enabled by a new block which can be added to the model; internally it relies on the Fast Fourier Transformation. The interactions of data acquisition and the computation of FFT are analyzed, and a numerical-efficient solution is proposed. The parametrization of the new block is more intuitive than recent implementations.

2) By definition, spectral criteria, such as total harmonic distortion, are identified at steady-state condition; this may occur after a long ramp-up phase to the operating point. A functional harmonic

model was implemented, which can consider detailed behavior up to switching characteristics. While the model is an approximation, initialization of the detailed model, using the variables of the approximated model, results in considerably better starting conditions, closer to the long-term periodic steady-state condition. Theoretical and practical aspects of automated initialization of this model are addressed, with special emphasis on a novel rectifier model in time and frequency domain.

3) It is not expected to find a solution closer to the long-term periodic steady-state condition analytically, due to the non-linearity of the system. The system's simulation converges to harmonic steady-state from the start condition, due to internal stability assumptions. The initially needed ramp-up time can only be found by testing the periodic steady-state condition. This thesis shows two new FFT-based steady-state detectors and compares them with two approaches from literature, the stochastic-based F-like test detector and a wavelet based detector. The new "THD-like" monitor is proposed as the best choice for the application. It can monitor the periodic signal without preconditioning, with medium computational overhead, and in relation to the theoretical minimum time, with little delay. Detailed instructions are given for the data processing and the parametrization of the underlying FFT algorithm.

8.3 Contributions in network stability and analysis of network interactions

Also, the generator parametrization has a direct influence on the impedance of the power source apparent to the local DC circuits; it also has an indirect influence, as local filters are designed for the power quality in the AC distribution network, which is affected by the generator's impedance. Therefore, the generator design process has an impact on local stability. Stability issues in the network can be considered using established methods for small-signal stability, e. g. Middlebrook criterion and Modal Analysis. This thesis compares them to an approach using elements from robust control, namely the structured singular value μ, the skewed-structured singular value ν, and μ sensitivity. The latter two methods give a much more global and direct result, for the influence of all components on stability. For cases where large signal stability needs to be ensured, an optimization-based approach is addressed. The stability problem is transferred to an optimization problem, for finding worst performance regarding stability criteria for a parameters range. In contrast to the afore mentioned methods, which are limited to small-signal stability with the necessity of averaging techniques and linearization, non-linear models may be used directly. The thesis proposes and examines model-based toolchains for all type of methods.

The last section is devoted to the analysis of network interactions, using detailed large-scale electrical network simulation. The virtual testing process in the aircraft system verification phase, demands high quality modeling of the components and of the integrated power network. But generic libraries and methods can be included in earlier phases of the system's development, to show design trade-offs.

The thesis proposes a Modelica-based solution for the virtual testing process of large-scale power systems in MEA. A dedicated library was developed for the simulation of the on-board electrical network. The thesis gives an overview of the virtual testing process of the electric power network of MEA. It shows the necessities of the infrastructure that had to be developed and the required modeling level of the components. Necessary tools are addressed and lessons learned from the study are documented. The scale and quality of models exceeds current implementations by far.

9 Future work

This thesis could show the potential of model and simulation-assisted design, with focus on network stability and quality. The relationships were analyzed qualitatively and quantitatively.

In the study of the large-scale electrical network simulation, the importance of mature and tested models, models of systems, and analysis scripts was found. Future model-based studies could benefit significantly from a reference library. For industrial applications, the automated testing of the design by requirements (Otter et al., 2015) from executable specifications (Kuhn et al., 2015) could introduce model-based knowledge earlier in the design, but requires more standardized libraries.

For the generator, the analysis of the power quality assumed the proper calculation of the machine's characteristic parameters, using the design function. However, the validity of the damper parametrization found by analytical functions, is often doubted in literature, for both real and virtual damper circuits. Especially for non salient-pole machines, the correct estimation is often subject to finite-element calculations or hardware tests. The estimation of the parameters could be improved, preferably by analytical or FEM-methods; some are mentioned in (Schlemmer, 2009). The same deficiencies of analytical functions apply for space harmonics from the winding scheme, estimation of the magnetic saturation for average current, and effects in the machine at high harmonic content. For the time-domain simulation, some improved Modelica models and analytic design tools were developed in project "Magmolib" (UPC, 2016). There is still need for more analytical design rules for proper parametrization of the "Magmolib" models.

Furthermore, the study only considered perturbations in the electrical system. However, it is known that the turbine and the shaft which move the generator, may not be seen as ideal stiff for high power generators anymore. This could drive development of advanced models with mechanical harmonics.

This thesis presents a new method for direct initialization in periodic steady-state condition, from harmonic functional models. The rectifier model assumed no commutation interval and no discontinuous current. Also, certain standards prescribe tests with asymmetric loads, which can not be considered with the recent implementation. In literature, some more general harmonic rectifiers can be found, for example (Sun et al., 2009). The replacement of the limited harmonic model by a generally valid model, or the dynamic selection of a suitable model, would allow for more proper initialization and robustness of the initialization approach.

Furthermore, the harmonic model only considers static, but complex, Fourier coefficients. (Ji, 2016) demonstrated the applicability of dynamic phasors, for modeling and analysis of the electrical network. A special type of representation, which is found by the "lifting" technique, uses magnitudes and phases rather than complex values. This is assumed to show better numerical performance. The work demonstrated the technique with examples. The approach could easily be combined with the object-oriented library concept for harmonic modeling of this thesis. A combined approach, using harmonic phasors for long-term simulation, and automatically initialized behavioral models for special short-time investigations, could combine the benefits of fast harmonic average models and the validity of behavioral models.

For periodic steady-state identification, a high interest and demand could be seen in the electrical community, but limited research activities. The novel THD-like test on periodic steady-state condition, showed good performance for the generator use case. Future studies should concentrate on more examples and further physical domains, and compare them with the alternative methods.

Lastly, this work showed some design improvements for the generator in terms of power quality and analysis of the integrated system. The integrated analysis of the source impedance and filters in the DC network, with combined criteria from network stability and power quality, exceeds the

scope of this thesis. Trade-off studies of the components and filters, could greatly improve the More Electric Aircraft network.

Appendix

A 1 Software used

A 1.1 MOPS

The software environment MOPS (Multi-Objective Parameter Synthesis)[27] was built to support the control engineer in setting up his design problem as a properly formulated multi-objective optimization task. To this end, MOPS offers a basic control system criteria library, a generic multi-model structure for multi-disciplinary problems and a generic multi-case structure for robust control law design, as well as visualization tools for monitoring the design progress. The user is provided with a clear application program interface and a graphical user interface both implemented in MATLAB. To solve the underlying optimization problem different powerful optimization procedures are available (Joos et al., 2002).

In MOPS, the parameters which are adapted by the optimization are called "tuners", to distinguish them from all other parameters appearing in a set-up, such as the ones describing model uncertainties. While the set of tuners remains always the same for an optimization run, different "Models" can be used, e.g. network wiring or level of detail. Identical models with different parametrization are treated as "cases".

MOPS has a built-in interface to construct optimization setups for and from Dymola models. MOPS utilises some MATLAB routines for translation of Dymola models, start of simulations and reading of results.

A 1.2 Modelica/Dymola

Modelica (ModelicaAssociation, 2017) is an object oriented multi-domain modeling language for component-oriented modeling of complex systems. In contrast to data flow-oriented languages with directed inputs and outputs, such as the widely known MATLAB and its associated Simulink tool, Modelica employs an equation based modeling, which results in a faster modeling process and a significantly increased reusability of the models. The language is developed under open source license since 1996 by the non-profit Modelica Association.

Many free Modelica libraries for different physical domains modeling are available. The Modelica standard library contains a large collection of components to model among others analogue and digital electronics, electrical machines, 1-dim. translational and rotational mechanical systems, as well as input/output control blocks. Modelica has also been used for simulation of electric power systems and power electronics components (Larsson, 2004), (Elmqvist et al., 1994). Free and commercial simulation environments acting as Modelica front-end are available with useful functionalities to graphically construct and simulate Modelica models and perform post-processing operations.

Modelica itself is similar to other modeling languages for physical systems in that as no causality has to be defined by the equations. For example it does not matter whether Ohm's law is written as $R = v/i$ or $v = R \cdot i$. In contrast to other numerical only implementations as Saber (Synopsys Inc., 2017) or Easy5 (MSC, 2017), all native Modelica code based simulation environments are able to perform some symbolic manipulation to the Modelica code based equation system. The symbolic manipulation can detect the causalities and can reorder the equations. In many cases the Differential Algebraic Equations can be reduced to lower-order explicit ordinary differential equations. Sym-

---

[27]Software developed by DLR, institute of System Dynamics and Control

bolic processing of the equation system is not a feature of Modelica itself but the simulators exploit its clear structure of the code.

The Modelica language based simulation program Dymola[28] has been selected for the building of a components library and simulation environment. Dymola provides the necessary functionality for graphical construction of Modelica models, handling of large libraries of components, efficient simulation and some post-processing operations. The transformed equations of Modelica code are provided as C-Code that is compiled and embedded in Dymola's own simulation engine, as stand-alone program or in other simulation environments (e.g. in Simulink or MATLAB). Parameter variations, initialization, pre- and post-processing of data can be automatically carried out. These operations can be performed directly in Dymola and can also be controlled via a MATLAB interface which is part of the distribution. Most of the calculations are carried out in analytical symbolic form, which simplifies the design, avoids a loss of precision, and decreases the computation burden which would result from iterative numerical procedure.

Dymola provides the necessary functionality for easy graphical construction of Modelica models, efficient simulation and some post-processing operations (Dassault Systèmes, 2017). The symbolic engine can handle algebraic loops and reduced degrees-of-freedom caused by constraints to some extent. This improves robustness and performance compared to a direct approach. These techniques and special numerical solvers enable real-time and Hardware-in-the-Loop Simulations (HIL). In a benchmark test of large scale electrical systems the good performance of Dymola could be demonstrated (Ji and Kuhn, 2013).
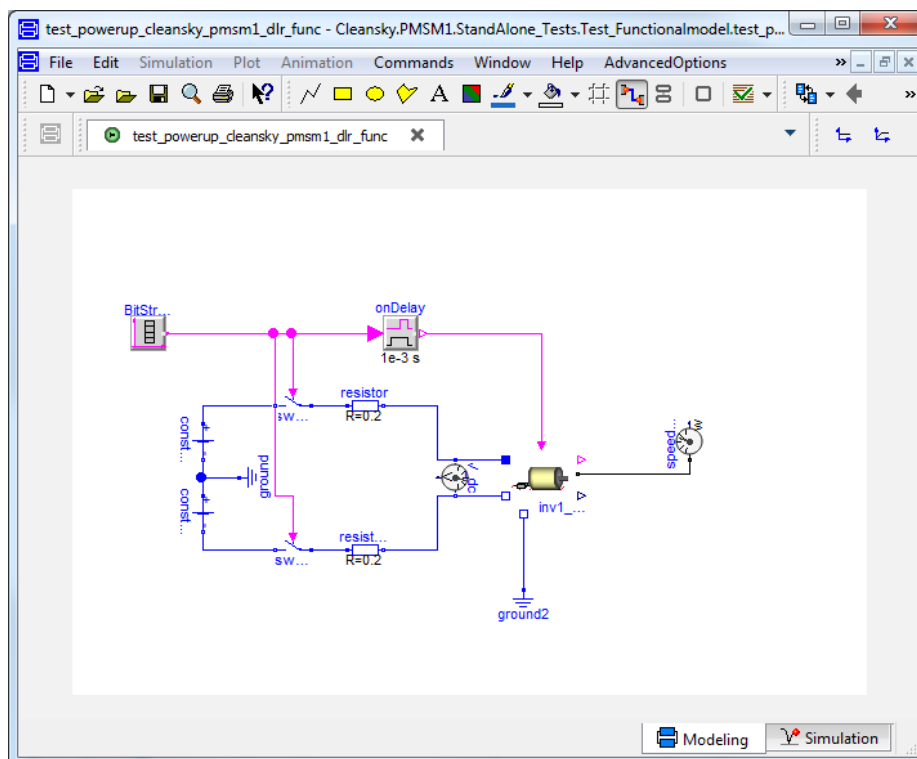
Figure A1: Example of a model of an electrical drive with Modelica/Dymola

Figure A1 shows an example of a Modelica model implemented in Dymola. The modeling can be performed intuitively in Dymola's Graphical User Environment (GUI). Models can be taken from the Modelica standard library, additional (commercial) libraries, and own libraries. All models rely on the underlying code. For example, the resistor is modeled by Ohm's law:

---

[28]"Dymola" by Dassault Systèmes, https://www.3ds.com/products-services/catia/products/dymola/

$$R = \frac{v}{i} \tag{226}$$

The Modelica code of the "resistor" model would look like this:

```
model resistor
  extends onePort;
  parameter Resistance R=1;
 equation
  v=R*i;
 end resistor;
```

and uses:

```
model onePort
  Voltage v;
  Current i;
  Pin p;
  Pin n;
 equation
  v=p.v-n.v;
  i=p.i;
  0=p.i+n.i;
 end resistor
connector Pin
  Voltage v;
  flow Current I;
 end Pin;
type Voltage = Real (unit="V");
type Current = Real(unit="A");
type Resistance = Real(unit="Ohm");
```

For clarity, the definition of the graphical layout of the circuit diagram is not shown.

The model "resistor" inherits (extends) all content of the sub-model "onePort". "onePort" declares the basic input/output relations of an electrical one-port model: There are two variables "v" and "i" of "type" Voltage and Current. Voltage and Current are both Real variables with unit "V" and "A". "onePort" declares two interfaces "p" and "n" of class "Pin". Each "Pin" contains a Voltage and Current itself. "flow" will be explained afterwards.

In the equation section of "onePort", the variable "i" is associated to the variable "p.i" of the positive pin "i=p.i". Furthermore, the input current equals the output current (Kirchhoff's rule): "0=p.i+n.i". The voltage "v" is the differential voltage of the two ports "v=p.v-n.v".

The "resistor" model itself is quite short. The variable "R" is a parameter of type resistance. The actual Ohm's law can be found in the equation section: "v=R*i". "R=v/i" would have worked as well since the causalities are not of importance in Modelica. The pins of the components are interlinked by the language elements "connect" such that they form one node. For example, the equation

```
connect(Resistor.p,Switch.n)
```

links the two "Pins" "Resistor.n" and "Switch.n". Variables of type "flow" are linked by a sum-to-zero equation:

```
Resistor.p.i+Switch.n.i =0;
```

(Kirchhoff's current law). All other variabels are linked by

```
Resistor.p.v=Switch.n.v;
```

(equilibrium of potential variables).

A 2 Component library for aircraft electrical network

The aircraft electrical network validation & verification process strongly relies on software based capabilities for modeling, simulation and analysis of the electrical components and systems. To ease the industrial process for future more electric aircraft, a dedicated Modelica based library was developed in the EU funded project "Clean Sky, Systems for Green Operation". The library is a reference implementation, with demonstration of

- Modeling of all major power suppliers, converters and loads of the electrical network
- Typical stand-alone and systems tests which are frequently performed
- Associated scripts for automated testing
- Dedicated scripts for post-processing, evaluation and documentation

A 2.1 Overview of library

The "Cleansky" library of components and systems for aircraft electrical network validation and verification can be seen in Figure A2. The structure follows the needs of the V&V procedure. For each equipment a separate sub-folder is made. These are

- 230 VAC variable frequency generator (VFG)
- Auto transformer unit (ATU)
- Auto transformer rectifier unit (ATRU)
- Rectifier unit (RU)
- Inverter and permanent magnet excited synchronous machine 1 (PMSM1)
- Inverter and permanent magnet excited synchronous machine 2 (PMSM2)
- 540 VDC to 28 VDC bidirectional converter (DCCU)

Each model was implemented twice with two levels of abstraction. Detailed modeling including high frequency effects up to 1 MHz is represented by the "BehaviouralModel". From this model the so-called "FunctionalModel" is derived, which reflects the time averaged behavior up to 100 Hz without high frequency switching behavior. All models rely on the Modelica standard library and specific sub-models which are placed in the individual "Components" section. Each component has to be tested individually where all tests are located in the "StandAlone_Tests". This includes coherency checks of hardware data against models and coherency checks of functional models versus behavioral models. Furthermore, specific tests like connection and disconnection tests may apply. Testing relies on dedicated test models, execution scripts and scripts for evaluation, post processing and documentation.

The large scale test benches of integrated systems are placed in the sub-folder "CommonTests". Some of them were already shown in the main part of the thesis. A more comprehensive overview of the industrial like test and some specific scripting can be found in (Kuhn and Ji, 2014).
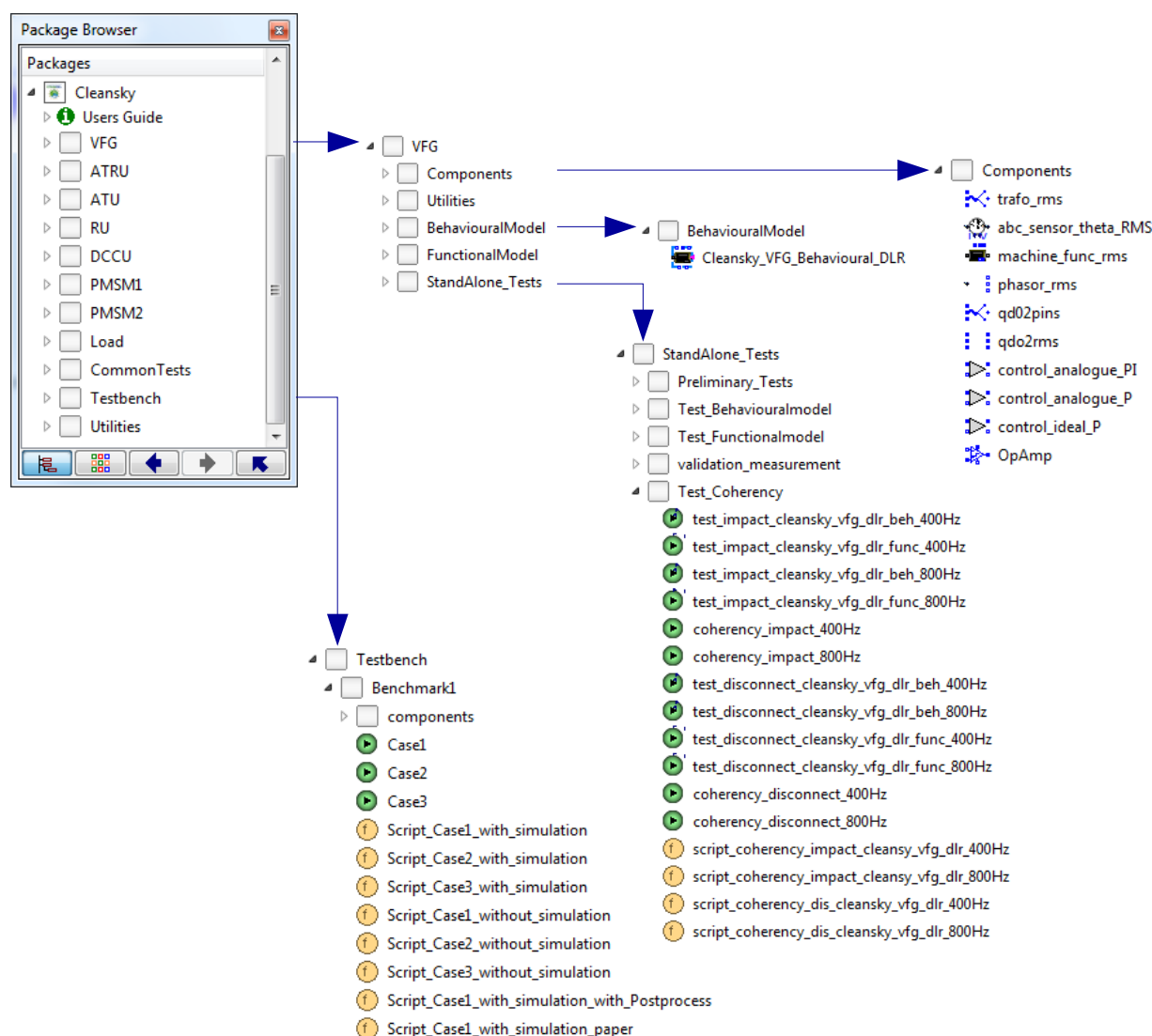
Figure A2: Overview of "Cleansky" library, for electrical systems V&V

A 2.2 Lessons learned from large scale systems simulation

The study could demonstrate the applicability of Modelica and Dymola for large scale testing of aircraft electrical systems in V&V studies successfully. All demands on new functionality, additional models and specialized scripts could be met within the project. It was found that the reliability of simulation highly depends on mature models. The developed library therefore is an important base for propagation to a Modelica based V&V process in aircraft electrical systems simulation.

In the main part of this thesis different types of initialization were discussed and analyzed mainly with the objective of elimination of the ramp-up phase. For the large-scale systems in many cases the simulation can not even start, since the complexity of the initialization prevents simulation. Therefore all identified methods for the small electric test circuit are also highly relevant for the integrated test benches.

The author's publication (Kuhn and Ji, 2014) reports some best-practice guidelines in modeling and identification of model errors.

A 3 Property monitors

[29]Instead of relying on written specifications, the model based specification approach specifies the basic behavior of systems and methods by models. Property monitors allow for automated checking of the requirements. In the following it is demonstrated how the property monitors can be implemented by recent Modelica based libraries, especially with the Modelica_Requirements library which was proposed in (Otter et al., 2015). Two new FFT-based requirement blocks are proposed which are used for the power quality checks in chapter 3.4.1.

Expression of high level requirements can be formulated in principle by any type of mathematical operation which results in an expression for requirement fulfilled/not fulfilled (or not yet evaluated). For example in (Kuhn, 2011) Modelica requirement models have been designed for band constraint signals or frequency domain constraints. The textual output of the requirement checking was based on Dymola proprietary scripting and at that time was missing systematic output and documentation concepts.

In parallel to the CleanSky SGO activities, the European ITEA projects EUROSYSLIB, OPENPROD, and their successor MODRIO also identified a strong need for requirements modeling. Their approach resulted in the Modelica_Requirements library[30] (Otter et al., 2015). One essential

R1: In normal operation mode, the envelope of the RMS value of the 400 Hz AC voltage after a voltage transient is given by the following figure and has to remain in the final limits.	
R2: In normal operation mode, the distortion spectrum of the variable frequency AC voltage has to remain below the limits given by the following figure.	

Table A12: Typical industrial requirements

---

[29]This chapter uses material published in the joint publication (Kuhn et al., 2015) and (Kuhn, 2011). The individual contributions of the author are stated in the main chapters of the thesis.

[30]At the time of writing this thesis, the library is not released. All references are related to the version which is addressed in (Otter et al., 2015)

advantage of this library is that it uses two- and three-valued logic to specify requirements. It is then possible to distinguish whether a requirement is satisfied, violated, or not tested during a simulation. It could be demonstrated in the JTI project, that the requirements library fulfills many needs for formulation of executable specifications of the electrical and the ECS system. In particular the LogicalBlocks, the TimeLocators and the ChecksInSlidingWindow have been used.

For the formalism of binding requirements to models, checking and indication, see the implementation in (Kuhn et al., 2015).

Table A12 shows some typical requirements in aircraft systems specification.

Requirement R1 of Table A12 could be implemented with the Modelica_Requirements library with several BandDuration blocks. A more convenient approach is sketched in chapter A 3.1 by using a newly designed and implemented "Funnel" block.

Frequency domain requirements, such as needed for Requirement R2, cannot be defined with the Modelica_Requirements library. Therefore, new requirement blocks have been developed based on the Fast Fourier Transformation (FFT), see chapter A 3.2.

A 3.1 Transient Limits monitor
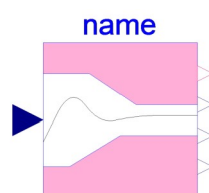
Figure A3: Funnel style transient limit block

The "Funnel" block, displayed in Figure A3, allows checking of transient time limits in funnel style. The upper and lower limits are defined via a table versus time. The initial start of the time varying limits is triggered by an initial overshoot of the limits. The initial limits are defined by the final band. This funnel type limit may be retriggered if one full period of the funnel style limitation has passed by. The output y indicates the fullfillment of the criterion. Further outputs are a scaled distance to the limits and the time varying upper and lower limits. The input is smoothed to suppress noise.

Code excerpt:

```
equation
der(itrans) = if started then max({low_lim-input,input-up_lim,0}) else 0;
y=if itrans/lim>1 or pre(y)==Property.Violated then Property.Violated else
 Property.Satisfied;
scaledDistance=max({(low_lim-input)/(up_lim-low_lim),(input-up_lim)/(up_lim-
 low_lim),0});
```

A 3.2 FFT-based frequency property monitor

A 3.2.1 Concept

Frequency based criteria are typical for industrial standards of electrical systems. For example, MIL-STD-704F (STD-704F, 2004) defines a maximum distortion in the spectrum of the 270Volts DC system. Standard tools/functions for FFT provide a user-unfriendly parametrization. This chapter proposes a convenient implementation. The efficient sampling of data in a simulation environment is addressed.
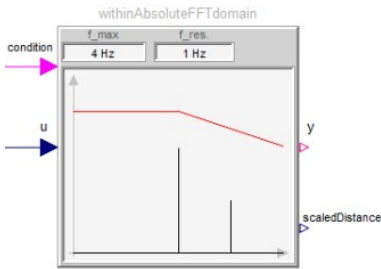
Figure A4: *Example of WithinAbsoluteFFTdomain block for the inputs:* $u=2+3{\cdot}\sin 2\pi f_1 t+1.5{\cdot}\sin 2\pi f_2 t$, $(f_1=2\,Hz,f_2=3\,Hz)$ *and* `condition = true`.
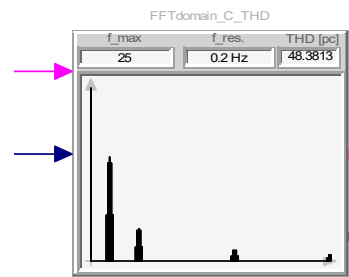
Figure A5: *Example of WithinAbsoluteFFTdomain_THD block with:* $u=5+3{\cdot}\sin 2\pi f_1 t+1.5{\cdot}\sin 2\pi f_2 t$, $(f_1=2\,Hz,f_2=5\,Hz)$ *"pulse" is the rectangular pulse function at frequency) and* `condition = true`.

Based on the implementation and practical experience with the FFT monitoring block of (Kuhn, 2011), two FFT blocks were newly designed and implemented with Modelica. An example of the user's view of the new FFT block `WithinAbsoluteFFTdomain` is shown in Figure A4. An alternative block with limits for total harmonic distortion (THD) is shown in Figure A5.

The user interfaces were designed to allow parametrization with a minimum of information and display the amplitudes over the frequencies in the icon.

In the icon of `WithinAbsoluteFFTdomain`, the two scalar parameters of this block are displayed, `f_max` – the maximum frequency of interest for the user, and `f_res` – the resolution of the frequency axis (so the increment of the frequency axis). Typically, the user is interested in a maximum frequency `f_max` that is an integer multiple of some base frequency (e.g. 50 Hz base for power distribution networks). The frequency resolution should be selected in such a way, that the spectral lines of particular interest are an integer multiple of the resolution (in order to get the most

accurate result). In the example `f_max = 4 Hz` and `f_res = 1 Hz`, so 5 frequency values are shown in the icon (0, 1, 2, 3, 4 Hz). For numerical reasons, in practice the resolution should be chosen high enough to distinguish well between adjacent peaks in the spectrum.

The constraints for the frequency amplitudes are defined via a polygon based on a tabular parameter input. Typically, there are two kinds of parametrization for spectral tests: Definition via absolute values for the constraints and definition in relation to the magnitude at a certain frequency. For relative definition, the user is requested for the respective base frequency. In case this frequency is not an integer multiple of the frequency resolution, the frequency closest to it is taken. With parameter `searchInterval` a search interval around this base frequency is defined, where the maximum peak in this region is taken as real base frequency. For example for the 50Hz net frequency of the European power grid, the frequency may vary by ±0.2Hz in regular operation mode. After initialization, the limits are displayed as red polygons in the icon.

Whenever the Boolean input `condition` has a rising edge, the Real input signal `u` is periodically sampled with a sample rate automatically computed from `f_max` and `f_res` and stored in a buffer. Once "sufficient" values are stored in the buffer (see chapter A 3.2.3), an FFT is computed, displayed in the icon as bar plot and stored on file. Additionally, the distance to the amplitude boundary is computed. If at least one amplitude is above the boundary, output y = Violated. If all amplitudes are below the boundary, y = Satisfied, and if the FFT has not yet been computed, y = Undecided.

In case a falling edge of `u` occurs before sufficient sample values are monitored or the simulation run is terminated, then the FFT spectrum is approximated via the partly-filled buffer with zeros for other values (called "zero-padding" technique).

A 3.2.2 Implementation

Standard tools/functions for FFT provide a user-unfriendly parametrization. Typical inputs are the sampling frequency and the number of data. In contrast to the definition, the user may be more interested in the maximum frequency of the spectrum and the frequency resolution. Therefore, the mapping of the parametrization of the *WithinAbsoluteFFTdomain* block to the underlying standard FFT parametrization is different to the standard practice. The non-trivial relations are shortly sketched:

In order that the amplitudes are computed by the FFT with sufficient precision, the FFT computation needs to be performed for a much larger frequency as of interest for the user. In the block a fixed factor of 10 is used. So, if $f_{max} = 4\,Hz$, then the FFT computation uses internally a maximum frequency $f_{max,FFT} \geq 40\,Hz$. The basic formulae for an FFT computation of real numbers with even number of sample points are summarized in equation (227):

$$f_s = \frac{n_s - 1}{T_s},$$

$$f = \left[0, \frac{f_s}{n_s}, \frac{2 f_s}{n_s}, \dots, \frac{f_s}{2} \right],$$

$$\Delta u_r = u(t_r) - u_{DC},$$

$$n_f = \frac{n_s}{2} + 1,$$

$$u_{FFT,k}(f_k) = \frac{1}{n_f} \sum_{r=0}^{n_f - 1} \Delta u_r \, e^{-j 2 \pi k \frac{r}{n_f}}$$

Where

- T_s is the sample period.
- n_s is the number of sample points
- f_s is the sample frequency $\left(f_{max,FFT} = f_s / 2 \right)$
- f_s / n_s is the frequency resolution (`f_res`)
- n_f is the number of frequency points
- u_{DC} is the arithmetic mean of the signal
- Δu_r is the difference of the input signal with respect to the arithmetic mean
- u_{FFT} is a complex number as function of a (real) frequency f_k, $k \in [1 .. n_s]$ and represents the FFT.

In order to be efficient, the original FFT algorithm by Cooley and Tukey (Cooley and Tukey, 1965) requires that the number of sample points is an integer multiple of 2: $n_s = 2^i, i = 1, 2, \dots$. Newer algorithms allow more prime numbers. The implemented blocks use the public domain C-code KISS FFT (Borgerding, 2015). This mixed-radix FFT code requires that the number of sample points must be an integer multiple of 2, 3 and 5: $n_s = 2^i 3^j 5^k$. For real signals, n_s must be additionally an *even* number.

The maximum frequency $10 f_{max}$ is now enlarged so that the number of sample points n_s fulfills the above restrictions. The sample period T_s is determined, so that the frequency resolution f_s / n_s has the required value. These computations are performed with the following Modelica code:

```
// Compute best ns according to f_max and f_resolution
ns:=2*integer(ceil(f_max/f_res));

// Make ns even
ns:=if mod(ns,2)==0 then ns else ns + 1;

// Find smallest ns that is even + expressed as 2^i*3^j*5^k
while true loop
    ns1 :=ns;
    while mod(ns1,2) == 0 loop ns1 :=div(ns1, 2);end while;
    while mod(ns1,3) == 0 loop ns1 :=div(ns1, 3);end while;
    while mod(ns1,5) == 0 loop ns1 :=div(ns1, 5);end while;
    if ns1 <= 1 then   break; end if;
    ns :=ns + 2;  // enlarge ns, but keep it even
end while;

// Enlarge maximum frequency by a factor of 10
```

```
ns:= 10*ns;

// Compute other FFT variables
f_max_FFT = f_resolution*div(ns,2);
Ts        = 1/(2*f_max_FFT) "Sample period";
T         = (ns-1)*Ts "Simulation time";
```

To understand the numbers above beforehand, utility function `showNumberOfFFTpoints(..)` is provided that computes them. For example calling the function as

```
showNumberOfFFTpoints(f_max=2000, f_resolution=27);
```

results in the following output:

```
Desired:
  f_max        = 2000 Hz
  f_resolution = 27 Hz

Calculated:
  Maximum frequency used  = 20250 Hz
  Number of sample points = 1500 (=2^2*3^1*5^3)
  Sample period           = 2.46914e-005 s
  Simulation time         = 0.0370123 s
```

Note, that

$$
\begin{aligned}
f_{max,FFT} &= (n_f - 1) \cdot f_{resolution} \\
&= \frac{n_s}{2} \cdot f_{resolution} \\
&= \frac{1500}{2} \cdot 27\,Hz \\
&= 20250\,Hz
\end{aligned}
\tag{228}
$$

In the "advanced" tab access is given to parameters less often used:

- $SearchInterval$ (search interval around base frequency)
- $TerminateAfterFFT$ (When true, the simulation is terminated after evaluation of the FFT)
- Parameterization of the "Window" type
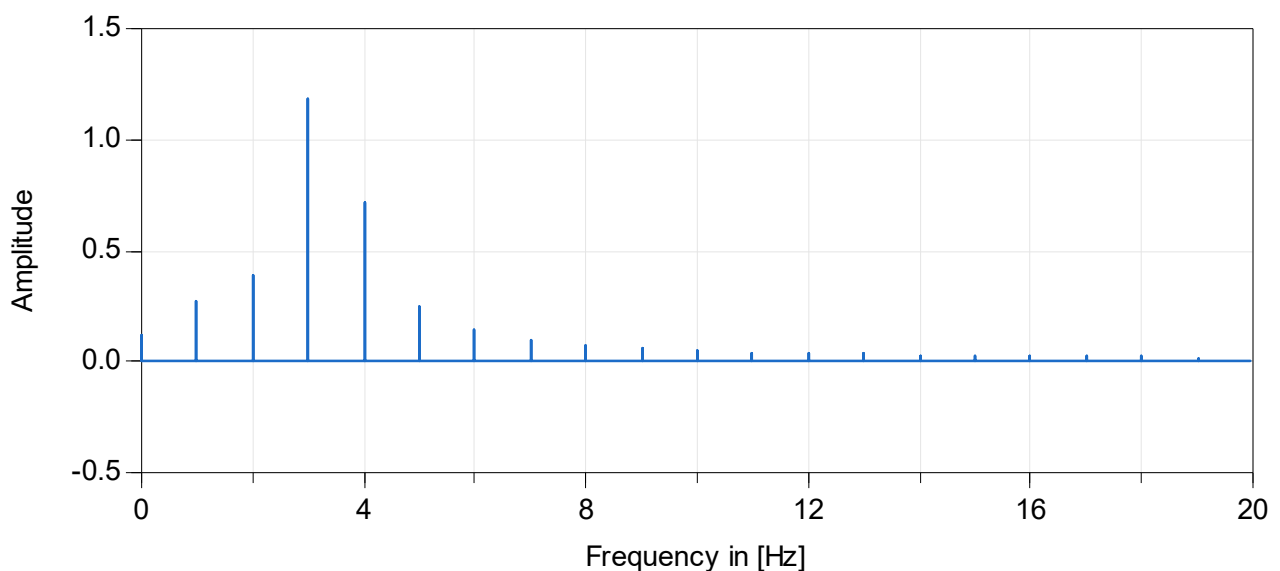
Figure A6: u=1.5 sin(2 π 3.4 t) at 1 Hz resolution

In case the sampled interval does not match a multiple length of the occurring waves, the spectrum would suffer from this "discontinuity" of non-matching levels at the start and the end point since the FFT assumes periodic signals. This can be circumvented by multiplication of the time series by a filter of the same length, called "window function". If this window function exhibits a shape with zero at start and end and some maximum in the middle, this discontinuity can be attenuated. By choice of a proper window function, erroneous high frequency signals will be diminished and the signal power at frequencies not precisely matched in the FFT output spectrum is smeared to the adjacent spectral points (called bins). For details see (Heinzel et al., 2002). The influence of windowing is demonstrated in Figure A6 and Figure A7. A sinusoidal signal of amplitude 1.5 and frequency 3.4 Hz is not matched by the FFT's output resolution of 1 Hz. Figure A6 shows a peak at 3 Hz with an amplitude of 1.2, some amplitudes in the adjacent bins and content for all higher frequencies. In contrast, Figure A7 is the FFT output of the signal which was windowed by the "Minimum sidelobe 3-term-at top window SFT3M" (Heinzel et al., 2002) of length n_s with the window:

$$w_i = 0.28235 - 0.52105 \cdot \cos\left(\frac{1 \cdot 2 \cdot \pi \cdot i}{n_s - 1}\right) + 0.19659 \cdot \cos\left(\frac{2 \cdot 2 \cdot \pi \cdot i}{n_s - 1}\right), i = 0..n_s - 1 \tag{229}$$

One can see from the plot, the original signal of 3.4 Hz occurs in the amplitudes of both frequencies, 3 Hz and 4 Hz. Also the next bins show a higher (erroneous) content while there are only low amplitudes at higher frequencies. As a consequence, it is not recommended to use flat windows in case where discrete peaks in the spectrum are expected, which may not be resolved well by the low resolution.

In addition to the `WithinAbsoluteFFTdomain` block, the `WithinAbsoluteFFTdomain_THD`, calculates the Total Harmonic Distortion (THD) from the FFT output. THD is a measure for the amplitudes of harmonics in relation to the amplitude of the base frequency. With the maximum number of harmonics M:

$$THD = \sqrt{\sum_{k=2}^{M} A \frac{\left[k \cdot f_{base}\right]^2}{A\left[f_{base}\right]}} \tag{230}$$

The maximum frequency of the FFT spectrum is defined as a function of M: $f_{base} \cdot M \leq f_{max,FFT}$
.
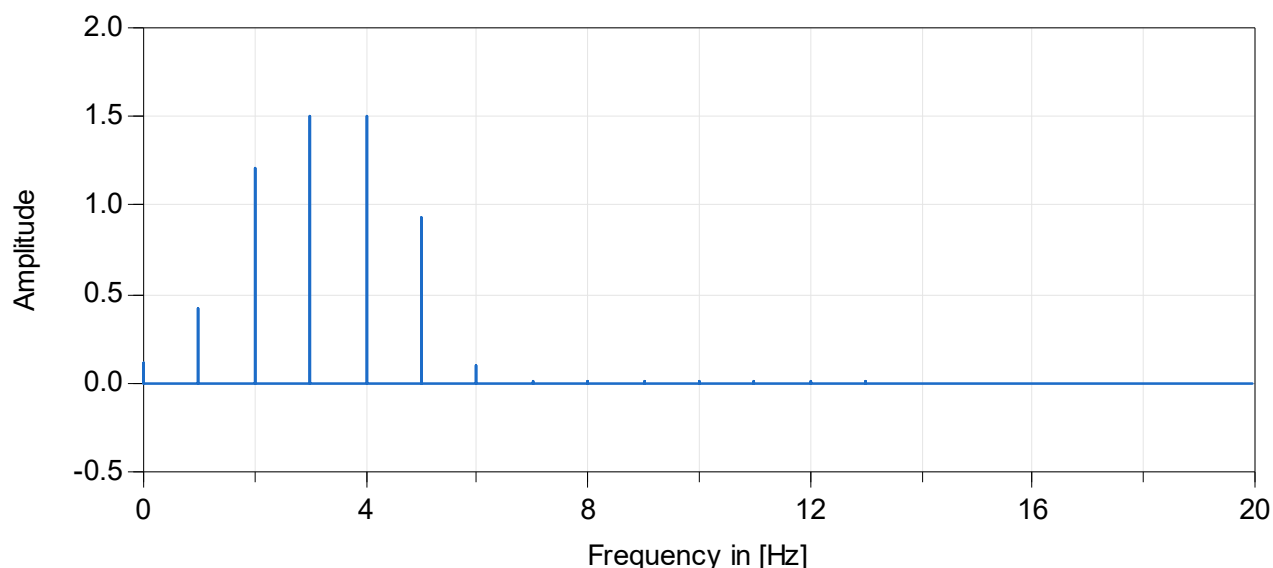
Figure A7: $u = 1.5 \cdot \sin(2\pi \cdot 3.4 \cdot t)$ *at 1 Hz resolution and flat top window.*

A 3.2.3 Sampling of data

The FFT algorithm works on past samples of the signal. The simulation environment could give direct access to the stored simulation data or data can be stored by parallel processes. Four methods for data storage were identified: This is

- use of the Modelica built in "Sampling" function, with a Modelica buffer,
- Modelica based "Sampling", with an external buffer,
- use of the Modelica function "delay" and
- by an event-free evaluation of an external C function and external buffer.

The sampling method seems most straight forward: After every sampling time interval $1/f_s$, the value of the selected signal is taken and stored in a buffer array. A test with Dymola 7.5 showed correct results of data storage and FFT but simulation time much suffered: In Dymola, the variable order integrator and solver was forced to stop at every sampling instance. The re-start of the integration algorithm is numerically expensive. This problem was identified within the "Modelica benchmark" activity and the manufacturer could deliver an improved version: For later Dymola versions the procedure changed for sampled data which are not inputs to state variables. The "sampling" can calculate the data by internal interpolation and extrapolation without interrupting the integration algorithm.

For the Modelica based buffering of data, Modelica's single assignment rule applies. All values of the buffer- array need to be set at every sample instant. If a value is not changed at the current sample instant, the value from the previous sample instant is copied (so at every sample instant $n_s - 1$ values are copied).

Alternatively, the buffer function can be implemented by an external function, which is triggered at every sampling. This prevents the copying of the full data array. Modelica supports embedded "C" functions for this purpose.

The third method relies on the Modelica specific "delay" function. It delays the input signal by a specified time. For n FFT points, n delays have to be added. The delay function uses the simulator's internally stored result values and the output of "delay" is calculated by interpolation of the sampled data from polynomials. Therefore, it does not need demand additional sampling with the FFT's sampling resolution. For this solution there appeared problems with the amount of data: Since "de-

lay" is just one-dimensional, for every instance of this function all internal polynomials are stored instead of joint use. This not only causes exhaustive memory usage but also, Dymola restricts the user to 2000 instances of "delay". The Modelica "delay" function should be improved to allow for single storage-multiple time data out.
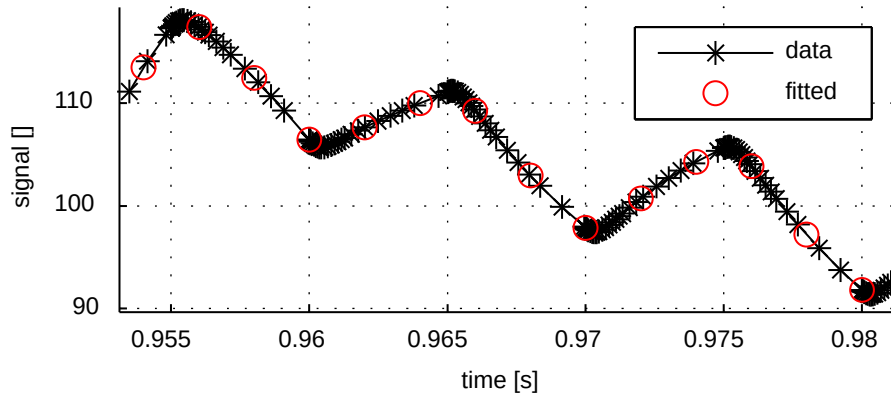
Figure A8: Interpolation of equidistantly sampled data from data generated at the evaluation points of the integration algorithm

The fourth method also relies on external "C" code. For all kinds of numerical integration, at every integration step the differential-algebraic equation system is evaluated. If some real or artificial states rely on an external function then this function is triggered at every evaluation step. Using a variable step solver like DASSL makes sure that the time steps are small enough to sample the signal with a resolution which covers the model's dynamics sufficiently. An external C function can store the data in a circular memory buffer. Variable step solvers use "back-stepping" in time in case the step width was taken too large. The C function has to consider this and also has to delete data sets from skipped time steps. The computation of the FFT starts with the request on a data set. An interface function extracts the stored data from memory, reduces the data set to the window of interest, adds zeros in case not enough data are gained to that moment ("zero padding") and interpolates the irregular sampled data to a regular sampled data set[31]. An example of the integrator step-size-triggered data generation and the equidistantly fitted data is shown in Figure A8.

In Figure A9 some benchmarks for different kinds of data storage of the n_s FFT points is given:

---

[31]The interpolation algorithm uses cubic hermetic splines. The implementation relies on the "CMATH" library of University of Queensland.
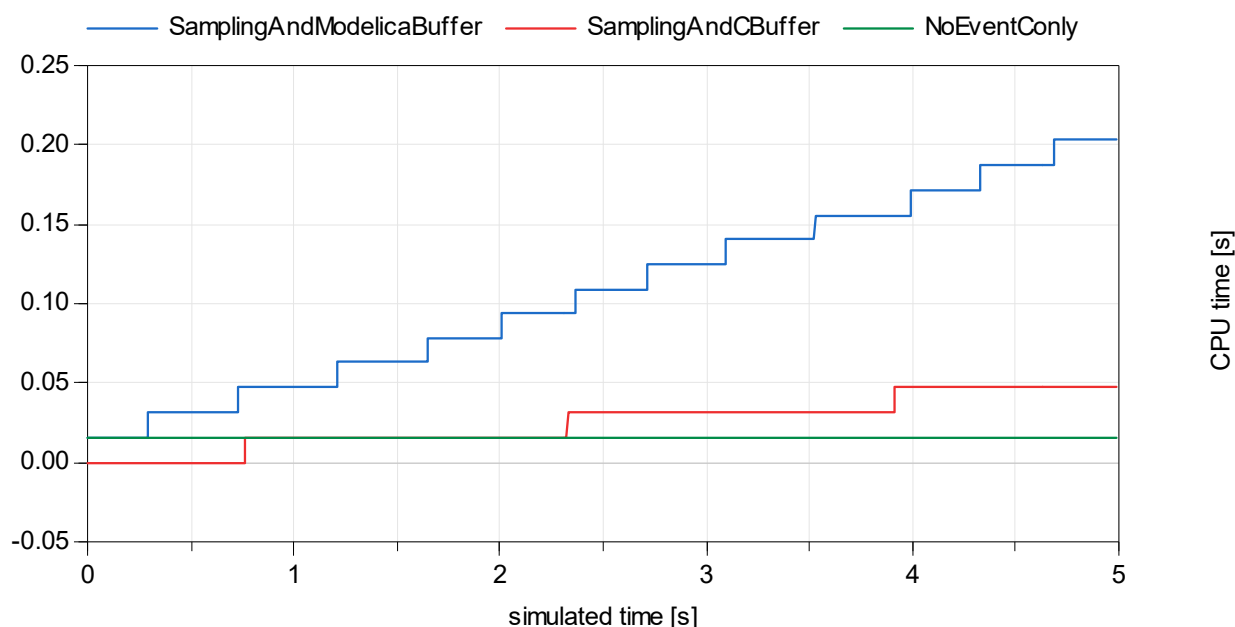
Figure A9: Comparison of CPU time [s] for three types of data storage for the FFT points.

- *SamplingAndModelicaBuffer* (= blue line) buffers the data at every sampling interval $1/f_s$ in a Modelica array. (Plots are based on a Dymola version with improved sampling function)
- *SamplingAndCBuffer* (= red line) invokes a C function at every sample instant that stores the actual value of the input signal into an internal C array.
- *NoEventConly* (= green line) stores the input value at every model evaluation into an internal C array.

As can be seen from Figure A9 *SamplingAndModelicaBuffer* is the slowest. *NoEventConly* is comparably fast as *SamplingAndCBuffer*. In other benchmarks, *SamplingAndCBuffer* is the fastest approach. Due to these benchmarks, and the easier sampling, the two blocks *WithinAbsoluteFFTdomain* and *WithinAbsoluteFFTdomain_THD* are implemented based on the *SamplingAndCBuffer* approach for data storage.

A 4 Filter weight determination

In an integrated analysis of the generation, distribution and consumption of electrical energy, the weight of the DC ripple filters has to be taken into account. The demands on the inverter's input filter in a local DC power system are twofold: Firstly, the filter shall effectively improve the power quality of the DC network. The filter has to attenuate the voltage and current harmonics coming from the transistors switching. The second need of the input filter is to stabilize the DC voltage at the terminals of the load. The specific demands result from stability considerations, and from the requirements defined in aerospace industrial standards on maximum voltage levels in static and transient behavior. The key issue for aircraft is the weight of the input filters which is dependent on the capacitors and inductors. Therefore, the design of an input filter becomes a typical constraint multi-objective optimization task: the weight of the input filter is the penalty function with various constraint criteria such as demands on current harmonics attenuation to the DC link, internal eigenvalue stability or DC voltage transient performance.

The following paragraph discusses the selection and weight determination of the filters. This chapter is intended to round off the design methods for the aircraft electrical network, with consideration of power quality and network stability.

The filter weight is considered as a function of the capacitors C and the inductors L. The first ones usually are selected from manufacturers data catalogs while the latter ones are manufactured to the needs. For the inverter filters, among aluminum, mica, mylar, polyester, and polypulse capacitors the polypropylene based capacitors were found to have a good efficiency. They show a very low dielectric loss to damp ratio and low temperature coefficient, high dielectric strength & stability, high volumetric energy and self healing capabilities, compact size, and excellent frequency and temperature characteristics. Compared to polyester capacitors they tolerate a wider temperature range. Compared to aluminum electrolytic capacitors they exhibit exceptionally low ESR, factor 10 ripple current, they are non-polar, have higher voltage rating, are based on a dry construction without electrolyte, and improved reliability (Tsiachris, 2009). For airborne applications the use of aluminium capacitors with their higher capacitance-to-weight ratio may be critical since evaporation of liquid parts will result in performance degradation. Health monitoring could help to preserve function and reliability. A method for health-monitoring of capacitors was proposed in (Ji and Bals, 2010) The lower weight would be faced by a higher technical effort and maintenance.

The following equations and plots characterize the polypropylene capacitors. The data were found by an investigation of the relations of weight/equivalent series resistance/capacitance and voltage. They are based upon a literature research with manufacturer data sheets[32].
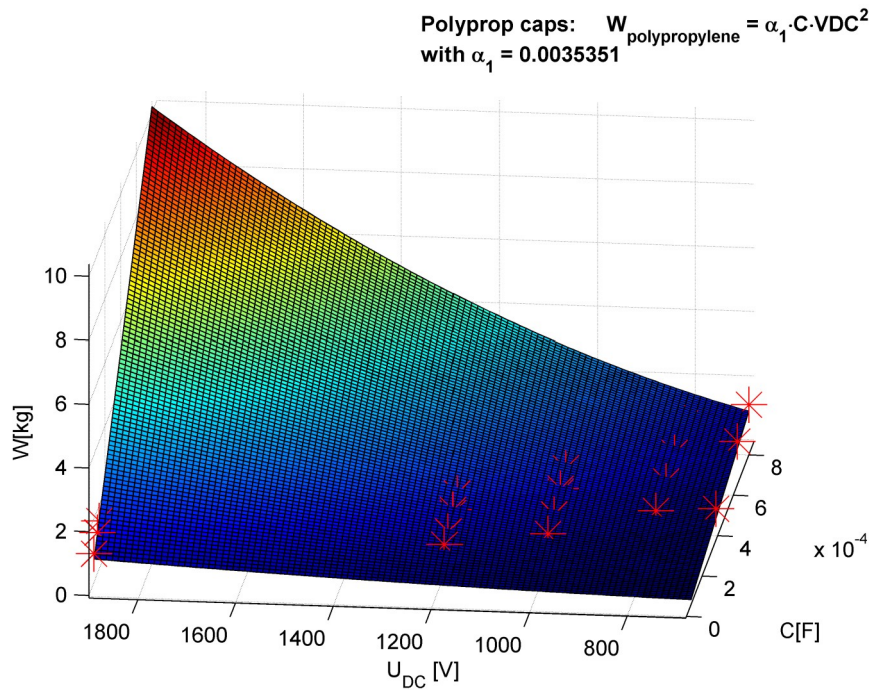
Figure A10: Relations ESR and weight of polypropylene capacitor

The capacitor weight can be approximated by

$$W_{polypropylene}[kg] = C[F] \cdot U_{dc\,max}[V]^2 \cdot 0.003535132 \qquad (231)$$

The equation relates the weight linearly to the stored energy $1/2 \cdot C \cdot U_{dc}^2$. More sophisticated formulas may consider a relation to the maximum (thermal) energy from the ripple current $W_{polypropylene} = (0.0036788 - 2.6357\mathrm{e}\text{-}7 \cdot I^2) \cdot C \cdot U_{DC}^2$.

The equivalent series resistance at 10kHz is approximated by

$$ESR_{poly}[\Omega] = 0.0037221 \cdot (C[F] \cdot 10^{-3})^{-0.84993} \cdot U_{DC}[V]^{-1.2793\mathrm{e}\text{-}8} \tag{232}$$

The approximation and the original capacitor data points are plotted in Figure A10.
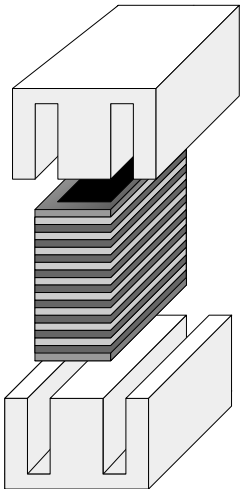
Figure A11: Filter inductor layout
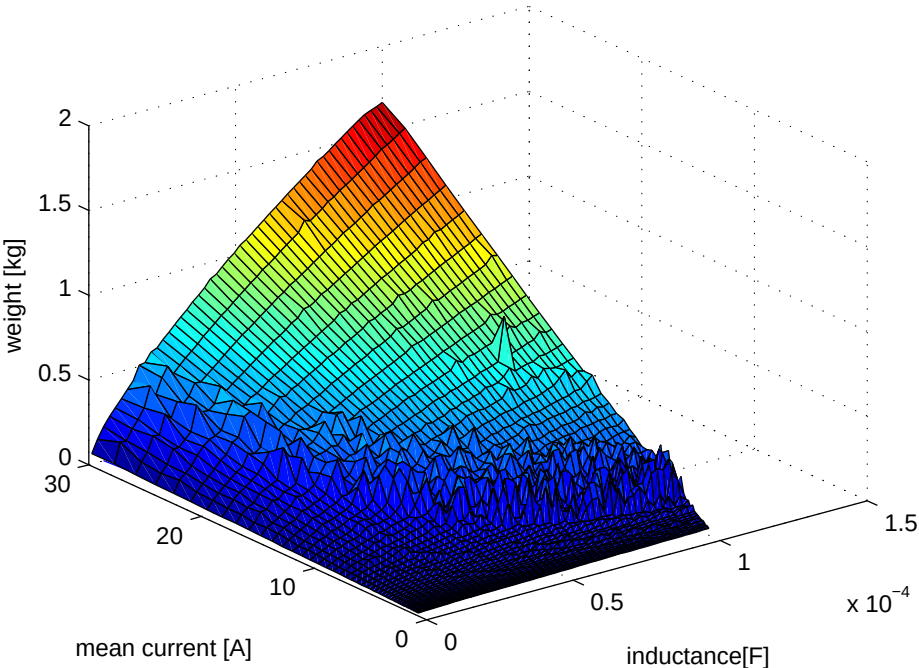
Figure A12: Inductor weight vs. mean current and inductance at ripple of 1.2*meancurrent

For the inductors, the procedure of (Gürdal et al., 2000) optimizes the mechanical dimensions of the inductor for a specific inductance value L, with constraints on performance and space. Here, an

inductor layout with an E core is assumed. The layout of the virtually manufactured inductor can be seen in Figure A11.

The inductor weight w_L can be calculated from an optimization-based function

$$w_L[kg] = f_L(L[F], i_{mean}[A], i_{ripple}[A])$$ (233)

with mean current i_{mean} and current ripple i_{ripple}. For details of the methodology and constraints, see (Gürdal et al., 2000). Some additional assumptions, which are known from in-house experience with motor design, are listed in Table A13.

Core material	Ferrite
Maximum flux density	0.3 T
Maximum Current density copper	8 A/mm^2
Window fill factor	0.6

Table A13: Inductor sizing parameters

Typical results for the inductor weight in relation to mean current and inductance are shown in Figure A12. The design function was implemented as a MATLAB routine. It uses a pattern search algorithm which is able to solve nonlinear constraint programming problems.

A 5 Abbreviations and Notations

β	steady state index of wavelet based test
ω_e, ω_{base}	angular velocity of electrical system, =angular velocity of base/fundamental
ω_{mec}	mechanical rotational speed
ϕ	flux linkages
ψ	Flux linkages per second
φ_{mec}, φ_e	mechanical/electrical phase angle
$\_{ds}, \_d$	variable of direct axis, associated to stator
$\_{fd}, \_{fd}$	variable of field winding
$\_{kd}$	variable of damper winding in direct axis, associated to rotor
$\_{kq}$	variable of damper winding in quadrature axis, associated to rotor
$\_{qs}$	variable of quadrature axis, associated to stator
$\_{rem}$	equivalent variables of remanence in rotor excitation
A/C	Aircraft
AC	Alternating Current
AEA	All Electric Aircraft
ATRU	Auto Transformer Rectifier Unit
ATU	Auto-Transformer Unit
B	magnetic flux density
$\boldsymbol{P}$	Park transformation with complex variables
$\boldsymbol{P}^{-1}$	Inverse Park transformation with complex variables
$\boldsymbol{T}^{-1}$	Inverse Park transformation
$\boldsymbol{T}$	Park transformation to qd0 system
CCM	Continuous Conduction Mode
CPL	Constant Power Load
DAE	Differential Algebraic Equation

DC	Direct Current
DCCU	DC/DC power converter
DCM	Discontinuous Conduction Mode
DFT	Discrete Fourier Transformation
ECS	Environmental Control System
f	frequency
FFT	Fast Fourier Transformation
GCU	Generator Control Unit
i/I	current (dynamic/static)
L_n, *Ln*	negative sequence inductance
LISN	Line Impedance Stabilization Network
LPV	Linear Parameter Varying
LTI	Linear Time Invariant representation
m	index of a harmonic
MEA	More Electric Aircraft
NLP	Non-Linear Programming
p	pole pair number; in chapter "levels of abstraction": differentiation operator
PMSMS	Permanent Magnet Synchronous Machine
PSO	Particle Swarm Optimization
R	steady state index of F-like test
RU	Rectifier Unit
s	Laplace operator; also used for the s-parameterization of a diode in time domain
SSI	Steady State Identification
V&V	Validation & Verification
v/V	voltage (dynamic/static)
VFG	Variable Frequency Generator
WIPS	Wing Ice Protection System
Zi	Input Impedance
Zs/Zo	Source Impedance

A 6 Trademarks and project acronyms

Clean Sky SGO ITD	EC funded project "CleanSky", Integrated Technology Demonstrator Systems for Green Operations
Dymola	software; registered trademark of Dassault Systèmes (developed by Dassault Systèmes Lund, formerly: Dynasim)
Maple	software; registered trademark of Waterloo Maple Inc.
MATLAB	software; registered trademark of The MathWorks, Inc.
Modelica	modeling language; registered trademark of the Modelica Association
MOET	EC funded project "More Open Electrical Technologies"
MOPS	Optimization environment by DLR, institute of System Dynamics and Control
Saber	software; registered trademark of Synopsys, Inc.
Simulink	software; registered trademark of The MathWorks, Inc.
VIVACE	EC funded project "Vale Improvement Through A Virtual Aeronautical Collaborative Enterprise"

Bibliography

Airbus (2002). **Airbus directive ABD100.1.8, part 1 - product, chap 8 - electric and installation requirements**.

Abel, A., and Nähring, T. (2008). **Frequency-Domain Analysis Methods for Modelica Models**. In *Proceedings of the 6th International Modelica Conference*.

SAE International (2016). **AIR6326: Aircraft Electrical Power Systems, Modeling and Simulation, Definitions**.

Ansorge, R., and Oberle, H.J. (2000). **Mathematik für Ingenieure**. WILEY-VCH Verlag.

ANSYS, Inc. (2017). **Simplorer**. http://www.ansys.com/en-GB/products/systems/ansys-simplorerSimplorer.

Areerak, K.-N., Bozhko, S.V., Asher, G.M., and Thomas, D.W.P. (2008). **Stability analysis and modelling of AC-DC system with mixed load using DQ-transformation method**. In *Proceedings of the IEEE International Symposium on Industrial Electronics (ISIE)*, p. 19-24.

Arrillaga, J., and Watson, N.R. (2003). **Power system harmonics**. Wiley.

ModelicaAssociation (2017). **Modelica**. https://www.modelica.org/.

Balas, G., Doyle, J., Glover, K., Packard, A., and Smith, R. (1998). **μ-Analysis and Synthesis Toolbox**. The Mathworks.

Bals, J., Fichter, W., and Surauer, M. (1997). **Optimization of Magnetic Attitude- and Angular Momentum Control for Low Earth Orbit Satellites**. In *Spacecraft Guidance, Navigation and Control Systems 381*, p. 559.

Bals, J., Ji, Y., Kuhn, M.R., and Schallert, C. (2009). **Model Based Design and Integration of More Electric Aircraft System using Modelica**. In *Moet Forum at European Power Electronics Conference and Exhibition*.

Barruel, F., Retiere, N., Schanen, J., and Caisley, A. (2005). **Stability Approach for Vehicle DC Power Networks: Application to Aircraft On-Board System**. In *IEEE Power Electronics Specialists Conference* 36.

Bauer, J. (2004). **Harnessing the swarm: communications policy in an era of ubiquitous networks and disruptive technologies**. In *Communications & Strategies* 54, p. 19-43.

Baur, M., Otter, M., and Thiele, B. (2009). **Modelica Libraries for Linear Control Systems**. In *Proceedings of the 7th International Modelica Conference*.

Becker, C., and Giese, T. (2011). **Application of model based functional specification methods to environmental control systems engineering**. In *SAE International Journal of Aerospace 4*, p. 637-651.

Besnerais, J.L., Fasquelle, A., Lanfranchi, V., Hecquet1, M., and Brochet, P. (2008). **Mixed-variable optimal design of induction motor**. In *International Conference on Engineering Optimization (EngOpt)*.

Bing, Z., Karimi, K.J., and Sun, J. (2009). **Input Impedance Modeling and Analysis of Line-Commutated Rectifiers**. In *IEEE Transactions on Power Electronics* 24, p. 2338-2346.

Blankenstein, G. (2005). **Power balancing for a new class of non-linear systems and stabilization of RLC circuits**. In *International Journal of Control* 78, p. 159-171.

Boglietti, A., Cavagnino, A., Tenconi, A., and Vaschetto, S. (2010). **Key design aspects of electrical machines for high-speed spindle applications**. In *Conference on IEEE Industrial Electronics Society (IECON) 36*, p. 1735-1740.

Bonfert, K. (1962). **Betriebsverhalten der Synchronmaschine**. Springer-Verlag, Berlin/G\"{o}ttingen/Heidelberg.

Bonwick, W.J. (1980). **Voltage waveform distortion in synchronous generators with rectifier loading**. In *IEE Proceedings B Electric Power Applications* 127, p. 13-19.

Borgerding, M. (2015). **Kiss FFT**. Available http://sourceforge.net/projects/kissfft/.

Braatz, R.P., Young, P.M., Doyle, J.C., and Morari, M. (1994). **Computational complexity of μ calculation**. In *IEEE Transactions on Automatic Control* 39, p. 1000-1002.

Brayton, R.K., and Moser, J.K. (1965). **A theory of nonlinear networks, part I**. In *Quarterly Applied Mathematics* 12, p. 1-33.

Breman, K., Campbell, S., and Petzold, L. (1989). **Numerical Solution of Initial-Value Problems in Differential-Algebraic Equations**. Elsevier Science Publishing Company, New York.

Brown, P.R., and Rhinehart, R.R. (2000). **Demonstration of a method for automated steady-state identification in multivariable systems**. In *Hydrocarbon processing* 79, p. 79-83.

Bünte, T. (2011). **Recording of Model Frequency Responses and Describing Functions in Modelica**. In *Proceedings of the 8th International Modelica Conference*.

Cao, S., and Rhinehart, R. (1995). **An efficient method for on-line identification of steady state**. In *Journal of Process Control* 5, p. 363 - 374.

Cao, W., Mecrow, B., Atkinson, G., Bennett, J., and Atkinson, D. (2012). **Overview of Electric Motor Technologies Used for More Electric Aircraft (MEA)**. In *Industrial Electronics, IEEE Transactions on* 59, p. 3523-3531.

Carpinelli, G., Iacovone, F., Russo, A., Varilone, P., and Verde, P. (2004). **Analytical modeling for harmonic analysis of line current of VSI-fed drives**. In *IEEE Transactions on Power Delivery* 19, p. 1212 - 1224.

Chandrasekaran, S., Ragon, S., Lindner, D., Gürdal, Z., and Boroyevich, D. (2002). **Optimization of an aircraft power distribution subsystem**. In *AIAA Journal of Aircraft* 40, p. 16-26.

Chen, H., Long, Y., and Zhang, X.-P. (1999). **More sophisticated synchronous machine model and the relevant harmonic power flow study**. In *IEE Proceedings- Generation, Transmission and Distribution* 146, p. 261-268.

Chiniforoosh, S. (2012). **Generalized dynamic average modeling of line-commutated converter systems in transient simulation programs**. Ph.D. thesis, The University of British Columbia.

Chua, L.O., Desoer, C.A., and Kuh, E.S. (1987). **Linear and nonlinear circuits**. McGraw-Hill.

Cooley, J.W., and Tukey, J.W. (1965). **An algorithm for the machine calculation of complex Fourier series**. In *Math. Comput.* 19, p. 297-301.

MSC Software Corporation (2017). **"Easy5", Advanced Controls & Systems Simulation**. http://www.mscsoftware.com/product/easy5.

Deb, K., Pratap, A., Agarwal, S., and Meyarivan, T. (2002). **A fast and elitist multiobjective genetic algorithm: NSGA-II**. In *IEEE transactions on evolutionary computation* 6, p. 182-197.

Debnath, L., and Shah, F.A. (2002). **Wavelet transforms and their applications**. Springer.

Delhasse, F., and Biais, F. (2006). **High Power Starter Generators for Airliners**. In *Changes in Aeronautical and Space Systems*.

Demiray, T. (2008). **Simulation of Power System Dynamics using Dynamic Phasor Models**. Ph.D. thesis, ETH Zurich.

Dinh, N.-Q. (1998). **Harmonic Domain Modelling of Direct Connected Generator and HVDC Converter units**. Ph.D. thesis, University of Canterbury, Christchurch, New Zealand.

Eiben, A., and Smith, J. (2007). **Introduction to Evolutionary Computation**. Springer.

Elmqvist, H., Cellier, F.E., and Otter, M. (1994). **Object-oriented modeling of power- electronic circuits using Dymola**. In *Proceedings of the First Joint Conference of International Simulation Societies (CISS)*.

Fan, N., Balan, R.V., and Rosca, J. (2004). **Comparison of wavelet- and FFT-based single-channel speech signal noise reduction techniques**. In *Proc. SPIE 5607*, p. 127-138.

Feng, X., Liu, J., and Lee, F.C. (2002). **Impedance Specifications for Stable DC Distributed Power Systems**. In *IEEE Transactions on Power Electronics 17*, p. 157-163.

Ferreres, G. (1999). **A Practical Approach to Robustness Analysis with Aeronautical Applications**. Kluwer Academic/Plenum Press.

Ferreres, G., and Biannic, J. (2003). **Skew Mu Toolbox (SMT): a presentation.**. Technical Report, ONERA, department of Systems Control and Flight Dynamics, Toulouse, France.

Fleischer, M. (2005). **Foundations of Swarm Intelligence: From Principles to Practice**. In *Transactions of Center for Satellite and Hybrid Communication Networks (CSHCN)*.

Florez-Lizarraga, M., and Witulski, A. (1996). **Input filter design for multiple-module DC power systems**. In *IEEE Transactions on Power Electronics 11*, p. 472-479.

Föllinger, O. (1993). **Nichtlineare Regelungen 2: Harmonische Balance, Popow-und Kreiskriterium, Hyperstabilität, Synthese im Zustandsraum**. Walter de Gruyter GmbH & Co KG.

Fortescue, C.L. (1918). **Method of Symmetrical Co-Ordinates Applied to the Solution of Polyphase Networks**. In *AIEE Transactions 37*, p. 1027–1140.

Gao, J., Ji, Y., Bals, J., and Kennel, R. (2014). **Wavelet library for Modelica**. In *Proceedings of the 10th International Modelica Conference*.

Giese, T., Schlabe, D., Slater, R., Crespo, M., Tichy, F., and Baumann, C. (2010). **Extended Design Office Concept Definition, D2.1.1**. CleanSky, ITD Systems for Green Operations.

Gürdal, Z., Ragon, S., and Lindner, D. (2000). **Global/Local Design Optimization of a Power Distribution System**. Available http://www.dtic.mil/get-tr-doc/pdf?AD=ADA396996.

Han, L., Wang, J., Griffo, A., and Howe, D. (2008). **Stability assessment of AC hybrid power systems for More Electric Aircraft**. In *Proc. IEEE Vehicle Power and Propulsion Conference (VPPC)*, p. 1-6.

Han, L., Wang, J., and Howe, D. (2006a). **Small-signal Stability Studies of 270V DC Power System for More Electric Aircraft Employing Switched Reluctance Generator Technology**. In *25th international congress of the aeronautical sciences*.

Han, L., Wang, J., and Howe, D. (2006b). **Small-signal Stability Studies of a 270V DC More-Electric Aircraft Power System**. In *The 3rd IET International Conference on Power Electronics, Machines and Drives*, p. 162-166.

Haumer, A., Kral, C., Gragger, J.V., and Kapeller, H. (2008). **Quasi-Stationary Modeling and Simulation of Electrical Circuits using Complex Phasors**. In *Proceedings of the 6th International Modelica conference*.

Hecker, S. (2006). **Generation of low order LFT Representations for Robust Control Applications**. VDI-Verlag.

Hecker, S., and Varga, A. (2005). **Symbolic Techniques for low order LFT-modelling**. In *Proceedings of IFAC World Congress, Prague, Czech Republic*.

Hecker, S., Varga, A., and Magni, J.-F. (2004). **Enhanced LFR-toolbox for MATLAB and LFT-based gain scheduling**. In *Proc. of ODAS 2004*, p. 80-89.

Heinzel, G., Rüdiger, A., and Schilling, R. (2002). **Spectrum and spectral density estimation by the Discrete Fourier transform (DFT), including a comprehensive list of window functions and some new at-top windows.**. Available http://www.rssd.esa.int/SP/LISAPATHFINDER/docs/Data_Analysis/GH_FFT.pdf.

Huang, V., Suganthan, P., and Liang, J. (2006). **Comprehensive Learning Particle Swarm Optimizer for Solving Multiobjective Optimization Problems**. In *International Journal of Intelligent Systems 21*, p. 209-226.

IEEE (2014). **Recommended Practice and Requirements for Harmonic Control in Electric Power Systems**. In *IEEE Std 519-2014 (Revision of IEEE Std 519-1992)*, p. 1-29.

Synopsys Inc. (2017). **Saber**. https://www.synopsys.com/verification/virtual-prototyping/saber.html.

Isermann, R.Springer (Ed.) (2006). **Fault-diagnosis systems: an introduction from fault detection to fault tolerance**. Springer Science & Business Media.

J.R. Hendershot, J., and Miller, T. (1994). **Design of Brushless Permanent-Magnet Motors**. Magna Physics Publishing.

Jeltsema, D., and Scherpen, J. (2005). **On Brayton and Moser's missing stability theorem**. In *IEEE Transactions on Circuits and Systems II: Express Briefs* 52, p. 550-552.

Ji, Y. (2016). **Model-based design and integration of the power network in more electric aircraft**. Ph.D. thesis, Technische Universität München.

Ji, Y., and Bals, J. (2010a). **A novel Modelica signal analysis tool towards design of more electric aircraft**. In *Proc. of the 3rd IEEE Int. Computer Science and Information Technology (ICCSIT) Conference 5*, p. 152-156.

Ji, Y., and Bals, J. (2010b). **Health Monitoring for the Electrical Network of More Electric Aircraft**. In *AIP Conference Proceedings 1247*, p. 86-99.

Ji, Y., and Kuhn, M.R. (2013b). **Modeling and simulation of large scale power systems in more electric aircraft**. In *IEEE 14th Workshop on Control and Modeling for Power Electronics (COMPEL)*, p. 1-6.

Ji, Y., and Kuhn, M.R. (2013a). **Physical modeling and simulation of inrush current in power transformers of more electric aircraft**. In *IEEE IFEEC conference*, p. 722-727.

Ji, Y., and Kuhn, M.R. (2014). **Model Based System Level Studies of More Electric Aircraft**. In *SAE Aerospace Systems and Technology Conference*.

Ji, Y., Pfeiffer, A., and Bals, J. (2010). **Optimization based Steady-State Analysis of Switched Power Electronic Systems**. In *12th IEEE Workshop on Control and Modeling for Power Electronics*, p. 1-6.

Jiang, T., Chen, B., and He, X. (2000). **Industrial application of Wavelet Transform to the on-line prediction of side draw qualities of crude unit**. In *Computers & Chemical Engineering* 24, p. 507-512.

Jiang, T., Chen, B., He, X., and Stuart, P. (2003). **Application of steady-state detection method based on wavelet transform**. In *Computers & Chemical Engineering* 27, p. 569 - 578.

Joos, H.-D. (2017). **MOPS - Multi-Objective Parameter Synthesis User's Guide V6.8**. German Aerospace Center (DLR).

Joos, H.-D., Bals, J., Looye, G., Schnepper, K., and Varga, A. (2002). **A multi-objective optimisation-based software environment for control systems design**. In *IEEE International Conference on Control Applications and International Symposium on Computer Aided Control Systems Design*, p. 7 - 14.

Kelly, J.D., and Hedengren, J.D. (2013). **A steady-state detection (SSD) algorithm to detect non-stationary drifts in processes**. In *Journal of Process Control* 23, p. 326-331.

Kennedy, J., and Eberhart, R. (1995). **Particle swarm optimization**. In *Proceedings of the 1995 IEEE International Conference on Neural Networks*, p. 1942-1948.

Korbel, M., Bellec, S., Jiang, T., and Stuart, P. (2014). **Steady state identification for on-line data reconciliation based on wavelet transform and filtering**. In *Computers & Chemical Engineering* 63, p. 206-218.

PC Krause, and Associates (2017). **FastSim Simulation Suite**. https://pcka.com/.

Krause, P., Wasynczuk, O., and Sudhoff, S. (2002). **Analysis of Electric Machinery and Drive Systems**. WileyBlackwell.

Krause, P.C., Wasynczuk, O., and REPLACED, S.D.S.T.B. (1998). **Analysis of electric machinery and drive systems**. Wiley-Interscience, Piscataway, New York.

Kuchar, R. (2012). **An integrated data generation process for flight dynamics modeling in aircraft design**. In *Deutscher Luft- und Raumfahrtkongress DLRK*.

Kuhn, M.R. (2011). **Advanced generator design using pareto-optimization**. In *IEEE Ninth International Conference on Power Electronics and Drive Systems (PEDS)*, p. 1061 -1067.

Kuhn, M.R. (2017). **Periodic Steady State Identification of electrical circuits**. In *Proceedings of the 12th International Modelica Conference*, p. 493-505.

Kuhn, M.R., Griffo, A., Wang, J., and Bals, J. (2009). **A components library for simulation and analysis of aircraft electrical power systems using Modelica**. In *Proceedings of the 13th European Conference on Power Electronics and Applications*.

Kuhn, M.R., and Ji, Y. (2014a). **Modelica for large scale aircraft electrical network V&V**. In *Proceedings of the 10th International ModelicaConference*.

Kuhn, M.R., and Ji, Y. (2014b). **Next generation design framework for the aircraft electric power system**. In *Greener Aviation: Clean Sky breakthroughs and worldwide status*.

Bibliography

Kuhn, M.R., Ji, Y., Joos, H.-D., and Bals, J. (2008b). **An approach for stability analysis of nonlinear electrical network using antioptimization**. In *Proc. of the IEEE Power Electronics Specialists Conf. (PESC)*, p. 3873-3879.

Kuhn, M.R., Ji, Y., and Schröder, D. (2007). **Stability Studies of Critical DC Power System Component for More Electric Aircraft using mu Sensitivity**. In *Proceedings of the 15th Mediterranean Conference on Control and Automation*.

Kuhn, M.R., Otter, M., and Giese, T. (2015). **Model Based Specifications in Aircraft Systems Design**. In *Proceedings of the 11th International ModelicaConference*.

Kuhn, M.R., Otter, M., and Raulin, L. (2008a). **A Multi Level Approach for Aircraft Electrical Systems Design**. In *Proceedings of the 6th International Modelica Conference*.

Kuhn, M.R., Rekik, M., and Bals, J. (2012). **Modelling and Use of an Aircraft Electrical Network Simulation for Harmonics Consideration in Generator Design**. In *SAE Technical Paper*.

Kundur, P. (1994). **Power System Stability And Control**. McGraw-Hill Education (India) Pvt Limited.

Kutt, F. (2012). **Models of Brushless Synchronous Generator for Studying Autonomous Electrical Power System**. Ph.D. thesis, Gdansk University of Technology.

Lafoz, M., Moreno-Torres, P., Torres, J., Blanco, M., and Navarro, G. (2016). **Design methodology of a high speed switched reluctance generator drive for aircrafts**. In *European Conference on Power Electronics and Applications (EPE ECCE Europe) 18*, p. 1-9.

Larsson, M. (2004). **ObjectStab-an educational tool for power system stability studies**. In *IEEE Trans. Power Systems 19*, p. 56-63.

Lian, K., Perkins, B., and Lehn, P. (2008). **Harmonic Analysis of a Three-Phase Diode Bridge Rectifier Based on Sampled-Data Model**. In *IEEE Transactions on Power Delivery 23*, p. 1088 -1096.

Liang, J., and Suganthan, P. (2005). **Dynamic multi-swarm particle swarm optimizer**. In *Proceedings of the IEEE Swarm Intelligence Symposium (SIS)*, p. 124-129.

Louganski, K.P. (1999). **Modelling and Analysis of a D.C. Power Distribution System in 21st Century Airlifters**. M.Sc. thesis, Virginia Polytechnic Institute and State University, Blacksburg Virginia.

Mallat, S. (2008). **A wavelet tour of signal processing: the sparse way**. Academic press.

Marcos, A., Bates, D., and Postlethwaite, I. (2005). **Control oriented uncertainty modelling using μ sensitivities and skewed μ analysis tools**. In *Proceedings of the 44th IEEE Conference on Decision and Control, and the European Control Conference*.

Marple, S.L., and Marino, C. (2004). **Coherence in signal processing: a fundamental redefinition**. In *Conference Record of the Thirty-Eighth Asilomar Conference on Signals, Systems and Computers 1*, p. 1035-1038 Vol.1.

Menon, P., Bates, D., and Postlethwaite, I. (2007). Optimisation-Based Flight Control Law Clearance. In Bates, D., and Hagström, M. (Ed.), **Nonlinear Analysis and Synthesis Techniques for Aircraft Control**, Springer.

Middlebrook, R. (1976). **Input filter considerations in design and application of switching regulators.**. In *IAS annual meeting 11*.

Modelica (2010). **Language Specification Version 3.2**. Modelica Association.

Moir, I., and Seabridge, A. (2008). **Aircraft Systems: Mechanical, Electrical and Avionics Subsystems Integration**. John Wiley & Sons.

Müller, G., Vogt, K., and Ponick, B. (2008). **Berechnung elektrischer Maschinen**. Wiley-VCH.

Oppenheim, A.V. (1999). **Discrete-time signal processing**. Pearson Education India.

Oppenheim, A.V., and Schafer, R.W. (1998). **Zeitdiskrete Signalverarbeitung**. Oldenbourg Wissenschaftsverlag.

Otter, M., Thiele, B., and Elmqvist, H. (2012). **A Library for Synchronous Control Systems in Modelica**. In *Proceedings of the 9th International Modelica Conference*.

Otter, M., Thuy, N., Bouskela, D., Buffoni, L., Elmqvist, H., Fritzson, P., Garro, A., Jardin, A., Olsson, H., Payelleville, M., and others (2015). **Formal requirements modeling for simulation-based verification**. In *Proceedings of the 11th International Modelica Conference*, p. 625-635.

Park, R.H. (1929). **Two-Reaction Theory of Synchronous Machine- Generalized Method of Analysis, Part I**. In *AIEE Transactions 48*, p. 716-727.

Pollok, A., and Bender, D. (2014). **Using Multi-objective Optimization to Balance System-level Model Complexity**. In *Proceedings of the 6th International Workshop on Equation-Based Object-Oriented Modeling Languages and Tools*, p. 69-78.

Rincón, F.D., Le Roux, G.A., and Lima, F.V. (2015). **A novel ARX-based approach for the steady-state identification analysis of industrial depropanizer column datasets**. In *Processes* 3, p. 257-285.

Roboam, X. (2011). **New trends and challenges of electrical networks embedded in "more electrical aircraft"**. In *IEEE International Symposium on Industrial Electronics (ISIE)*, p. 26-31.

Schallert, C. (2010). **Ein integriertes Entwurfswerkzeug für Elektrische Bordsysteme**. In *Deutscher Luft- und Raumfahrt Kongress*.

Schallert, C., Pfeiffer, A., and Bals, J. (2006). **Generator Power Optimisation for a More-Electric Aircraft by Use of a Virtual Iron Bird**. In *25th International Congress of the Aeronautical Sciences*.

Scherer, C. (2001). **Theory of Robust Control**. Lecture Note, Mechanical Engineering Systems and Control Group, Delft University of Technology, The Netherlands.

Schlabe, D., Bals, J., Sielemann, M., Kuhn, M., Ji, Y., Schallert, C., Zimmer, D., Widhammer, A., Giese, T., Bergman, M., Vial, S., Tichy, F., Bozhko, S., Martinez, M., Christmann, J.M.M., and Lemay, D. (2015). **Description of a standardized modelling and simulation process for energy systems, D2.1.2_1**. CleanSky, ITD Systems for Green Operations.

Schlabe, D., Sielemann, M., Schallert, C., Zimmer, D., Kuhn, M.R., Ji, Y., and Bals, J. (2012). **Towards a Model-Based Energy System DesignProcess**. In *SAE Power Systems Conference*.

Schlemmer, E. (2009). **Damping of synchronous machines-analytical estimations versus finite element results**. In *International Conference on Clean Electrical Power*, p. 751-754.

Schupp, G. (2003). **Numerische Verzweiungsanalyse mit Anwendungen auf Rad-Schiene-Systeme**. Ph.D. thesis, Universität Stuttgart.

Simon, H. (1982). **Models of Bounded Rationality**. Cambridge Univ. Press, Cambridge, MA.

Sinnett, M. (2007). **787 No-Bleed Systems**. Boeing. Available http://www.boeing.com/commercial/aeromagazine/articles/qtr_4_07/AERO_Q407_article2.pdf.

Soong, W. (2008). **Sizing of electrical machines**. In *Power Engineering Briefing Notes*, p. 17-18.

US Department of Defense (2004). **MIL-STD-704F: Aircraft electric power characteristic**. http://www.wbdg.org/ccb/FEDMIL/std704f.pdf.

Sudhoff, S, Glover, S, Lamm, P, Schmucker, D, and Delisle, D (2000). **Admittance space stability analysis of power electronics system**. In *IEEE Trans. on Aerospace and Electronic Systems* 36, p. 965-973.

Sun, J., Bing, Z., and Karimi, K.J. (2008). **Small-signal modeling of multipulse rectifiers for more-electric aircraft applications**. In *Proc. IEEE Power Electronics Specialists Conf. (PESC)*, p. 302-308.

Sun, J., Bing, Z., and Karimi, K.J. (2009). **Input impedance modeling of multipulse rectifiers by harmonic linearization**. In *IEEE Transactions on Power Electronics* 24, p. 2812-2820.

Dassault Systèmes (2018b). **CATIA**. https://www.3ds.com/products-services/catia/.

Dassault Systèmes (2018a). **Dymola**. https://www.3ds.com/products-services/catia/products/dymola/.

The MathWorks, Inc. (2017). **Simscape**. https://de.mathworks.com/products/simscape.html.

Tsiachris, F.K. (2009). **Study of High Voltage DC capacitors: Parametric Weight-, Volume- and ESR models**. MOET Report. Technological Educational Institute of Piraeus (TEIP).

UPC (2016). **MAGMOLIB (Modelica library of detailed magnetic effects in rotating machinery)**. Universitat Politècnica de Catalunya, MCIA group, https://magmolib.upc.edu/en.

Urfalioglu, O. (2004). **Robust estimation of camera rotation, translation and focal length at high outlier rates**. In *Proceedings of First Canadian Conference on computer and Robot Vision*, p. 464-471.

Varga, A. (2002). Optimisation-Based Clearance. In Fielding, C., Varga, A., Bennani, S., and Selier, M. (Ed.), **Advanced Techniques for Clearance of Flight Control Laws**, Springer-Verlag.

Wamkeue, R., Kamwa, I., and Dai-Do, X. (1998). **Numerical modeling and simulation of unsymmetrical transients on synchronous machines with neutral included**. In *Electric Machines and Power Systems* 26, p. 93-108.

Wang, L., and Liu, K.-H. (2005). **A study on randomly varying harmonic currents and total harmonic distortion of currents in power systems**. In *2005 International Conference on Future Power Systems*, p. 5 pp.-5.

Bibliography

Welch, P. (1967). **The use of fast Fourier transform for the estimation of power spectra: A method based on time averaging over short, modified periodograms**. In *IEEE Transactions on Audio and Electroacoustics* 15, p. 70-73.

Wiesmann, H. (2007). **SPOT 0.706**. Available https://github.com/modelica-3rdparty/Spot.

Zhou, K., and Doyle, J.C. (1998). **Essentials of robust control**. Prentice hall Upper Saddle River, NJ.

Ziske, J., and Bödrich, T. (2012). **Magnetic hysteresis models for Modelica**. In *Proceedings of the 9th International Modelica Conference*.